Fibre Laser Metal Deposition with Wire: Parameters Study and Temperature Control

Alexis G. Medrano Téllez

Thesis submitted to the University of Nottingham
for the degree of Doctor of Philosophy

July 2010

To my dear parents

Abstract

This research addresses the development of a laser metal deposition process with wire feeding and melt pool temperature control. The system consists of a 2 kW fibre laser, a CNC table, a wire feeder and a temperature monitoring and control system.

A study of the influence of the main parameters on the process and on the deposited bead geometry was performed. The parameters analysed were: laser power, traverse speed and wire feed rate. As a result of this study, a process window was established for metal deposition of stainless steel 308LSi (wire) on stainless steel 304 (plate). The influence of the parameters on the bead geometry (height and width) was analysed applying the Design of Experiments methodology, using a full factorial design 3^k. The results are presented, together with important practical considerations for laser metal deposition with wire.

A closed-loop temperature control system was developed: it controls the melt pool temperature by means of modifying the laser power. The melt pool temperature was measured by a two-colour pyrometer, whereas a single-colour pyrometer was used for monitoring the workpiece (upper layer) temperature. A model of the melt pool was derived from a heat balance equation. It was then utilized for the design of the controller in the discrete domain, using the root locus method. The control algorithm was developed in LabVIEW^{TM} software and executed in a computer.

The control system was implemented successfully and was utilized to build single-bead walls and cylinders of stainless steel 308LSi.

The study performed on the parameters and the developed temperature controller proved to be very effective tools to facilitate the transition to the deposition of titanium alloy Ti-6Al-4V, requiring only minimum adaptations. Single-bead walls and cylinders were also built in this material.

Stable and smooth metal deposition was achieved for both materials. During the experiments, several strategies for the automation of wire metal deposition of multi-layered structures were developed.

Finally, mechanical tests were performed. The mechanical properties of the deposited materials are comparable to those in wrought (annealed) condition and to similar alloys made by laser powder deposition systems.

The system developed in this work provides a means to perform stable and smooth wire metal deposition, achieving good mechanical properties. It also facilitates the the transition to deposit different materials. It has a flexible structure and can be expanded or adapted to be used in other wire metal deposition systems.

Acknowledgements

I would like to express my most sincere gratitude to my supervisor Dr Janet Folkes for her guidance and support over the course of this project. Without her help, this work would not have taken place. I would also like to express my gratitude to Dr Adam Clare for acting as internal examiner, and to Dr Stuart Barnes of the University of Warwick for acting as external examiner. I would also like to thank Dr Richard Cobb for his participation during the viva voce examination.

I am very grateful to all my colleagues and friends from the University of Nottingham. I would like especially to thank Dr Saúl López Arévalo for his friendship and advice. My thanks goes also to Dr Joel Segal for his help in this project. Special recognition goes to Mr Stuart Branston for his technical support and advice. I would also like to thank Taiwo Abioye (MSc) for his assistance in this work.

My deepest and sincere gratitude to my family for their unconditional love and support. They helped me to keep hoping and smiling on both sunny and rainy days. I owe special gratitude to all my friends, for the laughter in the good times and the encouragement in the difficult ones and for making my time so enjoyable.

I would like to acknowledge my sponsor, the Mexican Council of Science and Technology (CONACYT), who gave me the opportunity to study a PhD by granting me a scholarship. I would also like to thank the Ministry of Public Education of Mexico (SEP) for the complementary scholarship I received during my studies.

Finally, and above all, my gratitude to God.

Abbreviations

3D	Three-dimensional
A	Austenite solidification mode
ADC	Analogue to digital converter
AF	Primary austenite solidification mode
AM	Additive manufacturing
ANOVA	Analysis of variance
BCC	Body-centred cubic
CAD	Computer aided design
CNC	Computer numerical control
CW	Continuous wave
DAC	Digital to analogue converter
DAQ	Data acquisition
DOE	Design of experiments
EBM	Electron beam melting
EBW	Electron beam welding
ELI	Extra low interstitials
F	Ferrite solidification mode
FA	Primary ferrite solidification mode
FCC	Face-centred cubic
FN	Ferrite number
FRW	Friction welding
GMAW	Gas metal arc welding
GTAW	Gas tungsten arc welding
HAZ	Heat affected zone
HCP	Hexagonal close-packed

LBW	Laser beam welding
LED	Light emitting diode
LMD	Laser metal deposition
LPD	Laser powder deposition
MSE	Mean square of the error
MST	Mean square of the treatments
Nd:YAG	Neodymium: yttrium aluminium garnet
PAW	Plasma arc welding
PC	Personal computer
PI	Proportional-integral
PID	Proportional-integral-derivative
ppm	Parts per million
PTA	Plasma transferred arc
RTD	Resistance temperature devices
RW	Resistance welding
SMAW	Shielded metal arc welding
SSE	Sum of squares of error
SST	Sum of squares of treatments
Total SS	Corrected sum of squares
UTS	Ultimate tensile strength

Contents

1 Introduction 1

1.1 Aim of this Research 3

1.2 General Approach to the Problem 3

1.3 Overview of the Thesis 4

2 Literature Review 6

2.1 Lasers 6

2.1.1 Definition and Working Principle of a Laser 6

2.1.2 Lasers Used for Industrial Applications 8

2.2 Stainless Steel 16

2.2.1 Characteristics and Applications of Stainless Steels 16

2.2.2 Welding of Austenitic Stainless Steels 19

2.2.3 Stainless Steels 304 and 308 23

2.3 Titanium Alloys 24

2.3.1 Characteristics and Applications of Titanium Alloys 24

2.3.2 Welding of Titanium Alloys 27

2.3.3 Titanium Alloy Ti-6Al-4V 28

2.4 Temperature Measurement 30

2.4.1 Temperature Measurement Techniques 30

2.4.2 Thermocouples 31

2.4.3 Pyrometers 32

2.5 Design of Experiments 38

2.5.1 Basic Principles 38

2.5.2 General Methodology 40

2.5.3 Factorial Designs 41

2.5.4 Analysis of Results 42

2.6 Control Engineering 48

2.6.1 Closed-loop Control Systems 48

2.6.2 Mathematical Modelling of Systems 49

2.6.3 Root Locus Method 53

2.6.4 Discrete Time Systems 54

2.7 Additive Manufacturing 56

2.7.1 Description of the Process 56

2.7.2 Technologies for Metal Additive Manufacturing 57

2.7.3 Important Factors in Laser Metal Deposition 64

2.8 Control in Laser Metal Deposition 70

2.8.1 Melt Pool Size Control 70

2.8.2 Melt Pool Temperature Control 74

3 Experimental Setup and Procedures **78**

3.1 Experimental Setup 78

3.1.1 Laser 79

3.1.2 Laser Head 79

3.1.3 CNC Table 79

3.1.4 Wire Feeder 80

3.1.5 Temperature Sensors 80

3.1.6 Setup with Inert Gas Nozzle 81

3.1.7 Setup with Inert Gas Chamber 81

3.1.8 Data Acquisition Card 84

3.2 Materials 85

3.2.1 Austenitic Stainless Steel 85

3.2.2 Titanium Alloy Ti-6Al-4V 86

3.3 Procedures for Measurements and Tests 86

3.3.1 Measurement of Bead Geometry 86

3.3.2 Tensile Test 89

3.3.3 Metallographic Analysis of Stainless Steel 90

3.3.4 Hardness Test of Stainless Steel 91

4 Influence of Process Parameters on Metal Deposition 92

4.1 Bead-on-plate Metal Deposition Experiments 92

4.1.1 Bead-on-plate Deposition Without Inert Gas Chamber 92

4.1.2 Bead-on-plate Deposition Inside Inert Gas Chamber 94

4.2 Effects of the Main Factors on the Process 95

4.2.1 Effects of Laser Power, Traverse Speed and Wire Feed Rate . . 95

4.2.2 Process Window 96

4.2.3 Influence of Parameters on Porosity 100

4.3 Effects of the Main Factors on Bead Geometry 101

4.3.1 Effects on Bead Height 101

4.3.2 Effects on Bead Width 105

4.4 Practical Considerations for Laser Metal Deposition with Wire 110

4.4.1 Alignment and Position of the Wire 110

4.4.2 Wear of Wire Feeder Nozzle 111

4.4.3 Protection From Oxidation Inside Inert-gas Chamber 112

4.4.4 Temperature Inside Inert-gas Chamber 113

4.4.5 Change in Laser Focal Distance 113

5 Temperature Monitoring System for Metal Deposition 114

5.1 Analysis of Suitable Pyrometers 114

5.2 Experiments and Results 117

5.2.1 Raytek MM 2MH 119

5.2.2 Raytek MM 3ML 119

5.2.3 Impac IGAR 12-LO MB 22 122

5.2.4 Workpiece Temperature and Melt Pool Temperature 125

5.2.5 Impac IP 140-LO MB 7.5 125

5.2.6 Impac IGA 50-LO Plus MB 13.5 127

5.2.7 Precitec Photodiode 128

5.3 Optical Filters for Rejection of Laser Reflections 130

5.4 Actual Temperature Monitoring System 133

6 Development of Temperature Control System **136**

6.1 Development of the Model of the System 136

6.1.1 Derivation of the Transfer Function 137

6.1.2 Constants of the System 143

6.1.3 Transformation to the Discrete Domain 146

6.1.4 Root Locus Analysis and Controller Design 148

6.2 Controller Algorithm 154

7 Implementation of Temperature Control System **156**

7.1 Process Control of Non-continuous Metal Deposition (Walls) 156

7.1.1 Experimental Conditions 157

7.1.2 First Layers of a Wall 158

7.1.3 Strategy for the Start of a Bead 160

7.1.4 Strategy for the End of a Bead 161

7.1.5 Strategy for Building Multiple Walls 162

7.1.6 Workpiece Temperature 164

7.1.7 Deposition of Stainless Steel at 1750 and 2000 °C 167

7.1.8 Deposition of Ti–6Al–4V 172

7.2 Process Control of Continuous Metal Deposition (Cylinders) 174

7.2.1 Strategy for Metal Deposition of Cylinders 176

7.2.2 Deposition of Stainless Steel 179

7.2.3 Deposition of Ti-6Al-4V 182

8 Mechanical Properties **184**

8.1 Methodology of Metal Deposition of Walls for Mechanical Tests . . . 184

8.2 Tensile Test for Stainless Steel 308LSi 185

8.2.1 Conditions of the Test 185

8.2.2 Ultimate Tensile Strength 186

8.2.3 Elongation 190

8.3 Tensile Test for Ti-6Al-4V 193

8.3.1 Conditions of the Tests 193

8.3.2 Ultimate Tensile Strength 193

8.3.3 Elongation 195

8.4 Hardness Test for Stainless Steel 308LSi 196

9 Summary and Conclusions **199**

9.1 Summary and Conclusions 200

9.1.1 System Development 200

9.1.2 Effect of Parameters on the Process Condition 201

9.1.3 Influence of Parameters on Bead Geometry 202

9.1.4 Temperature Monitoring 203

9.1.5 Temperature Control 204

9.1.6 Mechanical Properties of Deposited Walls 206

9.2 Future Work 207

9.3 Publications Resulting from the Work 209

Appendices **223**

A Laser Power Measurement **223**

B Laser Focus Measurement **224**

C Means and Standard Deviations **231**

D Residual Plots **233**

List of Figures

2.1 Photon emission 7

2.2 Working principle of lasers 7

2.3 Optical resonator cavity 8

2.4 CO_2 laser 9

2.5 Diode 11

2.6 Diode laser strip 12

2.7 Diode laser stack 12

2.8 Fibre laser 15

2.9 Pseudo-binary diagram Fe-Cr-Ni 21

2.10 Schaeffler diagram 22

2.11 Reflection, absorption and transmission 32

2.12 Spectral characteristics of blackbody radiation 33

2.13 Relative spectral intensity 34

2.14 Digital pyrometer 35

2.15 Correct target size for single-colour pyrometer 36

2.16 Two-colour pyrometer 37

2.17 Example of two-colour pyrometer 38

2.18 2^K factorial design 42

2.19 Main effects plot 43

2.20 Interactions plot 43

2.21 Feedback loop 48

2.22 Cascade block diagram 50

2.23 Negative feedback block diagram 50

2.24 Unit step response 52

2.25 Influence of pole location 53

2.26 The Z - plane 56

2.27 Powder-bed additive manufacturing process 59

2.28 Powder nozzle 61

2.29 Four-nozzle powder delivery system 62

2.30 Wire feed 63

2.31 Reflectivity of selected metals 65

2.32 Wire setup 67

2.33 Wire height position 68

2.34 Sensors in Robotized Laser Metal-wire Deposition 72

3.1 Initial setup of the metal deposition system 82

3.2 Setup for inert gas chamber 83

3.3 Schematic diagram for the metal deposition system 85

3.4 Triangulation principle 87

3.5 Measurement of bead geometry 88

3.6 Tensile test sample 89

3.7 Tensile test 90

4.1 Bead-on-plate runs 94

4.2 Process window 98

4.3 Influence of the bead start conditions 99

4.4 Lack-of-fusion porosity due to inadequate parameters 100

4.5 Interaction plot for bead height 103

4.6 Main effects plot for bead height 104

4.7 Interaction plot for bead width 106

4.8 Main effects plot for bead width 107

4.9 Complete and incomplete cross section bead profile 109

4.10 Wire oscillations due to deteriorated wire feeder nozzle 112

5.1 Configuration of pyrometers 116

5.2 Setup of the experiments with pyrometers 118

5.3 Melt pool temperature using pyrometer Raytek MM 2MH 120

5.4 Aiming point of the pyrometer for workpiece temperature 121

5.5 Temperature of workpiece measured with Raytek MM 3ML 121

5.6 Pyrometer aiming spot for melt pool temperature measurement . . . 122

5.7 Effect of pyrometer misalignment 123

5.8 Melt pool temperature measured during the whole experiment 124

5.9 Alignment of laser and pyrometers 126

5.10 Monitoring of melt pool and workpiece temperatures 127

5.11 Measurements with pyrometers IGAR 12-LO and IGA 50-LOplus . . 128

5.12 Comparison of Precitec photodiode and pyrometers 130

5.13 Transmission graph of notch filter 132

5.14 Transmission graph of long-pass filter 132

5.15 Setup of temperature monitoring system 133

5.16 Alignment of melt pool pyrometer 134

6.1 Basic block diagram of temperature control system 137

6.2 Control volume 138

6.3 Longitudinal and transversal sections of the melt pool 146

6.4 Poles and zeros in the z-plane 150

6.5 Root locus of the system with a proportional controller 151

6.6 Root locus of the system with the proposed controller 152

6.7 Root locus of the system with the proposed controller (K = 0.7) . . . 153

6.8 Time response of the system with the proposed controller (K = 0.7) . 154

6.9 Interface of the controller 155

7.1 Deposition of second layer in a single-bead wall 159

7.2 Deposition of a bead: melt pool temperature and laser power 161

7.3 Excess deposit formed at the end of every layer and its effect 162

7.4 Problems when building multiple walls one at a time 163

7.5 Workpiece temperature at the beginning of a bead 164

7.6 Workpiece temperature of a 70-layer wall 165

7.7 Workpiece temperature and laser power extreme values 166

7.8 Stainless steel 308LSi wall deposited at 1750 °C 167

7.9 Graph of temperature control at 1750 °C (three beads) 168

7.10 Graph of temperature control at 1750 °C (20 beads) 169

7.11 Stainless steel 308LSi wall deposited at 2000 °C 170

7.12 Graph of temperature control at 2000 °C (three beads) 171

7.13 Ti–6Al–4V wall deposited at 1850 °C 173

7.14 Graph of temperature control of Ti–6Al–4V at 1850 °C (three beads) 174

7.15 Deposition of a cylinder inside argon chamber 176

7.16 Start of the spiral path in the deposition of cylinders 178

7.17 Deposition of a stainless steel 308LSi cylinder 180

7.18 Stainless steel 308LSi cylinder 182

7.19 Deposition of a Ti–6Al–4V cylinder 183

7.20 Ti–6Al–4V cylinder 183

8.1 Orientation of tensile test samples in walls 186

8.2 Single-bead wall used for tensile test samples 187

8.3 Main effects plot for UTS 188

8.4 Interactions plot for UTS 189

8.5 Main effects plot for elongation 191

8.6 Interactions plot for elongation 191

8.7 Main effects plot for UTS 194

8.8 Main effects plot for elongation 195

B.1 Setup for beam analysis 225

B.2 Focal distance vs laser power (86% radius definition) 227

B.3 Focal distance vs laser power (Second order moments) 227

B.4 Focal distance drift at 2 kW 228

B.5 Beam diameter out of focus at 1.5 kW 230

D.1 Residual plots for bead height 234

D.2 Residual plots for bead width 234

D.3 Residual plots for UTS of stainless steel 308LSi 235

D.4 Residual plots for elongation of stainless steel 308LSi 235

D.5 Residual plots for UTS of Ti-6Al-4V 236

D.6 Residual plots for elongation of Ti-6Al-4V 236

List of Tables

2.1 Wall plug efficiencies of industrial lasers 16

2.2 Chemical composition of stainless steel 304 and 308LSi 24

2.3 Mechanical properties of stainless steel 304 and 308 24

2.4 Physical properties of stainless steel 304 and 308 24

2.5 Chemical composition of Ti-6Al-4V 29

2.6 Mechanical properties of Ti-6Al-4V 29

2.7 Physical properties of Ti-6Al-4V 29

2.8 Thermocouple temperature ranges 31

2.9 ANOVA table 45

2.10 Characteristics of deposits made by commercial LPD systems 61

3.1 Analysis of shielding gas 83

3.2 Modules for NI cDAQ-9172 84

3.3 Chemical composition of stainless steel 304 and 308LSi 86

3.4 Chemical composition of Ti-6Al-4V 86

3.5 Parameters used for bead profile measurements 89

4.1 Analysis of variance for height (factors and interactions) 101

4.2 Analysis of variance for height (factors) 104

4.3 Analysis of variance for width (factors and interactions) 105

4.4 Analysis of variance for width (factors) 107

5.1 Pyrometers and characteristics 117

6.1 Time response characteristics of controller 152

8.1 Results for UTS of stainless steel 308LSi 187

8.2 Analysis of variance for UTS (factors and interaction) 188

8.3 Analysis of variance for UTS (factors) 189

8.4 Results for elongation of stainless steel 308LSi 190

8.5 Analysis of variance for elongation (factors and interaction) 190

8.6 Analysis of variance for elongation (factors) 192

8.7 Mechanical properties of wrought and deposited stainless steel 193

8.8 Results for UTS of Ti-6Al-4V 194

8.9 Analysis of variance for UTS 194

8.10 Results for elongation of Ti-6Al-4V 195

8.11 Analysis of variance for elongation 195

8.12 Mechanical properties of wrought and deposited Ti-6Al-4V 196

8.13 Hardness of stainless steel walls 197

8.14 Hardness of selected wrought stainless steels 198

A.1 Laser power measurement after 600 μm process fibre 223

B.1 Focal distance and diameter at different laser power settings 226

B.2 Focal distance drift at 2 kW 228

C.1 Means and standard deviations of bead height and width 232

Chapter 1

Introduction

Laser Metal Deposition (LMD) is a manufacturing process that uses a laser beam as a heat source to melt and deposit metal (in powder or wire form) onto a substrate. It has become a fundamental part of the Additive Manufacturing (AM) industry, that produces prototypes, tools and end-use parts directly from a Computer-Aided Design (CAD) model, building the piece layer upon layer.

Some of the typical applications of LMD are:

- Building a component
- Addition of features
- Cladding
- Repair work

It is used in areas such as aerospace, power generation, petrochemical, mould making, etc. It has been applied to improve the performance of components under conditions of wear and corrosion, and in the repair of high value products, for example, moulds, dies, turbine components, etc. [1].

The LMD process in industry has been dominated by powder-based technologies with several commercial systems available. However, the use of wire for laser metal deposition has gained attention in recent years due to some important advantages: 100% of the material is deposited, it is a cleaner process, it achieves high deposition rates and the simplicity of wire feeding systems. [2, 3].

Few publications have been made on the analysis of process factors and conditions of wire metal deposition with Nd:YAG [4], diode [5, 6, 2] and fibre lasers [7, 8]. In particular, in the area of wire deposition with fibre laser, the data is limited.

No comprehensive characterisation of the influence of the three main factors (laser power, traverse speed and wire feed rate) on the deposited bead geometry has been performed. There is the need to investigate the influence of the parameters and their interactions in order to gain a better understanding of the process to be able to apply it successfully in industry.

Even more, metal deposition systems are affected by process conditions such as the accumulation of heat as the part is built. This modifies the effects that the parameters have on the process, making it necessary to use a closed-loop control system to compensate for these changes in order to maintain the stability of the process and ensure the quality of the product.

Wohlers [9], has described the implementation of process control methods in AM as one of the key factors that "will have a profound impact on the future of rapid product development and manufacturing", especially for applications in which product failure has significant safety impact such as aerospace, automotive and medicine.

Different sensors can be used for the monitoring and control of metal deposition systems. Melt pool size and temperature measurements have been used in powder based deposition. One advantage of the melt pool temperature is that it can indicate microstructures and properties of the deposited material [10].

However, no process control system has been developed for melt pool temperature of

laser wire metal deposition. Therefore it is also necessary to investigate the development of such a control system.

This research addresses the development of a fibre laser wire metal deposition system, investigating both issues: process characterisation by analysing the influence of the three main parameters on the deposited bead geometry, and the design and implementation of a closed-loop melt pool temperature control system.

1.1 Aim of this Research

The aim of this research is to investigate the development of a metal deposition system with fibre laser and wire feeding.

Specific objectives are:

- To implement a metal deposition process with fibre laser and wire feeding
- To establish a process window for the main parameters
- To characterise the influence of the main parameters on the deposited bead geometry (width and height)
- To design and implement a closed-loop control system for the melt pool temperature

1.2 General Approach to the Problem

The approach to this research project have been summarized in the following stages:

- Literature Review

- Initial trials of fibre laser wire metal deposition
- Design and implementation of enclosure chamber and positioning fixtures
- Process characterisation of fibre laser wire metal deposition (bead-on-plate)
- Deposition of multi-layered structures
- Development of sensor system for temperature monitoring
- Derivation of theoretical model and transfer function of the system
- Design of controller
- Development of controller algorithm
- Practical implementation of the control system
- Mechanical tests of deposited material

Although presented here in a linear way for simplicity, the project has been an iterative process.

1.3 Overview of the Thesis

The remainder of this thesis is divided into the following Chapters:

Chapter 2 deals with the literature relevant to this research project. The basic theory of the different topics used in this work is explained. Also the previous research on additive manufacture and control of laser metal deposition processes is analysed.

In Chapter 3, the experimental setup is described, together with the materials used and the procedures for measurements and testing.

Chapter 4 presents the characterization of the wire metal deposition process. The effects of the parameters on the bead geometry are analysed and practical considerations for a successful process are explained.

In Chapter 5, the development of a temperature monitoring system is outlined. Practical issues regarding the temperature monitoring are analysed.

In Chapter 6, a mathematical model of the melt pool is developed, starting from a heat balance equation. This model is then transformed into the discrete domain and utilized to design a control system for the melt pool temperature, using the root locus method.

Chapter 7 deals with the practical implementation of the temperature control. The system is utilized to build single-bead walls and cylinders. The performance of the controller is analysed and different strategies for process automation are presented.

In Chapter 8 the results from the mechanical tests performed on the deposited material are presented and analysed.

Chapter 9 summarizes the conclusions of this research and presents recommendations for the future work that can be undertaken.

Chapter 2

Literature Review

2.1 Lasers

2.1.1 Definition and Working Principle of a Laser

The word Laser is an acronym for Light Amplification by the Stimulated Emission of Radiation [11]. It refers to the physical process used to produce a beam of light.

When an atom is in its normal level of energy, its electrons sit in a low orbit ("ground state"). If the atom receives more energy, the electrons can move to a higher orbit ("excited state") [12].

When atoms are excited, i.e. in an energy level higher than the normal, they will tend to return to the ground state by releasing the extra energy that they have. There are different ways to release this energy, one of them is the emission of light: an electron that is in a high energy level produces a photon (light) and drops to a lower energy level (see Figure 2.1). When this emission is produced without external intervention it is termed spontaneous emission, like the one occurring in a light bulb. This emission can be also stimulated, i.e. an atom that has excess energy can be stimulated to

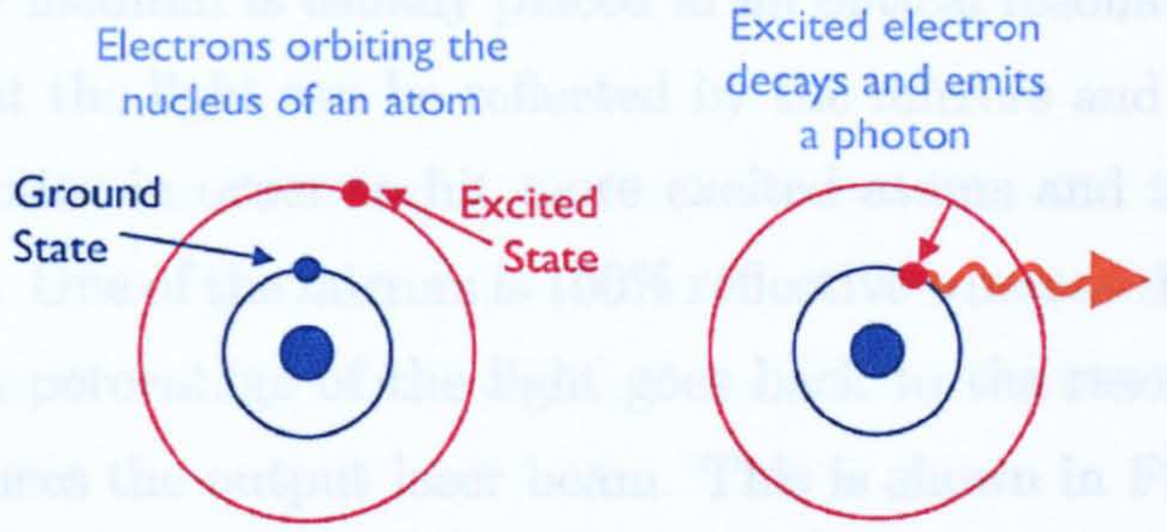

Figure 2.1: Photon emission [12]

release that energy as light, and that is the way lasers work.

A laser device normally consists of a medium (e.g. a gas, a crystal or a fibre) that is excited ("pumped") to achieve a condition called "population inversion", where the majority of atoms or molecules are excited.

When an electron is excited it normally gets to an unstable state, then it quickly moves to a meta-stable state with lower energy and stays there for a short period of time.

In this meta-stable state, some atoms release their extra energy in form of photons (light), and when this light reaches other excited atoms, they also release their energy in form of light with the same wavelength (stimulated emission). This induces a cascade effect that produces a light beam that is monochromatic and coherent [11]. Monochromatic means that the light waves have ideally the same wavelength (in practice the beam has a very narrow bandwidth). Coherent means that light waves are in phase with one another. The process is illustrated in Figure 2.2.

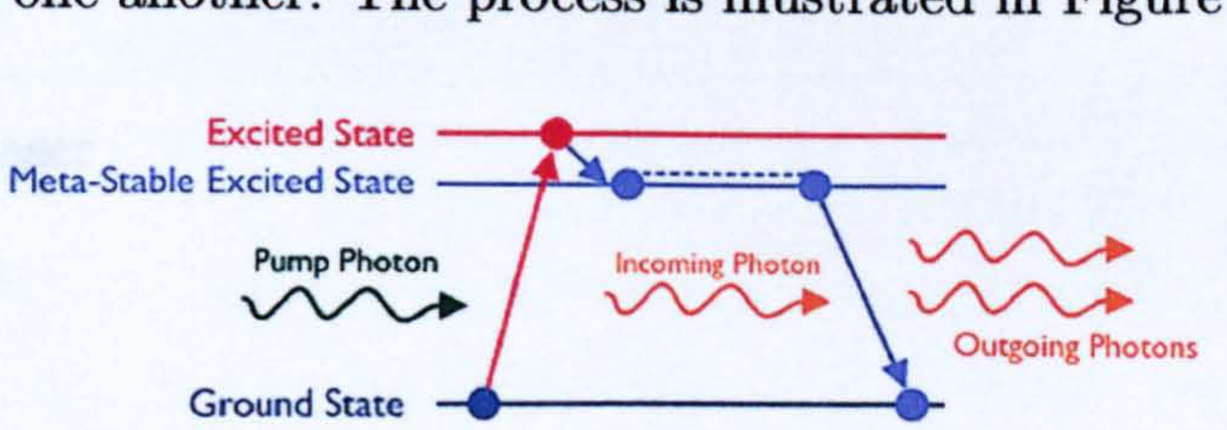

Figure 2.2: Working principle of lasers [12]

In laser devices the medium is usually placed in an optical resonator cavity, between two mirrors, so that the light can be reflected by the mirrors and travel many times in the cavity resonator in order to hit more excited atoms and thus make them to produce more light. One of the mirrors is 100% reflective whereas the other is partially reflective so that a percentage of the light goes back to the resonator and the rest goes out and produces the output laser beam. This is shown in Figure 2.3.

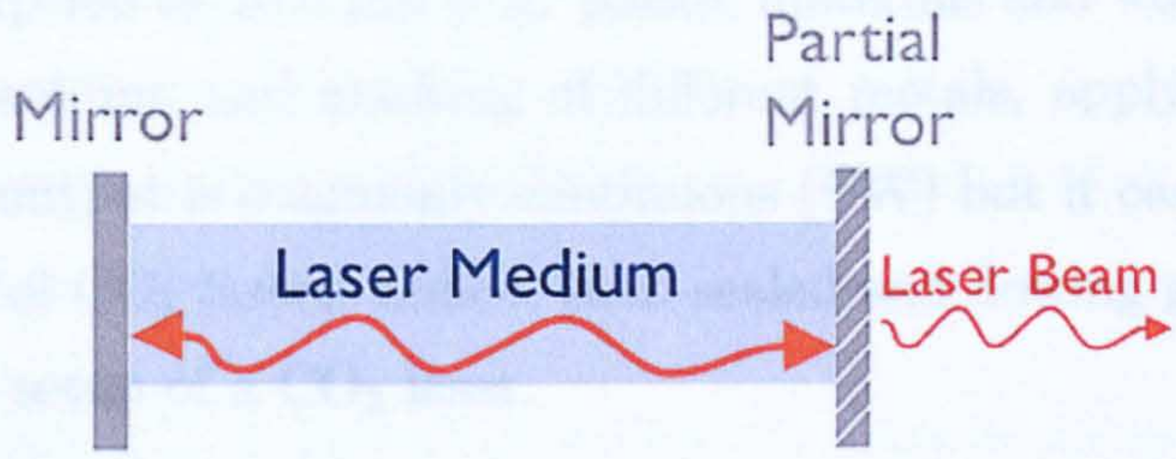

Figure 2.3: Optical resonator cavity [12]

2.1.2 Lasers Used for Industrial Applications

Among all the different types of laser devices, there are four that are commonly used for manufacturing applications (welding, cutting, drilling, marking, surface modification, metal deposition):

- CO_2 Laser
- Diode Laser
- Nd: YAG Laser
- Fibre Laser

CO_2 Lasers

In carbon dioxide (CO_2) lasers, the medium is a mixture of gases that contains carbon dioxide (CO_2), helium (He), nitrogen (N_2), and possibly some hydrogen (H_2), water vapor and/or xenon (Xe). CO_2 lasers emit at a wavelength of 10.6 μm.

They are commonly used in different manufacturing processes such as cutting materials with high absorption at 10.6 μm (e.g. plastic materials and wood). They are also used for cutting, welding and marking of different metals, applying multi-kilowatt powers. The laser output is commonly continuous (CW) but it can be pulsed. There are different types of CO_2 lasers: sealed, semi-sealed and flowing gas [13]. Figure 2.4 shows a schematic setup of a CO_2 laser.

Two important disadvantages of this laser are related to its wavelength: the absorptivity of a number of metals is lower at 10.6 μm than at $\approx$1 μm (the wavelength of Nd:YAG and fibre lasers). The second is that there are no optical fibres capable of transmitting a high power laser at 10.6 μm, so that the delivery of the beam is normally done by an arrangement of mirrors.

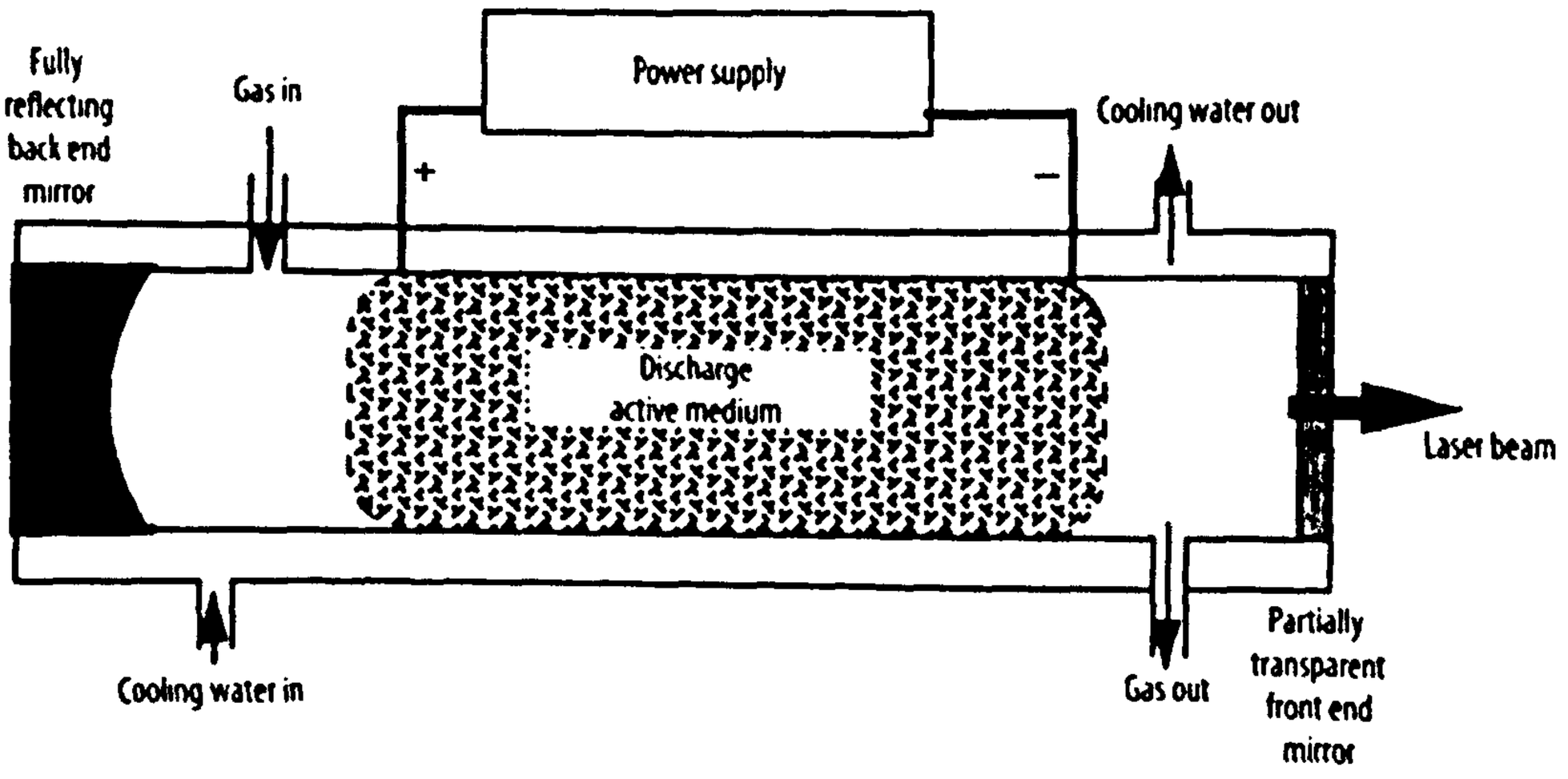

Figure 2.4: CO_2 laser [14]

The wall plug efficiency of CO_2 lasers is commonly in the range of 5–15% [15], but it can be up to 20% [16]. The term "wall plug efficiency" refers to the ratio of the energy of the output laser beam over the energy taken by the laser device from the wall plug (or another energy source), and it is an important value specially for industrial lasers, in which high power is needed. Industry requires efficiency because of cost.

Diode Lasers

In order to explain the operation of diode lasers it is important to review some basic principles of semiconductors and diodes.

The outermost electrons in a conductor are free to move in the material as electrical current. In a semiconductor, however, most of the outermost electrons are bound to the crystalline lattice, and only a few are able to escape and move in the material [17]. Semiconductors have just two energy bands in which electrons can fall. The lower energy band is the one for electrons that are bound to adjacent atoms of the crystal, it is called "valence band". The higher energy band is called "conduction band" and the electrons there are free to move and carry current. The difference in energy between the bottom of the conduction band and the top of the valence band is called the "band gap". The band gap depends on the material and is an important value because there are no energy levels in between, i.e. an electron must gain or lose at least the band gap energy in order to move between the valence and conduction bands. The band gap energy is related to a particular wavelength so that when an electron releases that energy in form of light, the light will have that particular wavelength [17].

Some semiconductor materials can be "doped" i.e. it is possible to add a few impurity atoms with more (or fewer) outer shell electrons in such a way that those extra electrons are not trapped in the lattice so the can move in the material as electrical current. If the impurity atoms have more electrons in the outer shell than the intrinsic semiconductor material, then the material is called n-type for it has negative current

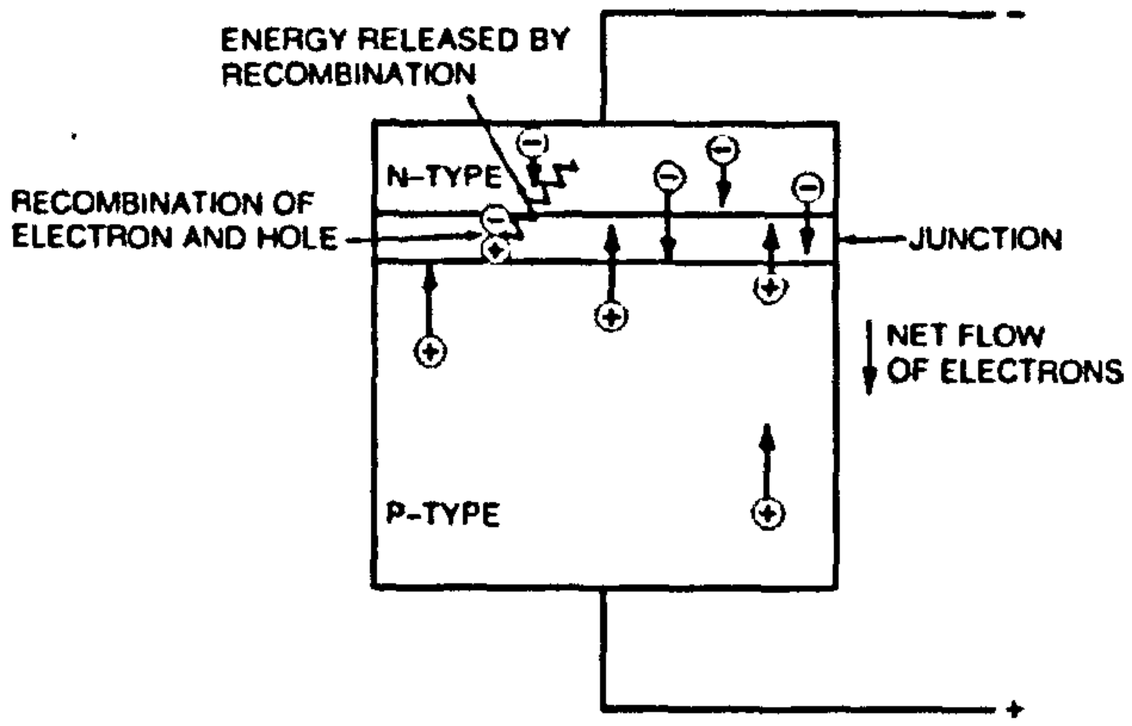

Figure 2.5: Diode [17]

carriers. If the impurity atoms have fewer electrons in the outer shell, the material is called p-type for it has positive carriers. The boundary zone between p-type and n-type regions is called "junction" and is the zone where light emission occurs [17].

A positive voltage is applied to the p-type part of the junction and a negative voltage is applied to the n-type part, this moves the positive and negative carriers to the other side and makes them to cross the junction. This is shown in Figure 2.5.

When electrons from the n-side (conduction band) recombine with p-carriers (valence band), they release the energy at the junction. This energy can be released in form of light, and that is the way a light emitting diode (LED) works. It is important to note that the light produced by LEDs is spontaneous emission.

As in other lasers, in a diode laser the stimulated emission is directed by two reflective surfaces. One of them may be totally reflective and the other is partially reflective so that some light is reflected back to stimulate light emission, while the rest passes through it to form the output laser beam. See Figure 2.6.

The output of a single diode laser element is a fraction of a Watt [13]. In order to make a high power diode laser, a laser bar is made i.e. a large chip with several active stripes. The laser bar is soldered to a heat sink with water-cooling channels in order

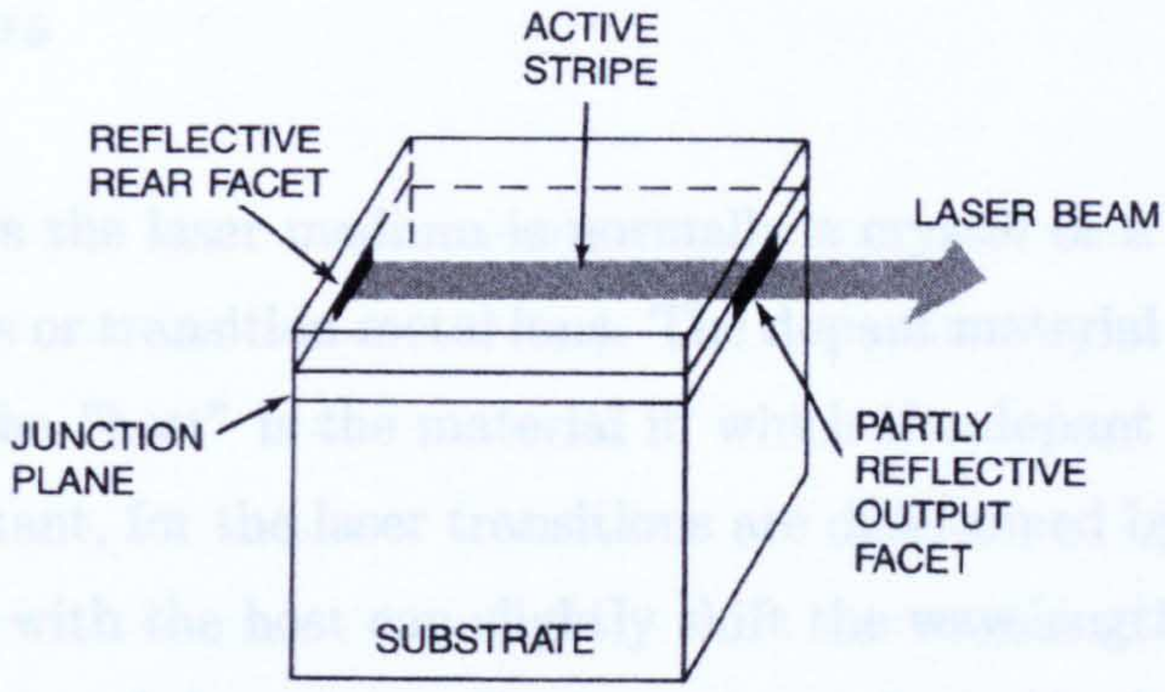

Figure 2.6: Diode laser strip [17]

to take away the heat. Then a number of laser bars are stacked and some optical components are added to focus the laser radiation, as shown in Figure 2.7.

The result is that high power diode lasers can only be focused on a relatively large area (compared to other industrial lasers such as CO_2, Nd:YAG or Fibre lasers). They are used as pump sources for other laser types and also in applications that require only low power density, such as surface heat treatment, surface melting, cladding, conduction welding and also plastic welding.

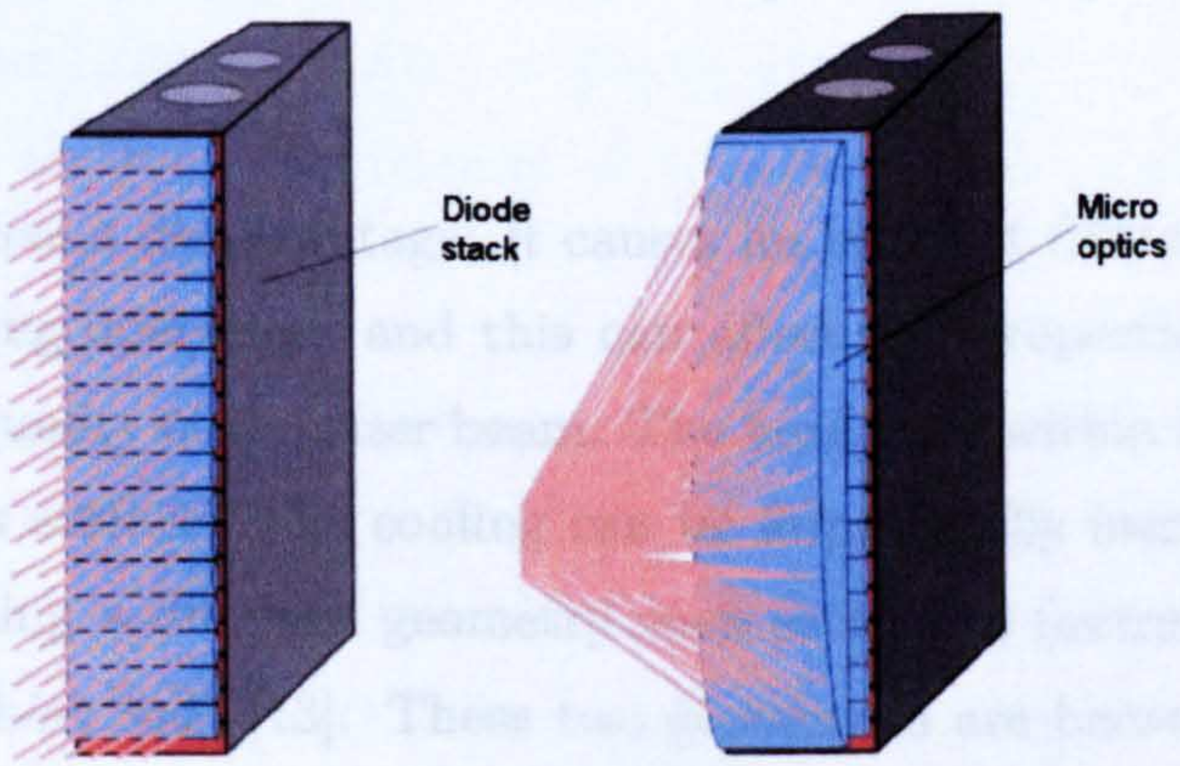

Figure 2.7: Diode laser stack [18]

Solid-State Lasers

In solid-state lasers the laser medium is normally a crystal or a glass that is doped with rare earth ions or transition metal ions. The dopant material is called the "active species" whereas the "host" is the material in which the dopant is embedded. Both of them are important, for the laser transitions are determined by the active species, but its interaction with the host can slightly shift the wavelength. The thermal and mechanical properties of the gain media depend mainly on the host [16].

Solid state lasers can be optically pumped by lamps or diode lasers. A number of them are pumped by flash lamps or arc lamps. These lamps are relatively cheap and can provide high powers, but they lead to poor wall plug efficiency and moderate lifetime [19]. As an alternative, diode lasers are compact, have long lifetime and high efficiency, and are widely used for pumping solid-state lasers.

The laser medium can be produced in different shapes such as rod, disc, slab and fibre. Rod, disc and slab lasers are commonly known as "bulk lasers" for their medium is a bulk doped crystal or glass. Rod-shaped crystals have been used in industrial solid-state lasers for over 30 years. The rods commonly have an aspect ratio of 15:1, the size of a pen [13].

The rod geometry has a disadvantage: it causes an inherent difficulty to extract the heat produced during operation, and this can affect the properties of the medium, compromising the quality of the laser beam. The heat from within the rod is removed by water cooling its surface. The cooling can be improved by increasing the surface to volume ratio, using a different geometry such as a fibre (extremely long rod) or a disc (extremely short rod) [13]. These two geometries are becoming important in materials processing; they are pumped by diode lasers.

Nd:YAG Lasers

Nd:YAG lasers are solid-state lasers based on neodymium-doped YAG crystals as the medium (YAG is the acronym for yttrium aluminum garnet $Y_3Al_5O_{12}$) [20]. They are optically pumped by a diode laser or a lamp. When pumped by a lamp, the efficiency is in the range of 1.5–2%, whereas Diode-pumped YAG lasers have an efficiecy of 10–20% [15]. The most common Nd:YAG emission wavelength is 1064 nm. From this wavelength, it is possible to generate outputs at 532 nm by frequency doubling, 355 nm (frequency tripling) and 266 nm (frequency quadrupling) [20].

Nd:YAG lasers can operate in continuous wave (CW), and can be pulsed and Q-switched. Q-switching means that the laser is optically switched while pumping is continued, so that the energy builds up within the laser medium and is then liberated in a short and powerful pulse [13].

Fibre Lasers

The term "fibre lasers" usually refers to those lasers in which the medium is a doped optical fibre. In most cases the fibre is doped with a rare earth element such as erbium, ytterbium, thulium, neodymium or praseodymium. They are pumped by one or several diode lasers [21].

An optical fibre consists of a core that guides the light, surrounded by a cladding layer. In this single-clad fibre the doped core is able to guide the light of the pump beam (directed into the core) and the stimulated emission generated inside the core. It can be used for low-power lasers [16].

For high power fibre lasers, a double-clad fibre is required, consisting of a doped core, an inner clad and an outer sheath, as shown in Figure 2.8. The pump beam is directed into the inner cladding. While guided in this inner cladding, the pump light will cross the doped core many times, exciting the active species and generating a

population inversion. Stimulated emission takes place inside the core and is guided along it. Reflective structures, such as Bragg gratings, are located at the ends of the fibre, and they act as the mirrors of the laser cavity.

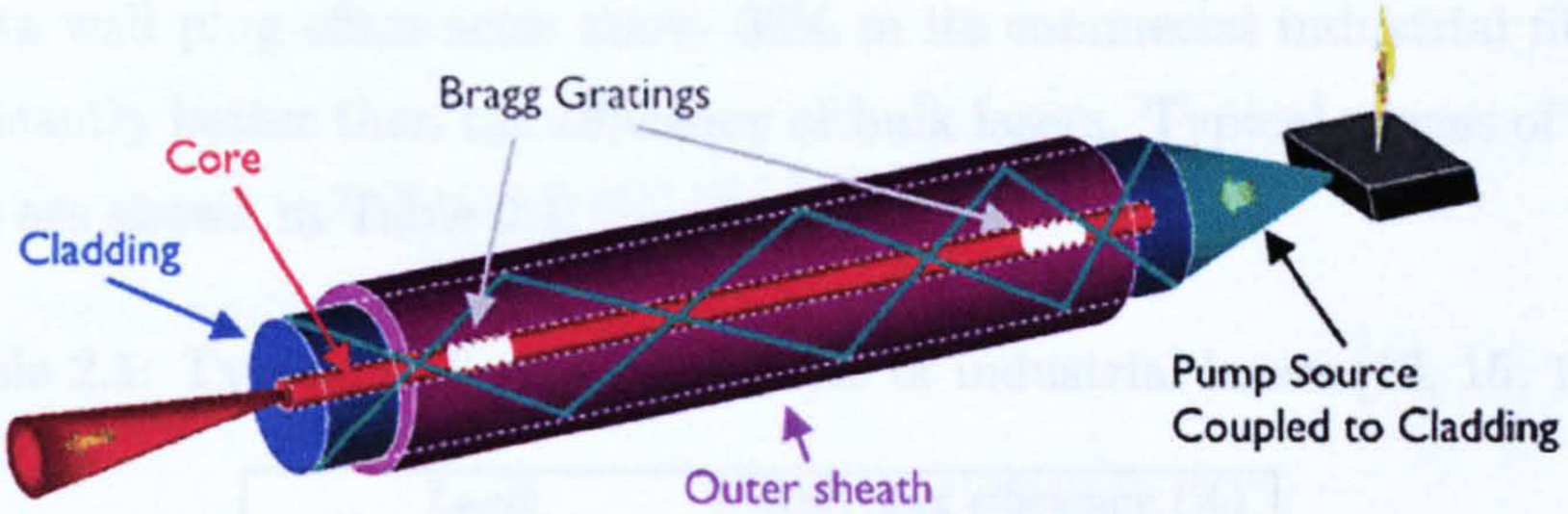

Figure 2.8: Fibre laser [12]

The three most important dopants for fibre lasers are ytterbium, erbium and thulium. They can emit laser radiation in the ranges of 1030–1120 nm, 1520–1620 nm and 1750–2200 nm respectively [16].

Ytterbium-doped are the most powerful type of fibre lasers. They can be pumped at 975, 936 and 915 nm (the main pump line is at 975 nm). The peak laser output is at 1070–1080 nm. Their main application is in materials processing [16].

The emission of fibre lasers can be continuous or pulsed. They can also be Q-switched. However, fibre devices for Q-switching have a limited performance, and fibre lasers with bulk-optical devices (such as an acousto-optic Q switch) are less robust, and are also less powerful than bulk Q-switched lasers [22].

There are important advantages of fibre lasers, and in recent years they have been "the fastest growing part of solid-state laser market" [16]. Among these advantages one can cite:

- High efficiency
- Compact size

- Ease of operation
- Good beam quality

IPG reports wall plug efficiencies above 30% in its commecial industrial fibre lasers [23], significantly better than the efficiency of bulk lasers. Typical ranges of wall plug efficiencies are shown in Table 2.1.

Table 2.1: Typical wall plug efficiencies of industrial lasers [13, 15, 16]

Laser	Wall plug efficiency (%)
Fibre (Ytterbium)	25–30+
Lamp-pumped YAG	1.5–2
Diode-pumped YAG	10–20
Disc	15–25
CO_2	5–20
Diode	up to 50

2.2 Stainless Steel

2.2.1 Characteristics and Applications of Stainless Steels

Stainless steels are iron-base alloys that contain at least 10.5% Cr and no more than 1.5% C [24, 25]. They achieve their high corrosion resistance through the formation of a chromium-rich oxide surface film, which produces the effect of passivation, i.e. the oxide film works as a layer that protects the material from corrosion. This passive layer rebuilds itself spontaneously when mechanically damaged.

Some of the most common applications of stainless steels are [24]:

- Cooking utensils
- Fasteners

- Cutlery
- Decorative architectural hardware
- Equipment for use in:
  - Chemical plants
  - Dairy and food processing plants
  - Health and sanitation applications
  - Petroleum and petrochemical plants
  - Textile plants
  - Pharmaceutical industry
  - Transportation industry

The selection of a specific stainless steel may depend on corrosion resistance, mechanical properties in specific temperature ranges, fabrication characteristics, physical properties (thermal and electrical), availability and cost. From these, corrosion resistance and mechanical properties are usually the most important factors for selection [24].

There are five groups of stainless steels, according to their microstructure:

- Ferritic stainless steels
- Martensitic stainless steels
- Precipitation-Hardening ("maraging") stainless steels
- Duplex ferritic-austenitic stainless steels
- Austenitic stainless steels

Ferritic stainless steels have a body-centred cubic (BCC) crystal structure and are ferromagnetic. Their main alloy element is chromium (10.5–30%), but they may

contain other elements such as molybdenum, silicon, aluminium, titanium and niobium. They can have good ductility. Their high-temperature mechanical properties are lower than those of austenitic grades [24].

Martensitic stainless steels can be hardened by heat treatment. Their two main alloy elements are chromium (10.5–18%) and carbon (may exceed 1.2%). They may have carbides to improve wear resistance. Their corrosion resistance is not as good as that of austenitic stainless steels [24].

Precipitation-Hardening stainless steels contain high chromium and nickel and also some elements that can be precipitated such as copper, aluminium or titanium. They can be hardened by heat treatment and can obtain high strength by precipitation hardening ("aging") of the martensitic structure [24].

Duplex stainless steels have a microstructure that contains both ferrite and austenite. They have good corrosion resistance and higher tensile strengths that austenitic grades.

Austenitic stainless steels will be considered in more detail in the next section.

Austenitic Stainless Steels

The chemical compositions of austenitic stainless steels are based on a combination of elements that promote the formation of ferrite and elements that promote austenite formation. The most important ferritizing element is chromium, but molybdenum, niobium, titanium, aluminium, tungsten and vanadium also promote ferrite. Similarly, the most important austenitizing element is nickel, but carbon, nitrogen, manganese and copper also promote formation and/or stabilization of austenite [25]. Thus, these steels are able to retain austenite at room temperature because of the influence of these austenitizing elements.

Some important characteristics of austenitic stainless steels are [24]:

- FCC (face-centred cubic) crystal structure (austenite)
- High corrosion resistance
- Non-magnetic
- Can be hardened by cold work
- Cannot be hardened by heat treatment
- Excellent cryogenic properties
- Good high-temperature strength
- High ductility
- Chromium content is usually 16–26%
- Nickel content is usually 8–35%
- Carbon content is usually 0.03–0.15%

2.2.2 Welding of Austenitic Stainless Steels

Among the different groups of stainless steels, the austenitic grades are in general the easiest to weld (apart from the free-machining grades), producing welded joints with high toughness [24]. However, it is important to pay attention to issues such as cracking, contamination and porosity, in order to develop a good welding procedure.

Similarly to other single-phase FCC alloys, austenitic stainless steels are susceptible to hot cracking [24]. Welding procedure and filler-metal selection usually depend on corrosion resistance and avoidance of cracking.

Hot cracking can occur at temperatures just below the bulk solidus temperature of the alloy(s) being welded. This can appear as "large weld-metal cracks, usually along the weld centreline"; but it can also appear as "small, short cracks (micro-fissures)

in the weld-metal or in the heat affected zone (HAZ) at the fusion line and, usually, perpendicular to it" [25]. A common solution to avoid hot cracking is to add a mostly-austenitic filler metal that has a small percentage of ferrite [25].

A critical aspect of austenitic stainless steels welding is the solidification mode of the weld metal. There are four solidification modes, which depend mainly on the weld metal composition: Austenite (A), Primary Austenite (AF), Primary Ferrite (FA) and Ferrite (F).

Austenite solidification (A): The metal solidifies entirely as austenite and remains in this phase to room temperature [25].

Primary austenite solidification (AF): The metal solidifies as austenite in the early stages of solidification. However, some ferrite will form in the later stages of solidification. If the material cools down under equilibrium conditions, the ferrite will transform to austenite. But under rapid cooling, some ferrite will remain to room temperature [25].

Primary ferrite solidification (FA): The metal solidifies as ferrite in the early stages of solidification. Then, some austenite will form in the later stages of solidification. When cooling down the metal under equilibrium conditions, the ferrite can be transformed to austenite. However, under rapid cooling, some ferrite will remain to room temperature [25].

Ferrite solidification (F): The metal solidifies entirely as ferrite. When cooling down, it may transform partially or totally to austenite. If the percentage of austenitizing elements is too low, the metal will remain entirely as ferrite (i.e. a ferritic stainless steel) [25].

Stainless steels that solidify in the primary ferrite mode (FA) are the most resistant to hot cracking [25]. The solidification mode can be analysed form the phase diagrams. Figure 2.9 shows a pseudo-binary phase diagram of 70% Fe alloy with chromium and nickel being the rest of the composition and indicates where the different solidification

modes take place.

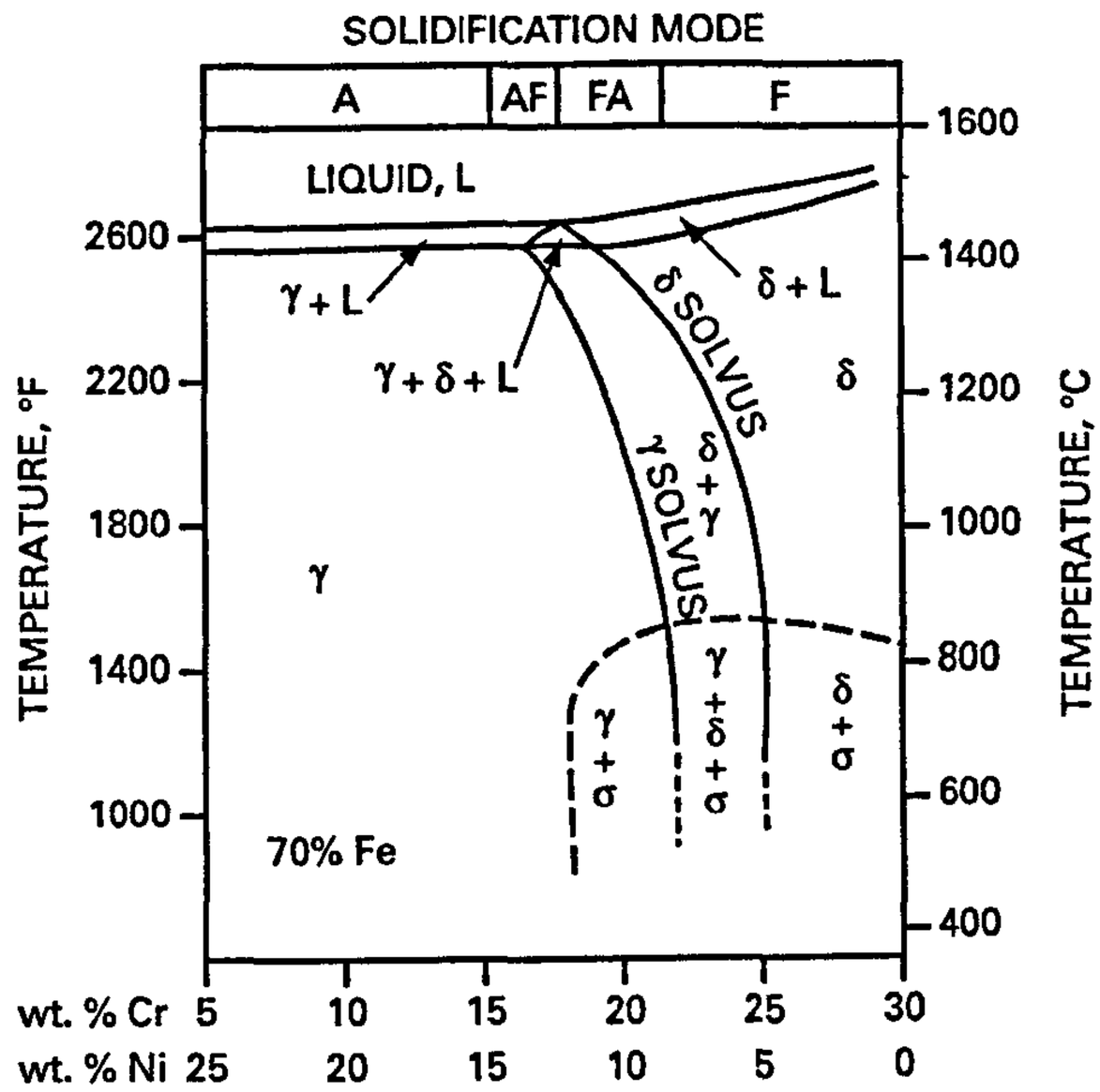

Figure 2.9: Pseudo-binary diagram Fe-Cr-Ni (70% Fe) [26]

In practice, to avoid microfisuring in a weld metal, a suitable filler metal is selected in order to obtain some ferrite in the final microsturcture. The ferrite content should be at least 4% (ferrite number FN 4). Actual measurements of ferrite can be made with a magnetic analysis device. When developing a welding procedure, the Schaeffler diagram (see Figure 2.10) is normally used to predict the approximate amount of ferrite to be obtained in a weld, based on the chemical composition. [24, 25].

Nitrogen from the air can affect the formation of ferrite. The disturbance of shielding gas in gas-shielded welding can permit the nitrogen from the air to enter the weld and to reduce the amount of ferrite and make the weld susceptible to hot cracking (as nitrogen is an austenitizing element).

It is important to ensure that the weld is protected from air all the time. It is also crucial to clean the workpiece before welding in order to avoid weld contamination.

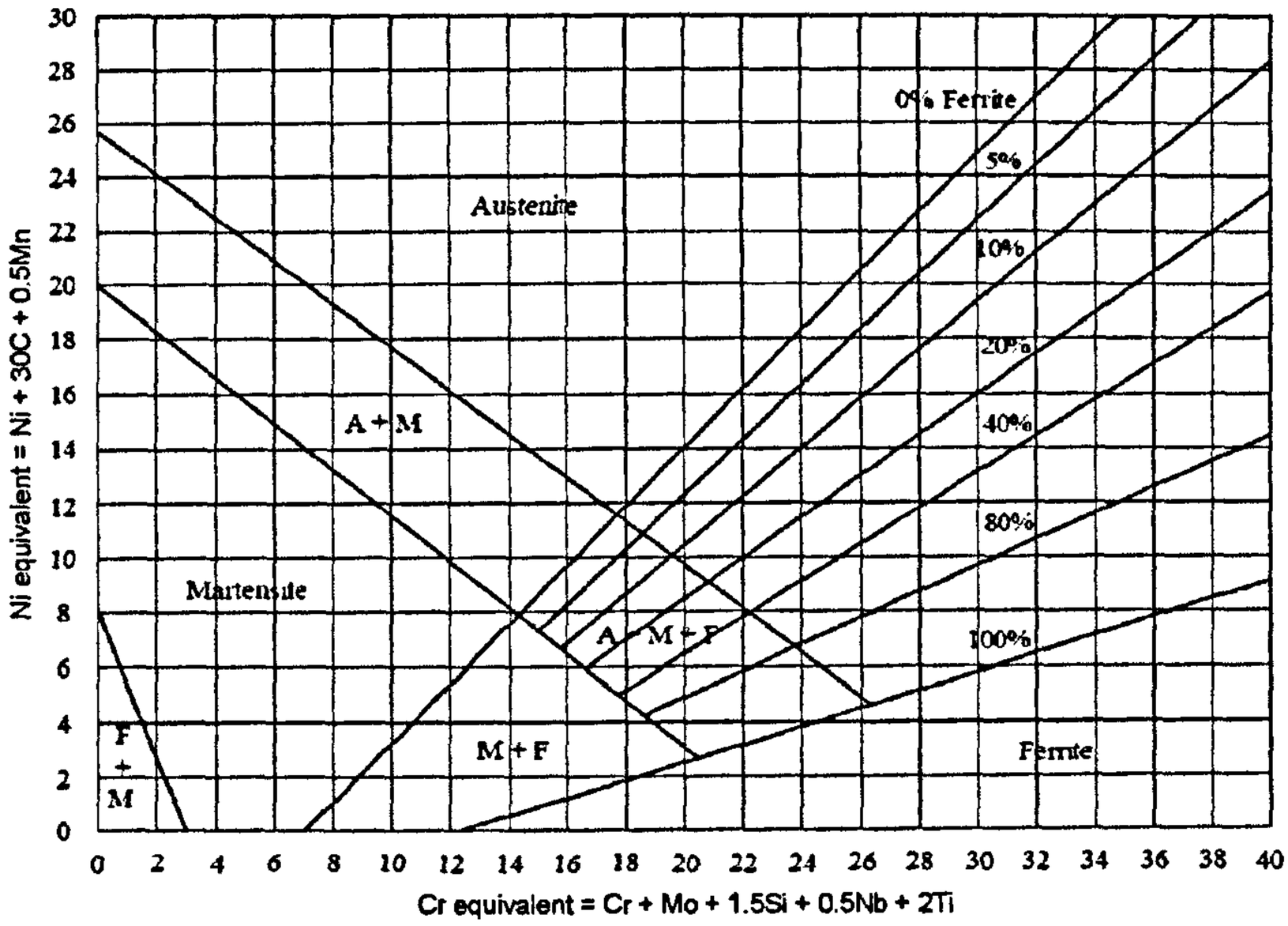

Figure 2.10: Schaeffler diagram [27]

A number of welding processes are utilized to weld austenitic stainless steels, including [24, 26]:

- Shielded Metal Arc Welding (SMAW)
- Gas Metal Arc Welding (GMAW)
- Gas Tungsten Arc Welding (GTAW)
- Plasma Arc Welding (PAW)
- Electron Beam Welding (EBW)
- Laser Beam Welding (LBW)
- Friction Welding (FRW)
- Resistance Welding (RW)

2.2.3 Stainless Steels 304 and 308

Grade 304 is the standard 18/8 austenitic stainless steel; it is a very versatile steel that is used in a variety of products. It has excellent formability and weldability. It has also excellent corrosion resistance in a wide range of environments and has found many applications in industry, architecture and transport, for example. [28].

Some typical applications include [28]:

- Food processing equipment
- Kitchen benches, sinks, equipment and appliances
- Architectural panels, railings
- Chemical containers
- Heat exchangers
- Threaded fasteners
- Springs

Austenitic stainless steel 308 has chemical composition and mechanical properties close to those of grade 304. It has, however, higher chromium and nickel. It is used primarily for welding austenitic stainless steels, for its chemical composition produces some ferrite (308 is the alloy normally recommended to weld grade 304).

The grade used in this work is 308LSi i.e., lower carbon and higher silicon than grade 308. Low carbon versions of stainless steels help to avoid intergranular corrosion due to sensitization (presence of chromium carbides at the grain boundaries, and reduction of chromium content in the grains). Silicon helps to enhance the resistance to scaling and increases the fluidity of the melted metal, improving wetting of the weld metal to the base metal [24, 26].

The chemical compositions of these steels are shown in Table 2.2. The mechanical and physical properties are shown in Tables 2.3 and 2.4 respectively.

Table 2.2: Chemical composition of stainless steel 304 and 308LSi (wt%) [24, 29]

Grade		C	Mn	Si	P	S	Cr	Ni	Mo	Fe
304 [24]	Min	-	-	-	-	-	18.0	8.0	-	Bal.
	Max	0.08	2.0	1.0	0.045	0.03	20.0	10.5	-	
308LSi [29]	Typical	0.012	1.9	0.85	0.02	0.002	19.5	10.5	0.05	Bal

Table 2.3: Typical mechanical properties of stainless steel 304 and 308 [24]

Material	Condition	Tensile Strength (MPa) min.	Yield Strength 0.2% Proof (MPa) min.	Elongation (% in 50mm) min.	Hardness (HR B) max.
SS 304	Annealed	515	205	40	92
SS 308	Annealed	515	205	40	88

Table 2.4: Typical physical properties of stainless steel 304 and 308 [24]

Material	Density (kg/m^3)	Elastic Modulus (GPa)	Mean Coefficient of Thermal Expansion ($\mu m/[m\ K]$)			Thermal Conductivity at 100°C (W/[m K])	Thermal Conductivity at 500°C (W/[m K])	Specific Heat at 0-100°C (J/[kg K])	Melting Range (°C)
			0-100°C	0-315°C	0-538°C				
SS 304	8000	193	17.2	17.8	18.4	16.2	21.5	500	1400-1450
SS 308	8000	193	17.2	17.8	18.4	15.2	21.6	500	1400-1420

2.3 Titanium Alloys

2.3.1 Characteristics and Applications of Titanium Alloys

Titanium and titanium alloys have acquired a significant importance in the last 50 years due to the advantages they offer to the industry, as the high strength-to-weight ratio (high strength and low density) and high corrosion resistance.

Because of their strength-to-weight ratio, titanium alloys are widely used in the aerospace industry, in pieces that work at low to moderately-high temperatures. Many components of the jet engine, especially in the compressor, and the airplane frame are made of titanium alloys.

Another important industry that takes advantage of titanium alloys is the chemical industry due to the excellent corrosion resistance of titanium. Titanium has a strong affinity to oxygen and forms a very stable microscopic oxide film on the surface, this passivating oxide layer protects titanium from corrosion. The medical field also uses titanium to make surgical implants and prosthesis as this material is well tolerated by the human body.

Titanium is a non-magnetic, silvery coloured metal. Pure titanium is a ductile material, it presents 15 to 25% elongation and an ultimate tensile strength of approximately 207 MPa at room temperature [30]. Some of its physical properties are:

Melting point:	1670 °C
Boiling point:	3260 °C
Coefficient of thermal expansion:	8.41 μm/[m °C] at 20 °C
Density:	4510 kg/m^3

Titanium can exist in two crystal forms. From room temperature to approximately 880 °C, titanium presents a hexagonal close-packed (HCP) structure known as alpha phase. Above this temperature, it transforms to a (BCC) structure known as beta phase. The temperature at which all the structure has been transformed to the beta phase is known as "beta transus" temperature.

The alloying elements of titanium can be classified in three groups:

- Alpha phase stabilizers
- Beta phase stabilizers
- Interstitial elements (impurities)

The alpha phase stabilizers, also known as alpha substitutional elements, have preferential solubility in the alpha phase, and they raise the beta transus. The most important alpha stabilizer is aluminium, which increases tensile strength, creep strength and the elastic modulus. The amount of aluminium in titanium alloys is limited to 6%, as above this percentage it promotes the formation of Ti_3Al which is associated with embrittlement [31].

Beta phase stabilizers, also known as beta substitutional elements, lower the beta transus. Among these elements are molybdenum, vanadium, niobium and tantalum.

The elements that form interstitial solid solution with titanium are: carbon, hydrogen, nitrogen and oxygen. These interstitial elements are considered as impurities in titanium and its alloys. Carbon, nitrogen and oxygen are more soluble in the alpha phase, whereas hydrogen is more soluble in the beta phase.

Titanium and titanium alloys are classified according to their structure in the annealed condition. There are four groups [30]:

- Commercially pure titanium
- Alpha alloys
- Alpha-beta alloys
- Metastable beta alloys

For commercially pure titanium, the differences among the grades are based on their impurity limits.

Alpha alloys have essentially all-alpha microstructures, and are used in applications that require good strength at moderate-elevated temperatures. They cannot be strengthened by heat treatment, and their principal microstructural variable is the grain size. Near-alpha alloys contain small additions of beta stabilizers and are considered marginally heat treatable [30, 31].

Alpha-beta alloys have beta stabilizers and their microstructures present both, alpha and beta phases. They can be heat treated, and are normally used in two conditions: annealed (with excellent fracture toughness), and solution heat treated and aged (with excellent strength-to-density ratios). Alpha-beta alloys give good creep performance up to $\approx$ 400 °C. The most used alpha-beta alloy is Ti-6Al-4V [30].

Metastable beta alloys contain high percentage of beta stabilizers, and their microstructure is 100% beta phase at room temperature. They have excellent formability [30].

It is worth noting that there are some alloys produced with "extra low interstitials" (ELI), which are used in applications where good ductility and toughness are needed [30].

2.3.2 Welding of Titanium Alloys

Most titanium alloys can be welded using the equipment and procedures used to weld austenitic stainless steels [32]. The processes used are GTAW, GMAW, PAW, EBW, LBW, FRW and RW.

One of the most important issues when processing titanium and titanium alloys is their propensity to absorb impurities when the material is hot. This characteristic must be considered when welding titanium alloys, and the necessary precautions must be taken.

When exposed to air, moisture or hydrocarbons at temperatures above 500 °C, titanium absorbs interstitial elements (impurities) such as oxygen, nitrogen, carbon and hydrogen. The presence of air promotes the absorption of oxygen; moisture promotes the absorption of hydrogen and oxygen; and residual oils, cleaning agents and other contaminating substances promote the absorption of hydrogen and carbon. The presence of interstitial atoms (especially in alpha-titanium) distorts the crystal lattice and reduces the number of active slip planes, so the plastic deformation is inhibited and

thus the ductility is reduced. At a certain level of impurities, the stresses generated during welding may cause weld metal cracking [30].

Exposure to contaminants and porosity can be minimized following these recommendations [30]:

- Remove surface films from the area to be welded (e.g. with a stainless steel brush)
- Degrease the joint with acetone before welding
- Provide sufficient inert gas shielding during welding, and maintain this shielding until the weld and the surrounding areas have cooled below 260 °C
- Use a shielding gas with oxygen content lower than 60 parts-per-million (ppm) and H_2O content lower than 34 ppm (dew point of -51 °C or lower)
- Keep the hot end of the filler wire inside the shielding atmosphere in order to avoid oxygen and nitrogen pick up
- Welding at slow traverse speeds facilitates the escape of gas pores
- Welding in the flat position or uphill in the vertical position also facilitate the escape of gas pores

2.3.3 Titanium Alloy Ti-6Al-4V

Ti-6Al-4V is the most widely used titanium alpha-beta alloy. It has many applications in the aerospace industry in the engine compressor's disks and blades, as well as in the structural components of the airframe. It is processed to provide annealed structures and sometimes it is solution treated and aged. It has an useful creep resistance up to 300 °C and excellent fatigue strength. It is also used for chemical-processing equipment and for prosthetic implants. It has fair weldability and can be used in the as-welded condition for most applications. The ELI grade improves ductility and

toughness, and is used for cryogenic applications and for fracture-critical aerospace applications [31].

Alpha-beta alloys, in the annealed condition, have lower toughness than pure titanium. Alpha beta alloys are heat treatable and can be significantly strengthened by aging. However, this heat treatment reduces the ductility and fracture toughness of these alloys.

The chemical composition of the alloy Ti-6Al-4V is shown in Table 2.5. The mechanical and physical properties are shown in Tables 2.6 and 2.7 respectively.

Table 2.5: Nominal chemical composition of Ti-6Al-4V (wt.%) [30]

Material	Al	V	C *	N *	O *	H *	Fe *	Ti
Ti-6Al-4V	6	4	0.10	0.05	0.2	0.0125	0.3	Bal

* maximum (impurity limit)

Table 2.6: Typical mechanical properties of Ti-6Al-4V [30, 31, 33]

Material	Condition	Tensile Strength (MPa)	Yield Strength (MPa)	Elongation (%)	Hardness (HR C)
Ti-6Al-4V	Annealed	931	896	15	36
Ti-6Al-4V	Annealed (from cast)	930	855	12	–

Table 2.7: Typical physical properties of Ti-6Al-4V [31, 34]

Material	Density (kg/m^3)	Elastic Modulus (GPa)	Mean Coefficient of Thermal Expansion ($\mu m/[m\ K]$)			Thermal Conductivity at 100°C (W/[m K])	Specific Heat (J/[kg K])	Melting Range (°C)
			20–100°C	20–315°C	20–540°C			
Ti-6Al-4V	4430	114	8.6	9.2	9.5	6.6-6.8	526	1604–1660

2.4 Temperature Measurement

2.4.1 Temperature Measurement Techniques

There are different types of sensors for temperature measurement. Among the most common, one can mention:

- Thermocouples
- Resistance temperature devices (RTD)
- Infrared temperature sensors (pyrometers)
- Bimetallic thermometers
- Fluid-expansion thermometers

Thermocouples are made of two wires or strips of dissimilar metals that are joined at one end. Changes in temperature at the junction will produce a voltage between the other ends. This voltage can be correlated to the temperature [35].

Resistance Temperature Devices work on the principle that the electrical resistance of material changes according to its temperature. There are two main types: the sensors that use metals are normally called RTDs, whereas the sensors that use a ceramic semiconductor are called thermistors [36].

Infrared temperature sensors measure the thermal radiation emitted by an object and calculate the temperature according to that radiation. They are non-contact sensors.

Bimetallic thermometers use strips of two metals with different thermal expansion coefficients. These strips are bonded together and are linked to a pointer that indicates the temperature (e.g. on a dial temperature scale). When heated, one metal will expand more and bend the bimetallic element, moving the pointer to the new temperature value [36].

Fluid-expansion thermometers use the principle of thermal expansion in a fluid to indicate the temperature. The classical example being the household mercury thermometer. Other liquids are also used instead, in order to avoid the environmental impact associated with mercury [36].

2.4.2 Thermocouples

Thermocouples are temperature sensors based on a junction of two dissimilar metals that produce a voltage (in the order of millivolts) which can be correlated to a temperature value. There is a number combinations of metals or "calibrations", that are useful in different temperature ranges and environments. The most common are J, K, T and E. Their temperature ranges are shown in Table 2.8.

Table 2.8: Common thermocouple temperature ranges [35]

Calibration	Temperature Range (°C)	Standard Limits of error (whichever is greater)
J	0–750	2.2 °C or 0.75%
K	-200–1250	2.2 °C or 0.75%
E	-200–900	1.7 °C or 0.5%
T	-250–350	1.0 °C or 0.75%

It is worth noting that the maximum temperature of the thermocouple depends on both the calibration and the diameter of the thermocouple wire (i.e. if the wire is too thin, it may not be able to reach the maximum nominal temperature of that calibration).

Thermocouples are widely used in industry, they provide an accurate way for contact temperature measurement. The temperature values can be easily recorded. Time response of thermocouples varies depending on the probe used and its diameter. It may be in the range of a fraction of a second to a few seconds.

2.4.3 Pyrometers

Thermal Radiation

Pyrometers are infrared temperature sensors that work based on the principle that all bodies with a temperature above the absolute zero (- 273.15 °C) emit thermal radiation, which depends on their temperature.

The radiation received by a body can be absorbed, reflected or transmitted, as shown in Figure 2.11. The sum of the absorptance, reflectance and transmittance equals 1 (the value of these coefficients lay between 0 and 1). In a similar way, the radiation that comes from a body can be emitted, reflected or transmitted. The sum of the emittance, reflectance and transmittance equals 1. In opaque bodies there is no transmission, thus the radiation from it can only be emitted or reflected (emittance + reflectance = 1).

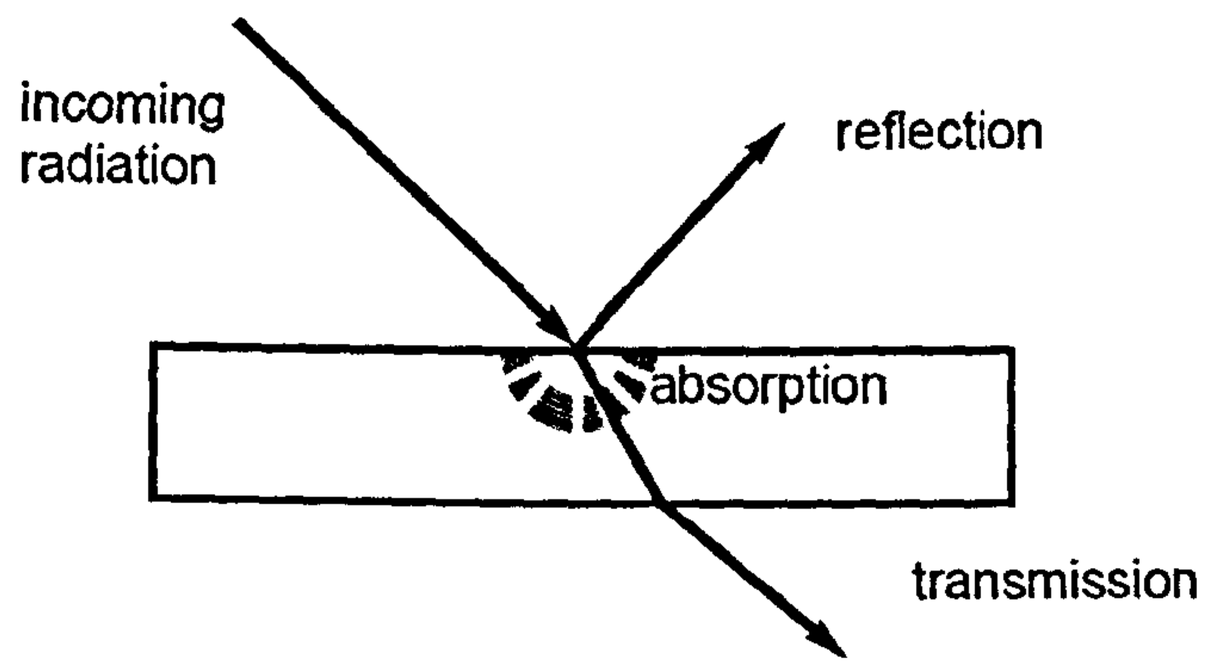

Figure 2.11: Reflection, absorption and transmission [37]

A blackbody is an opaque object that absorbs all incoming radiation i.e., absorptance = 1. Its reflectance and transmittance equal 0. Thus, its emittance equals 1. Figure 2.12 shows the spectral characteristics of blackbody radiation at different temperatures. It is important to note that [38]:

- The emitted radiation varies with the wavelength

- At a specific wavelength, the amount of radiation increases with higher temperatures
- The spectral distribution changes with temperature: as the temperature increases, the peak of the radiant energy concentration shifts toward the left (i.e. shorter wavelengths)

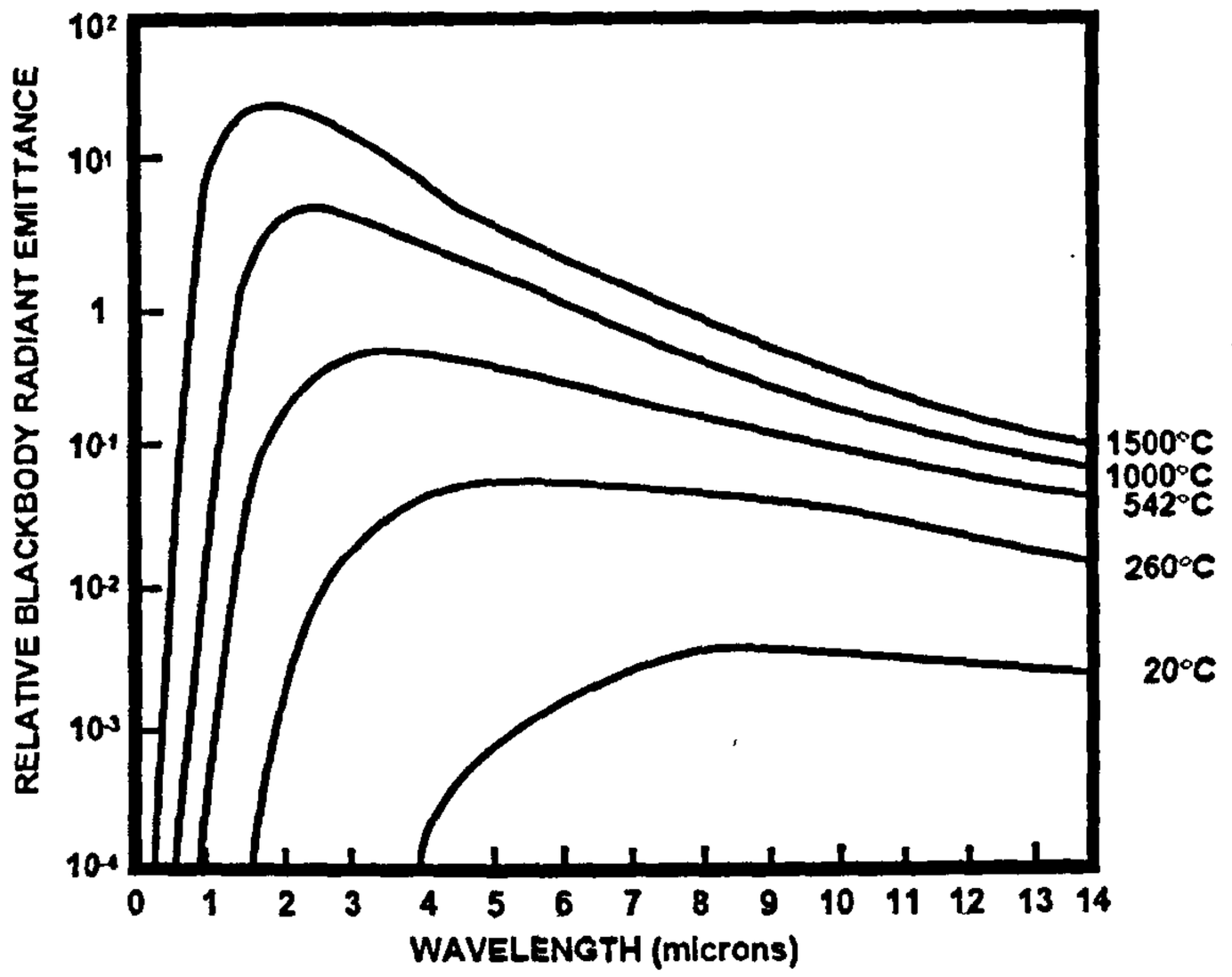

Figure 2.12: Spectral characteristics of blackbody radiation at different temperatures [38]

However, normal real objects do not behave as blackbodies. The emissivity, ϵ, is "the ratio of radiation emitted by an object to that of a blackbody at the same temperature and wavelength" [38]. A blackbody has an emissivity of 1. A graybody has a constant emissivity, lower than 1. A non-graybody (or "real radiation body") does not behave as a graybody, but has an emissivity that changes with wavelength [38], as shown in Figure 2.13.

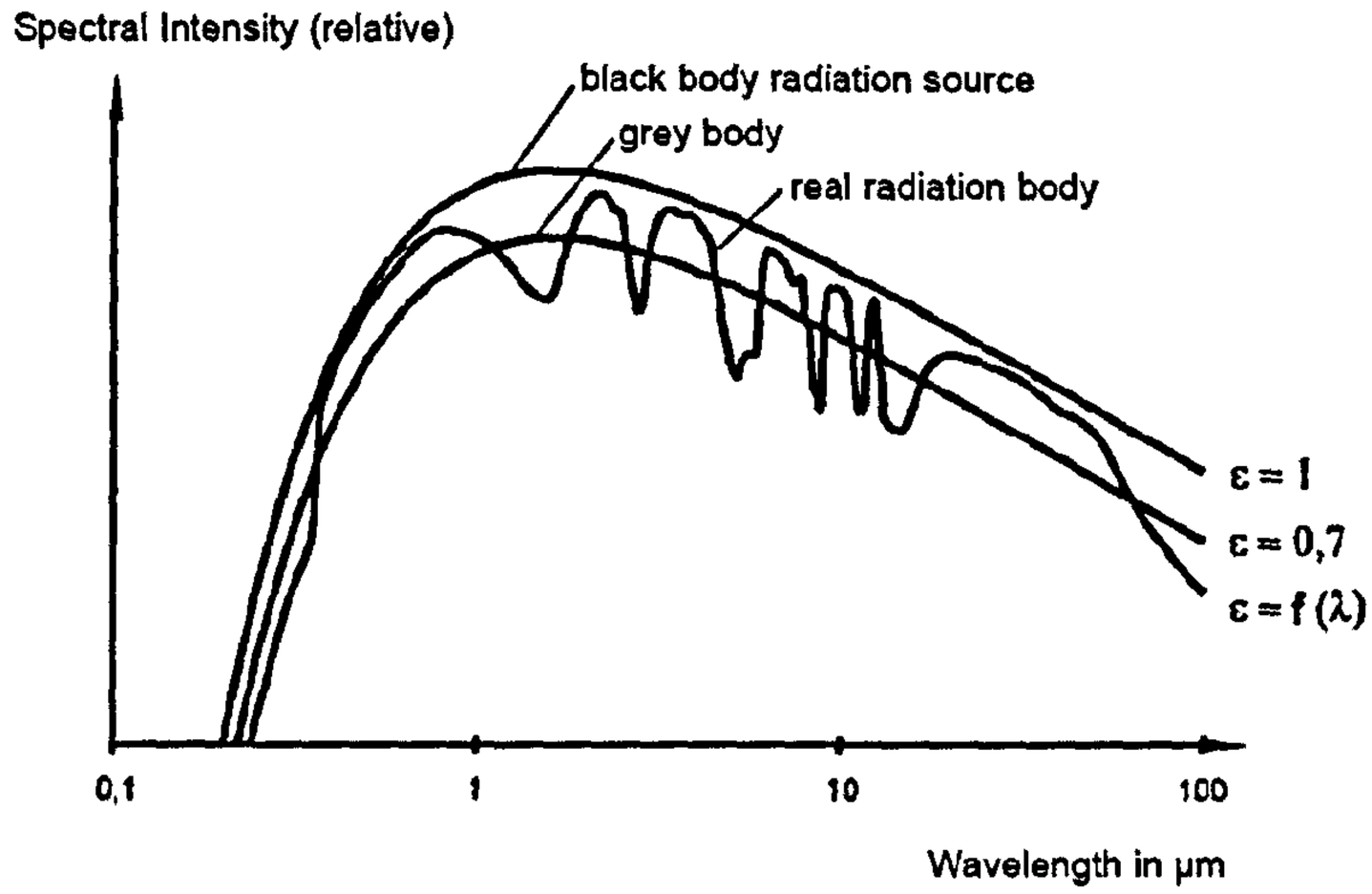

Figure 2.13: Relative spectral intensity [37]

Pyrometers

A pyrometer is a sensor that measures radiation from an object, in a specific range of wavelengths, and correlates this radiation to a temperature value. This way it is possible to perform a non-contact temperature measurement. Pyrometers provide a number of advantages, among them one can mention:

- Fast response (normally in the order of milliseconds)
- It does not damage the measured object (scratching)
- It does not affect the temperature of the object
- It is possible to measure the temperature of objects with difficult access (e.g. moving objects, high temperature, electricity conducting)

Modern pyrometers are digital: they have a microprocessor that performs all the calculations. The construction of a digital pyrometer is shown in Figure 2.14.

The sensor receives the infrared radiation and produces a signal. This signal is directly digitized (or digitized after an analogue pre-amplifier) via an analogue-to-digital converter (ADC). A microprocessor performs the required mathematical calculations and outputs a temperature value. This output can be communicated digitally (using a digital interface) or in an analogue way via a digital-to-analogue converter (DAC) [37]. Some advantages of digital pyrometers are:

- Higher accuracy in the measured value
- Mathematical functions are performed without the need for peripheral electronic equipment
- The pyrometer can be controlled via a personal computer (PC) to enter the parameters
- The temperature data can be saved directly in the PC

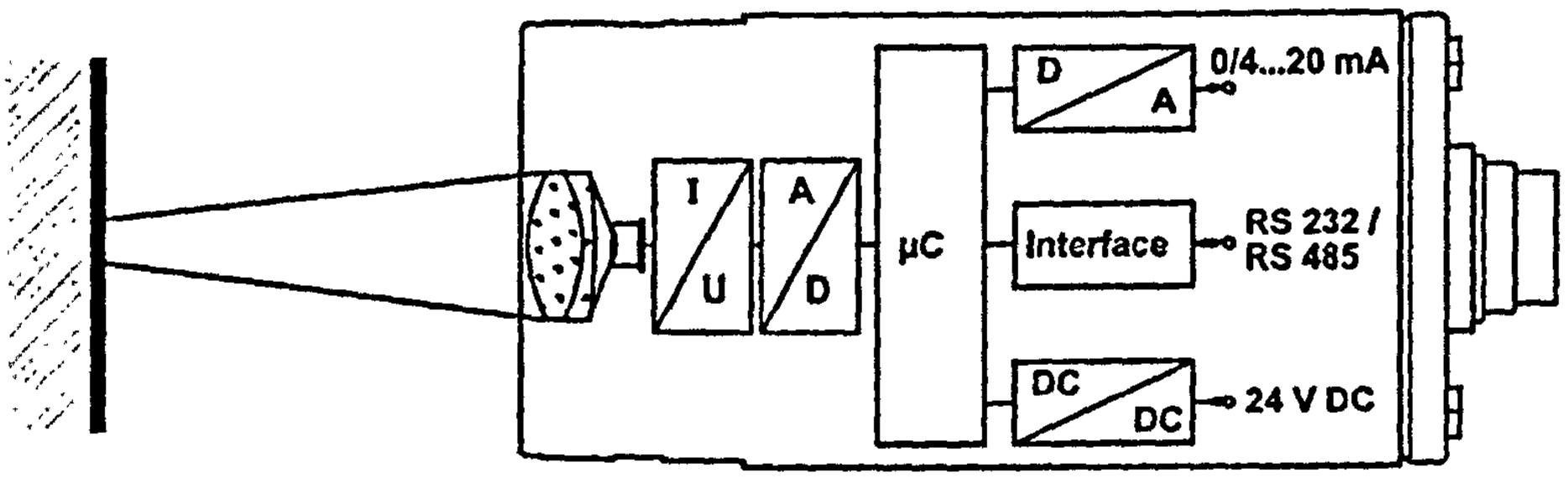

Figure 2.14: Construction of a digital pyrometer [37]

Single-colour Pyrometers

There are two main types of pyrometers: single-colour and two-colour (ratio principle). Single-colour pyrometers measure the radiation in a single range of wavelengths to calculate the temperature. It is necessary to input the emissivity value of the surface of the object. This value depends on the material and the surface condition of the object, and also on the wavelength range of the pyrometer.

They average the temperature of the spot that they measure. For this reason, the object should fill the whole spot size, as shown in Figure 2.15. It is worth noting that they can be affected by conditions such as smoke or dirty windows, for these will reduce the radiation detected by the pyrometer.

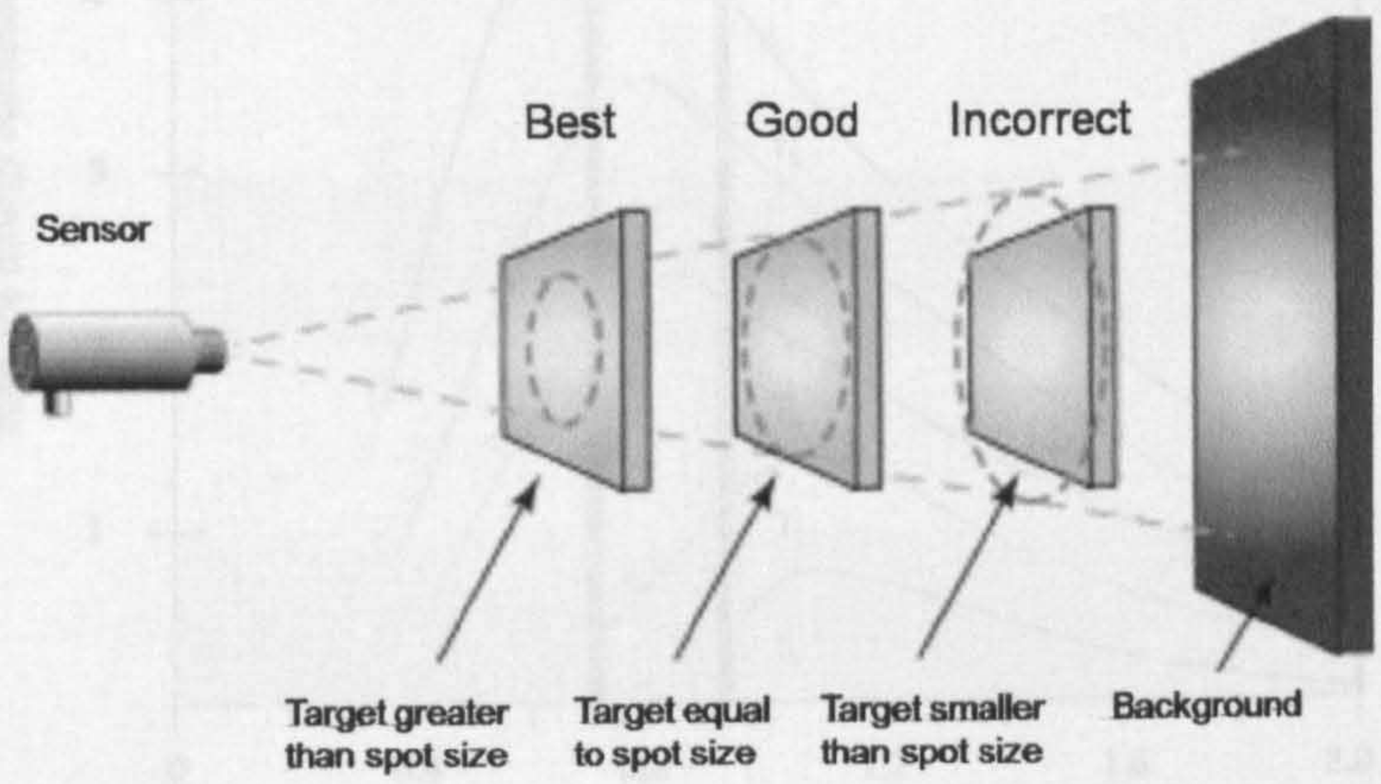

Figure 2.15: Correct target size for single-colour pyrometer [39]

Two-colour Pyrometers

Two-colour pyrometers measure the radiation in two adjacent narrow wavelength bands. The ratio of the two energies is a function of the temperature of the object [40]. This principle is illustrated in Figure 2.16.

The wavelength bands are close together in order to have (as much as possible) the same emissivity in both. This equal emissivity can be assumed for a number of materials and surface conditions. In case the emissivity is different, then it is necessary to adjust the emissivity-slope K (where $K = \epsilon_1/\epsilon_2$) so that the pyrometer can calculate the temperature accurately.

Using this ratio principle a number of issues can be overcome, provided they affect the radiation in both wavelengths in the same way (i.e. that the ratio is not affected). Some important advantages of two-colour pyrometers are [37]:

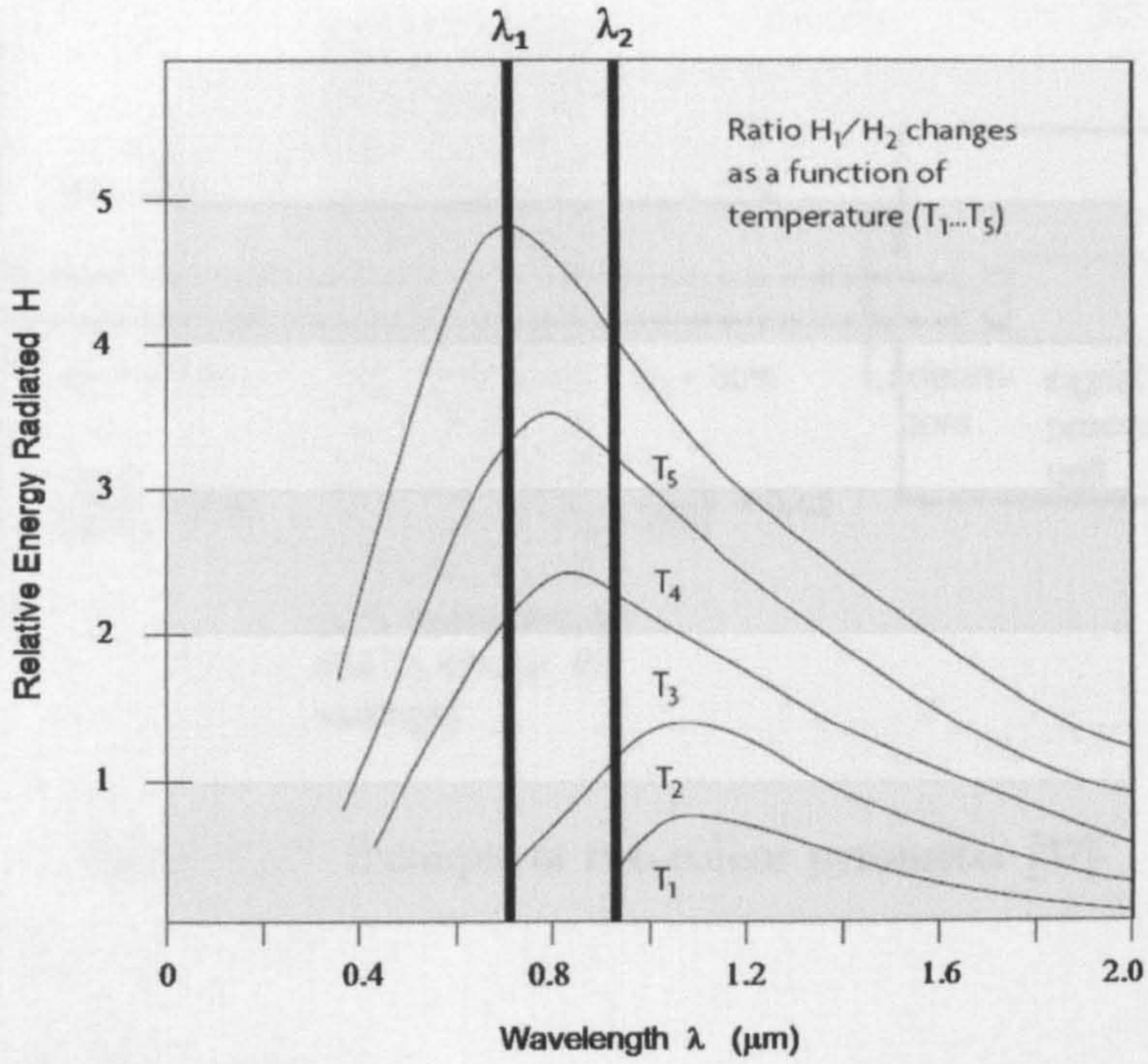

Figure 2.16: Working principle of two-colour pyrometer [40]

- The temperature measurement is unaffected by dust, smoke or dirty windows
- The temperature measurement is independent of the emissivity of the surface in wide ranges
- The target can be smaller than the spot size

Figure 2.17 shows an example of the working principle of a two-colour pyrometer: although the smoke reduces the radiation detected by the sensor, the ratio does not change (thus, the temperature reading is not affected).

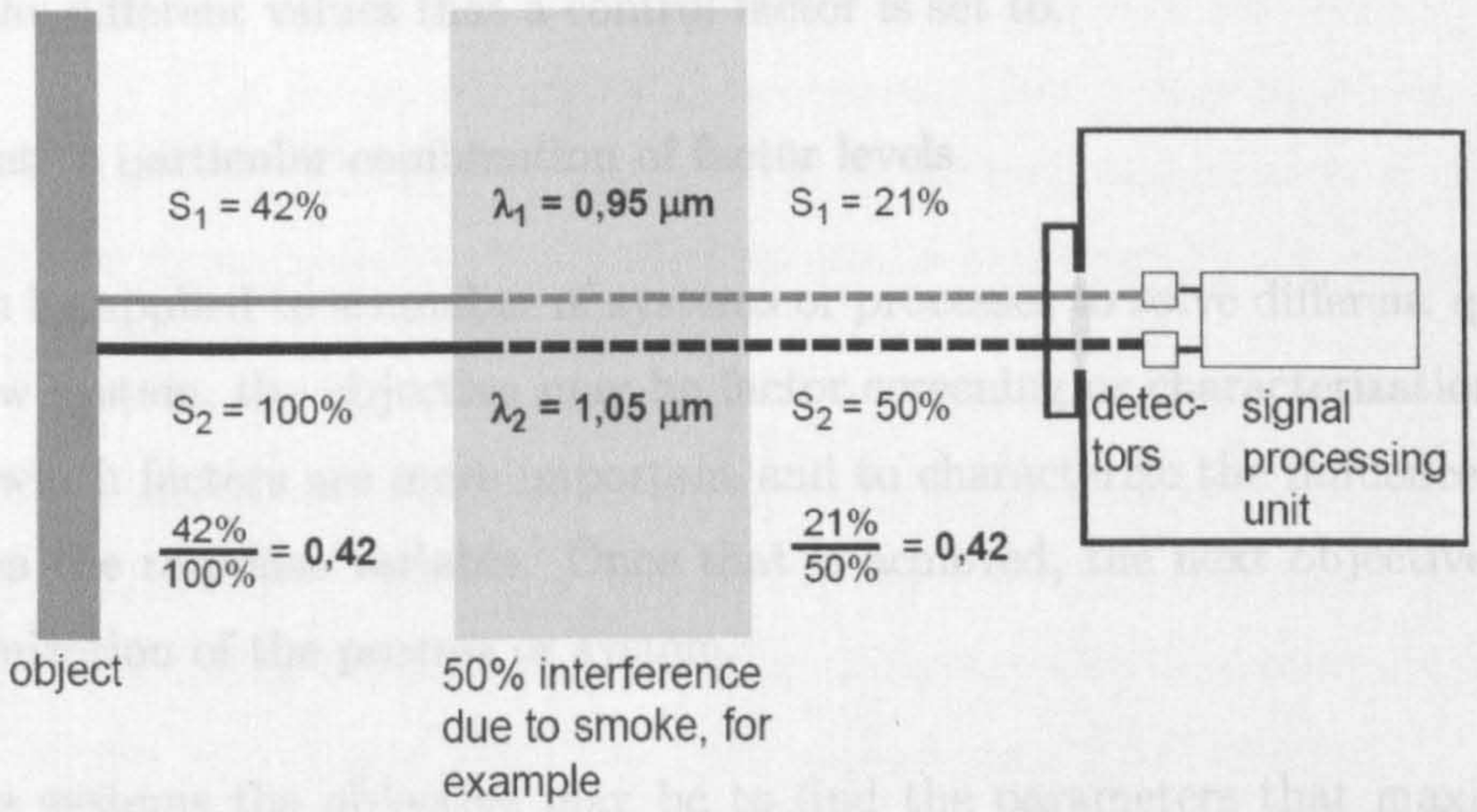

Figure 2.17: Example of two-colour pyrometer [37]

2.5 Design of Experiments

2.5.1 Basic Principles

Design of Experiments (DOE) provides a powerful means to achieve sound conclusions in industrial experiments and also in research and development environments.

As defined by Montgomery [41], "Statistical design of experiments refers to the process of planning the experiment so that appropriate data that can be analysed by statistical methods will be collected, resulting in valid and objective conclusions".

It is convenient to define now some basic terms frequently used in DOE, for they will be used throughout this section. These terms are [42]:

Response variable: the process output, i.e. the dependent variable.

Control factors: the process inputs that the experimenter manipulates in order to cause a change in the response variable (sometimes they are called just "factors").

Levels: the different values that a control factor is set to.

Treatment: a particular combination of factor levels

DOE can be applied to a number of systems or processes to solve different questions. For a new system, the objective may be factor screening or characterization, i.e. to identify which factors are more important and to characterize the influence of those factors on the response variable. Once that is achieved, the next objective may be the optimization of the process or system.

For some systems the objective may be to find the parameters that maximize the production, or those that minimize the variability, for example.

There are three basic principles for DOE [41]:

- Randomization
- Replication
- Blocking

Randomization means that the individual runs of the experiment must be performed in a random order; the allocation of materials has to be random as well. The statistical methods used for the analysis assume that the observations (or errors) are independently distributed random variables, and this assumption is usually true with randomization [41]. Randomization helps to average out the influence of external factors on the process (e.g. a change in the calibration of an instrument over time or changes in the performance of a machine due to heating-up).

Replication refers to the number of independent runs performed of each treatment. If the experiment has four treatments and three replicates, then the experiment has a total of twelve runs. Replication makes it possible to estimate the experimental error. This experimental error can be then compared to the results obtained for different treatments in order to obtain statistical conclusions.

If the means of two treatments are different ($\bar{y}_1 \neq \bar{y}_2$), and the experimental error is very small compared to the difference of the means, then it may be possible to conclude that there is a statistical difference between the response variable of "treatment 1" and that of "treatment 2". This difference would be caused by the influence of the control factors.

Conversely, if the experimental error is relatively large (compared to the difference of the means), the conclusion may be that there is not statistical difference between the results of the two treatments. The control factors may not have an important influence on the response variable (for the range of parameters selected).

That is, replication makes it possible to compare the variability within the treatments (experimental error) to the variability between the treatments (which may be caused by the influence of the control factors). In practice, this comparison is done by performing an Analysis of Variance (ANOVA).

Blocking is a technique used to deal with the effects of known changes in which the experimenter is not directly interested, such as different operators or different batches of raw material. Thus, the runs performed with "raw material batch 1" would be put in a block, whereas runs made with "raw material batch 2" would be in another block.

2.5.2 General Methodology

Montgomery [41] suggests the following procedure for design of experiments:

1. Recognition and statement of the problem

2. Selection of the response variable

3. Choice of factors, levels and ranges

4. Choice of experimental design

5. Performing the experiment

6. Statistical analysis of the data

7. Conclusions and recommendations

It is highly recommended to perform a sequential series of experiments instead of doing only one big experiment. Sequential experiments are more effective because they allow the experimenter to learn at every stage and apply that new knowledge in the following stages. This strategy gives flexibility to the experimenter to change the control factors, ranges and levels according to the results of previous experiments. As a general rule, during the first experiment, no more than 25% of the resources should be used [41, 43].

2.5.3 Factorial Designs

There are different approaches to design an experiment. When several factors are studied, the correct approach is a factorial design, for this kind of designs offer important advantages. First, they are more efficient than the "one factor at a time" approach (less runs are needed to analyse the same number of factors and levels). Factorial designs also allow the analysis of the interactions between the factors [41]. An *interaction occurs* "when the effect of one factor on a response depends on the level of another factor(s)" [42].

A full factorial design is one that includes all possible combinations of the levels of the input factors. A design with K factors in which each factor has two levels is called "2^K design"; and if the factors have three levels each, it is called "3^K design". This indicates the number of runs that each replication of the experiment will have.

Figure 2.18 shows an example of a 2^K factorial design with three factors X_1, X_2, and X_3 ($2^3 = 8$, thus a total of eight runs per replication).

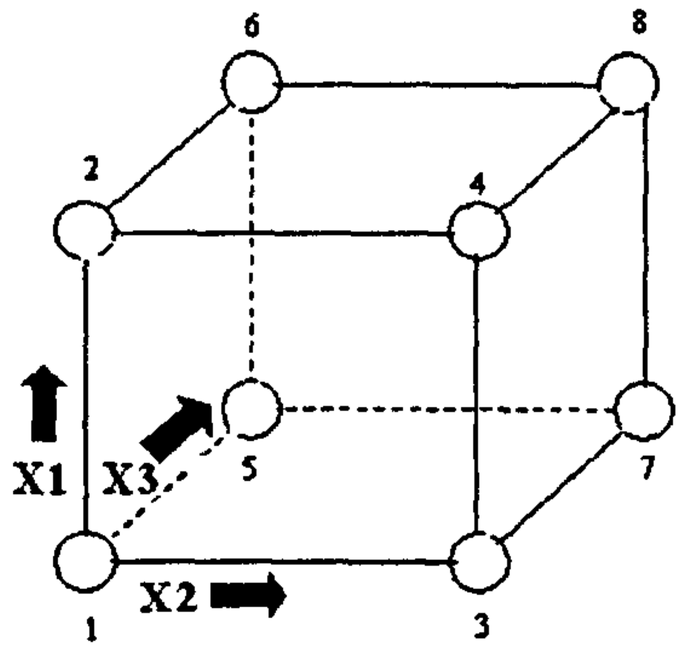

Figure 2.18: 2^K factorial design with three factors [42]

2.5.4 Analysis of Results

There are a number of different tools (e.g. graphs and statistical tests) that can be used to analyse the data. Among the most important one can mention:

- Main Effects Plot
- Interactions Plot
- ANOVA
- Regression Models

Main Effects and Interactions Plots

The main effects plot shows one factor against the response variable. A steep graph indicates a strong effect of the factor on the response, for the particular range used in that factor. A positive slope shows a positive effect, i.e. that increasing the factor would increase the response. A negative slope indicates that increasing the factor would decrease the response, as shown in Figure 2.19. From this graph it is possible to see which factors have a strong effect on the response and whether that effect is positive or negative.

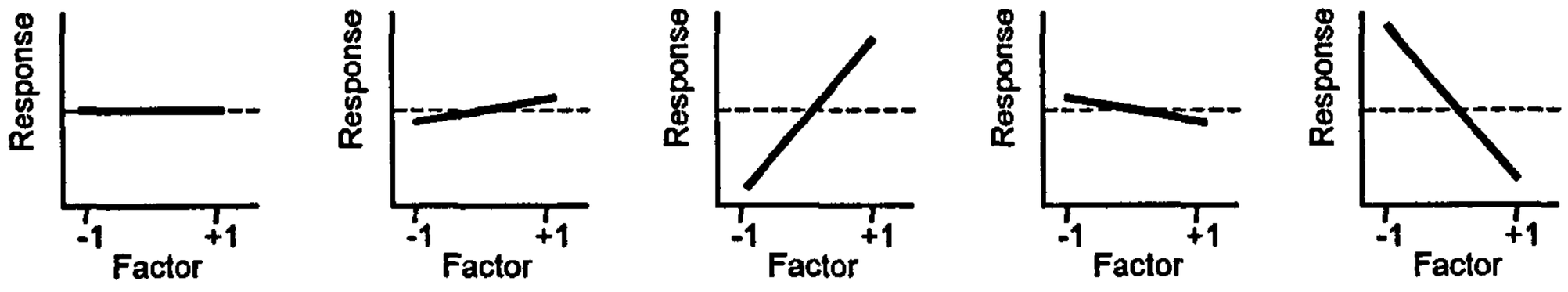

Figure 2.19: Main effects plot (after [44])

The interactions plot shows whether the effect of one factor depends on the level of other factor(s), i.e. whether there is any interaction between the factors. If the lines of the levels of a factor are parallel, then there is no interaction. If there is an angle between the lines, there is interaction, as shown in Figure 2.20.

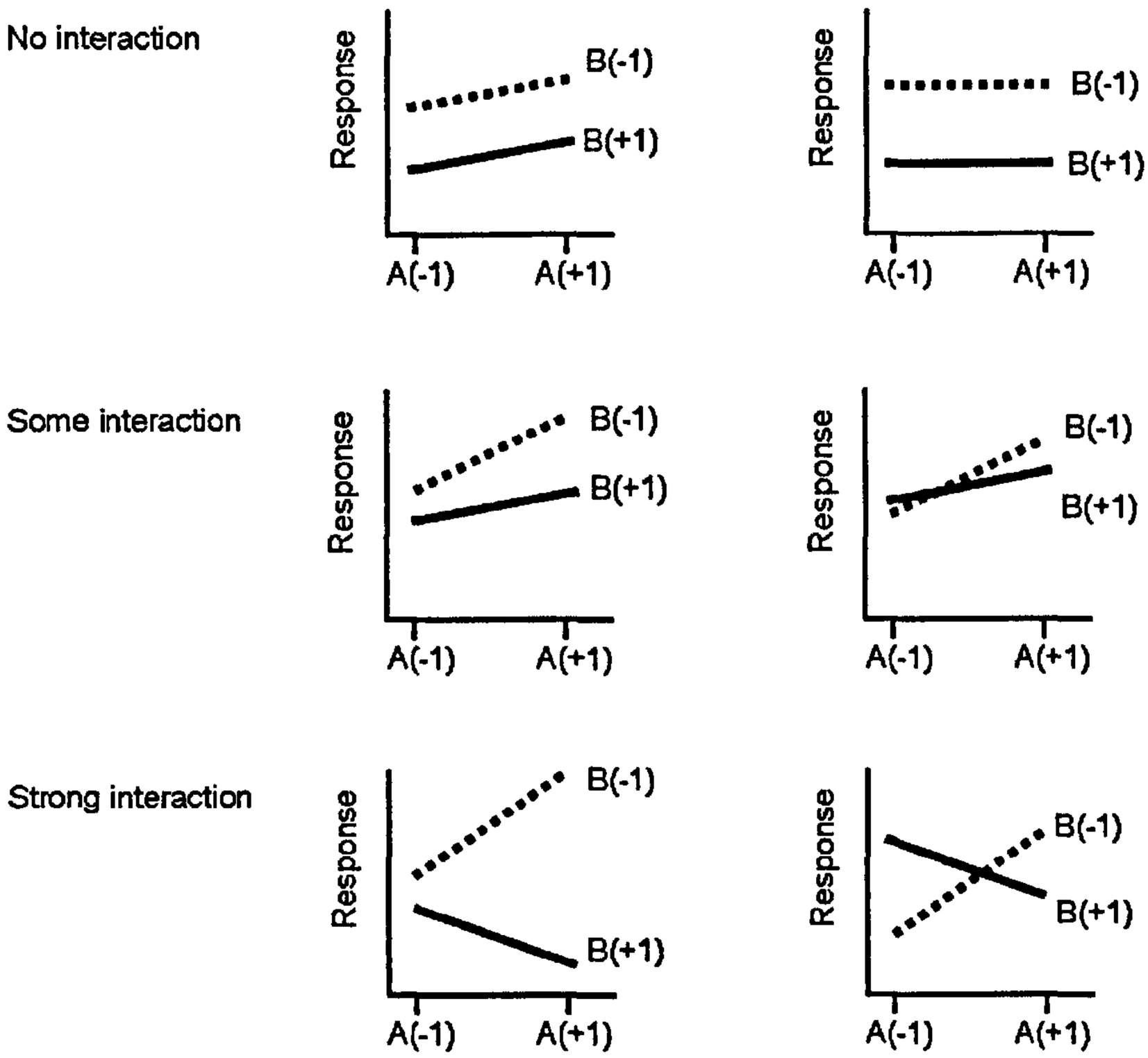

Figure 2.20: Interactions plot (after [44])

Analysis of Variance (ANOVA)

ANOVA is a statistical technique utilized to test the hypothesis of equal means, i.e. whether the means among two or more groups (e.g. treatments) are equal. It has the assumption that the sampled populations have a normal distribution [42].

The null hypothesis is that: there is no difference in the (response variable) means of a factor. This hypothesis is tested for all the factors and for all the possible interactions. The alternative hypothesis for each case is that the means are not equal.

In order to show the ANOVA procedure, the simple case of a fixed-effects one-way ANOVA (i.e. when there is only one factor and the levels are fixed) is explained next. It is important to keep in mind that the objective is to split the variation in two: a part due to the random error and a part due to the changes in the control factor(s).

The variance is given by:

$$s^2 = \frac{\sum_{i=1}^{n} (y_i - \overline{y})^2}{n+1}$$

where $\overline{y}$ is the mean and n is the number of measurements. The numerator is called sum of squares of deviations of the mean; it is also called "corrected sum of squares" (usually abbreviated as "Total SS"). The denominator is called the degrees of freedom [42].

The total SS can be divided into two components, the "sum of squares of treatments" (SST) and the "sum of squares of error" (SSE) in this way [42]:

$$Total\ \ SS \quad = \quad SST \quad + \quad SSE$$

$$\sum_{i=1}^{k}\sum_{j=1}^{n_i} (y_{ij} - \overline{y}_{..})^2 \;=\; \sum_{i=1}^{k} n_i (\overline{y}_{i.} - \overline{y}_{..})^2 + \sum_{i=1}^{k}\sum_{j=1}^{n_i} (y_{ij} - \overline{y}_{i.})^2$$

Where

k is the number of treatments

$\overline{y}_{..}$ is the overall mean

n_i is the number of observations for treatment i

These values are utilized to calculate the mean square of the treatments (MST) and the mean square of the error (MSE), which are used in the ANOVA table. They are obtained by dividing the sum of squares by the correspondent degrees of freedom. Defining N as the total number of observations ($N = \sum n_i$), then:

Degrees of freedom for treatment $= k - 1$

Degrees of freedom for error $= N - k$

Thus,

$$MST = \frac{SST}{(k-1)}$$

$$MSE = \frac{SSE}{(N-k)}$$

If the hypothesis of equal means (null hypothesis) is true, then MST and MSE should have similar value, i.e. the ratio MST/MSE should be close to 1. If the null hypothesis is false, then MST should be bigger than MSE [42]. The statistic utilized to test the equality of means is:

$$F_0 = \frac{MST}{MSE}$$

These values are normally presented in an ANOVA table, as shown in Table 2.9.

Table 2.9: ANOVA table [42, 41]

Source of Variation	DF	SS	MS	F_0
Treatments	$k-1$	SST	$SST/(k-1)$	MST/MSE
Error	$N-k$	SSE	$SSE/(N-k)$	
Total	$N-1$	SS		

If the alternative hypothesis is true, then $MST > MSE$ and the test statistic F_0 would be larger than 1. The null hypothesis H_0 should be rejected for large values of F_0. This requires the use of a test with an upper-tail, one-tail critical region [41]. The test is done using the F distribution, and the null hypothesis should be rejected

if

$$F_0 > F_{\alpha,k-1,N-k}$$

Where

α is the significance level

$k-1$ is the degrees of freedom for treatment

$N-k$ is the degrees of freedom for error

The significance level α (or "type I error") is chosen by the experimenter; typical values are 0.05 and 0.01. A significance level of 0.05 means that the experimenter would inadvertently reject the null hypothesis 5% of the times when it is actually true [42].

An important issue with this α-approach is that it only establishes whether the null hypothesis is rejected or not. It does not give extra information to rank the factors or to know whether the test statistic is close to the chosen significance level of far into the critical region.

To overcome this issue, a tactic that is commonly used for decision making is the "P-value" approach. The P-value is "the smallest level of significance that would lead to rejection of the null hypothesis H_0" [41].

If the experimenter has chosen a significance level (e.g. $\alpha = 0.05$), then the null hypothesis is rejected if the P-value is lower than the chosen significance level (e.g. $P < 0.05$). The advantage of the P-value approach is that it allows the experimenter to rank the factors: the lower the P-value the more significant the factor.

It is important to note that statistical methods do not prove that a factor has a specific effect on the response, however, they do allow the experimenter to "measure the likely error in a conclusion" [41]. They allow a more objective experimental analysis.

Regression Models

Regression models are utilized to calculate a mathematical relationship (empirical model) between a response variable and one (or several) control factor(s). Linear regression models are commonly applied, using the method of least squares for the calculation of the coefficients. A linear regression model is described by the equation:

$$Y = \beta_0 + \beta_1 X_1 + \beta_2 X_2 + \ldots + \beta_k X_k + \epsilon$$

Where

Y is the response variable

X_1, $X_2 \ldots X_k$ are the control factors

β_0, $\beta_1 \ldots \beta_k$ are the regression coefficients

ϵ is the error

The coefficient β_j is the expected change in the response variable Y per unit change in the factor X_j when all the other factors are kept constant [41].

It is worth noting that this method can also include quadratic terms because terms such as $\beta_{11} X_1^2$ can be dealt with if the quadratic factor is treated as one single variable X_2 (where $X_2 = X_1^2$). The same principle applies for a multiplication term $\beta_{12} X_1 X_2$ (such as the ones produced by interactions), in which the multiplication of factors can be treated as one factor X_3 (where $X_3 = X_1 X_2$) [41].

In an experiment with k factors, the experimenter will have a number of n observations (where $n > k$). Every observation will have a response Y_i, and a number of control factors X_{ij} (the ith observation of the factor X_j). The equation, in terms of the observations, becomes:

$$Y_i = \beta_0 + \beta_1 X_{i1} + \beta_2 X_{i2} + \ldots + \beta_k X_{ik} + \epsilon_i$$

For this equation, the method of least squares calculates the β's that minimize the sum of the squares of the errors, ϵ_i [41].

2.6 Control Engineering

2.6.1 Closed-loop Control Systems

Closed-loop systems are widely used in the industry for control of processes and devices. A typical block diagram is shown in Figure 2.21. A sensor measures the output and sends the feedback signal. This signal is compared to the desired response, obtaining an error. The error signal is sent to the controller, which performs a corrective action in order to reduce/eliminate the error. This kind of control systems are error-driven, because the control effort is a function of the difference between the desired output and the actual output [45].

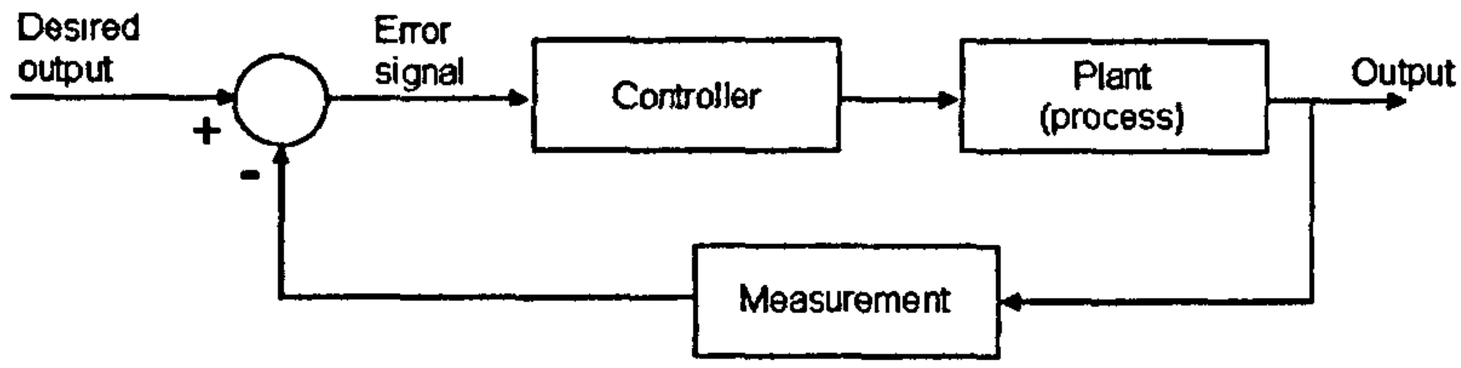

Figure 2.21: Feedback loop

When a controller is going to be designed, it is necessary to choose the variable to control. Also to define the configuration of the system (plant and feedback elements).

Once the configuration of the system is established, the next step is to obtain a mathematical model of the system. This can be obtained by physical principles or by experimental trials (measuring the input and output signals). This model is normally obtained in the time-domain.

Some of the techniques utilized for control design work in the s-domain (Laplace). If the controller is designed for implementation in a digital device (e.g. a computer), the design is performed in the z-domain (discrete time). The model is transformed from the time-domain to the s-domain (or z-domain) and the controller can be designed using techniques such as the root locus method.

Once the controller has been designed, it is necessary to analyse the performance and tune the parameters until a satisfactory outcome is achieved. This is an iterative process.

2.6.2 Mathematical Modelling of Systems

The methodology for control design described in this section applies only to linear systems. The use of linear systems allows the application of the Laplace transformation. A linear system must satisfy two conditions: superposition and homogeneity.

When a system is at rest, an excitation $x_1(t)$ will cause a response $y_1(t)$. If it is subjected to an excitation $x_2(t)$, the system will give a response $y_2(t)$. The superposition principle for a linear system requires that the excitation $x_1(t) + x_2(t)$ produces the response $y_1(t) + y_2(t)$. A system characterized by the equation $y = x^2$ is not linear because it does not satisfy the superposition principle [46].

The property of homogeneity indicates that the magnitude scale factor has to be preserved. In a system, an input x will cause a response y. If the input is multiplied by a constant k it will become kx and, in a linear system, it must cause a response ky. A system characterized by the equation $y = mx + b$ is not linear: the homogeneity property is not satisfied [46].

Transfer Function

The transfer function of a system or element is defined as "the ratio of the Laplace transform of the output variable to the Laplace transform of the input variable with all initial conditions assumed to be zero" [46].

Transfer functions can be defined only for linear systems. The system must also be stationary, i.e. with constant parameters (Laplace transforms may not be utilized for time-varying systems) [46].

It is important to note that a transfer function describes only a relationship between the input and the output of a system. It does not provide any information about the internal structure and behavior of the system [46].

The use of transfer functions is very important in control engineering. They can be represented in the elements of a block diagram. Each element has a transfer function (e.g. $G(s)$), and the elements can be combined to obtain the transfer function of the whole system.

Figure 2.22 shows two elements connected in cascade. The transfer functions of these elements are multiplied to obtain a transfer function of the system or subsystem:

$$\frac{\theta_o}{\theta_i} = G_1(s)\, G_2(s)$$

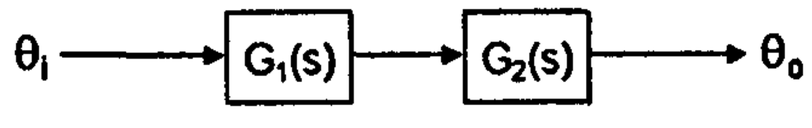

Figure 2.22: Cascade block diagram

For elements connected in a negative feedback loop, as shown in Figure 2.23, the closed loop transfer function of the system is:

$$\frac{\theta_o}{\theta_i} = \frac{G(s)}{1 + G(s)\, H(s)}$$

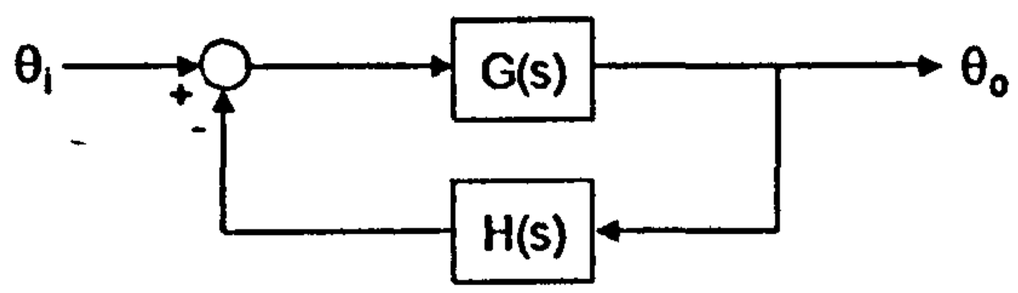

Figure 2.23: Negative feedback block diagram

Poles and Zeros

The transfer function of a system can be separated into numerator and denominator:

$$\frac{\theta_o}{\theta_i} = G(s) = \frac{N(s)}{D(s)}$$

The characteristic equation of a system is obtained when the denominator of the transfer function is equated to zero, i.e. $D(s) = 0$. In the closed loop system shown in Figure 2.23, this equation is: $1 + G(s)\,H(s) = 0$.

The roots of the characteristic equation are called poles. The number of poles determine the order of the system (e.g. a second order system will have two poles). Similarly, if the numerator is equated to zero (i.e. $N(s) = 0$), the values of s that solve the equation are called zeros.

The number and location of the poles in the s-plane are closely related to the dynamic response of the system. The s-plane has two axes: the real axis (σ) and the imaginary one ($j\omega$), which correspond to the components of the complex variable $s = \sigma + j\omega$. If the poles are located on the real axis, the system will be non-oscillatory. If they have a component in the imaginary axis, the system will oscillate. This applies for both open-loop and closed-loop systems.

A first-order system will have only one pole, located in the real axis, producing a non-oscillatory response. A second-order system will have two poles: if they are located on the real axis the system will not oscillate; but if they have a component on the imaginary axis, the system will oscillate.

The unit step response of a closed-loop stable oscillatory system is shown in Figure 2.24. The response of such system is commonly described by the following terms:

Rise time T_{r_1}: time for the response to change from 10% to 90% of the desired value.

Peak time T_p: time at the peak of the response.

Overshoot: the percentage of the response that go above the desired value.

Settling time T_s: time for the response to settle inside the tolerance band $\pm\ \delta$. Typical values for the tolerance band are $\pm$ 2% and $\pm$ 5%.

Steady-state error e_{ss}: the difference between the desired value and the steady state

response.

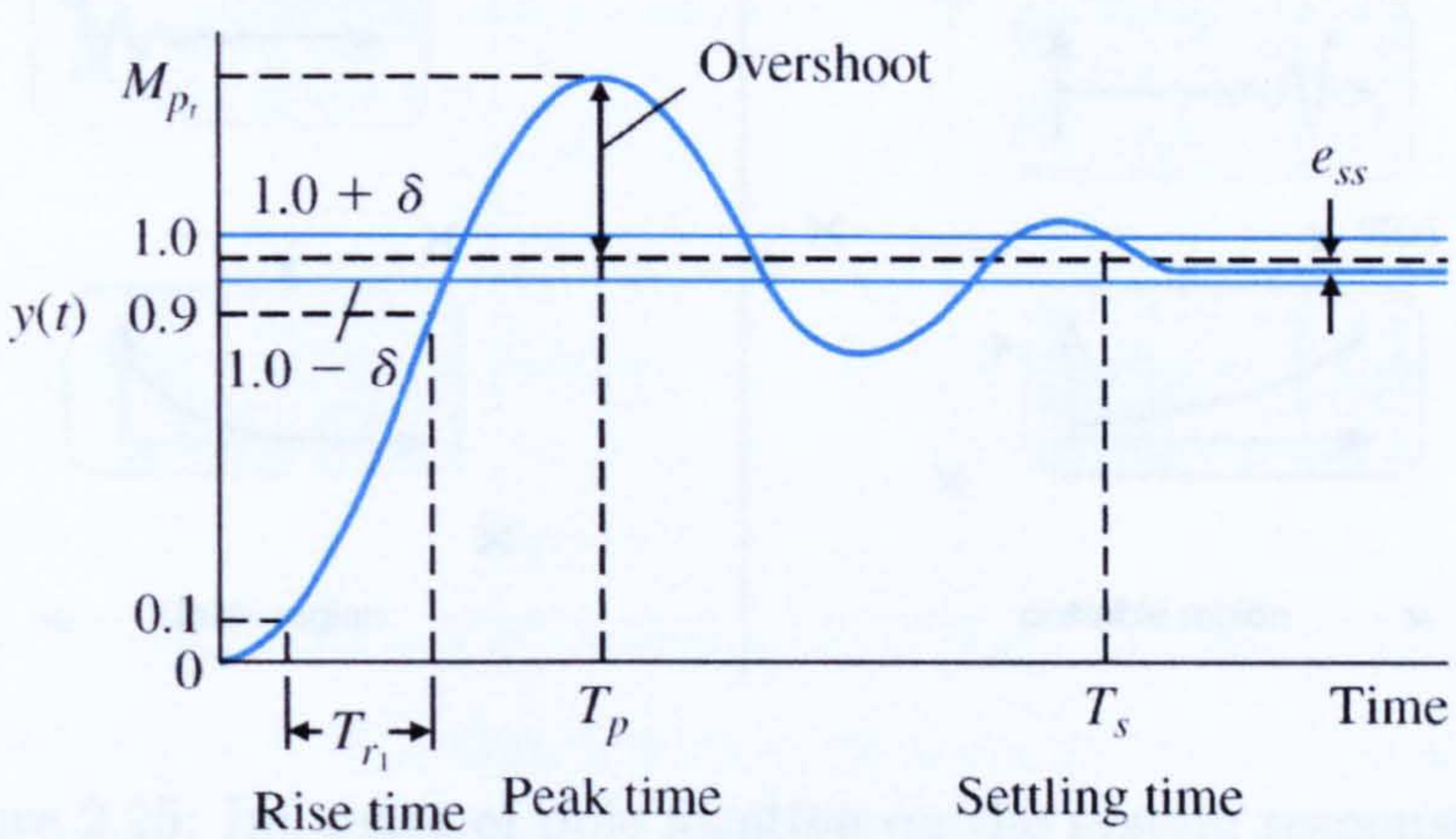

Figure 2.24: Unit step response for a stable oscillatory 2nd-order system [47]

Stability

The stability of a system is a crucial factor in control design, and it can be analysed in the s-plane. If all the poles are located in the negative side of the s-plane, the system is stable. If at least one pole is located in the positive side of the s-plane, the system is unstable. If at least one pole is located on the imaginary axis (i.e. $s = 0 + j\omega$), the system is marginally stable (provided that there are no poles in the positive side of the plane). Figure 2.25 shows the influence of the location of the poles on system response.

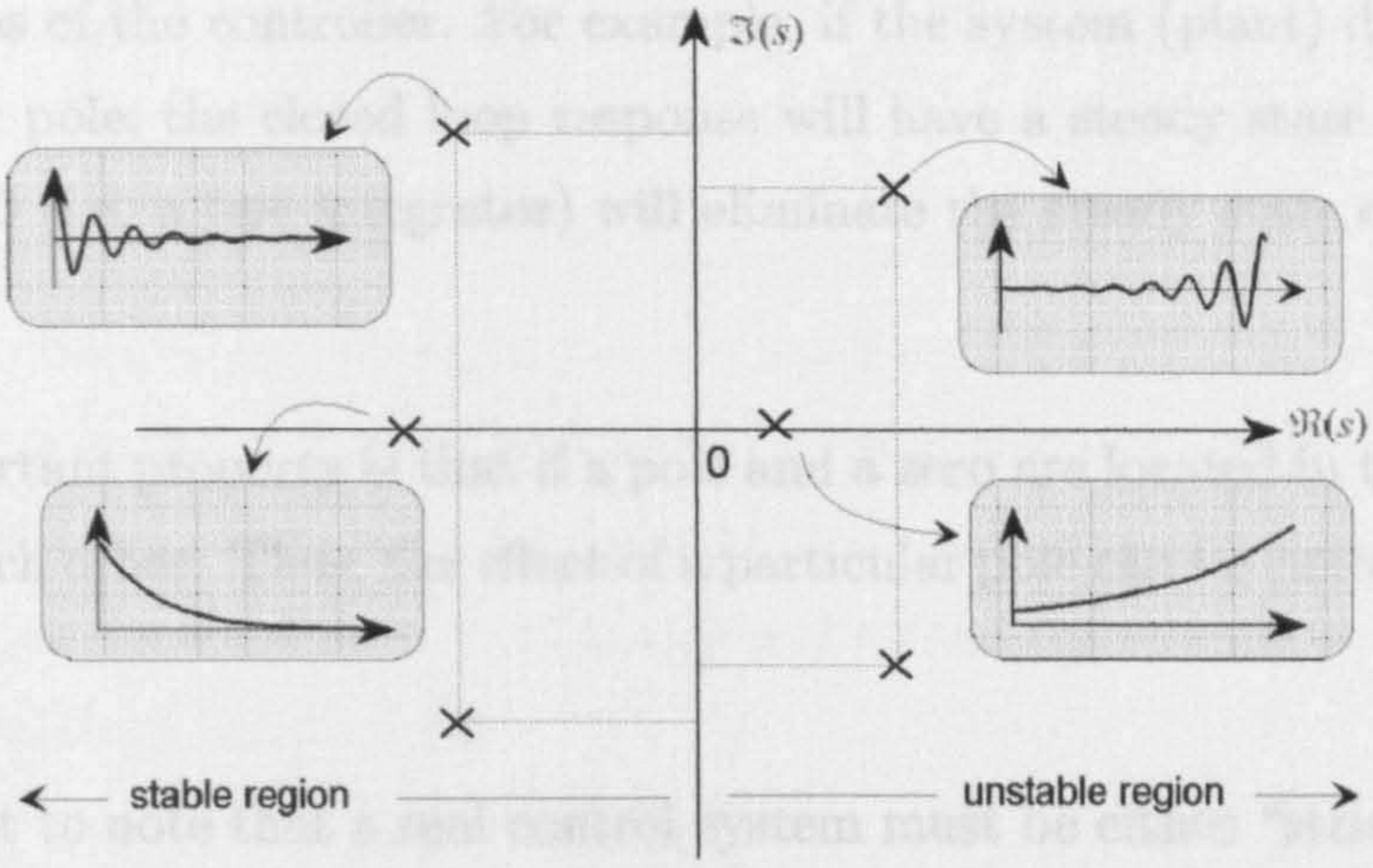

Figure 2.25: Influence of pole location on the system response [48]

2.6.3 Root Locus Method

The root locus method traces the path of the roots of the closed-loop characteristic equation (i.e. closed-loop poles) in the s-plane as the controller gain K (or another parameter) is varied. Normally the objective is to choose an adequate value for the controller gain in order to achieve the desired performance.

Some important aspects of the root locus method [49, 46]:

- The controller gain K is usually varied from 0 to ∞
- Each locus (or "branch") starts at an open-loop pole (when $K = 0$) and ends at an open-loop zero or at infinity (when $K = \infty$)
- The number of branches is equal to the number of open-loop poles
- The root loci is always symmetrical with respect to the horizontal real axis (σ-axis)

When designing a controller, it is important to choose a convenient location for the

poles and zeros of the controller. For example, if the system (plant) does not have a free integrator pole, the closed loop response will have a steady state error. Adding a pole in $s = 0$ (i.e. a free integrator) will eliminate the steady state error for a step input.

Another important property is that if a pole and a zero are located in the same place, they cancel each other. Thus, the effect of a particular pole can be canceled by placing a zero on it.

It is important to note that a real control system must be either "strictly proper" or "proper". A strictly proper system has more poles than zeros. A proper system has the same number of poles and zeros. A system with more zeros than poles cannot be implemented in reality.

Once the number and location of poles and zeros have been decided, the root locus is utilized to choose an adequate controller gain K. The design of a controller is actually an iterative process.

2.6.4 Discrete Time Systems

The use of computers for process monitoring and control can offer important characteristics [45]:

- High performance
- Versatility
- Flexibility
- Reliability
- Cost effective system
- Ability to perform complex calculations

- User-friendly interface

Process variables and signals are usually continuous time. However, when a computer is used for process control, these signals are sampled via an analogue-to-digital converter (ADC), and the computer performs the calculations with the sampled values (discrete time signal). Then the signal is converted via a digital-to-analogue converter (DAC). A system in which both continuous and discrete time signals are present are called "sampled-data systems" [45].

Continuous time signals are defined for a continuous range of time; the can change its value at any time (e.g. voltage and current). Conversely, discrete time signals are defined only at particular instants of time and only can vary its value at those instants [45].

Regarding the modelling of systems, it is important to note that continuous time systems can be modeled using transfer functions in the s-domain (Laplace). However, discrete time systems are modeled using a different domain: the z-domain. Discrete time transfer functions are obtained in this domain by means of the z-transform. The approach used with the z-transform is similar to that used in continuous time systems with the Laplace transform [45].

The transfer function of a discrete time system is called "pulse transfer function", and it is defined as "the z-transform of the output divided by the z-transform of the input" [45].

Once the pulse transfer function has been obtained, it can be analysed using the root locus method. The root locus is traced on the z-plane.

Similar to the s-plane, the axes of the z-plane are: σ (real) and $j\omega$ (imaginary). Here the stable region of the system lays inside the unit circle. If a closed-loop pole lays outside this circle the system is unstable, as shown in Figure 2.26.

If the dominant poles are on the σ-axis, on the section $0 \leq z \leq 1$ the system will be stable and non-oscillatory. If they are on the section $-1 \leq z < 0$ the system will be stable but oscillatory. If they have a component in the imaginary axis, the system will be oscillatory as well.

In the z-plane, the location of a free integrator is in $z = 1$.

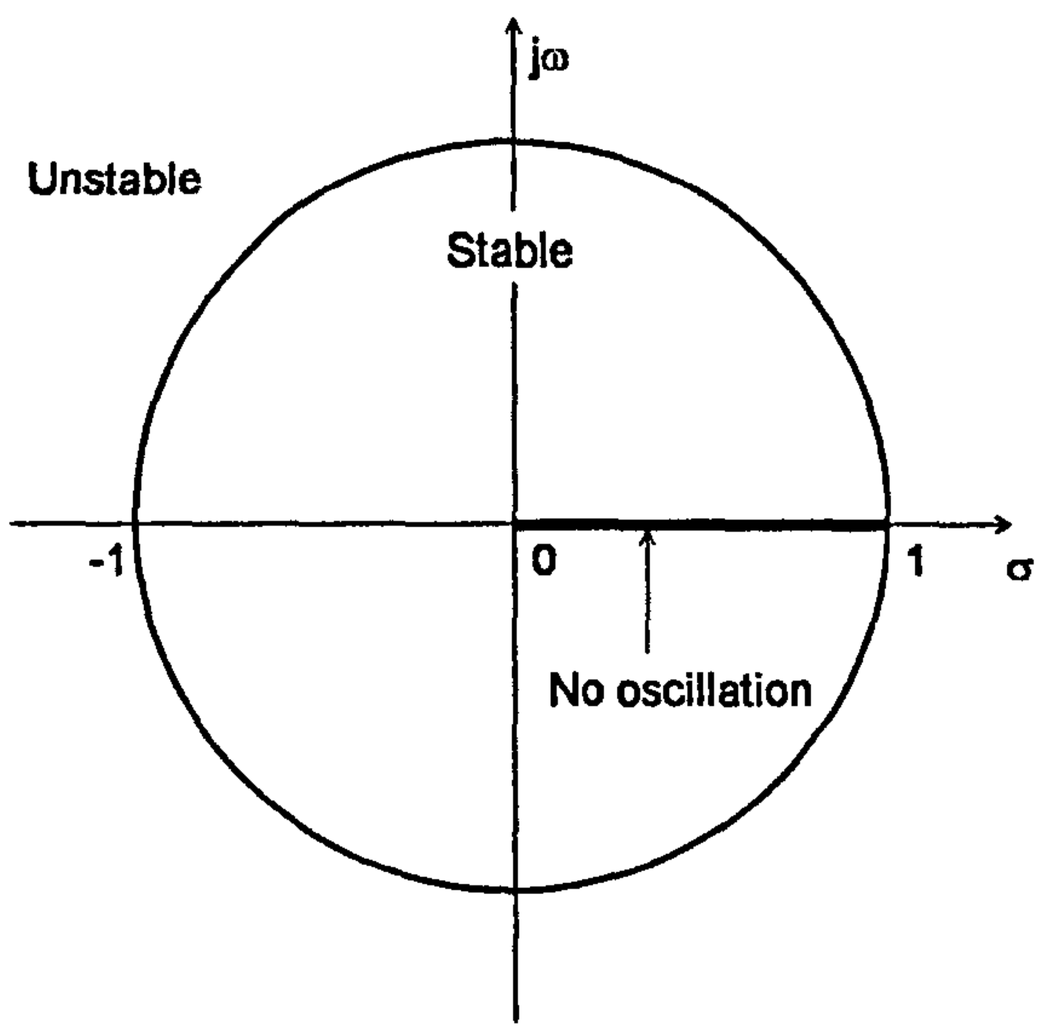

Figure 2.26: The Z - plane

2.7 Additive Manufacturing

2.7.1 Description of the Process

Additive Manufacturing (AM) consists of technologies that manufacture parts or components building the piece by depositing material layer by layer. A 3D model of the piece is generated using a Computer Aided Design (CAD) software, then the model is sliced into several thin layers and the AM software calculates the path to deposit the material. Then, the piece is built layer by layer. Commonly, additive techniques produce near-net shape parts which require some finishing operation, such as machining, to improve the surface quality.

Additive manufacturing is referred in a number of different ways such as: Solid Freeform Fabrication, Layer-based Manufacture, Direct Manufacturing, Direct Fabrication, Rapid Manufacture, Additive Fabrication, Layer Manufacturing, Additive Techniques, Additive Processes and Additive Layer Manufacturing [50, 51, 52].

AM can be used to build components in a range of materials such as polymers, metals and ceramics. This section focuses on those technologies that produce metallic parts.

2.7.2 Technologies for Metal Additive Manufacturing

The technologies used for metal additive manufacturing require a heat source to melt the metal and also a material delivery system to feed the metal (powder or wire) into the process. The heat source is one of a welding process, whereas the material delivery systems can be classified in three most common cases: power bed, powder nozzle and wire.

Heat Source

Metal deposition is performed by using the heat source of a welding or cladding process, including Gas Metal Arc Welding [53, 54], Gas Tungsten Arc Welding [54, 55], Plasma Transfer Arc [56], Electron Beam [57] and Laser Beam [2, 4, 58, 59, 60].

Among these heat sources, laser beam stands out due to its characteristics:

- Flexibility: a laser beam can be focused on a small area or on a bigger area
- When focused on a small area it allows the use of low heat input, leading to a small heat affected zone (HAZ)
- Laser power is easy to control

- Large stand-off distance, allowing space for sensors and reducing the risk of the deposition head clashing with the workpiece
- Some lasers require only low maintenance (e.g. diode and fibre lasers)
- No vacuum needed

However, lasers have also some disadvantages:

- Lasers are more expensive than electric arc systems
- Less efficient heat sources than electric arcs (wall plug efficiency and material absorptivity)
- Difficulty to process very reflective materials such as gold, copper and aluminium

Powder Bed

An image of a typical powder-bed process is shown in Figure 2.27 in order to illustrate the concept. It is usually called Selective Laser Sintering when polymers are used, and Selective Laser Melting when metallic components are built. Systems designed for metals use normally a Nd:YAG or a fibre laser due to the better absorptivity of the metals to a 1.06 μm wavelength compared do that of a 10.6 μm CO_2 laser [50].

A layer of powder is placed and spread on the build platform by a powder-leveling roller. A laser beam is scanned on the platform, according to the particular layer of the CAD file, and the powder is melted to form that layer of the workpiece. The build platform is lowered (the thickness of one layer), a new layer of powder is placed and leveled, and the laser beam scans the new layer. The process is repeated until the workpiece is finished. The process is performed inside an enclosed chamber with controlled atmosphere [50].

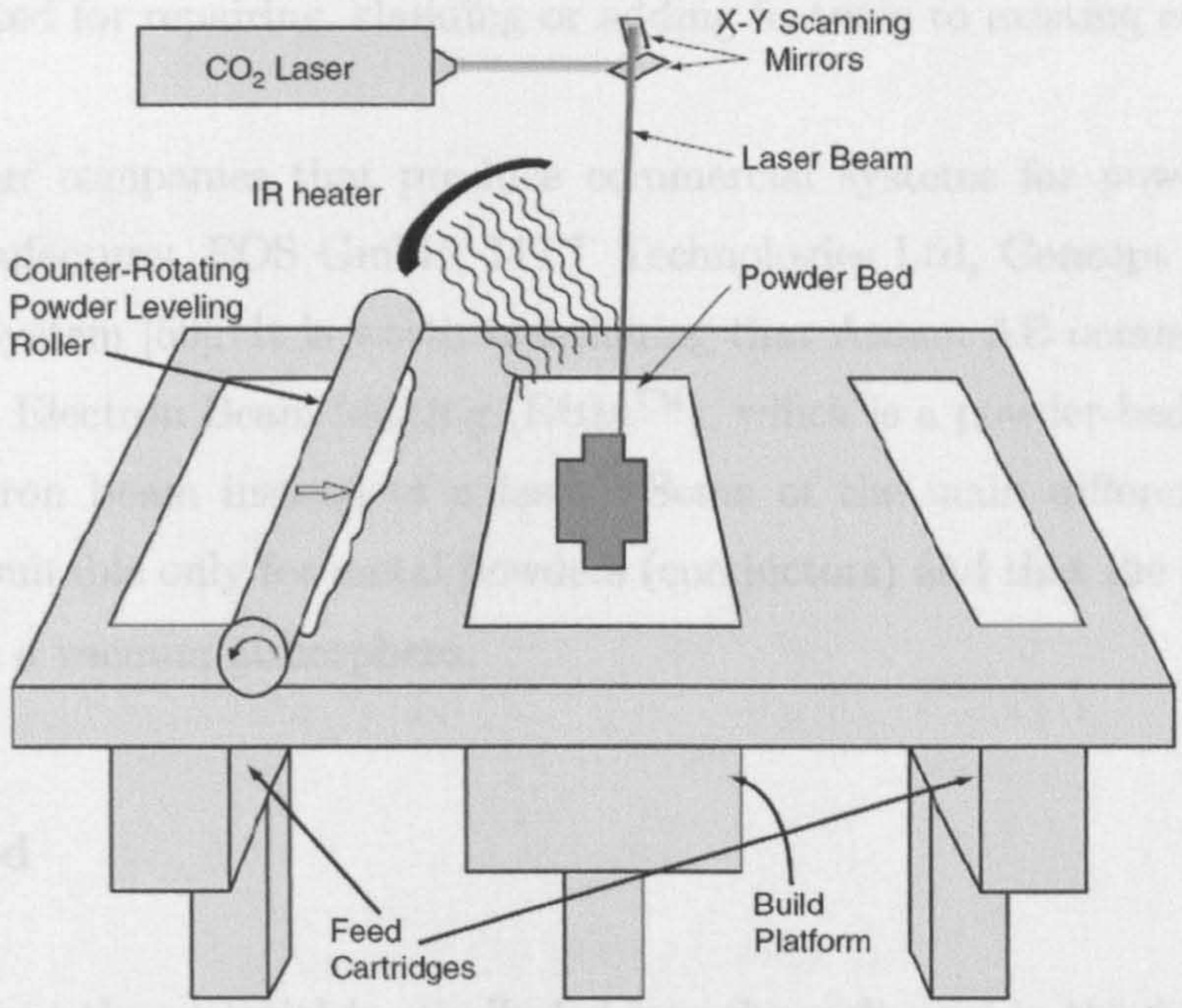

Figure 2.27: Powder-bed additive manufacturing process [50]

Heaters may be located above the workpiece and at the build platform in order to maintain an elevated uniform temperature. This allows uniform thermal expansion and contraction, preventing warping of the workpiece [50].

Among the capabilities of these systems are [50]:

- They can produce fully dense metallic parts with good mechanical properties
- They can build very complex geometries
- Higher accuracy than powder nozzle and wire feeding systems
- A number of pieces can be built on the same platform in a single build

Some limitations:

- Depending on the material, the powder may be recycled but its quality may be affected

- Not suited for repairing, cladding or adding features to existing components

There are four companies that produce commercial systems for powder-bed laser additive manufacture: EOS GmbH, MTT Technologies Ltd, Concept Laser GmbH and Phenix System [50]. It is worth mentioning that Arcam AB commercializes the system called Electron Beam Melting (EBM™), which is a powder-bed process that uses an electron beam instead of a laser. Some of the main differences are that EBM™ is suitable only for metal powders (conductors) and that the process needs to be done in a vacuum atmosphere.

Powder Feed

In these systems the material is usually fed into the melt pool in the form of powder using a single nozzle (lateral), a conical nozzle coaxial to the laser beam or a multi-nozzle system (normally three or four nozzles). Figure 2.28 illustrates the use of a coaxial nozzle and a lateral one. A number of technologies for laser metal deposition work with powder feeding, such as Laser Engineered Net Shaping (LENS™) [58], Direct Metal Deposition (DMD™) [59] and Laser Net Shape Manufacturing (LNSM) [60]. This process is commonly called Laser Powder Deposition (LPD) [61].

Lateral single nozzle is simple to implement, but it has the disadvantage that the deposition rate depends on the scan direction. Thus, it is not suitable for many metal deposition applications [61]. Conical coaxial nozzle and multi-nozzle systems have the advantage of providing a more flexible multi-directional process. The four-nozzle approach used in LENS™ is shown in Figure 2.29.

The coaxial feeding system allows a higher powder capture efficiency. There is a shielding gas that helps to focus the powder stream and to protect the melt pool from oxidation when the deposition is done without a controlled atmosphere chamber [50].

LPD systems can produce fully dense parts with good mechanical properties. They

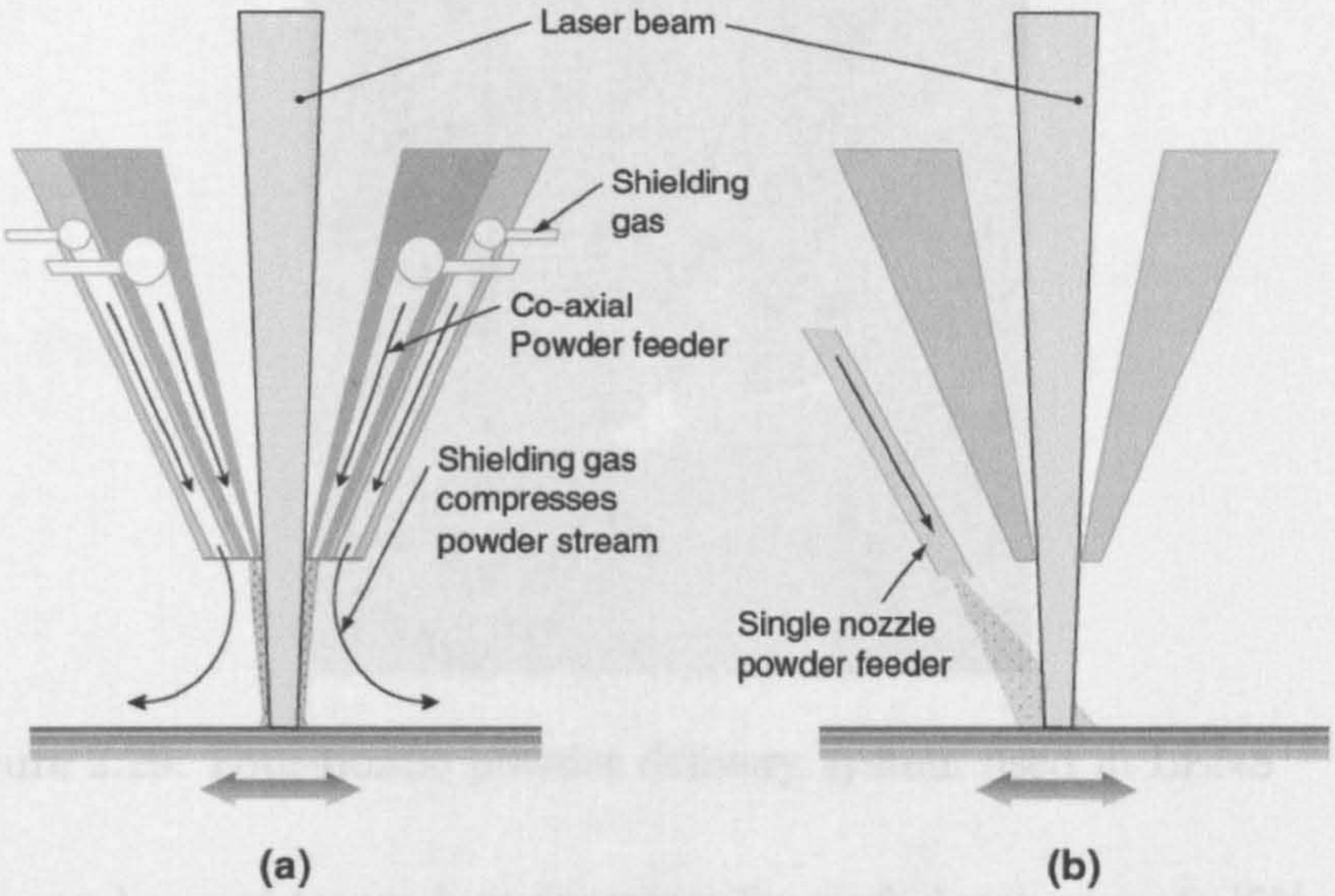

Figure 2.28: Powder nozzle [50]
(a) Coaxial nozzle. (b) Single nozzle

are commonly applied for cladding in order to improve the surface properties in terms of resistance to wear and/or corrosion. They are also used for repairing defective or service-damaged parts. Adding features to existing components is another important application that adds value and takes advantage of the capabilities of metal deposition systems. Table 2.10 shows the dimensional characteristics of the deposition made by different commercial systems.

Table 2.10: Characteristics of deposits made by commercial LPD systems [61]

Company or university	System	Minimum feature size (mm)	Achievable accuracy (μm)	Maximum part overhang angle (°)	Minimum surface roughness (μm)
POM	DMD 105D	1	75	45	Ra 10
Optomec	LENS 850-R	0.3	250	30	Ra 12
RCAM at SMU*	Prototype	1	200	45	Ra 15

* Research Center for Advanced Manufacturing at the Southern Methodist University

One crucial characteristic of LPD systems is their capability to change the chemical composition and microstructure of the deposited material during the deposition process. This can be achieved by means of modifying the powder mixtures, i.e. using several powder feeders with different materials and changing their individual feed

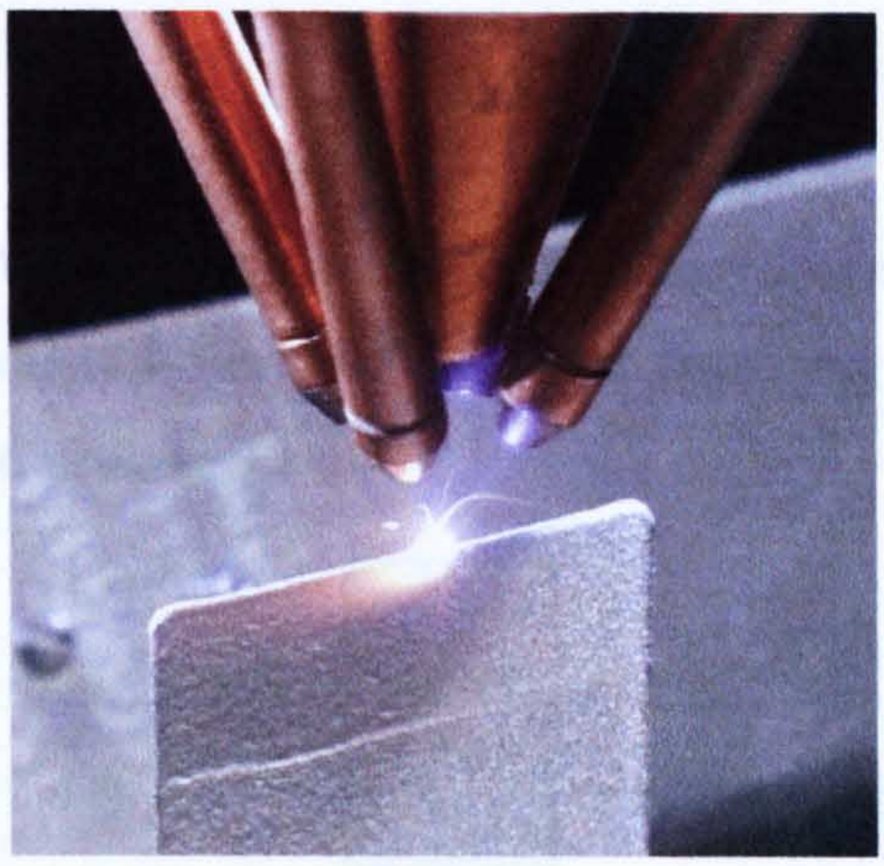

Figure 2.29: Four-nozzle powder delivery system used in LENS^{TM}[62]

rates. This can be used to produce functionally graded components [61].

LPD process also has some disadvantages. In many cases powder feeding exhibits low deposition rates typically about 25–40 g/h, leading to long build times. Also, post processing operations, such as finish machining, are commonly required due to poor surface finish [50].

Material use efficiency can also be low, depending on the system and parameters used. Syed et al. [63] reported that the deposition efficiencies of laser powder deposition are usually below 30%.

If the deposition process is not made in a sealed chamber, some powder is blown to the surroundings, causing potential hazard to the operators and the environment [2]. Also the optical components of the laser are vulnerable to be soiled [64].

Because only a percentage of the powder is actually deposited, variations in the process conditions may alter the powder catchment efficiency and thus the material deposition rate, adding a source of variability to the process [61].

Wire Feed

Laser wire deposition systems also produce fully dense deposition with good mechanical properties, and are suitable for cladding and repairing of metallic components. Figure 2.30 illustrates the process.

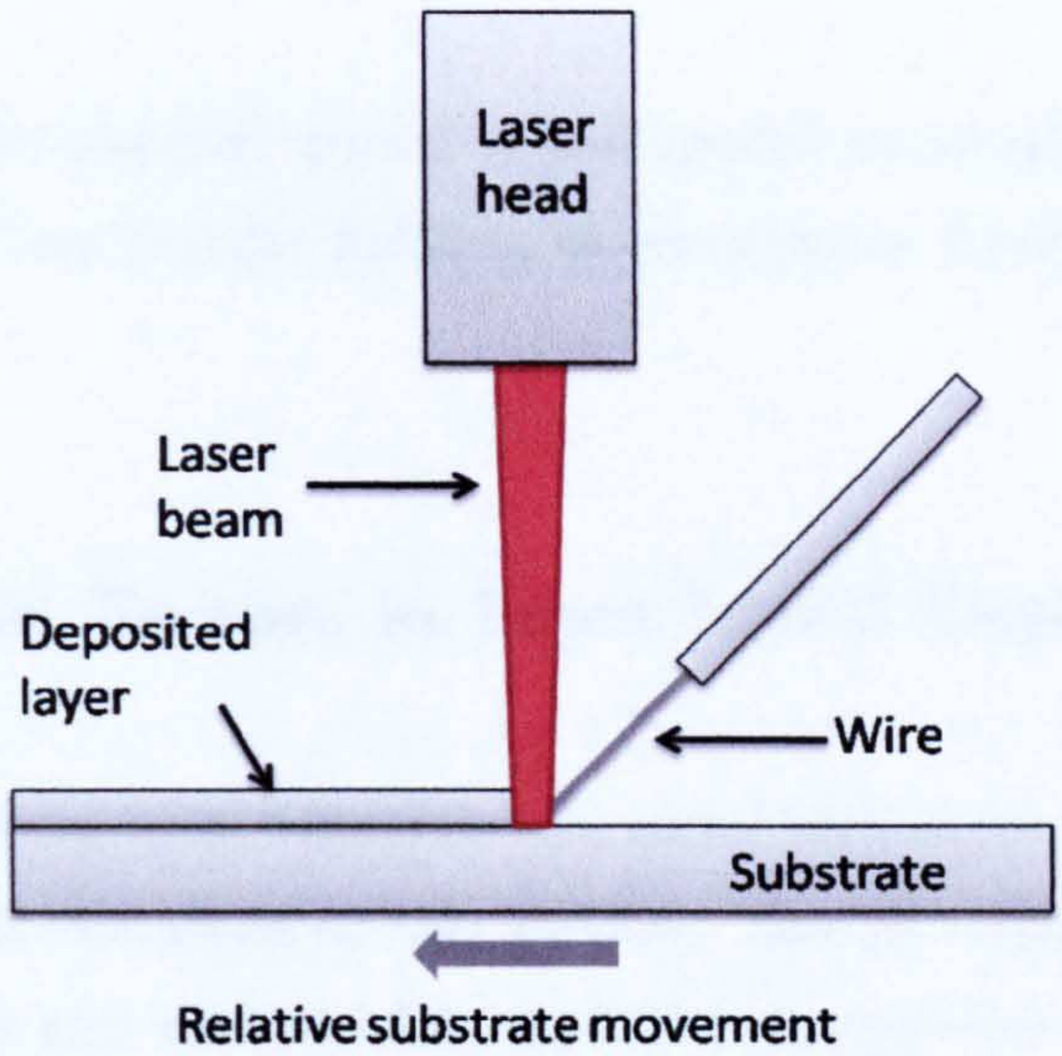

Figure 2.30: Wire feed

Laser metal deposition with wire offers important advantages: practically 100% of the material is used. It is also a clean (dust-free) process that lowers the risks to the operators and it achieves high metal deposition rates [2]. Because it deposits all the material that is fed, the actual deposition rate is known all the time and can be controlled (not the case for LPD systems).

Syed et al. [6] reported an average surface roughness of 40 to 60 μm (Ra) for wire deposition with a diode laser. In the same study they reported an average surface roughness between Ra 70 and 90 μm for powder deposition with a lateral single nozzle and diode laser.

One important limitation of wire metal deposition is that the process is direction-dependent. Front feeding achieves a more consistent deposition, whereas back feeding can cause disturbances in the process and side feeding may result in incomplete

melting of the bead [2, 4]. This makes the system unsuitable for complex geometries in which change of feeding direction would be needed.

Although there are a great amount of materials available in wire and, in many cases they are cheaper than metal powders [4], there are some materials that are not available in wire.

It is worth noting that material mixtures and graded materials have been produced by simultaneous wire and powder feeding, as reported by Syed et al. [65] and Wang et al. [66].

2.7.3 Important Factors in Laser Metal Deposition

There are several factors that influence the metal deposition process, some of the most relevant ones are described in this section. This discussion is focused on laser metal deposition with wire and powder nozzle (i.e. no powder-bed processes).

Laser

The laser used has a very important effect on the capabilities of the process. The reflectivity of materials depends on the wavelength of the radiation. Many metals have very high reflectivity at 10.6 μm (CO_2 laser), and a lower one for wavelengths around 1 μm such as Nd:YAG (1.06 μm), fibre (1.07 μm) and some diode lasers (0.808 μm and 0.940 μm). A metal deposition system with a CO_2 laser will require higher power to process most metallic materials. Figure 2.31 shows the reflectivity of different metals against wavelength of radiation.

The spot size and shape also depends on the laser used. High power diode lasers have normally large spot sizes with a rectangular shape (e.g. 2.5 mm $\times$ 3.5 mm or 1.8 $\times$ 6.8 mm). They are suitable for cladding but not for deposition of small features. CO_2, Nd:YAG and fibre lasers can normally be focused on very small areas, being suitable

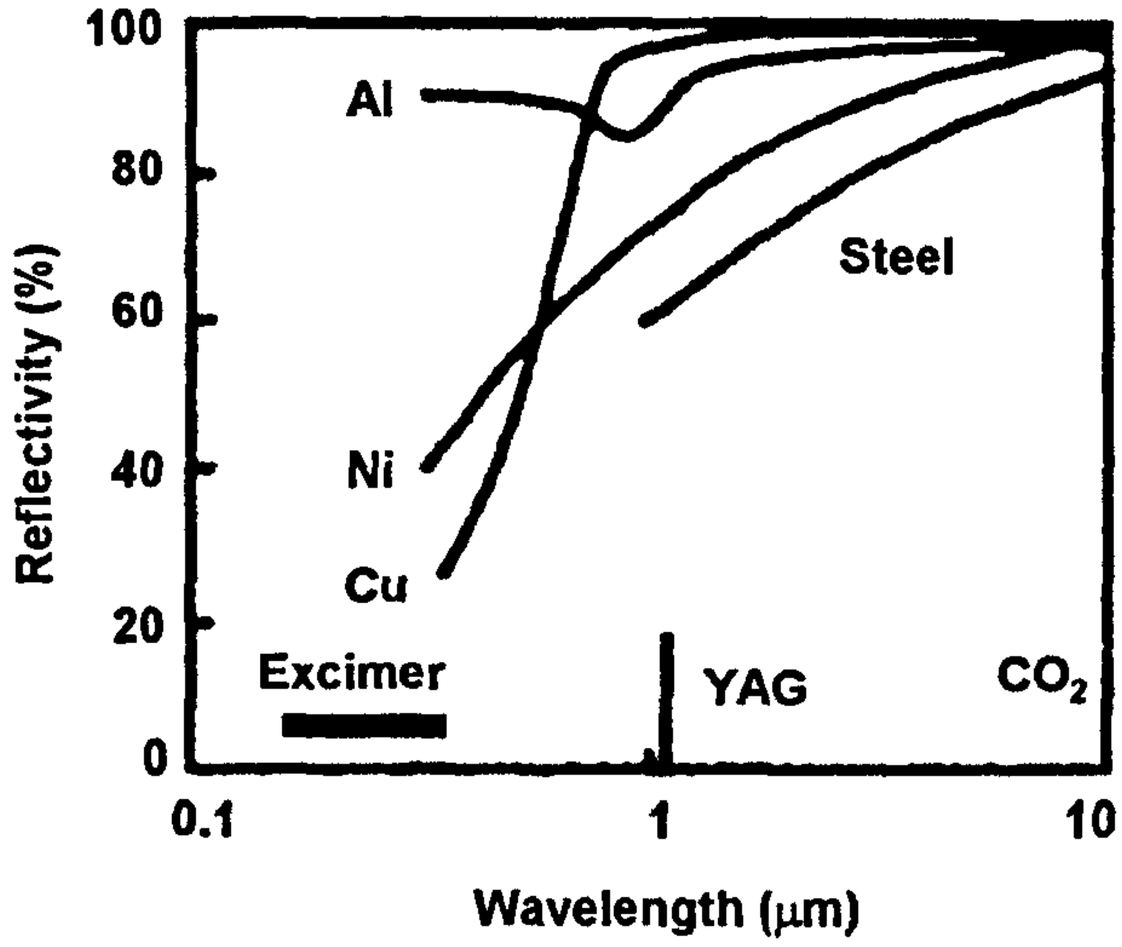

Figure 2.31: Reflectivity of selected metals [14]

for deposition of small features. They can also perform cladding and deposition of wide beads if used out of focus.

Process Factors for Laser Metal Deposition

Laser metal deposition is a complex process that is influenced by several factors, among them: laser power, laser spot size, traverse speed, shielding gas flow, material properties (e.g. absorptivity, thermal properties), material delivery method and material feed rate [2, 10, 50, 67]. The factors that have greater influence on the weld bead are [1, 68]:

- Laser spot size
- Laser power
- Traverse speed
- Material feed rate (powder or wire)

The laser spot size is controlled by modifying the defocus distance. Once this distance is chosen, it is kept constant and the wire feeder (or powder feeder nozzle) is aligned accordingly.

The laser power provides the heat to melt the material that is being fed and part of the substrate (or previous layer). When powder feed is used, increasing the laser power will normally increase the height of the deposit [50, 67]. This is because not all the powder is melted, and increasing the laser power can increase the amount of melted powder and thus increase the thickness of the bead. Syed et al. [6] reported an increase of the deposition efficiency from 8% at low laser power (700 W) to 40% at higher power (1300 W), when all the other factors were kept constant. Conversely, when wire feed is used, 100% of the material is melted, so that increasing the laser power will not increase the amount of deposited material. Heralić et al. [69] reported an increase in the melt pool width when the laser power is increased.

Increasing the traverse speed will decrease both the width and height of the deposited bead [67], because less material is being deposited per unit length of substrate, thus the cross section of the bead is smaller. This occurs for both wire feed and powder feed systems.

Increasing the powder feed rate normally increases the bead height [50, 67]. However, the effect depends on the laser power and other process conditions, because higher powder feed rate does not necessarily mean more material being deposited.

For wire feed, the bead height is determined mainly by the wire feed rate (in combination with the traverse speed) [8]. Increasing the wire feed rate will increase the bead height.

It is worth noting that the main parameters (laser power, traverse speed and material feed rate) are all interrelated. And that a successful deposition (fusion bonded, porosity free) depends on selecting an adequate combination of them [50, 61, 70].

Although the general relationships between the parameters and the deposited bead have been described here, it is important to emphasize that the actual way (how and how much) in which the factors affect the deposition depends on the specific process conditions, the deposition system, materials and range of parameters used [61]. These relationships will also be affected by variations in the process, such as heat accumulation in the workpiece or changes in the stand-off distance (between the deposition head and the melt pool).

Parameters for Laser Wire Deposition

Apart from the main factors, there are some parameters that are specific to metal deposition with wire feedstock. They are related to the setup, as shown in Figure 2.32 [8]:

- Feeding direction
- Feeding angle
- Wire tip longitudinal position in the melt pool
- Wire stick-out from the wire feeding nozzle

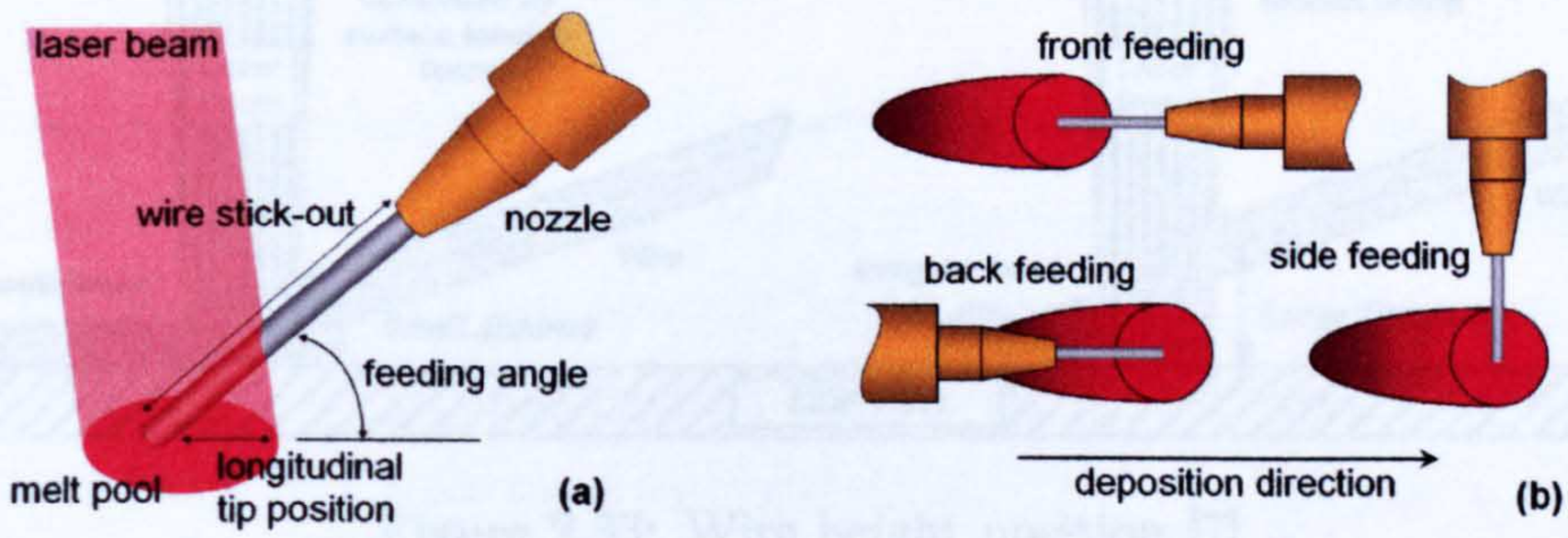

Figure 2.32: Wire setup [8]
(a) Wire setup in relation to the melt pool. (b) Wire feeding direction.

Mok et al. [2] reported that front feeding at 45° is preferred because it produces a more consistent deposition and allows higher deposition rates. Syed et al. [6]

reported good quality beads with front feeding at angles in the range of 20–60 °. Both experiments were performed using high power diode lasers.

There are three main modes of metal transfer from the wire to the workpiece: plunging, smooth transfer and droplet-like transfer; smooth transfer being the one that achieves a stable process [8].

The transfer mode depends on the main parameters (laser power, wire feed rate and traverse speed) and also on the wire setup. In order to achieve smooth deposition, the wire tip should be melted "close to the intersection with the melt pool" [8], so that the melted tip touches the substrate (melt pool) before detaching from the wire [7].

If the distance between the wire tip and the substrate is large, then the melted tip will form droplets that will fall due to gravity, producing an irregular bead, as shown in Figure 2.33 [7].

Plunging transfer mode occurs when the wire is melted by the heat of the melt pool, by plunging the wire into it. However, with this mode there is the risk of feeding too much wire, so that there is not enough energy available to melt it completely, resulting in lack-of-fusion defects [8].

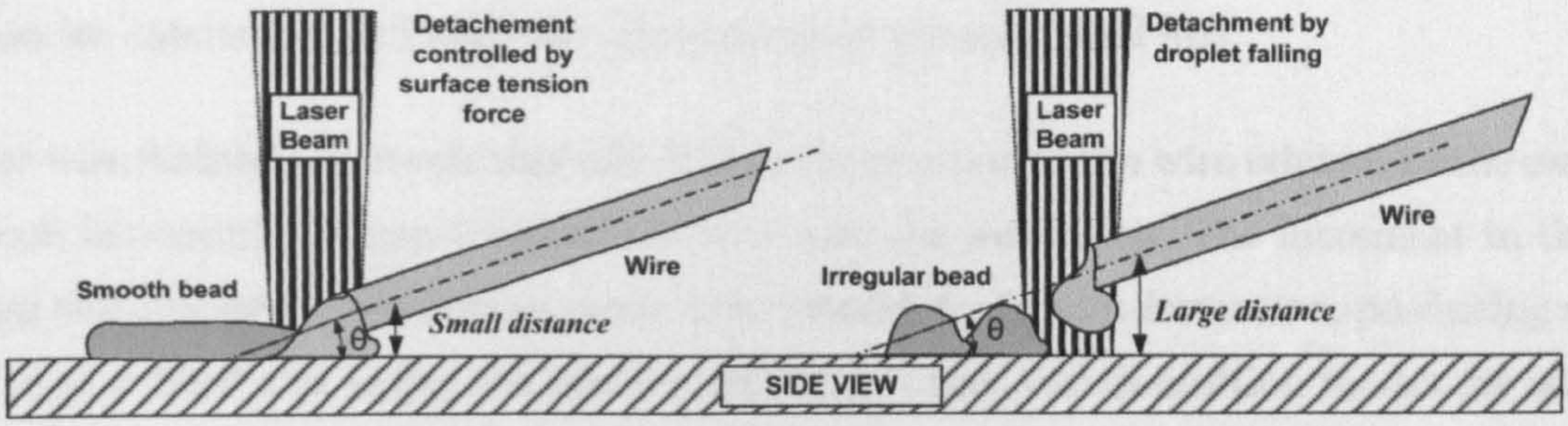

Figure 2.33: Wire height position [7]

Heat Accumulation

As the piece is being built, the heat accumulates in it, and the process conditions are affected. It has been reported that this heat accumulation leads to wider and deeper melt pools, which produces an increase in the width and a decrease in the height of the deposited bead [61].

The cooling rate of the deposited material is also affected. When the first layer is deposited on a cool substrate, the cooling rate is high. As the deposition is performed layer by layer the heat accumulates, thus the thermal gradient between the melt pool and the workpiece is lower. Then, there is a reduction in the cooling rate [61].

Also for single walls, as the height of the wall increases, the heat transfer becomes bi-dimensional. The heat transfer is lower than when the deposition is performed on the substrate (three-dimensional heat transfer).

If the deposition becomes wider and lower, then there will be a difference between the pre-determined height (programmed in the CNC table or robot) and the actual height of the bead. When subsequent layers are deposited this error will progressively increase, and the stand-off distance between the deposition head and the melt pool may increase to a significant level. For powder feedstock systems this will affect the powder catchment and alter the dimensions of the melt pool [61].

For wire feedstock systems this will change the position of the wire relative to the melt pool, increasing the gap between the wire and the workpiece. The increment in this gap will change the deposition mode from smooth to droplet-formation, producing an irregular bead and losing the process stability. These two deposition modes for wire feeding were previously illustrated in Figure 2.33.

The process factors have to be adjusted to compensate for the variations in the deposition conditions. For instance, because the workpiece is hot and the heat transfer is lower, the heat input required to make a melt pool and keep depositing material is lower. Thus, it is necessary to reduce the heat input (e.g. by means of reducing the

laser power) and to control it. For this reason it is crucial to develop control systems for metal deposition, in order to ensure a stable process.

2.8 Control in Laser Metal Deposition

The industry requires high quality and reliable processes and, in order to achieve these characteristics, online process monitoring and control systems have become a fundamental part of the laser metal deposition technologies. Research has been carried out in the past on different approaches for closed-loop process control, using a variety of sensors such as photodiodes, pyrometers and cameras. Commonly they use feedback signals from the melt pool, which can be divided into the following main categories:

- Melt pool size
  - For Laser Powder Deposition
  - For Laser Wire Deposition
- Melt pool temperature (or photodiode signal) for Laser Powder Deposition

2.8.1 Melt Pool Size Control

The literature shows different research efforts made on melt pool size closed-loop control. Two approaches are commonly found: control of the size (number of pixels) [71, 72, 73] and control of the width [8, 74]. Coaxial systems with melt pool size measurements prevail. One important advantage is that they provide a direction-independent system.

Melt Pool Size Control in Powder Deposition

Hofmeister et al. [71] reported the development of a melt pool size (number of pixels) control system for the LENS^{TM} process. They used a high-speed digital camera for visible light radiation to measure the melt pool size. The camera was coaxial to the Nd:YAG laser beam and had a narrow band notch filter to block the laser radiation. The control action was performed by a Proportional-Integral-Derivative (PID) control algorithm run from a PC. The algorithm output was utilized to modify the laser power in order to maintain a constant melt pool size. The control system improved the dimensional accuracy of the workpiece, compared to open-loop operation.

Hu and Kovacevic [72] developed a very similar system using an infrared camera coaxial to the laser beam. Two optical filters were used so that the camera received radiation at wavelengths from 0.7 to 1.06 μm, in order to block the Nd:YAG laser radiation, to reduce the high intensity light from the melt pool and to avoid the image noise from the metal powder. A grey level value was calibrated to define the boundary of the melt pool and the number of pixels was used as the feedback signal for the controller. The laser power was varied in order to maintain a constant melt pool size. An improvement in the geometry accuracy was also reported.

Melt pool width has also been used for control. Hofman et al. [74] used an infrared camera, coaxial to the Nd:YAG laser, to obtain the melt pool images. Optical filters were used so that only radiation between 0.7 and 0.9 μm was received by the camera. They extracted the melt pool width from the images and used it for online control of laser cladding with powder process. The system was tested only for one-layer cladding (i.e. not additive manufacturing). It maintained a constant bead width by means of adjusting the laser power.

Mazumder et al. [59] reported the development of a height control system based on three photodetectors. The system limits the maximum height of the deposition. The sensors detect when a section of the layer is building-up higher than the specified limit; then, the system shuts off the laser until it has passed the section of excess

deposition.

Melt Pool Size Control in Wire Deposition

Laser powder deposition has obtained great attention whereas wire feeding has been overlooked. Although there are some articles about the influence of process factors on the deposition, the topic of online control remains practically unexplored. There are only few publications on laser wire deposition monitoring and closed-loop control.

Heralić et al. [3] reported on the development of closed-loop control for bead width. The AM system consists of a 6 kW fibre laser and a wire feeding system mounted on a jointed-arm robot. A camera, placed at one side of the laser head, is used to obtain the width of the melt pool. Then the laser power is adjusted in order to maintain a constant width. A height control system has also been developed. The deposition head and sensors are shown in Figure 2.34.

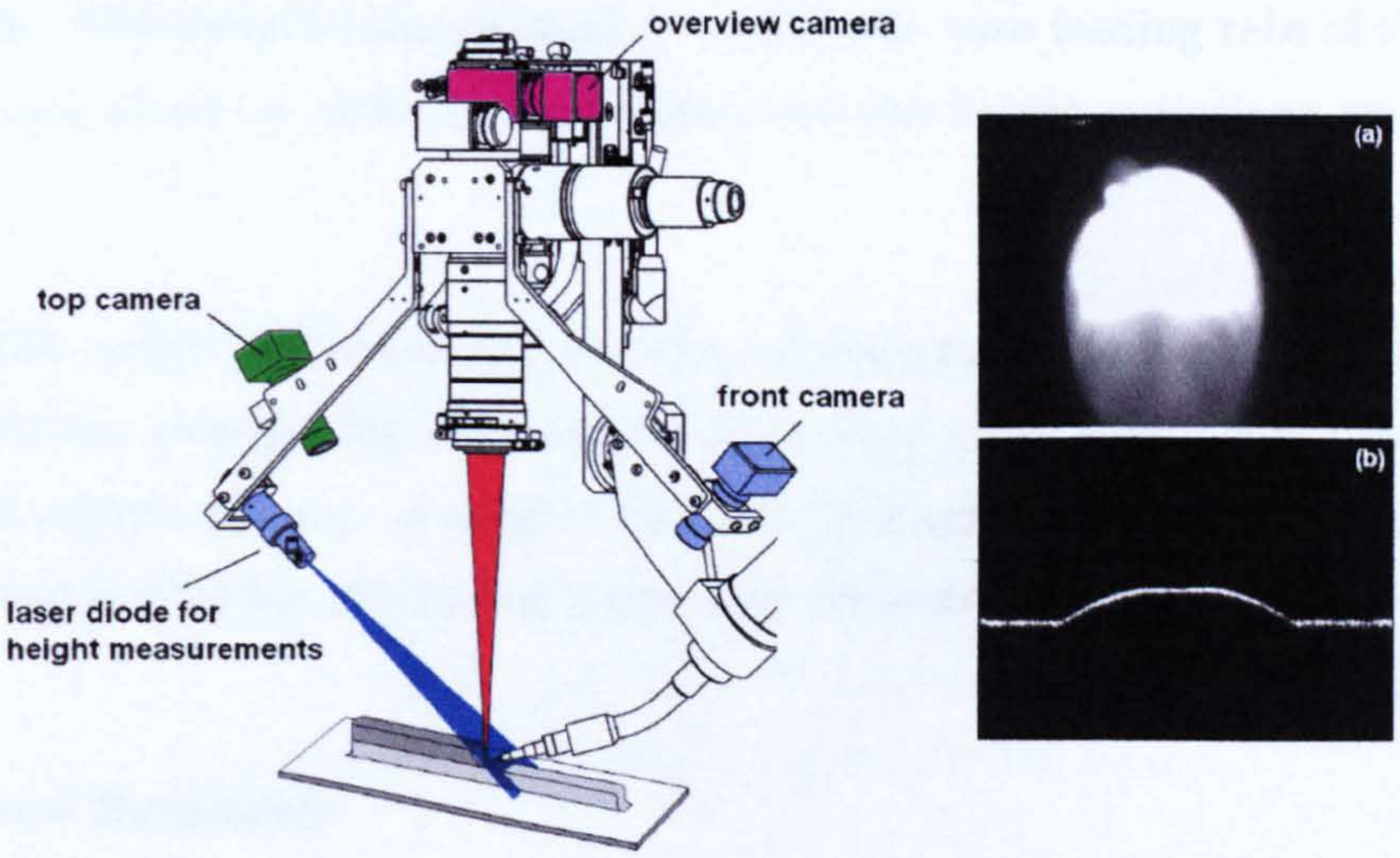

Figure 2.34: Sensors in Robotized Laser Metal-wire Deposition [8]
Melt pool images (a) are obtained by the "top camera" for width measurement, whereas the "front camera" captures the projected diode laser line (b) for height measurements.

The width controller uses a Proportional-Integral (PI) control algorithm. The controller has been used successfully to deposit single-bead walls. However, some limitations were also reported. Due to the convex shape of the top layer, after some layers have been deposited, the edges of the melt pool get out of focus and the camera is unable detect the complete melt pool. The middle part appears brighter than the edges and the system gives a measure that is smaller the actual width. Since the error is predictable, the approach taken was to change the reference width value (set-point) of the different layers in order to match it to the measurements (instead of the real width) [3]. Although this strategy may work for known conditions (materials and geometries previously deposited), it is not addressed how it would perform for other conditions (e.g. taller walls, different geometries or materials).

The height control system uses a low power diode laser (409 nm wavelength) for illumination and a camera captures the projected laser line, which is used to calculate the height of the last deposited layer (see Figure 2.34). That is, it does not measure online the height of the bead that is being deposited, but the one that was deposited previously. This height value is used to modify the wire feeding rate of the bead that is being deposited, in order to compensate for the height variations or the previous layer.

The height control improves the stability of the system, but a limitation is that it only works for straight line deposition. Also, only small components were produced with this system [8], e.g. a single-bead wall 215 mm long and 25–30 mm high. Its control capabilities for producing larger size components have not been established.

Melt Pool Boundary

Obtaining an adequate grey level for the limit of the melt pool can be a complicated and time-consuming task. The process applied by Hu and Kovacevic [72] consisted of mounting an ultra high speed camera on one side of the laser head. A nitrogen laser (337 nm wavelength) was used for illumination, and this camera was provided

a narrow band pass filter so that it would only receive the radiation at wavelengths close to 337 nm. Images of the melt pool were taken with this system and were processed to find the edge of the melt pool. Then, using a coordinate transformation, the position of the melt pool edge was mapped to the corresponding images of the infrared coaxial camera, and the grey level was selected to match the melt pool edges.

It is important to note that metals have different emissivity values. The grey level may be material-dependent and thus, for a new material a new calibration may be needed in order to obtain an accurate measurement of the melt pool area or width. Heralić [8] suggested that the calibration might need revising when the process parameters used produce a significantly different heat input to that of the original calibration conditions.

2.8.2 Melt Pool Temperature Control

Another approach is to monitor and control the temperature of the melt pool, measured by a single-colour or a two-colour pyrometer [10, 68, 75, 76]. Also, instead of a temperature, some works use a photodiode signal [1, 77, 78, 79] . The main difference is that a pyrometer is calibrated to give a temperature value (in °C, °F or K), and can be a very sophisticated and accurate device as it was shown in section 2.4.3; whereas a simple photodiode is an uncalibrated sensor that converts the radiation into an electric signal.

This strategy of temperature control has been applied only for LPD. No publication was found on laser temperature control of laser wire deposition.

Melt Pool Temperature (or Photodiode Signal) Control in Powder Deposition

Bi et al. [1, 77, 78] used a Ge photodiode, coaxial to the laser beam, to monitor and control the LPD process. The sensor had a functional wavelength of 1.3–1.6 μm.

They deposited single-bead walls and concluded that the photodiode signal had good correlation with the powder deposition process and the quality of the walls, and that it can be used for process monitoring and control [77]. Then they developed a PID control system, modifying the laser power to maintain a constant photodiode signal. The controller reference value (set-point) was modified at the edges of the wall in order to avoid excessive deposition there. The control system improved the dimensional accuracy and the microstructure homogeneity of the walls [78].

However, an important drawback is the sensor used. It is not calibrated to a temperature scale and it has the disadvantages of single-colour sensors: the target must fill the sensor spot, they are susceptible to emissivity variations and interference from smoke or powder particles (as explained for single-colour pyrometers in section 2.4.3). An alternative approach is the use of two-colour pyrometers.

Salehi and Brandt [76] used a two-colour pyrometer for melt pool temperature control in laser cladding. A PID algorithm in LabVIEW^{TM} software was applied. The controller improved the quality of the clad and a more uniform and narrower HAZ was obtained. However, they concluded that the control of the temperature alone is not enough to achieve the desired clad (in terms of dilution and size of the HAZ).

Song and Mazumder [10, 68, 75] developed a multi-sensor monitoring system with a two-colour pyrometer for melt pool temperature monitoring and three cameras that were used for measuring the pool size and height. They showed that the melt pool size (area) and the temperature had the same trend, and suggested that melt pool temperature monitoring had a similar function to melt pool size monitoring (this was for low laser power Direct Metal Deposition^{TM}, 700–900 W, CO_2 laser). They

reported that the temperature signal had less noise than the melt pool size signal. Then they developed and implemented a predictive control algorithm to maintain a constant melt pool temperature by means of varying the laser power.

However, it has been reported that pyrometers are not adequate sensors for process control of LPD because "the melt pool temperature does not provide a reliable indication of the actual melt pool size" [61]. Krantz and Nasla [80] reported that an increase in the laser power tends to increase the size of the melt pool, not its temperature. They proposed that the convection currents in the melt pool take the heat to the edges, melting the surrounding material and increasing the size of the melt pool.

The correlation between melt pool temperature and size may depend on the system (e.g. type of powder-delivery nozzle and diameter of the powder stream) and the parameters used (laser power, traverse speed, powder feed rate, beam size). The powder catchment is an important factor that is affected by the system, process parameters and process conditions (such as heat accumulation). For instance, an increase in the process heat input (laser power and/or workpiece temperature) may cause an increase in the powder catchment, then the deposition will become wider/higher (i.e. a bigger melt pool). If most of the extra heat is used to melt the additional powder, the melt pool temperature may remain practically without change. This increase on powder catchment with constant melt pool temperature was reported by Salehi and Brandt [76].

Melt Pool Temperature Control in Laser Wire Deposition

As previously explained, laser wire deposition offers important advantages over powder deposition, such as 100% material use, high deposition rates, a clean (dust-free) process. Thus, industry is looking with interest at the capabilities of the process.

In order to achieve the quality, reliability and automation demanded by the industry, it is necessary to develop closed-loop control systems. Melt pool size and temperature are the signals that have been successfully used for process control of laser powder

deposition.

However, process control for laser wire deposition remains highly unexplored. Very few publications have been made on melt pool width control, and no publication was found on temperature control of this process, showing that there is an important gap in the process knowledge and development. Hence the importance of doing research on this topic.

Chapter 3

Experimental Setup and Procedures

This chapter presents the equipment and the materials used for the experiments. It also describes the methods for the measurements and tests performed during this project.

3.1 Experimental Setup

The fibre laser metal deposition system at the University of Nottingham involves a 2 kW Fibre Laser mounted on a CNC table, a wire feeder, temperature sensors, an inert gas chamber, a computer for control and a DAQ card for input/output of signals. This system was gradually developed during this work. Experiments were performed with different setups, as explained in chapters 4, 5 and 7. The elements of the system are described next.

3.1.1 Laser

The laser used in this study was an IPG^{TM}, Ytterbium Fibre Laser, YLR–2000. This 2 KW laser has a wavelength of 1070 ± 6 nm. Its fibre has a diameter of 100 μm, and is coupled to a 600 μm diameter fibre that is utilized to deliver the beam to the laser head. The laser is connected to a computer, via an Ethernet cable, and it is controlled using the software LaserNet^{TM}. The laser power can be also controlled externally using an analogue signal 0-10 V dc. The power measurements of the laser are shown in appendix A. The measurements of the beam diameter and the focal distance are shown in appendix B

3.1.2 Laser Head

The laser head used in this study was a Precitec^{TM}YC 50 cladding head. It has sensors integrated for monitoring the cladding process. Among these sensors it is important to note a Ge photodiode for temperature monitoring and a camera that is used for alignment of the system and for monitoring the deposition process. Both the photodiode and the camera are coaxial to the laser beam.

The focusing lens has a focal length of 200 mm. The working distance of the cladding head at focus is 192 mm measured from the edge of the head (not from the position of the lens). The wire metal deposition is undertaken at a working distance of 212 mm, i.e. 20 mm out of focus, in order to get a bigger laser beam spot, approximately 3-3.5 mm diameter.

3.1.3 CNC Table

A CNC table by Talmont Control Systems LTD, fitted with an E.C.S 1400 D control, was utilized. It has four axes of movement: the laser head moves up and down in the Z axis whereas the table, in addition to the X and Y axes, has a rotational axis A.

3.1.4 Wire Feeder

Two different wire feeders were used in this project:

- The first wire feeder was a Jupiter–501, by Planetics Welding Systems Ltd. Some of the control features have been disabled, so that it was used with a manual on/off control.

- The second wire feeder was a WF200DC by Redman Controls & Electronics Ltd. It can be controlled manually or via analogue signals: 0-10 V dc for the wire feed rate, and a relay for the on/off control. It has a closed-loop control to achieve a constant feed rate.

Both wire feeders were calibrated before the experiments. The second wire feeder was used in order to integrate it to the automatic control system developed during this work, and to ensure a more constant wire feed rate.

3.1.5 Temperature Sensors

Different infrared temperature sensors "pyrometers" were tested in order to analyse their performance in temperature monitoring of laser metal deposition with wire (as described in chapter 5). After those trials, two pyrometers from IMPAC^{TM} were acquired for this project.

The pyrometer "IGAR 12-LO MB 22" was selected for measuring the melt pool temperature. It was a two-colour pyrometer with wavelengths of 1.28 and 1.65 μm and a temperature range of 500-2200 °C. Its response time was 2 ms.

The pyrometer "IGA 50-LO plus MB 13.5" was utilized to measure the workpiece temperature (upper layer). It was a single-colour pyrometer with a wavelength range of 1.45–1.80 μm and a temperature range of 250-1350 °C. Its response time was 1 ms.

Both pyrometers had a fibre optic cable and optical head which could stand temperatures up to 250 °C. There were two different optical heads; the optical head 1 had a minimum spot size of 1.2 mm whereas the optical head 2 had a minimum spot size of 0.45 mm. The pyrometers could use either optical head.

The optical heads of both pyrometers had an optical filter that rejects the wavelength of the laser in order to protect the pyrometers from the laser reflections. They could stand temperatures of about 150 °C.

Both pyrometers had a digital output that could be directly acquired by a computer using the software Infrawin^{TM}. They also had an analogue output signal of 0-20 mA that corresponds linearly to the temperature range that was used.

There was also a K-type thermocouple that is positioned inside the enclosure, close to the optical heads of the pyrometers in order to measure the temperature in the chamber and ensure that the maximum working temperature of the optical filters of the pyrometers was not exceeded.

3.1.6 Setup with Inert Gas Nozzle

The initial setup of the metal deposition system is shown in Figure 3.1. A nozzle delivers argon to the process in order to protect the melt pool from oxidation. It can be noticed that the laser head, the argon nozzle and the wire feeder nozzle were attached to the Z axis of the CNC, so that they move in the Z direction every time a new layer is deposited.

3.1.7 Setup with Inert Gas Chamber

An enclosure chamber was developed during this project in order to perform the metal deposition process in an inert-gas atmosphere (to avoid the oxidation of the

Figure 3.1: Initial setup of the metal deposition system
(1) Laser head. (2) Wire feeder nozzle. (3) Argon nozzle.
(4) Workpiece (38 mm diameter cylinder).

workpiece) and to be able to align and position accurately the different elements of the system such as the wire and pyrometers.

A top plate is attached to the laser head, and a transparent flexible plastic drape is attached to this plate and to a base plate to form the chamber. The wire and the optical fibres of the pyrometers pass through the top plate, whereas the positioning elements for the wire and optical heads are attached to it. The top plate is water cooled to avoid its overheating due to the laser reflections. The chamber and the elements inside it are shown in Figure 3.2.

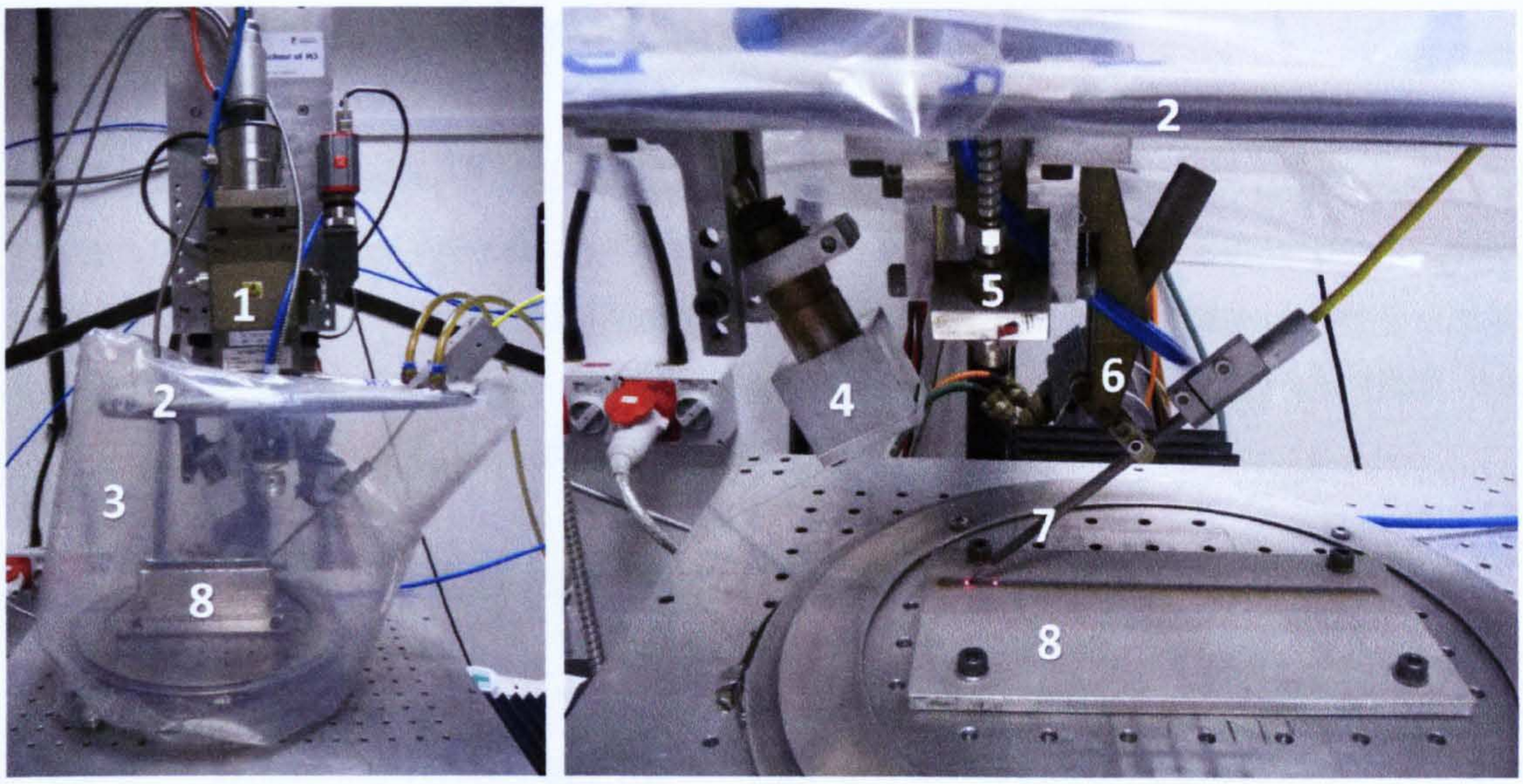

Figure 3.2: Setup for inert gas chamber

(1) Laser head. (2) Top plate. (3) Plastic chamber. (4) Optical head of melt pool pyrometer. (5) Optical head of workpiece pyrometer. (6) Wire positioning system. (7) Wire feeder nozzle. (8) Workpiece.

The inert gas used for this work was BOC™ "Pureshield Argon", with a 99.998% minimum purity specification. A typical analysis of this gas is shown in Table 3.1 (from manufacturer).

Table 3.1: Typical analysis of shielding gas BOC Pureshield Argon (from manufacturer)

Argon	99.999%
Oxygen	2 ppm*
Nitrogen	5 ppm*
Carbon dioxide	1 ppm*
Carbon monoxide	1 ppm*
Hydrogen	1 ppm*
Hydrocarbons	1 ppm*
Moisture (H_2O)	2 ppm*
Dew Point	-90 °C

* Parts per million in terms of volume

3.1.8 Data Acquisition Card

A National Instruments™ NI cDAQ-9172 was acquired in order to connect the different elements of the system to the computer. It was a modular device which could hold up to eight modules for different signals. This system only utilizes four modules, which are described in Table 3.2. The card connects to the computer via USB. The schematic diagram of the system is shown in Figure 3.3.

Table 3.2: Modules for NI cDAQ-9172

Module	No. of Chanels	Module Signal	Task and actual signal
NI 9215	4	± 10 V dc Analogue input	Acquire signal from CNC controller (0–10 V)
NI 9203	8	± 20 mA Analogue input	Acquire temperature signals from pyrometers (0–20 mA)
NI 9263	4	± 10 V dc Analogue output	Send signal to IPG Laser to control laser power (0–10 V) Send signal to wire feeder to control wire feed rate (0–10 V)
NI 9472	8	24 V dc Digital output	Send signal to relay to switch on/off wire feeder (24 V)

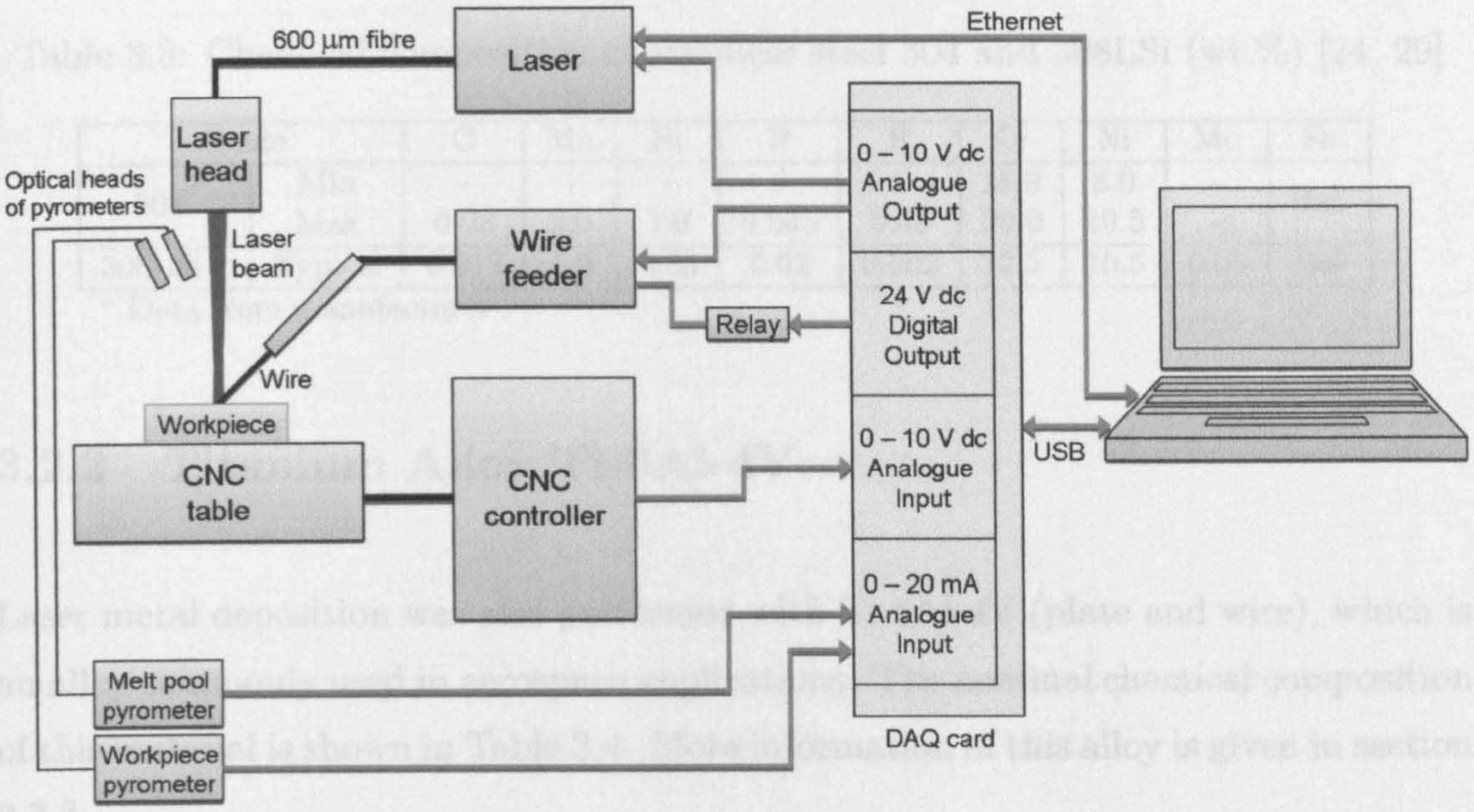

Figure 3.3: Schematic diagram for the metal deposition system

3.2 Materials

3.2.1 Austenitic Stainless Steel

The materials used in most of the experiments in this research are stainless steel, grade 304 (plate) and grade 308LSi (wire). These austenitic stainless steels have good weldability, tensile strength and corrosion resistance. Austenitic structures avoid the embrittlement of martensitic steels. For these reasons, these steels can be considered suitable for additive manufacture. Their chemical compositions are described in Table 3.3. The steel grade 308LSi has lower carbon content than 308. It also has higher silicon, which increases the fluidity of the weld pool [29]. More details of these materials, including mechanical and physical properties, are given in section 2.2.3.

Table 3.3: Chemical composition of stainless steel 304 and 308LSi (wt.%) [24, 29]

Grade		C	Mn	Si	P	S	Cr	Ni	Mo	Fe
304	Min	-	-	-	-	-	18.0	8.0	-	Bal.
	Max	0.08	2.0	1.0	0.045	0.03	20.0	10.5	-	
308LSi *	Typical	0.012	1.9	0.85	0.02	0.002	19.5	10.5	0.05	Bal

* Data from manufacturer

3.2.2 Titanium Alloy Ti-6Al-4V

Laser metal deposition was also performed with Ti-6Al-4V (plate and wire), which is an alloy commonly used in aerospace applications. The nominal chemical composition of this material is shown in Table 3.4. More information of this alloy is given in section 2.3.3.

Table 3.4: Nominal chemical composition of Ti-6Al-4V (wt.%) [30]

Material	Al	V	C *	N *	O *	H *	Fe *	Ti
Ti-6Al-4V	6	4	0.10	0.05	0.2	0.0125	0.3	Bal

* maximum (impurity limit)

3.3 Procedures for Measurements and Tests

3.3.1 Measurement of Bead Geometry

The measurement of the bead geometry (width and height) for the bead-on-plate experiments was done using a surface profiler Taylor Hobson Talysurf CLI 1000, which utilizes the laser triangulation principle.

Figure 3.4 illustrates the triangulation principle for distance measurement. A diode laser (1) emits a beam that is focused by a lens (2) onto the object to be measured (6). Part of the reflected radiation is collected by a lens (3) and displayed onto a

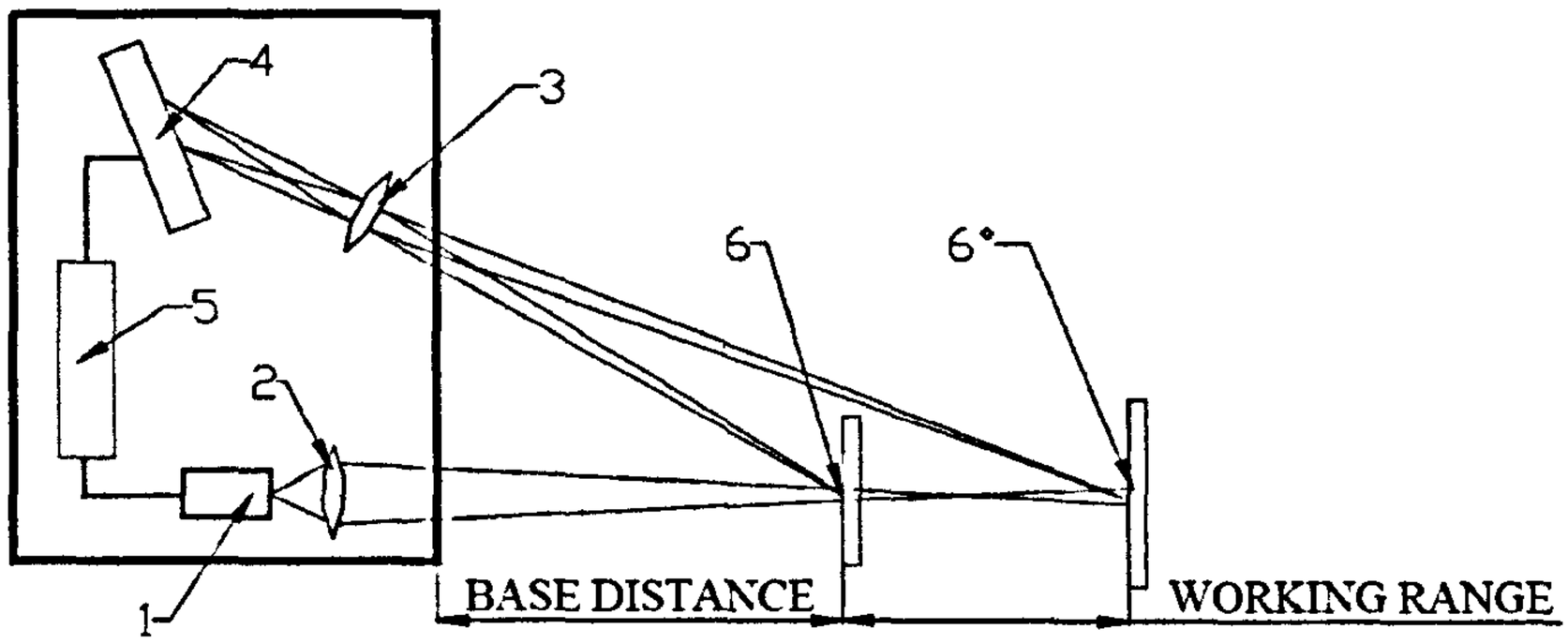

Figure 3.4: Triangulation principle [81]

linear CMOS array (4). A signal processor (5) calculates the distance to the object, based on the position of the light spot on the array [81].

The parameters used in the measurements are shown in Table 3.5, whereas the procedure is illustrated in Figure 3.5. The procedure for the measurement was:

1. The plate was placed on the measurement area.

2. The beam profiler scanned three lines to measure the transversal profile of the bead. These lines had a pitch of 5 mm.

3. The profile of each measurement was then displayed graphically and levelled in order to eliminate the error due to the bend of the plate.

4. From these three profiles the height values were measured and averaged. The same was done to the width values, so that every bead had one average height and width.

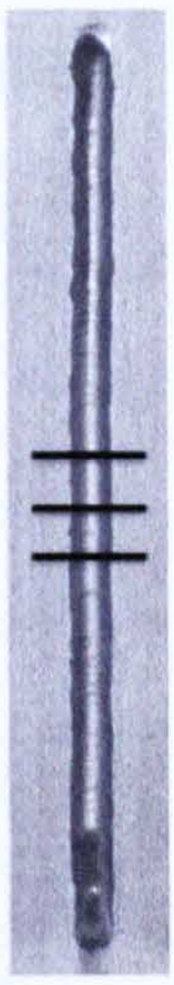

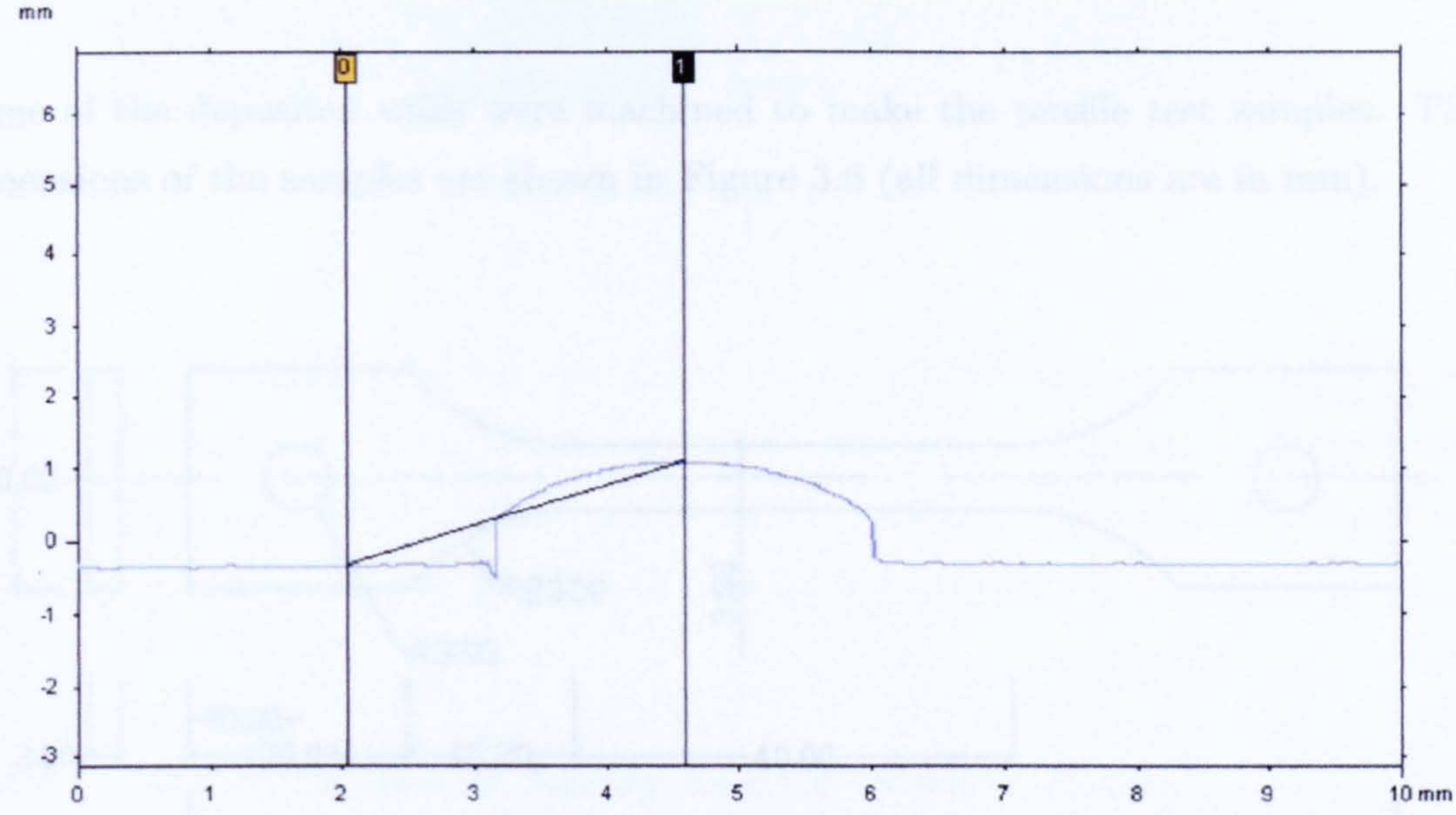

Figure 3.5: Measurement of bead geometry

(a) Talysurf CLI 1000. (b) Scanning a bead. (c) Three traces were scanned on each bead. (d) Height and width were measured by calculating the vertical and horizontal distances between two points.

Table 3.5: Parameters used for bead profile measurements

Parameter	Value	
Gauge to use	Laser	
Range to use	Single	
Measurement speed	1 mm/s	
Speed to return	3 mm/s	
	X	Y
Length	10 mm	10 mm
Resolution	10000 points	3 traces
Spacing	1 μm	5000 μm

3.3.2 Tensile Test

Some of the deposited walls were machined to make the tensile test samples. The dimensions of the samples are shown in Figure 3.6 (all dimensions are in mm).

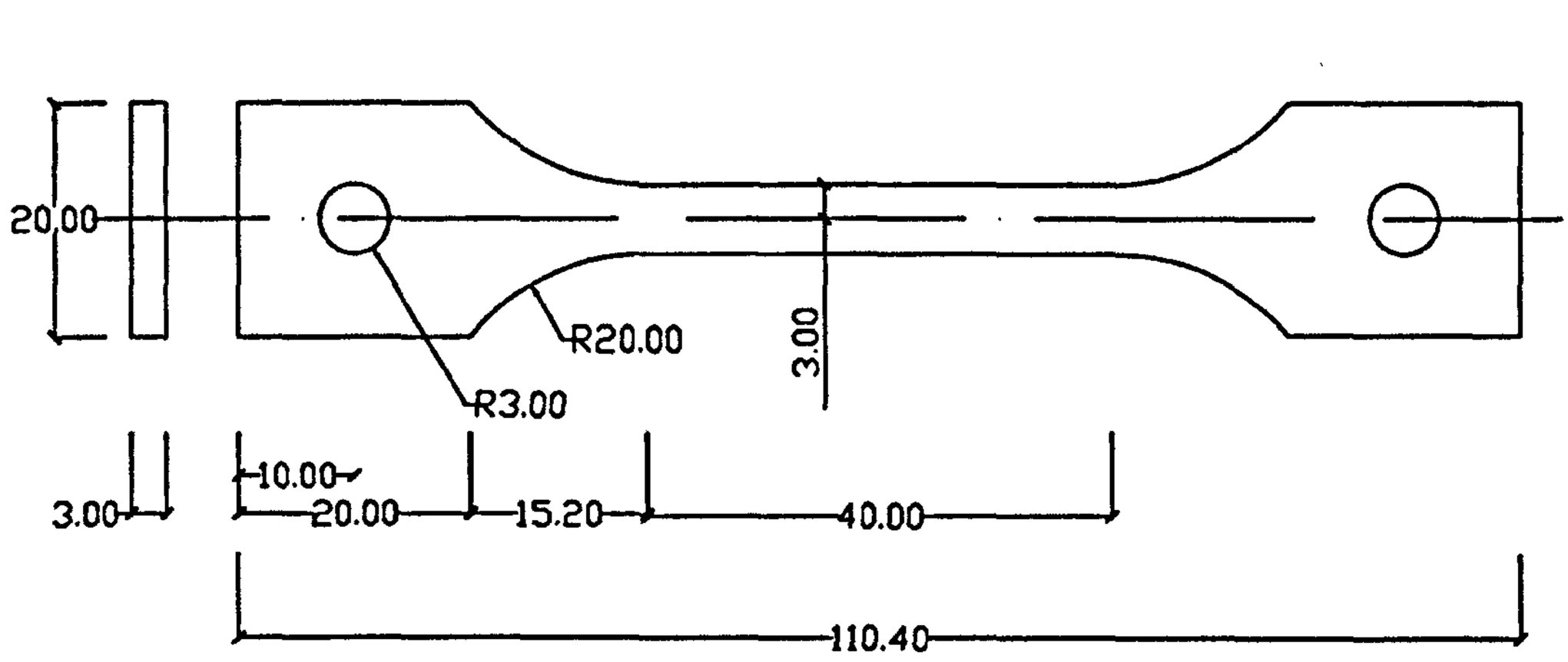

Figure 3.6: Tensile test sample

The tensile tests for the stainless steel samples were performed using the Instron^{TM} 5569, shown in Figure 3.7.

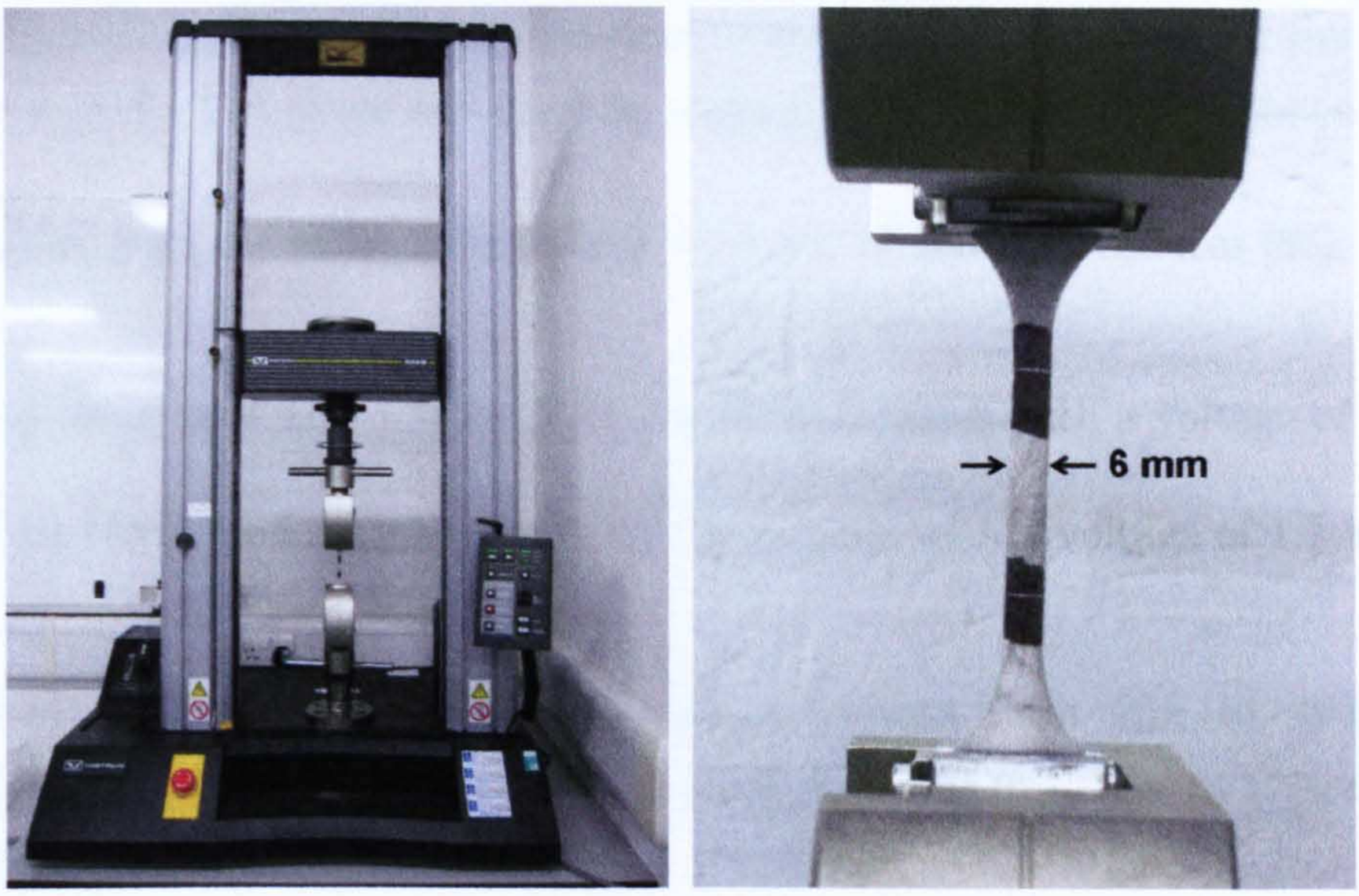

Figure 3.7: Tensile test

Two marks were made on every sample, in the parallel section, with a separation of 30 mm. The samples were mounted and tested using an extension rate of 2 mm/min. After a sample was broken, it was removed from the machine and the distance between the marks was measured to calculate the elongation at break.

3.3.3 Metallographic Analysis of Stainless Steel

Samples of deposited stainless steel were cut and machined for metallographic analysis in both transversal and longitudinal directions.

The samples were mounted in non-conductive black epoxy mounting resin or in bakelite resin. Grinding was performed by a Struers^{TM} LaboPol-5 automatic grinding/polishing machine, utilizing a MD piano disc grit 220 for 3 min., applying a force of 25 N with an angular speed of 250 rpm. The fine grinding was carried out utilizing a MD piano disc grit 1200 for 3 min., applying a force of 25 N with an angular speed of 125 rpm. This procedure ensures a flat surface with a roughness equivalent to

grit 1200 grinding. The polishing was done manually on a cloth with 6 μm diamond abrasive, and the last stage was done on a cloth with 1 μm diamond abrasive.

The samples were electrolytically etched with one of these procedures [82]:

- 10 g oxalic acid and 100 ml H_2O, for 15–30 seconds with a voltage of 6 V.
- 60 ml HNO_3 and 40 ml H_2O for 20–40 seconds with a voltage of 1.1 V.

A Nikon^{TM} optical microscope with magnifications from 25x to 400x and a Keyence^{TM} VHX Digital Microscope with magnifications from 25x to 175x were used for analysis of the samples.

3.3.4 Hardness Test of Stainless Steel

Some of the stainless steel samples were used for hardness test. Vickers hardness was measured applying a load of 20 Kg. The measurements were spaced 4 mm from each other in order to avoid any influence between them due to the cold-work hardened area.

Chapter 4

Influence of Process Parameters on Metal Deposition

This chapter deals with the influence of parameters and process conditions on fibre laser metal deposition with wire. The first three sections show a study on the main process parameters: laser power, traverse speed and wire feeder rate. The fourth section deals with the practicalities of the fibre laser metal deposition process.

4.1 Bead-on-plate Metal Deposition Experiments

4.1.1 Bead-on-plate Deposition Without Inert Gas Chamber

Three bead-on-plate experiments have been carried out during this project. The first two were done with the setup described in section 3.1.6 i.e., a nozzle was used to deliver argon gas to the melt pool area in order to protect it from oxidation (no inert gas chamber). The Jupiter 501 wire feeder was utilized in these two experiments. The plates were sand-blasted in order to increase their absorptivity to the laser beam; they were then cleaned with acetone. The conditions of the process were:

Argon flow rate:	15 L/min
Plate:	stainless steel 304, 190x100x6 mm
Wire:	stainless steel 308LSi, 1.2 mm diameter
Length of beads:	80 mm
Pitch:	10 mm

The objective was to find the process window, varying the parameters with the following values:

Laser power:	1250 – 1500 – 1750 – 2000 W
Traverse speed:	200 – 300 – 400 – 500 mm/min
Wire feed rate:	0.6 – 0.8 – 1.0 – 1.2 – 1.4 – 1.6 – 1.8 – 2.0 – 2.2 – 2.4 m/min

The method for the experiment was: selecting a combination of laser power and traverse speed, deposit beads with different wire feed rate, starting from 0.6 m/min and increasing it by 0.2 m/min until the deposition process shows an excess of wire; for example:

Laser power:	1500 W
Traverse speed:	200 mm/min
Wire feed rate:	0.6 – 0.8 – 1.0 – 1.2 – 1.4 – 1.6 – 1.8 – 2.0 m/min

Then, the procedure was repeated for the other treatments of laser power and traverse speed. The order of these combinations was randomized. An example of such bead-on-plate experiments is shown in Figure 4.1. It is important to note that for some of the treatments metal deposition was impossible to perform, for example, those with low laser power and high traverse speed because insuficient melting ocurred. For those in which metal deposition was possible, only one run of each treatment was made.

A second experiment was performed in the same way, to investigate the performance of the process with lower traverse speeds, around 200 mm/min, and with middle-range laser power, for these conditions gave good results during the first experiment i.e. straight beads with more consistent deposition. The parameters were:

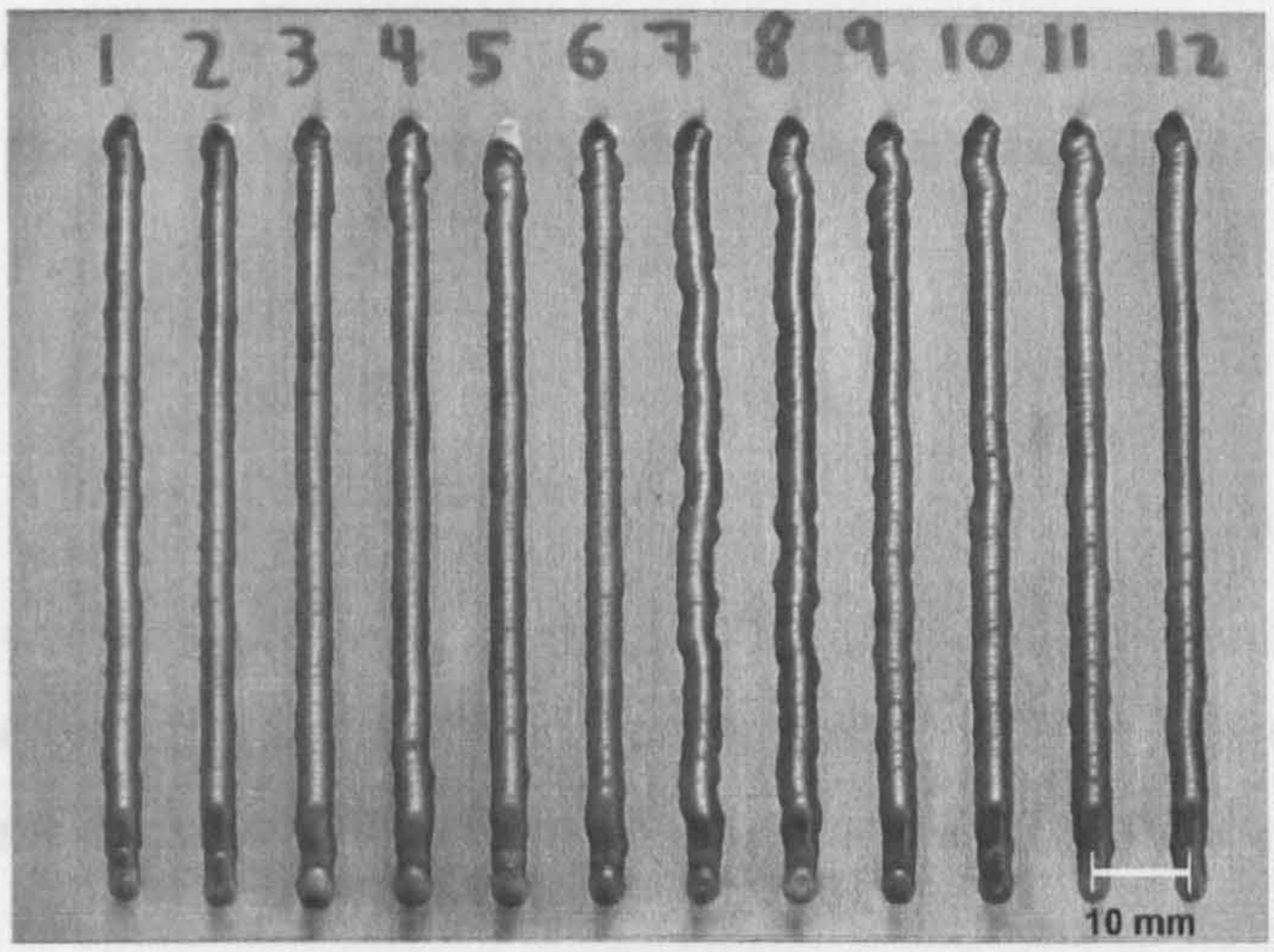

Figure 4.1: Bead-on-plate runs

Laser power: 1400 – 1500 – 1600 W

Traverse speed: 150 – 200 – 250 mm/min

Wire feed rate: 0.6 – 0.8 – 1.0 – 1.2 – 1.4 – 1.6 – 1.8 – 2.0 m/min

4.1.2 Bead-on-plate Deposition Inside Inert Gas Chamber

The third and final bead-on-plate experiment was performed inside the inert-gas enclosure, with the setup described in section 3.1.7, with the WF200DC wire feeder. The objectives of this experiment were:

- To define a process window for metal deposition with stainless steel 308LSi inside an argon atmosphere
- To analyse the influence of the parameters on the bead geometry (width and height).

This experiment was planned with the DOE methodology. A factorial design was selected in order to be able to analyse possible interactions and also possible non-

linear relations between the factors and the response variables. The control factors were again laser power, traverse speed and wire feeder rate. The levels were:

Laser power: 1700 – 1850 – 2000 W
Traverse speed: 175 – 200 – 225 – 250 mm/min
Wire feed rate: 0.8 – 1.0 – 1.2 m/min

Three replicates were made, giving a total of 108 beads, which were deposited in random order. The argon flow inside the enclosure was 30 L/min. The other parameters were kept the same as in the experiment described in section 4.1.1.

4.2 Effects of the Main Factors on the Process

It is widely accepted that the most important factors for laser metal deposition are: laser beam size , laser power, traverse speed and wire (or powder) feed rate [1, 60, 68, 83]. It is essential to realise that these factors have to be in the right combination in order to achieve a stable and reliable process. There are other process conditions that are also crucial to achieve good quality deposition and those will be explained later.

4.2.1 Effects of Laser Power, Traverse Speed and Wire Feed Rate

The function of the laser beam is to provide enough energy at a sufficient rate (power) to create and maintain a wide enough melt pool and to melt the wire that is fed in. The laser beam diameter should be selected according to the desired size for the melt pool. The laser power has to be selected according to the material used, the combination of traverse speed and wire feed rate and the process conditions that affect the heat flow such as the geometry and the temperature of the workpiece.

The traverse speed is a vital factor in wire metal deposition for it controls the time that the substrate interacts with the laser beam. This interaction time must be enough to allow the creation of a wide enough melt pool. When an excessively fast traverse speed is used, this interaction may be too short, so that the substrate may not get sufficient energy and time to form a uniform wide enough melt pool, leading to an unstable process. Conversely, too low traverse speed will promote the formation of wider/higher beads and will limit the maximum amount of wire that can be fed into the melt pool for a stable process (for a given laser power). In this experiment, using a wire feed rate of 1.2 m/min and a laser power of 1700 W, beads were successfully deposited at a traverse speed of 225 mm/min, whereas conditions of oscillations and severe stubbing occurred at 175 mm/min as illustrated in Figure 4.2 (region 5).

The wire feed rate also plays an important role in the metal deposition process. Too low wire feed rate (for a given laser power and traverse speed) would cause the wire to melt before it reaches the melt pool, i.e. it will start dripping instead of depositing the wire into the melt pool (see Figure 4.2, region 1). Conversely, too high wire feed rate (for a given laser power and traverse speed) would produce a wavy bead. This occurs because too much wire is going into the melt pool, so that the wire struggles to build-up a higher and wider bead. The wire hits the material that has been already deposited and is forced to move sidewise (Figure 4.2, region 5).

4.2.2 Process Window

The experiment performed inside the inert gas chamber (described in section 4.1.2) was utilized to define a process window for bead-on-plate laser metal deposition of stainless steel 308LSi wire. In order to accommodate different traverse speeds in the same graph, the process factors have been converted to "energy per unit length" (J/mm) and "deposited volume per unit length" (mm^3/mm) in the following way:

$$\text{Energy Per Unit Length} = \frac{\text{Laser Power}}{\text{Traverse Speed}}$$

$$\text{Dep. Volume Per Unit Length} = \frac{\text{Cross Section Area of Wire} \times \text{Wire Feed Rate}}{\text{Traverse Speed}}$$

The process window is shown in Figure 4.2. It illustrates the transition from dripping conditions to smooth metal deposition to stubbing/oscillating and to waving conditions. The traverse speed is indicated by the different shapes in the graph.

This process window is valid for 1.2 mm diameter wire, with the wire feeder nozzle aimed at the centre of the melt pool. That is, the wire tip is positioned at the centre of the same spot where the laser hits the substrate. If the alignment wire tip is moved towards the front of the melt pool, the process window would be expected to move towards the left due to shorter interaction time (the influence of the wire alignment is explained in section 4.4.1).

As shown in Figure 4.2, process conditions in regions 6 and 7 are likely to produce wavy beads, which seem to be the result of combining high traverse speeds and relatively low wire feed rates.

The formation of wave-like beads was previously reported by Hung and Lin [84] in laser cladding of tubes with wire feeding. In their process, the wire was fed horizontally, tangentially to the surface of the tube, and the laser aimed on the wire tip. They observed that an increment on the speed of the substrate (tangential speed of the tube) led to thiner beads, i.e. lower height; and a further increment resulted in the formation of thin wave-like beads. They developed a mathematical model of the system, and the analysis revealed a lack of heating of the substrate which caused lack of melting.

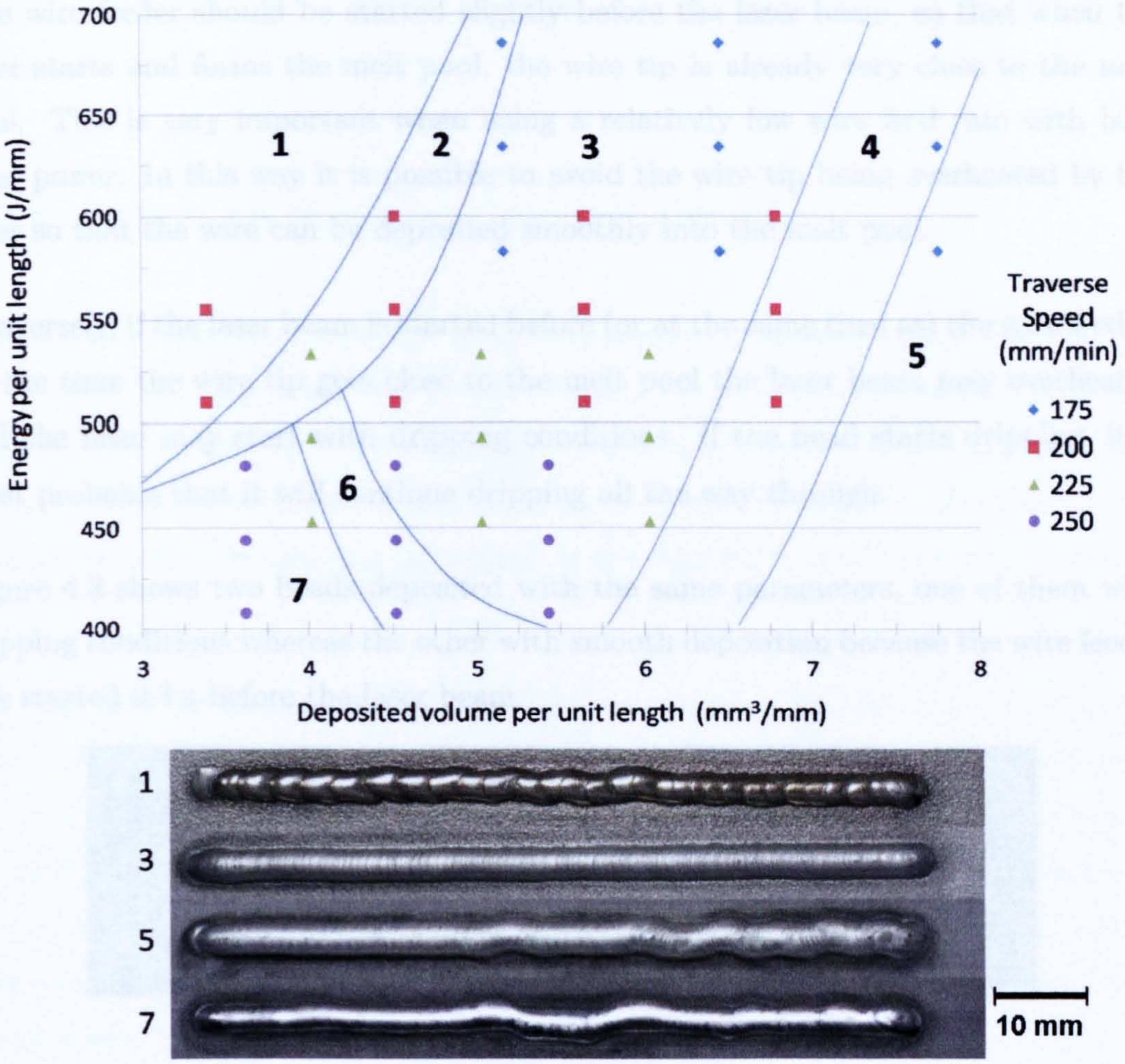

Figure 4.2: Process window

(1) Droplets formation. (2) Droplets formation may occur. (3) Smooth metal deposition. (4) Stubbing may occur. (5) Stubbing and oscillations. (6) Wavy beads may occur. (7) Wavy beads.

Region "2" of the process window, i.e. the area in which dripping conditions may occur, depends partly on the way the bead is started. At the beginning, the wire tip is 10 mm away from the zone of interaction between the laser and the workpiece (where the melt pool will be formed), and it will take some time to reach this zone, depending on the wire feeding rate.

The wire feeder should be started slightly before the laser beam, so that when the laser starts and forms the melt pool, the wire tip is already very close to the melt pool. This is very important when using a relatively low wire feed rate with high laser power. In this way it is possible to avoid the wire tip being overheated by the laser so that the wire can be deposited smoothly into the melt pool.

Conversely, if the laser beam is started before (or at the same time as) the wire feeder, by the time the wire tip gets close to the melt pool the laser beam may overheat it and the bead may start with dripping conditions. If the bead starts dripping, it is most probable that it will continue dripping all the way through.

Figure 4.3 shows two beads deposited with the same parameters, one of them with dripping conditions whereas the other with smooth deposition because the wire feeder was started 0.3 s before the laser beam.

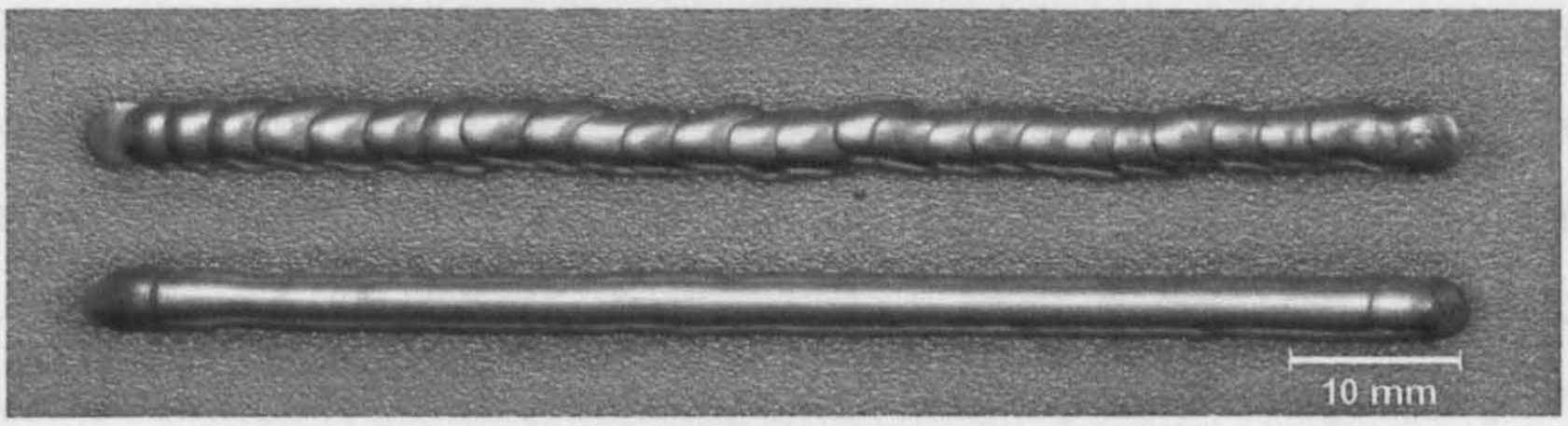

Figure 4.3: Influence of the bead start conditions
Beads deposited with laser power = 1850 W, traverse speed = 200 mm/min, wire feed rate = 0.8 m/min. Top: dripping conditions due to the wire feed starting at the same time than the laser. Bottom: smooth deposition due to the wire feed starting 0.3 s before the laser.

It is important to mention that, when depositing multi-layered structures (such as walls), after a few layers have been deposited, lower energy per unit length (i.e. lower laser power) is required due to the higher temperature of the workpiece and also to the lower heat conduction. This reduction in the heat conduction is due partly to the increase in the temperature of the workpiece; so that the temperature gradient is lower and the heat conduction is thus lower. Another reason is that the geometry may

produce a change in the heat flow mode from three-dimensional to bi-dimensional, as in the case of single-bead walls.

4.2.3 Influence of Parameters on Porosity

Porosity is an important problem in metal deposition processes. There are different types of porosity [70], one is due to lack of fusion during the metal deposition process and is caused mainly by the combination of parameters used [76], that leads to lack of laser power and/or excess in the material feed (wire or powder). Another type of porosity is caused by gas that is trapped in the deposition and is not able to escape [70].

Some samples in the first two experiments were affected by lack-of-fusion porosity, as it is illustrated in Figure 4.4. It is important to note that some non-melted areas are present in the microstructure of the longitudinal section, showing the lack of fusion during the metal deposition process. In this case the combination of high wire feed rate, relatively high traverse speed and low laser power lead to lack of fusion. However, when a right combination of parameters was used, no porosity was found in the beads (they were analysed through optical microscopy).

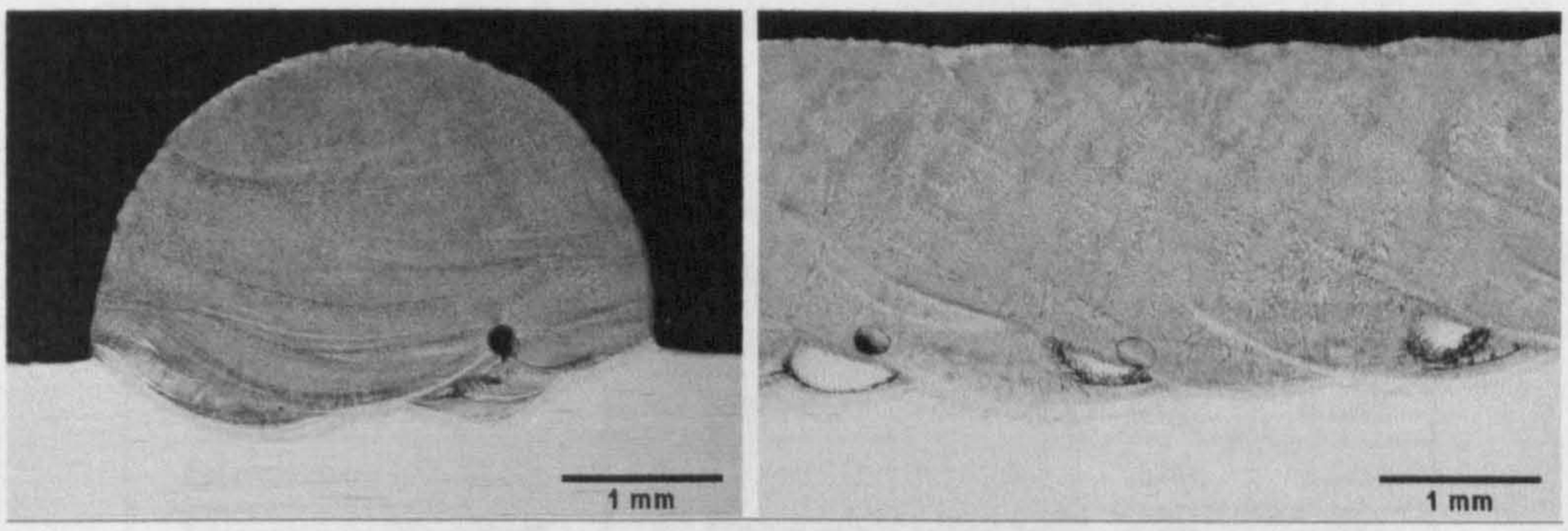

Figure 4.4: Lack-of-fusion porosity due to inadequate parameters
Transversal (left) and longitudinal (right) sections of a deposited bead.
Laser power = 1600 W. Traverse speed = 250 mm/min. Wire feed rate = 1.8 m/min

4.3 Effects of the Main Factors on Bead Geometry

This section deals with the effects of the parameters on the bead geometry (width and height). This study was done on the experiment described in section 4.1.2 i.e. the process was performed inside the argon chamber. However, due to the fact that a few of the beads deposited with a traverse speed of 250 mm/min were wavy, this speed was not considered for the analysis. The analysis was done with traverse speeds of 175, 200 and 225 mm/min, giving a total of 81 beads. The means and standard deviations of the bead height and width are provided in appendix C.

4.3.1 Effects on Bead Height

One of the important advantages of a factorial design is that it is possible to analyse not only the main effects of the factors but also whether their interactions are significant.

The result of the ANOVA for the bead height, including the interactions between the factors, is shown in Table 4.1.

Table 4.1: Analysis of variance for height (factors and interactions)

Source	DF	SS	MS	F	P
Laser Power (LP)	2	0.02883	0.01441	8.76	0.001
Traverse Speed (TS)	2	0.94903	0.47451	288.34	< 0.001
Wire Feed Rate (WFR)	2	3.55434	1.77717	1079.90	< 0.001
Interaction LP TS	4	0.00425	0.00106	0.65	0.632
Interaction LP WFR	4	0.01579	0.00395	2.40	0.061
Interaction TS WFR	4	0.03839	0.00960	5.83	0.001
Interaction LP TS WFR	8	0.00453	0.00057	0.34	0.944
Error	54	0.08887	0.00165		
Total	80	4.68402			
S = 0.0405670		$R^2 = 0.9810$		R^2(adj) = 0.9719	

From Table 4.1 it is easy to identify the most important factors: those which have a bigger F-value (or a smaller P-value). With a significance level of $\alpha = 0.99$ a factor is significant if its P-value is equal or smaller than 0.01.

From Table 4.1 the most important factors are: wire feed rate, traverse speed, laser power and the interaction between traverse speed and wire feed rate. The other interactions are not significant.

It is also possible to analyse graphically the interactions of the factors. An interaction occurs when "the difference in response between the levels of one factor is not the same at all levels of the other factors" [85]. Graphically, an interaction can be identified when the lines are not parallel in the interaction plot.

Figure 4.5 shows the interaction plot for bead height. It can be seen that, in the plots of the interaction between traverse speed and wire feed rate, the lines are fairly parallel, indicating that the interaction is low. Even more, the F-value of this interaction is smaller than that of the main factors. For these reasons that interaction is not going to be considered, and the analysis will focus on the three main factors.

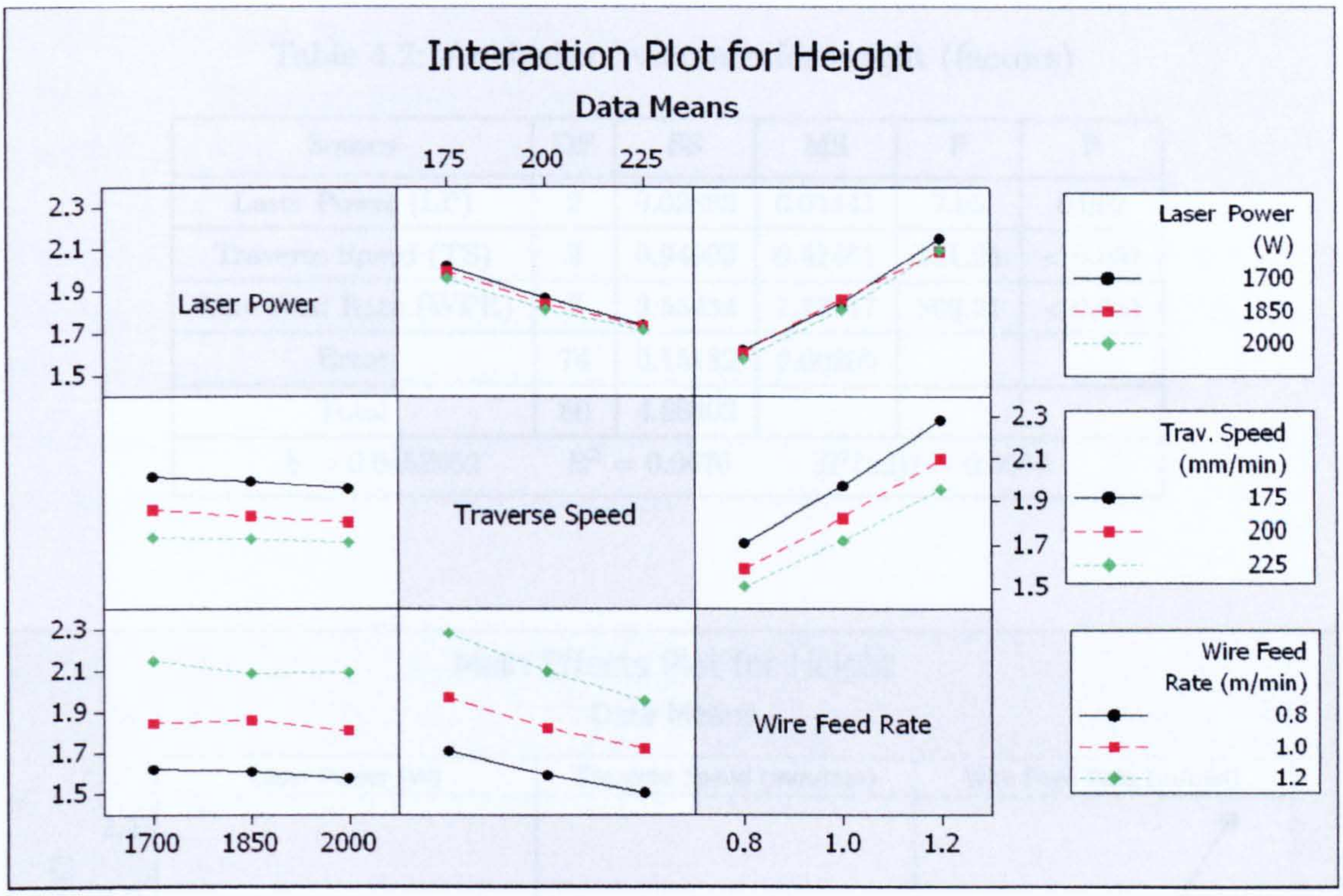

Figure 4.5: Interaction plot for bead height

A second ANOVA can be run considering only the significant factors. The ANOVA table for the three main factors (without interactions) is shown in Table 4.2. For these experimental conditions, the most significant factor is the wire feed rate, followed by the traverse speed. Laser power has very little influence on bead height compared to the other two factors. The residual plots are presented in appendix D. Figure 4.6 shows the main effects of the three control factors. It can be seen that:

- An increase in Wire Feed Rate will increase the height
- An increase in Traverse Speed will decrease the height
- An increase in Laser Power will slightly decrease the height

Table 4.2: Analysis of variance for height (factors)

Source	DF	SS	MS	F	P
Laser Power (LP)	2	0.02883	0.01441	7.03	0.002
Traverse Speed (TS)	2	0.94903	0.47451	231.28	< 0.001
Wire Feed Rate (WFR)	2	3.55434	1.77717	866.21	< 0.001
Error	74	0.15182	0.00205		
Total	80	4.68402			
$S = 0.0452952$		$R^2 = 0.9676$		$R^2(\text{adj}) = 0.9650$	

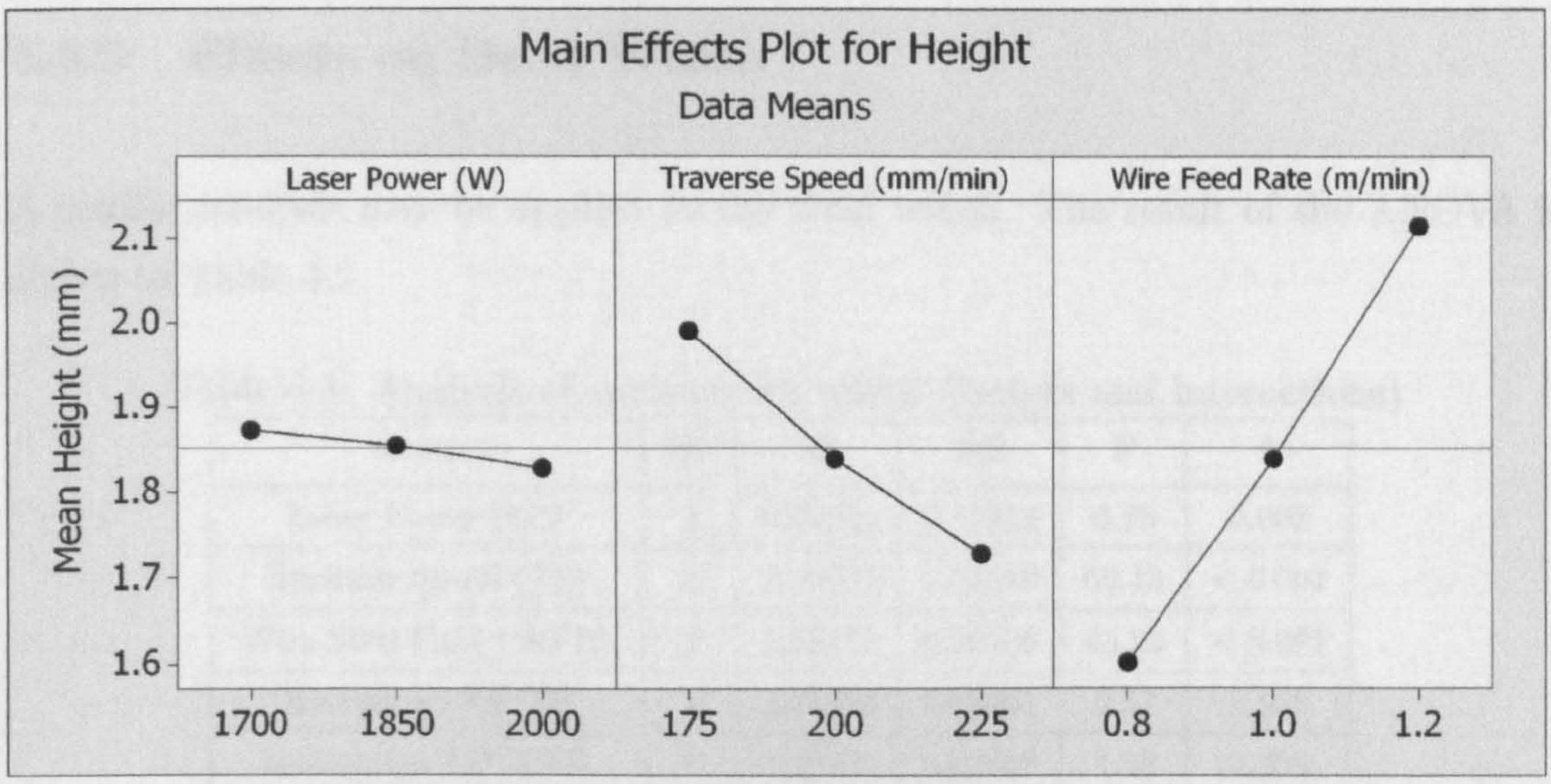

Figure 4.6: Main effects plot for bead height

It is also possible to calculate a regression equation for the height, using the method of least squares. The result of the equation is:

$$Height = 1.91 - 0.000153\ LP - 0.00528\ TS + 1.28\ WFR$$

Where

LP	=	Laser Power	(W)
TS	=	Traverse Speed	(mm/min)
WFR	=	Wire Feed Rate	(m/min)

The R^2 value for this regression model is 0.9640. This value can be regarded as the fraction of the variability in the data that can be "explained" by the ANOVA model [85]. It indicates that there is a very good correlation between the factors and the bead height. This way it is possible to estimate the height value for a particular combination of parameters (within the range used in this experiment).

4.3.2 Effects on Bead Width

A similar analysis may be applied to the bead width. The result of the ANOVA is shown in Table 4.3.

Table 4.3: Analysis of variance for width (factors and interactions)

Source	DF	SS	MS	F	P
Laser Power (LP)	2	0.22829	0.11414	6.73	0.002
Traverse Speed (TS)	2	2.04032	1.02016	60.13	< 0.001
Wire Feed Rate (WFR)	2	1.53472	0.76736	45.23	< 0.001
Interaction LP TS	4	0.03846	0.00961	0.57	0.688
Interaction LP WFR	4	0.10390	0.02598	1.53	0.206
Interaction TS WFR	4	0.05236	0.01309	0.77	0.548
Interaction LP TS WFR	8	0.11977	0.01497	0.88	0.537
Error	54	0.91613	0.01697		
Total	80	5.03396			
S = 0.130251	$R^2 = 0.8180$		R^2(adj) = 0.7304		

From this initial analysis it is possible to conclude that the most significant factors are: Laser Power, Traverse Speed and Wire Feed rate; and that the interactions between the factors are not important.

It can be seen that, within the parameters used in this experiment, the most influential

factor for the width of the bead is the Traverse Speed; the second factor is the Wire Feed Rate, and the third one is Laser Power (which is far less influential than the previous two).

As is can be seen in Figure 4.7, in this case most of the lines are fairly parallel. There is a small interaction between Wire Feed Rate and Laser Power; however, it is not a significant one (P-value = 0.206) and can be ignored.

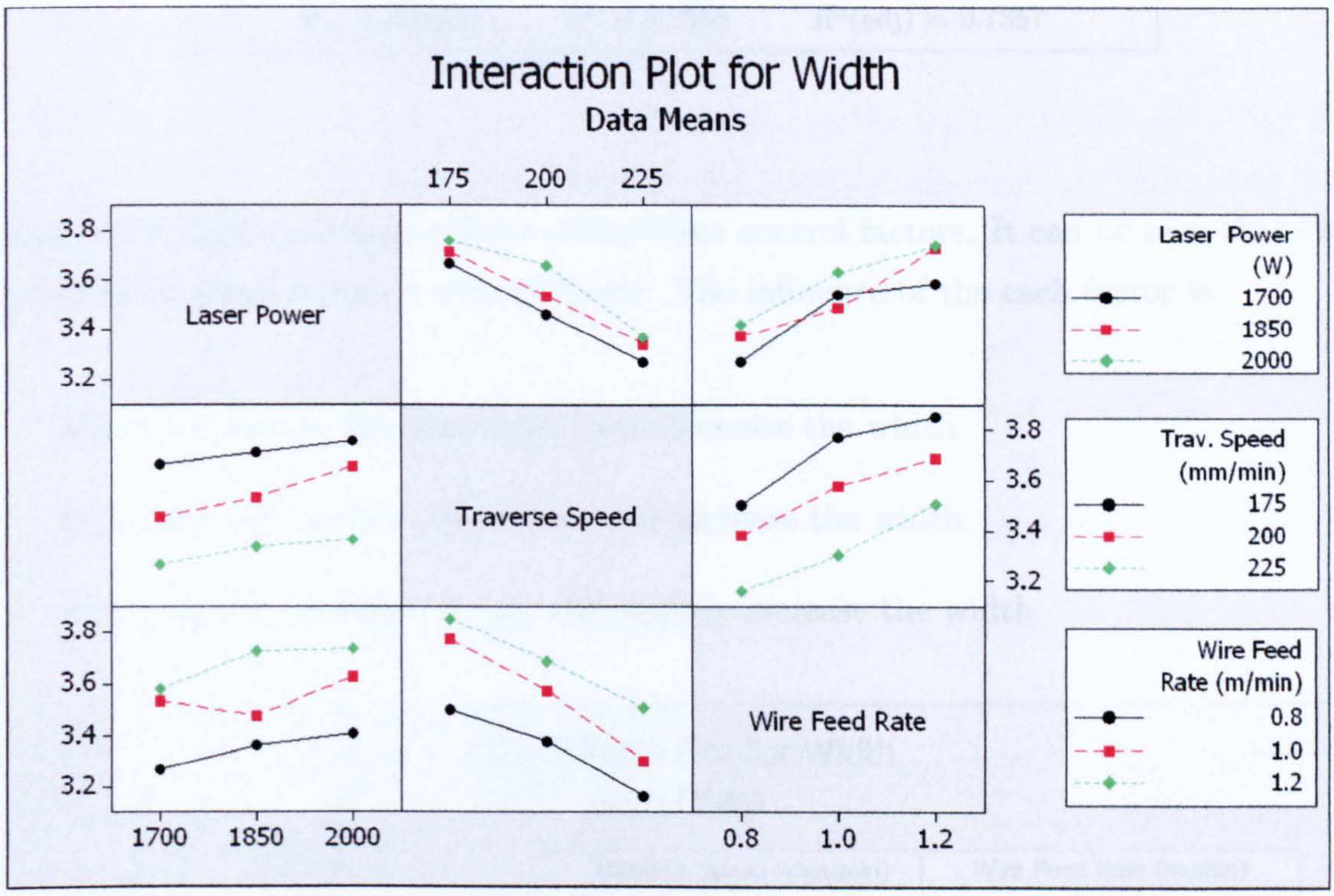

Figure 4.7: Interaction plot for bead width

A second ANOVA can be run considering only the significant factors. The result is shown in Table 4.4. The residual plots are presented in appendix D and it can be seen there that the ANOVA assumptions have not been violated.

Table 4.4: Analysis of variance for width (factors)

Source	DF	SS	MS	F	P
Laser Power (LP)	2	0.22829	0.11414	6.86	0.002
Traverse Speed (TS)	2	2.04032	1.02016	61.34	< 0.001
Wire Feed Rate (WFR)	2	1.53472	0.76736	46.14	< 0.001
Error	74	1.23063	0.01663		
Total	80	5.03396			
S = 0.128958	$R^2 = 0.7555$		R^2(adj) = 0.7357		

Figure 4.8 shows the main effects of the three control factors. It can be seen that the plots of all three factors are fairly linear. The influence of the each factor is:

- An increase in Traverse Speed will decrease the width
- An increase in Wire Feed Rate will increase the width
- An increase in Laser Power will slightly increase the width

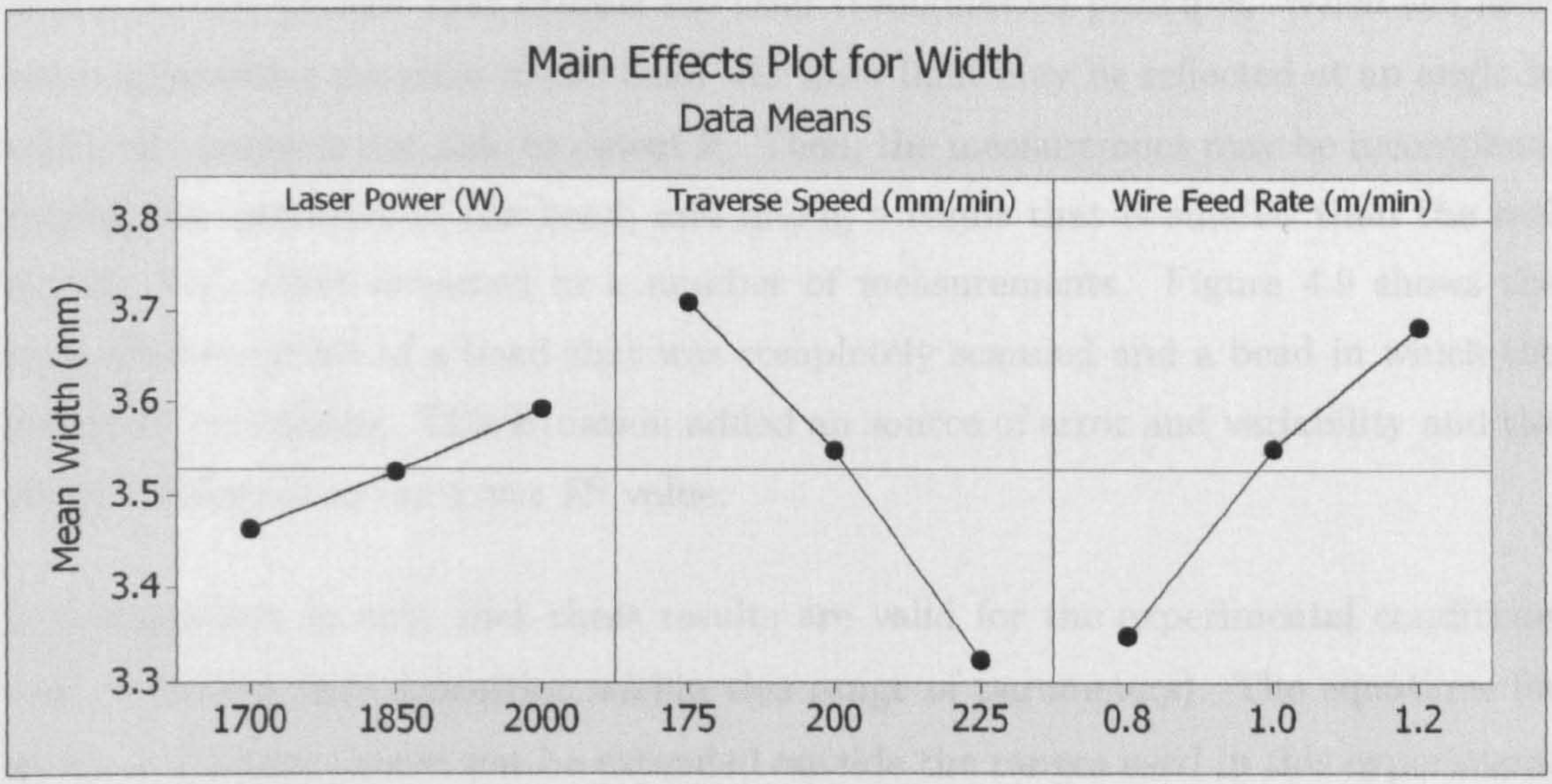

Figure 4.8: Main effects plot for bead width

A regression equation was also calculated for the bead width:

$$Width = 3.437 + 0.000433\ LP - 0.00774\ TS + 0.837\ WFR$$

Where

LP	=	Laser Power	(W)
TS	=	Traverse Speed	(mm/min)
WFR	=	Wire Feed Rate	(m/min)

The beam diameter has a very strong influence on the melt pool size and thus on the bead width. It can be noticed that, in the equation, the constant term (3.437) is close to the beam diameter.

With this equation it is possible to get an approximation of the width for a particular combination of parameters. The R^2 value for this empirical model is 0.748. The R^2 value of the width is lower than that of the height (0.9640). This indicates a lower correlation, which can be explained by the error in the measurement of the width.

As explained in section 3.3.1 the measurement of the bead geometry was performed with a surface profiler that utilizes the laser triangulation principle. When the laser beam approaches the sides of the bead, the laser light may be reflected at an angle in which the sensor is not able to detect it. Then, the measurement may be incomplete, missing the extremes of the bead, and giving a result that is smaller than the real width. This effect occurred in a number of measurements. Figure 4.9 shows the cross section profile of a bead that was completely scanned and a bead in which the extremes are missing. This situation added an source of error and variability and the effect is reflected in the lower R^2 value.

It is important to note that these results are valid for the experimental conditions used (bead-on-plate deposition within this range of parameters). The equations for width and height should not be extended outside the ranges used in this experiment. For practical applications, it is vital to ensure that the combination of factors is inside the process window (show in Figure 4.2).

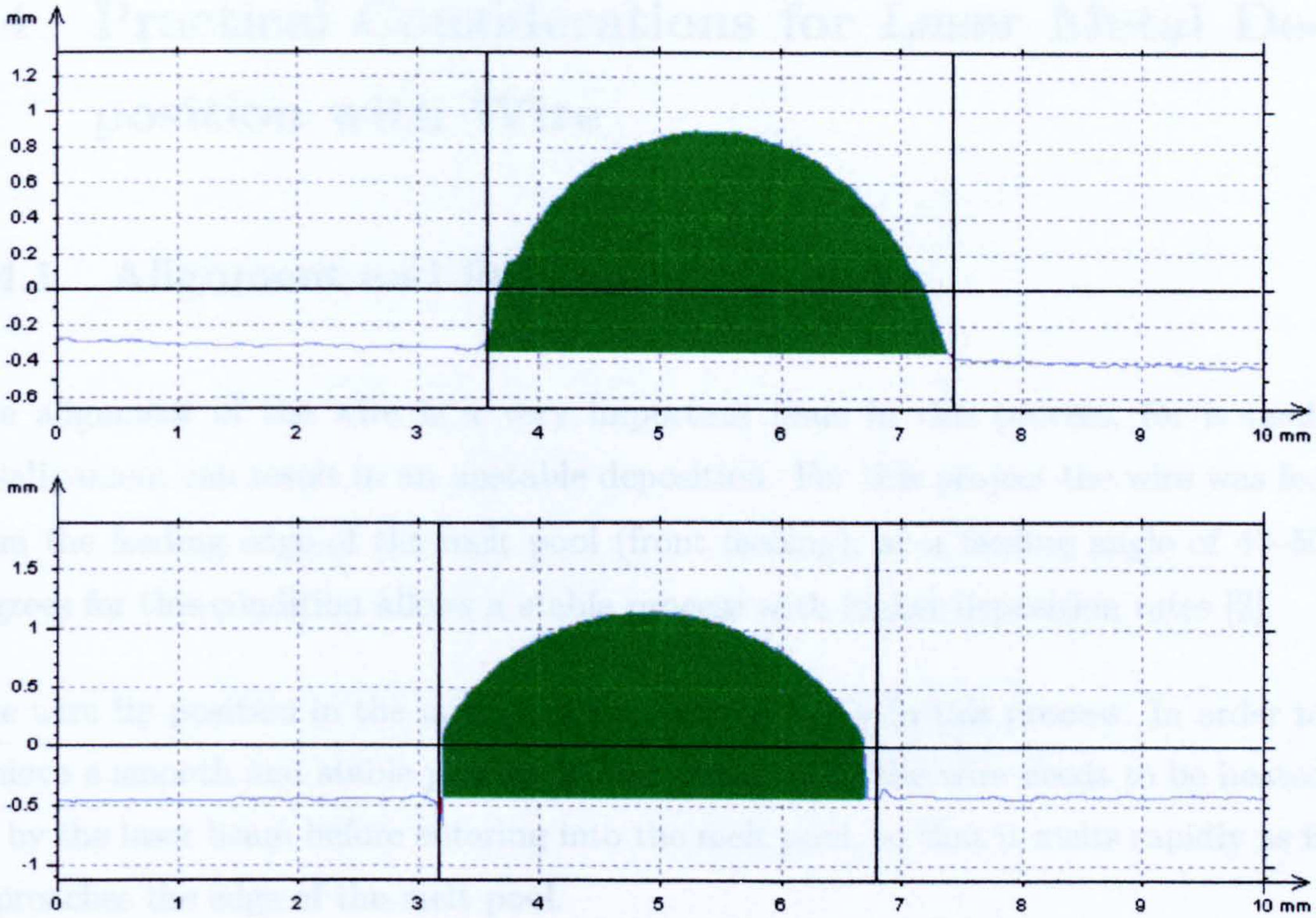

Figure 4.9: Complete (top) and incomplete (bottom) cross section bead profiles

For different process conditions, the influence of the parameters on the bead geometry will be different. It was observed that, when depositing multi-layered structures such as walls and cylinders, the laser power has an important influence on the bead geometry. Higher laser power produces a lower and wider bead. Conversely, a reduction in laser power produces a higher and narrower bead.

4.4 Practical Considerations for Laser Metal Deposition with Wire

4.4.1 Alignment and Position of the Wire

The alignment of the wire is a very important issue in this process, for a small misalignment can result in an unstable deposition. For this project the wire was fed from the leading edge of the melt pool (front feeding), at a feeding angle of 40–50 degrees for this condition allows a stable process with higher deposition rates [2].

The wire tip position in the melt pool is a critical factor in this process. In order to achieve a smooth and stable process, a key issue is that the wire needs to be heated up by the laser beam before entering into the melt pool, so that it melts rapidly as it approaches the edge of the melt pool.

As previously reported by Heralić [8] , if it stays too long under the laser beam, it will melt before reaching the weld pool and will start dripping. If it stays too little under the laser beam, it will be too "cold" and it may not melt smoothly; the wire tip may oscillate and/or hit the solid metal at the bottom of the melt pool ("stubbing"). Both situations are undesirable because they lead to an unstable process.

The optimum positioning for the wire tip depends on how long it needs to be under the laser beam for a particular setting of parameters such as laser power and feeding angle. Following this logic, a thin wire will need a short time to heat up, so that it does not melt before reaching the melt pool. It may be more convenient to be placed close to the front of the melt pool. In contrast, a thicker wire will need more time to heat up, so it may be more convenient to place it towards the centre of the melt pool.

The wire feed rate also plays an important role. A fast wire feed rate means that a segment of the wire will spend less time under the laser beam; thus, the wire may be positioned towards the centre of the melt pool. Conversely, a slow wire feed rate

means that the wire spends more time under the laser, so it may be more convenient to place the wire close to the front of the melt pool.

In this project the wire used has a diameter of 1.2 mm, and the feed rate was between 0.8 to 1.2 m/min. It was found that best deposition is achieved when aiming the wire to the centre of the melt pool. If the wire was aligned closer to the front of the melt pool, it started to oscillate. If it was aligned at the back of the melt pool, it started dripping.

For other systems it may be more convenient to align the wire closer to the front of the melt pool. Syed et al. [6] utilized a 0.8 mm diameter wire for diode laser metal deposition and they reported that good results were obtained when positioning the wire at the leading point of the melt pool, whereas a poor clad was obtained when positioning the wire at the centre or back of the melt pool.

4.4.2 Wear of Wire Feeder Nozzle

The wire feeder nozzle will eventually wear out, especially at its tip. This will cause the wire to have some play at the tip of the nozzle. This issue can be identified when the wire tip starts oscillating even when good metal deposition parameters are used. When the nozzle gets severely worn, these oscillations become wider and lead to an unstable process. Figure 4.10 shows the oscillations caused by a worn nozzle, seen from the camera that is coaxial to the laser beam.

Another problem regarding the wire feeder nozzle is that its fixture may eventually get a bit loose, and this could cause some misalignment of the nozzle. For this reason it is important to check it is tight when doing the setup for metal deposition.

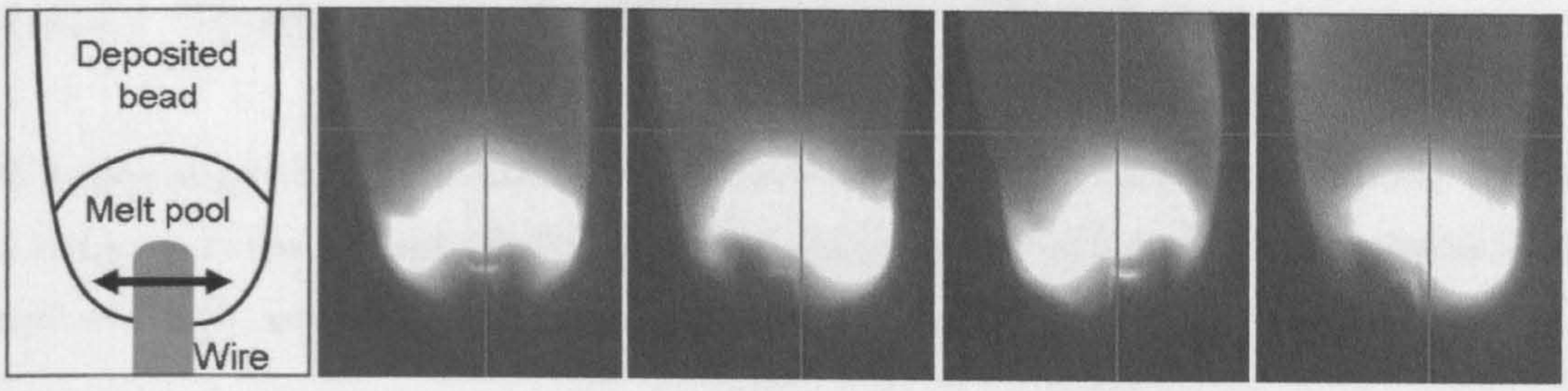

Figure 4.10: Wire oscillations due to deteriorated wire feeder nozzle
Top view from camera coaxial to laser beam.

4.4.3 Protection From Oxidation Inside Inert-gas Chamber

When the inert gas chamber is used it is important to ensure that the gas flows into the chamber for enough time to purge out the air inside it before the metal deposition starts. In the system used in this project, it takes about 5 minutes with an argon flow rate of 30 L/min.

During the metal deposition process it is important to monitor the condition of the chamber. Due to the high temperatures inside it, the plastic chamber may deteriorate and loose its properties. A few minutes later it may even get a small hole which will allow some oxygen to enter into the enclosure, causing some oxidation in the metal deposition process.

Oxygen inside the enclosure causes a number of problems. Regarding the material, oxidation may affect significantly the properties of the material, especially those that are more sensitive to it such as titanium alloys.

Regarding the process, if a layer gets oxidized, then the next layer will require higher laser power to melt the oxides and the metal. If the temperature controller is used, the laser power will be limited (maximum and minimum) to a particular setting; thus, if the maximum power limit is below the power required to melt the oxides and the metal, the wire will struggle to melt, causing a non-smooth process.

4.4.4 Temperature Inside Inert-gas Chamber

It is also important to monitor the temperature inside the enclosure chamber; so that it does not exceed about 150 °C. Very high temperature will damage the optical filters and will also deteriorate the plastic enclosure faster.

Damage in the optical filters will affect their properties such as cut-on wavelength and its slope. This will have an effect on the temperature reading of the pyrometers. For example, the ThorLabs optical filter was exposed to temperatures higher than its maximum working temperature, then it started to deteriorate and the melt pool temperature reading was lower than expected, causing the controller to increase the laser power in excess (the description of the optical filters is given in section 5.3).

4.4.5 Change in Laser Focal Distance

An issue of the laser system is that when the focusing lens gets hot it changes the focal length. As the lens gets hot, the focus distance gets shorter; thus the beam diameter at a working distance of 212 mm will get wider. Then, the melt pool may be expected to get wider as well. This focus shift in fibre laser processing was also identified by Heralić [8].

When depositing a long bead (e.g. 170 mm) it is possible to spot a small difference in the bead width at the start and the end of the bead. This difference may be due partly to the heating of the plate and partly to the change in the laser beam diameter. A study on this change of focus distance is shown in appendix B.

Chapter 5

Temperature Monitoring System for Metal Deposition

This chapter presents an analysis of the suitability and performance of different pyrometers for temperature monitoring of laser metal deposition with wire, and describes the development of a system that measures both the melt pool and workpiece (upper layer) temperatures.

5.1 Analysis of Suitable Pyrometers

Two important characteristics of pyrometers are that they are non-contact sensors and they have a fast response, in the order of milliseconds. These characteristics make them a very good option for temperature measurement of cladding or metal deposition applications.

There are different types of pyrometers, the most common being "single-colour", which means that they measure the signal in a single range of wavelengths to calculate the temperature. An alternative is the use of two-colour (ratio principle) pyrometers,

which measure the radiated energy of an object at two narrow wavelength bands; the ratio of the two energies is a function of the temperature of the object [40]. A more detailed description of the working principles, advantages and disadvantages of these pyrometers is provided in section 2.4.3.

There are basically two configurations of pyrometers:

1. Integrated electronics and optics: The electronics and optics are integrated in one piece (see Figure 5.1, left). They can normally stand maximum working temperatures of around 60 °C. For higher temperatures they would need a cooling system (air or water cooling devices are available from the pyrometer's manufacturer). They also need more space and are heavier. The advantages of these pyrometers are: they are cheaper, and there are more options to choose from (in terms of temperature ranges and wavelengths).

2. Fibre optic cable and optical head: The electronics are connected to a small optical head via a fibre optic cable (see Figure 5.1, right). They have the following advantages:

   - The optical head can stand temperatures up to 250 °C
   - The optical head is small and light, so it can be placed close to the target whereas the electronics of the sensor can be situated away from the process

Five different pyrometers and one photodiode have been tested in this project in order to analyse their suitability for temperature monitoring of laser metal deposition with wire. The aim of these experiments was to measure the temperature of the melt pool (high temperature pyrometers) and the temperature of the workpiece just few millimetres before the metal deposition (lower temperature pyrometers). The pyrometers and their characteristics are shown in Table 5.1

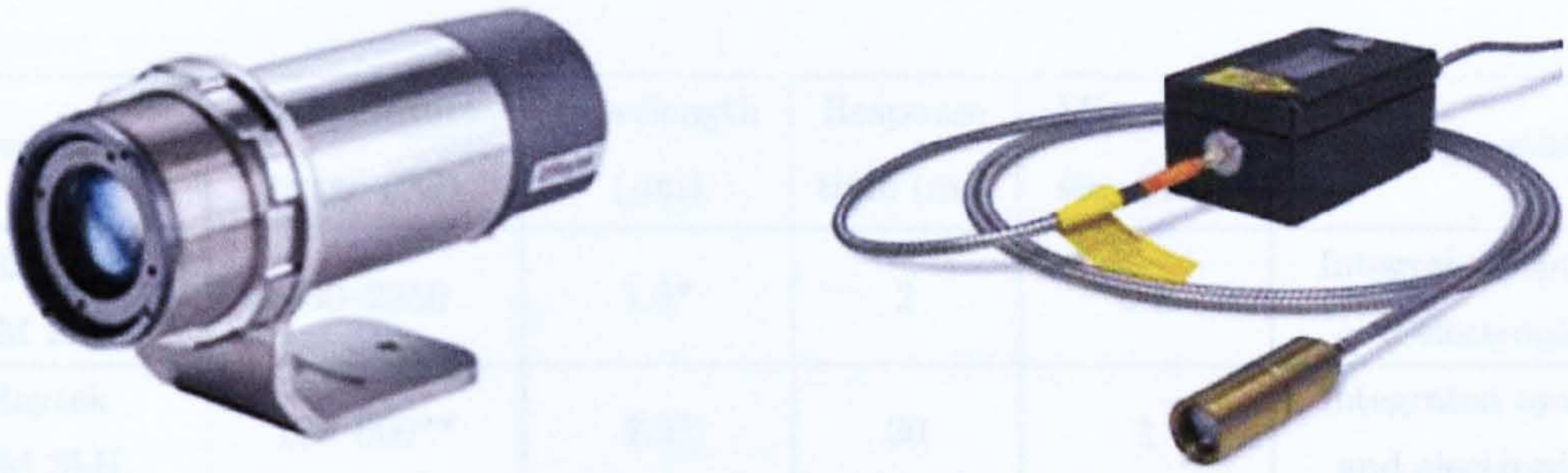

Figure 5.1: Configuration of pyrometers
Left: Integrated electronics and optics (Raytek MM series) [86].
Right: Fibre optic cable and optical head (Impac IGA 50-LOplus) [87].

These pyrometers were chosen considering the following factors:

- Wavelength of the pyrometer must be different to that of the laser (1070 nm)
- Both one-colour and two-colour pyrometers should be included in the trials
- Both configurations (integrated optics/electronics and fibre cable/optical head) should be included in the trials
- Fast response time
- Small spot size
- Adequate temperature range
- Analogue output signal

Table 5.1: Pyrometers and characteristics

Pyrometer	Temperature range (°C)	Wavelength (μm)	Response time (ms)	Min. spot size (mm)	Configuration
Raytek MM 2MH	450–2250	1.6*	2	0.5	Integrated optics and electronics
Raytek MM 3ML	100–600**	2.3*	20	1	Integrated optics and electronics
Impac IGAR 12-LO MB 22	500–2200	1.28/1.65 (two-colour)	2	1.2 (OH1) 0.45 (OH2)	Optical head and fibre optic cable
Impac IP 140-LO MB 7.5	130–750	2–2.6	1.5	3.4 (OH1) 1.1 (OH2)	Optical head and fibre optic cable
Impac IGA 50-LOplus MB 13.5	250–1350	1.45–1.8	1	1.2 (OH1) 0.45 (OH2)	Optical head and fibre optic cable
Precitec photodiode	Non-calibrated Ge photodiode	1.3–1.6	***	***	Incorporated inside cladding head, coaxial to laser

* 95% Spectral response

** The range can be extended to 50–900 °C, according to the manufacturer

*** Unknown

(OH1) Optical head type 1

(OH2) Optical head type 2

5.2 Experiments and Results

In order to measure the temperature in a continuous way, the experiments consisted of building cylinders, moving the workpiece with the rotational axis, and moving the laser head up with the Z axis as the piece was built. Figure 5.2 shows the setup of the experiment, using different pyrometers. The dimensions of the cylinders and the

process parameters were:

Diameter of cylinder (centreline):	38 mm
Height:	40–60 mm
Traverse speed:	200 mm/min
Wire feed rate:	1.4 m/min
Laser power:	Varied from 1200 to 2000 W
Step in Z:	1.9 mm
Argon flow rate:	15 L/min
Plate:	stainless steel 304, 100x100x6 mm
Wire:	stainless steel 308LSi, 1.2 mm diameter

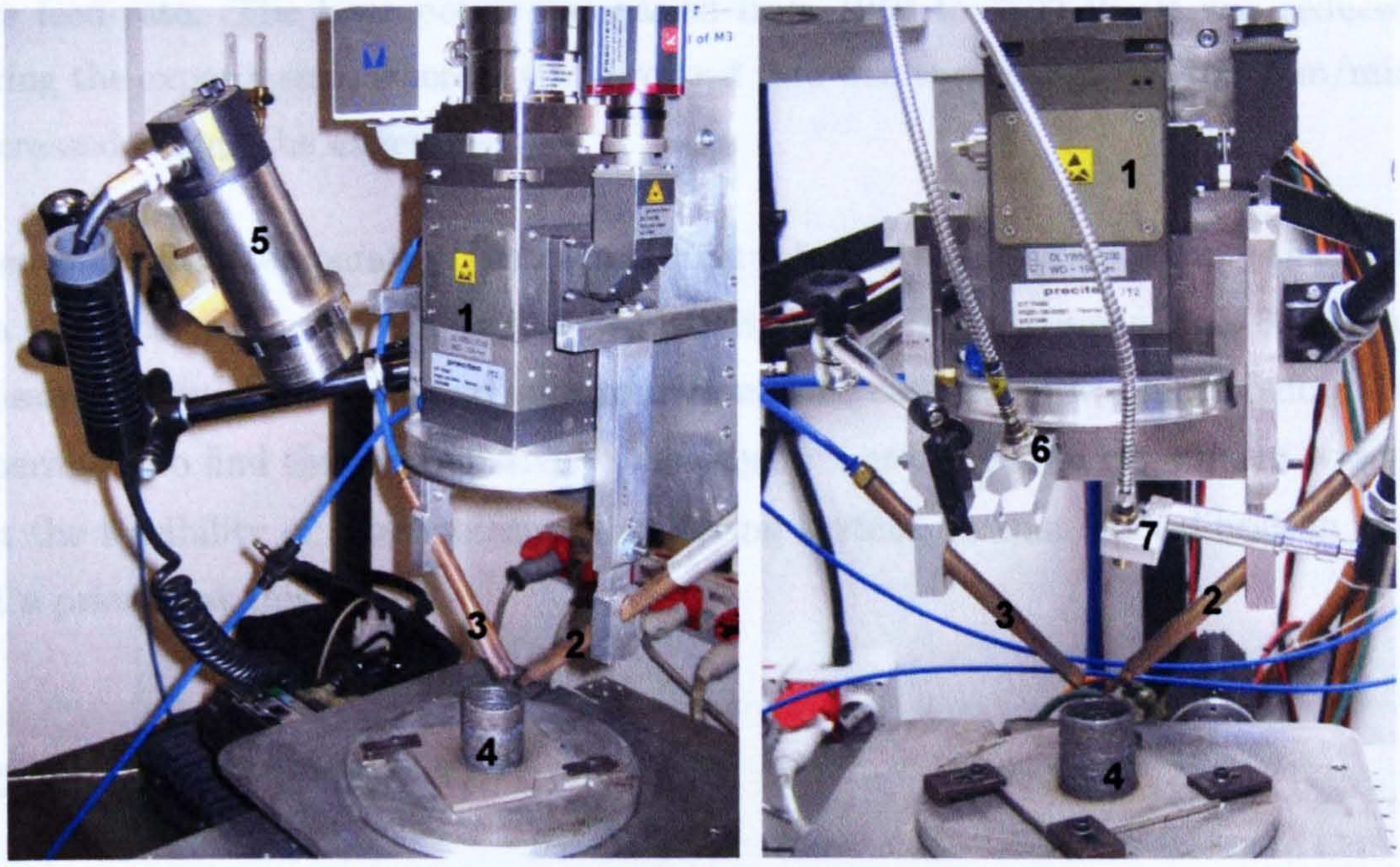

Figure 5.2: Setup of the experiments with pyrometers
(1) Laser head. (2) Wire feeder nozzle. (3) Shielding gas nozzle. (4) Workpiece. Left: (5) Pyrometer Raytek MM2 MH. Right: (6) Pyrometer Impac IGAR 12-LO. (7) Pyrometer Impac IGA 50-LO plus. The deposited cylinders have a diameter of 38 mm.

The data acquisition of the Raytek pyrometers was carried out by connecting directly the pyrometer to a computer and using Raytek's software with a sampling rate of 1 Hz. The data acquisition of the Impac pyrometers was accomplished by connecting their

analogue output signal (0–20 mA) to a data acquisition card and using LabVIEW™ to acquire and save the data with a sampling rate of 20 Hz; and the same for the Precitec photodiode, using a voltage signal of 0–10 Vdc.

5.2.1 Raytek MM 2MH

The pyrometer Raytek MM 2MH was tried first. This was a one-colour pyrometer with integrated optics and electronics (no fibre optic cable and head). The pyrometer was aimed at the melt pool and a cylinder was built, trying to keep the melt pool temperature relatively constant by means of modifying manually the laser power and wire feed rate. The laser power was varied from 1250 to 1500 W (it was reduced during the experiment), whereas the wire feed rate was varied from 1.0 to 1.6 m/min (increased during the experiment).

The result of the temperature is shown in Figure 5.3. It is important to note that this is a single-colour pyrometer, and the emissivity set in the instrument was 0.3. This emissivity, however, was just an approximation as no calibration was made before the experiment to find the real emissivity (the objective of this initial experiment was to test the feasibility of a temperature monitoring system, so that the calibration was not a priority at this stage).

5.2.2 Raytek MM 3ML

This was a one-colour pyrometer with integrated optics and electronics. The temperature range for this pyrometer is nominally 100–600 °C; however, the actual range that it can measure is 50–900 °C, according to the manufacturer.

The pyrometer was aimed at the upper layer of the cylinder, opposite the melt pool in order to monitor the temperature of the workpiece as it was being built. The measuring point is shown in Figure 5.4. A cylinder was built, trying to keep the

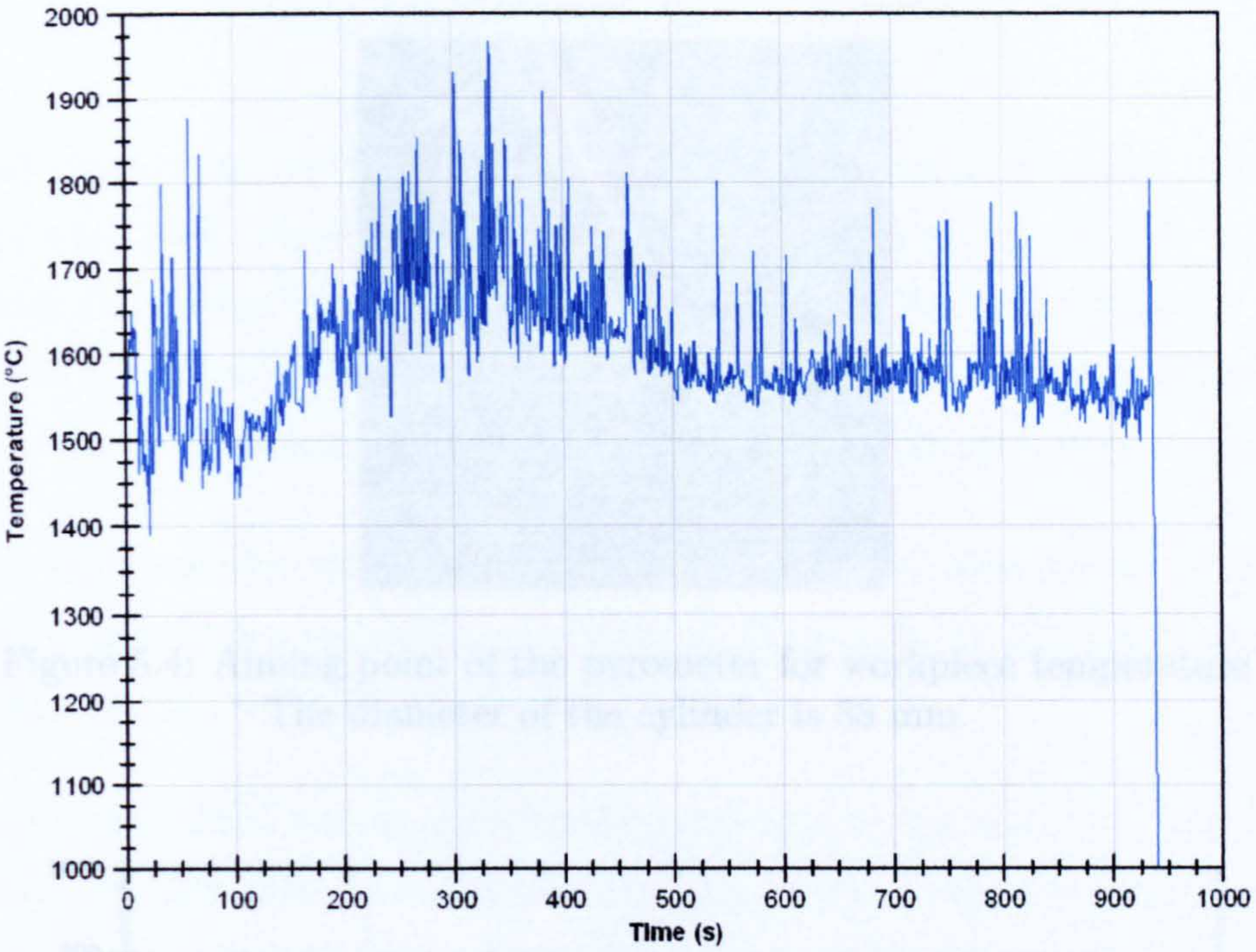

Figure 5.3: Melt pool temperature using pyrometer Raytek MM 2MH

workpiece (upper layer) temperature relatively constant by means of modifying the laser power and wire feed rate.

The emissivity set in the instrument was 0.6 (the setting was different to the one used with the Raytek MM 2MH because the pyrometers work at a different wavelength). This emissivity, however, was just an approximation as no calibration was made before the experiment to find the real emissivity. The result of the temperature is shown in Figure 5.5.

Figure 5.4: Aiming point of the pyrometer for workpiece temperature
The diameter of the cylinder is 38 mm.

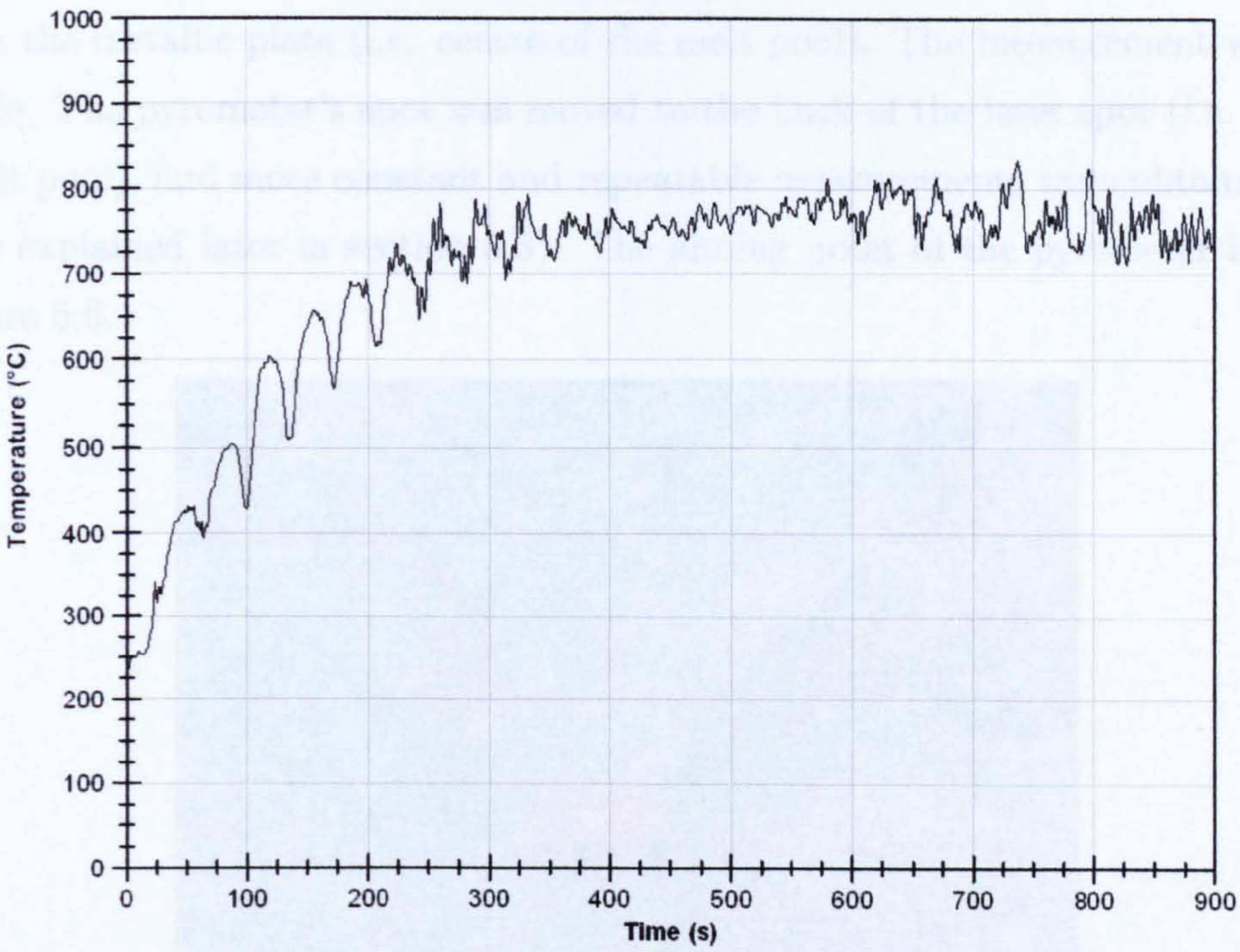

Figure 5.5: Temperature of workpiece measured with Raytek MM 3ML

5.2.3 Impac IGAR 12-LO MB 22

The next experiment was performed using the pyrometers from Impac. Three pyrometers were used: IGAR 12-LO, IP 140-LO and IGA 50-LOplus; all with fibre optic cable and optical head. The setup of the system is shown in Figure 5.2. Impac pyrometers have laser aiming and it is important to mention that in these pyrometers the size of the laser aiming spot is actually the spot size that the sensor is measuring.

IGAR 12-LO pyrometer was used to measure the melt pool temperature. It is a two-colour pyrometer with a temperature range from 500 to 2200 °C. The same experiment was performed, i.e. building stainless steel cylinders.

A problem arose when aiming the pyrometer directly to the same point of the laser spot on the metallic plate (i.e. centre of the melt pool). The measurement was very unstable. The pyrometer's spot was moved to the back of the laser spot (i.e. back of the melt pool), and more constant and repeatable measurements were obtained (this issue is explained later in section 5.3). The aiming point of the pyrometer is shown in Figure 5.6.

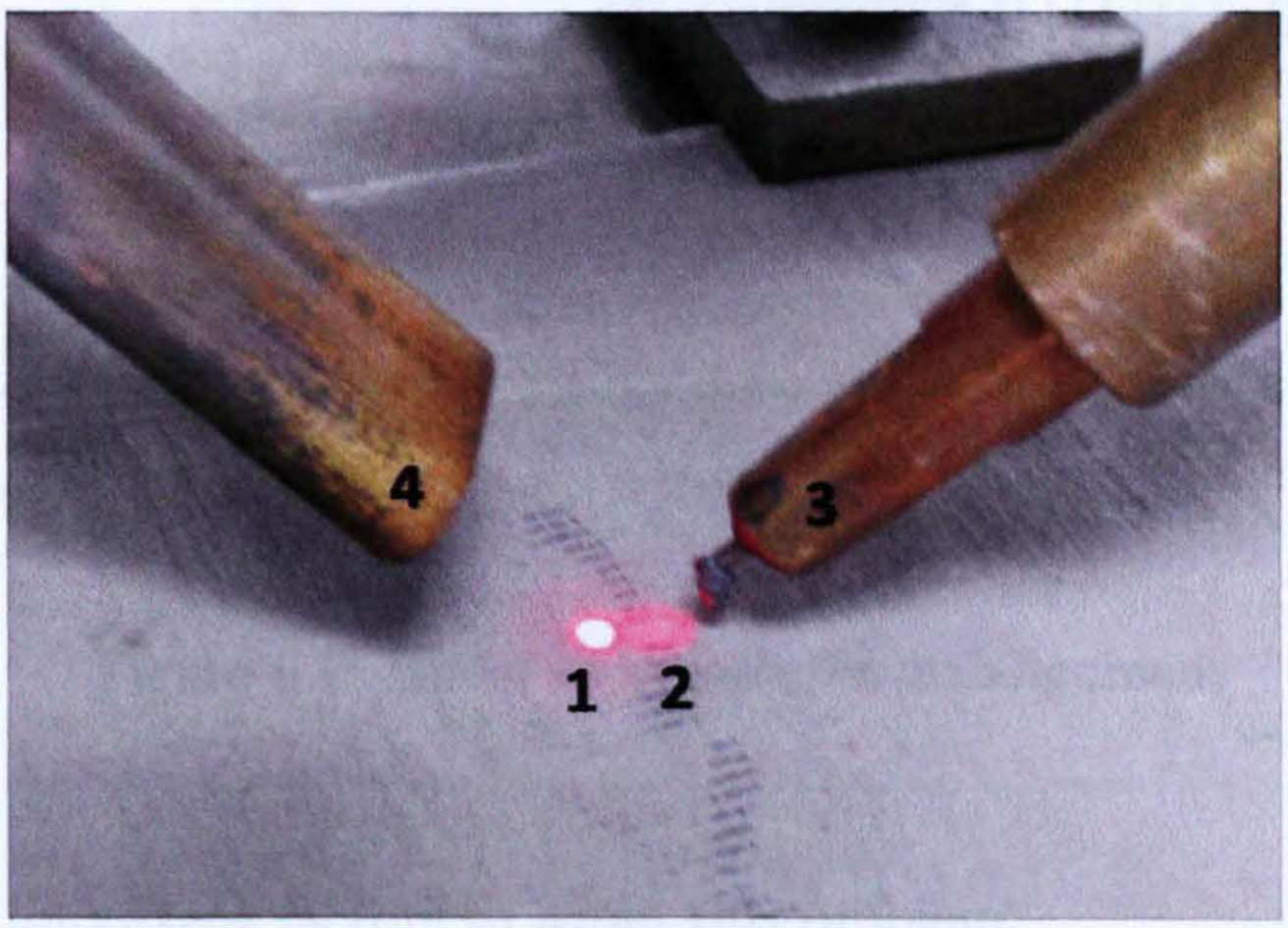

Figure 5.6: Pyrometer aiming spot for melt pool temperature measurement
(1) Pyrometer spot. (2) Laser spot. (3) Wire feeder nozzle. (4) Shielding gas nozzle.

As it can be seen in Figure 5.2, the pyrometer was at one side of the deposition line.

When depositing a multi-layer structure, if the Z step programed in the CNC machine was higher than the actual layer thickness then, after a few layers, the pyrometer aimed above the workpiece and partially missed the melt pool.

Figure 5.7 shows the temperature profile when this problem occurred. After a period with too high laser power (in this case the temperature was higher than in other cylinders due to the high power) the height of the metal deposition bead became lower and, after few layers, the pyrometer partially missed the melt pool and gave a very unstable reading.

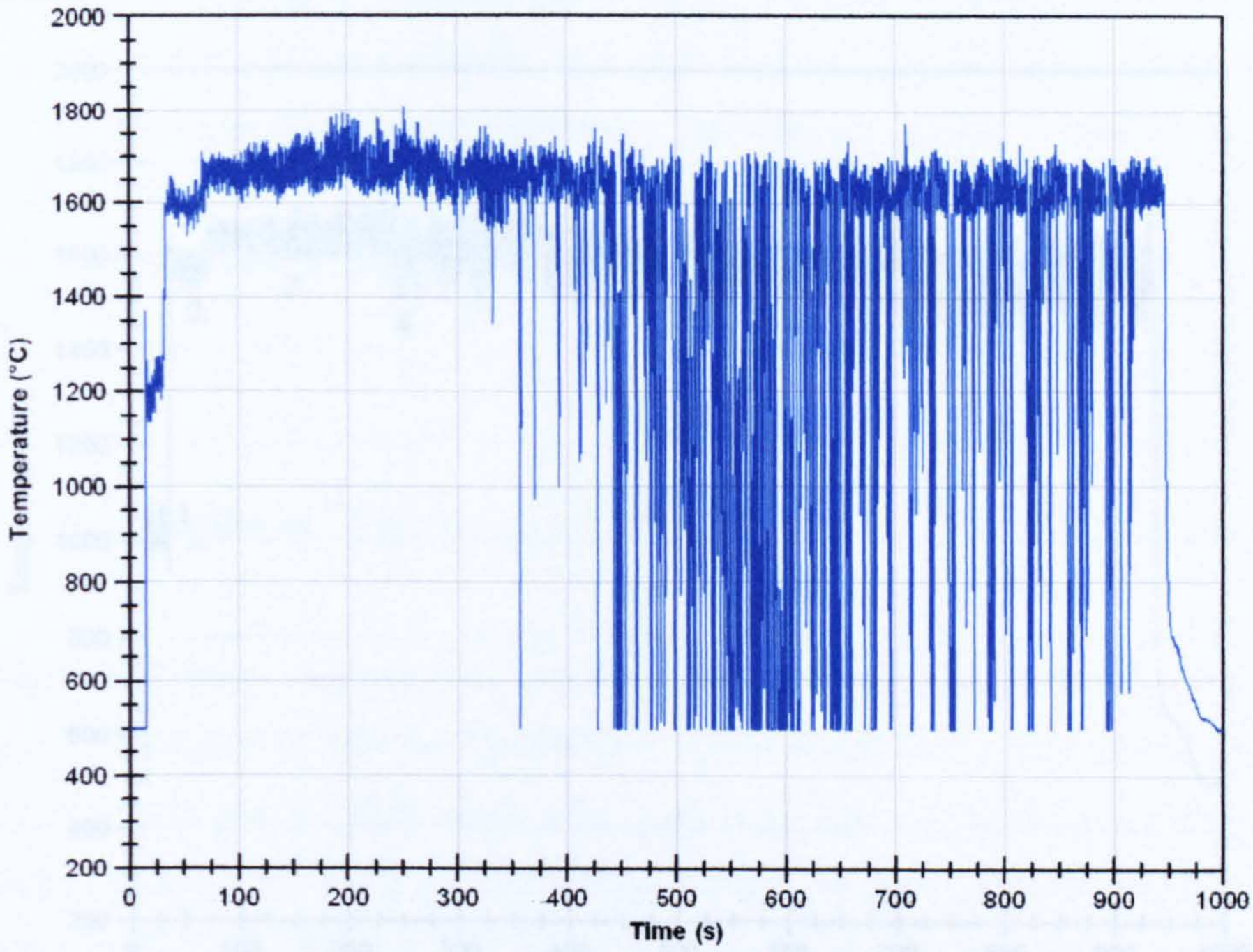

Figure 5.7: Effect of pyrometer misalignment

There are some important factors to avoid this problem:

- The angle of incidence of the pyrometer should be as small as practically possible
- Choose the right Z step in the CNC program, according to the laser power used.

Higher laser power will produce a flat and wider bead, i.e. the bead height will be smaller.

- It is better to locate the pyrometer in line with the deposition process (e.g. from the back) rather than at one side.

After these considerations, a temperature monitoring system for the melt pool in laser metal deposition with wire was achieved. Figure 5.8 shows the temperature of the melt pool of a cylinder in which the sensor was aiming properly during the whole experiment.

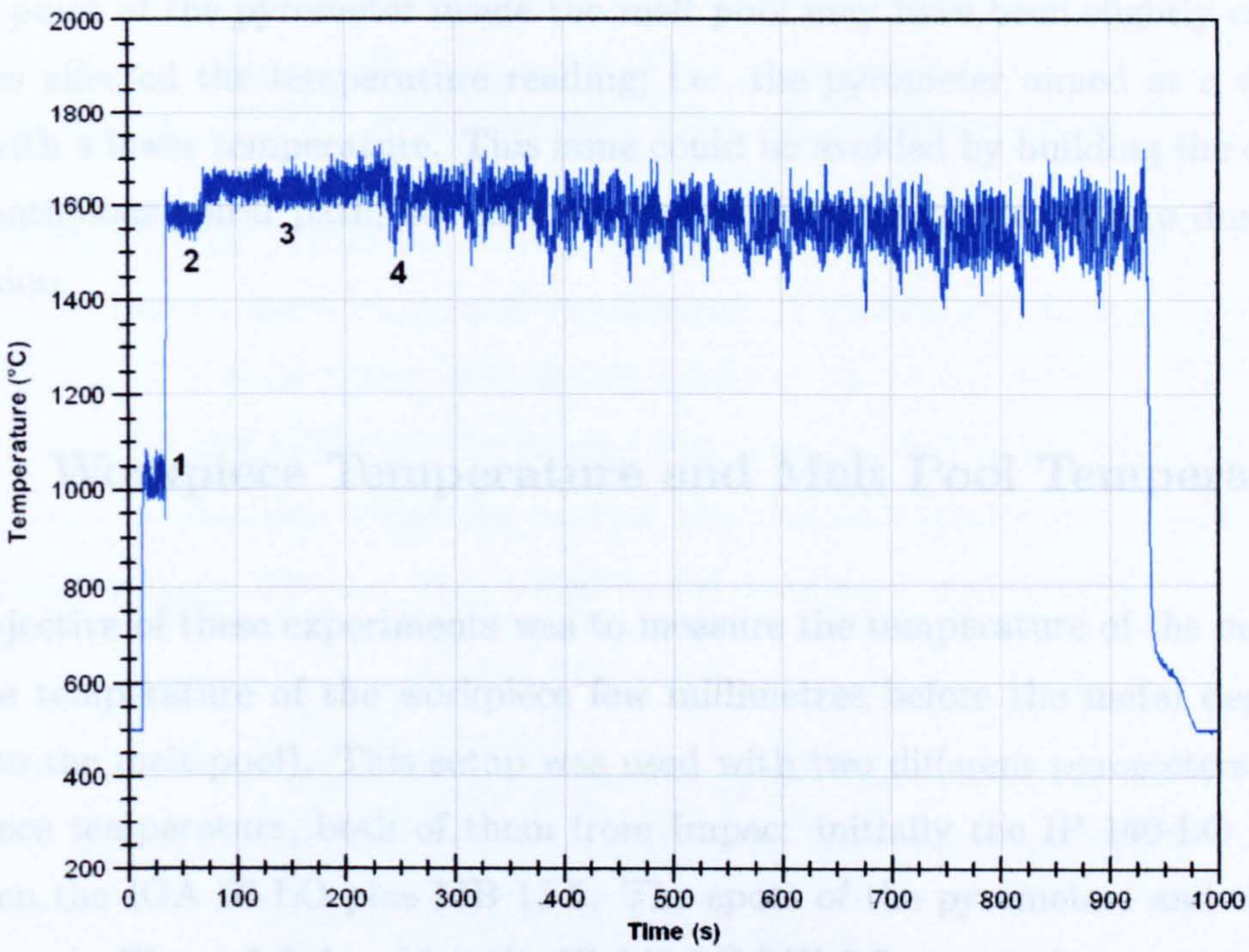

Figure 5.8: Melt pool temperature measured during the whole experiment (1) Preheating lap. (2) First deposition lap. (3) Laser reduced from 1600 W to 1400 W in steps. (4) Laser reduced to 1300 W.

It is worth noticing that in this and other cylinders there was a cyclic profile in the temperature graph, where each cycle corresponded to one revolution in the cylinder (in this case, 36 seconds). This behaviour can be explained considering the way the cylinders were deposited.

A preheat lap (only laser without wire feed) was done in order to start the deposition on a warmer plate. The wire was then deposited in a continuous way until the cylinder was finished, whereas the laser power was reduced in steps (manually) as shown in Figure 5.8. In each lap the deposition was performed during 315° of the lap with a constant Z, and then the Z axis was ramped-up 1.9 mm (i.e. the Z step) for 45°. This process was repeated every lap until the cylinder was finished.

The temperature reading was stable during around 31.5 seconds, time that corresponds to 315° of one lap; and then it went down during approximately 4.5 seconds, which corresponds to 45° of one lap. Apparently, when the Z axis was ramping-up the aiming point of the pyrometer inside the melt pool may have been slightly changed, and this affected the temperature reading; i.e. the pyrometer aimed at a different point with a lower temperature. This issue could be avoided by building the cylinder in a continuous spiral path, so that the aiming point does not change during the deposition.

5.2.4 Workpiece Temperature and Melt Pool Temperature

The objective of these experiments was to measure the temperature of the melt pool and the temperature of the workpiece few millimetres before the metal deposition (close to the melt pool). This setup was used with two different pyrometers for the workpiece temperature, both of them from Impac: initially the IP 140-LO MB 7.5 and then the IGA 50-LO plus MB 13.5. The spots of the pyrometers and the laser are shown in Figure 5.9, in which the IP 140-LO MB 7.5 was used.

5.2.5 Impac IP 140-LO MB 7.5

This pyrometer was used to measure the workpiece temperature. It is a single-colour pyrometer with a temperature range from 130 to 750 °C.

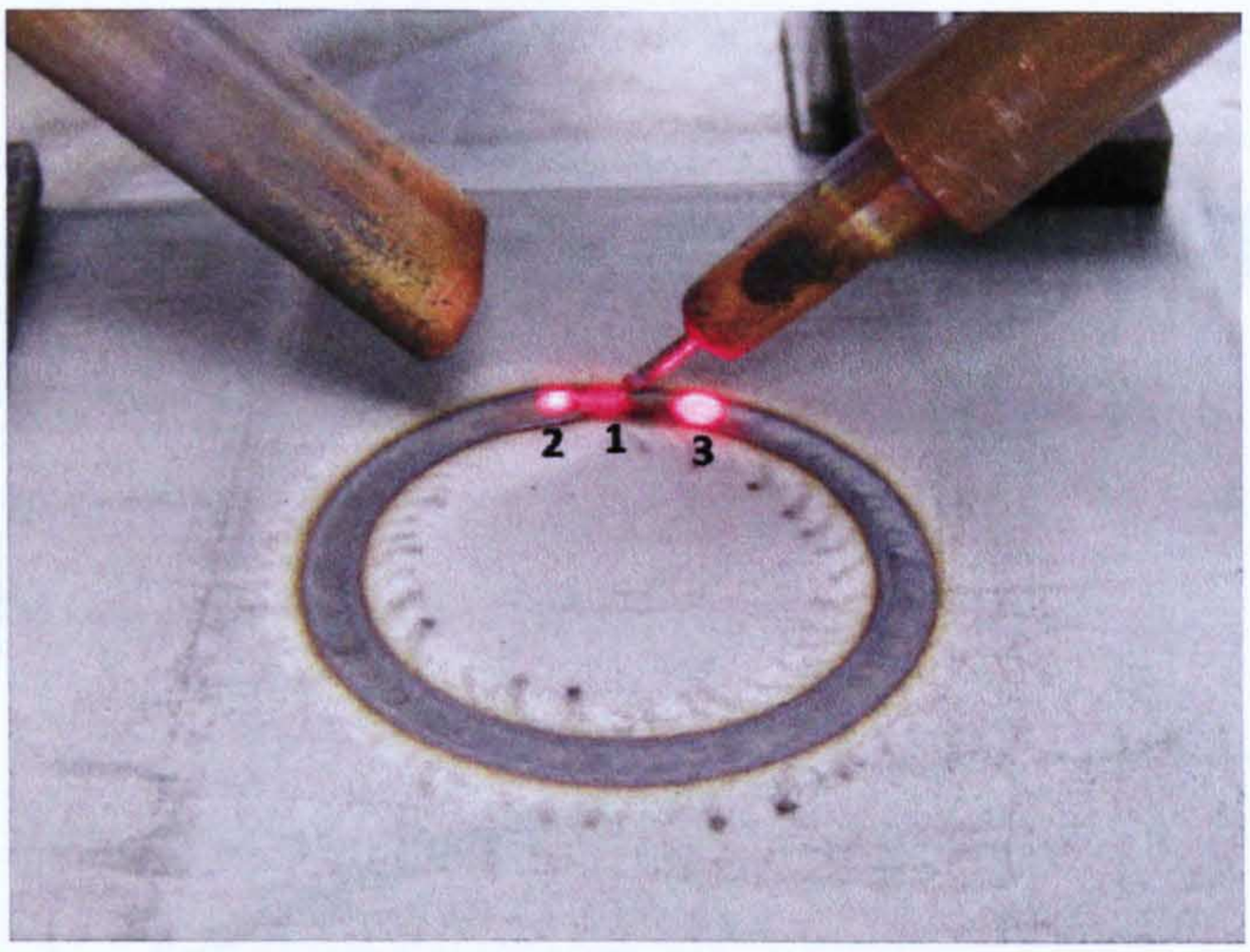

Figure 5.9: Alignment of laser and pyrometers
(1) Laser spot. (2) Melt pool pyrometer spot. (3) Workpiece pyrometer spot.

Being a single-colour pyrometer, it was necessary to find the emissivity of the material in this temperature range and wavelength. To achieve this, both pyrometers were aimed at the same point in order to measure the temperature with the two-colour pyrometer and calibrate the single-colour one according to that temperature (i.e. to find the adequate emissivity so that the temperatures would match in both pyrometers). The pyrometers were aimed at the workpiece (upper layer) as in Figure 5.4.

As the minimum temperature for the two-colour pyrometer was 500 °C, the calibration was made from 550–750 °C. The emissivity value was varied gradually, obtaining better results with a value of 0.70 (i.e. 70%).

This pyrometer performed well during the experiments; however, it was limited to a maximum temperature of 750 °C. When measuring the temperature of the workpiece with the pyrometer IGAR 12-LO during the deposition of one cylinder it raised up to 860 °C. So the temperature range of the pyrometer IP 140-LO was not high enough to analyse the whole experiment. Figure 5.10 shows the temperature measurements (melt pool and workpiece) of one cylinder. It can be noticed that towards the end the workpiece temperature was higher than 750 °C.

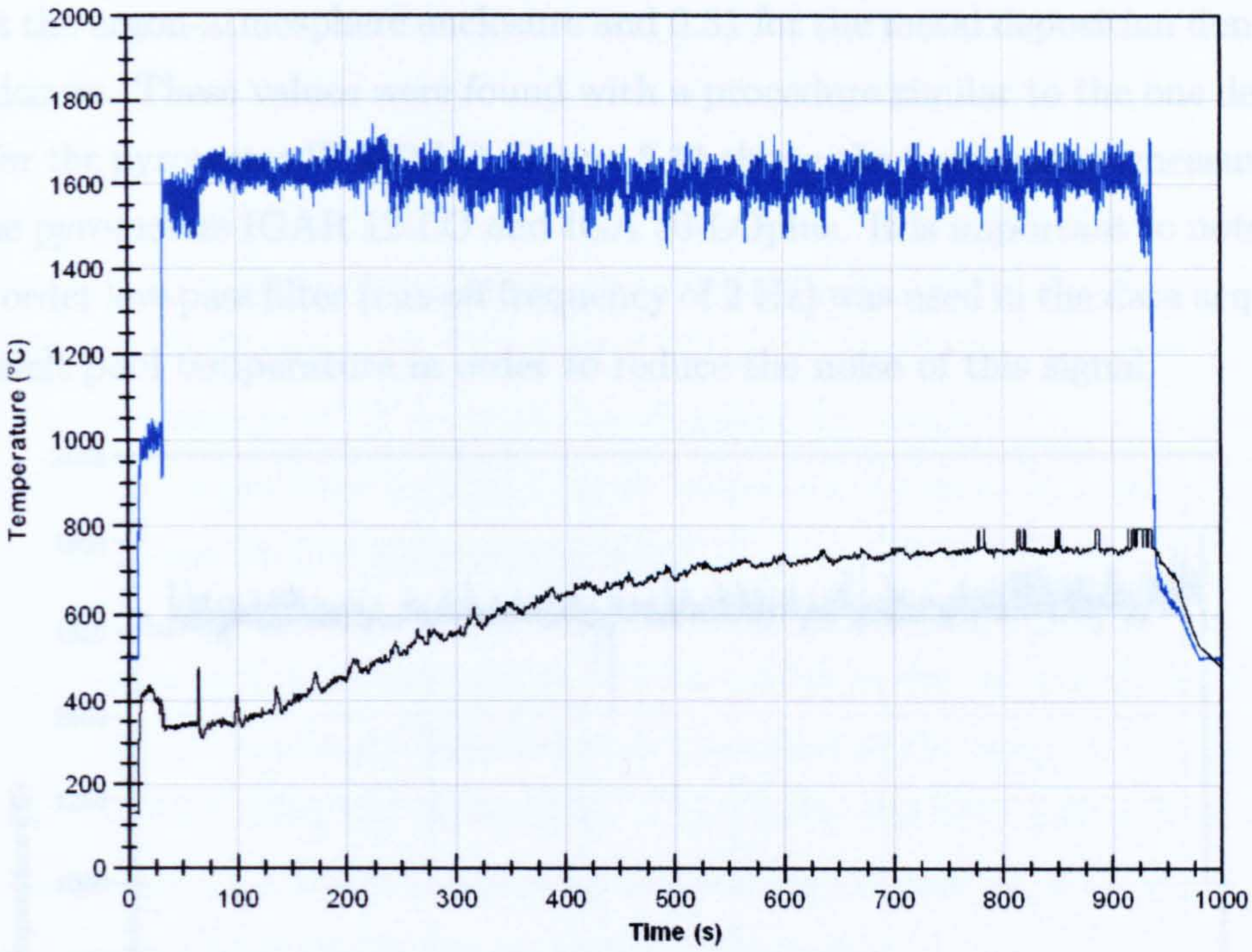

Figure 5.10: Monitoring of melt pool and workpiece temperatures
Blue: Melt pool temperature. Black: Workpiece temperature (upper layer).

5.2.6 Impac IGA 50-LO Plus MB 13.5

This pyrometer was used to measure the workpiece temperature, so it can be compared to the pyrometer IP 140-LO (see Table 5.1). It is a single-colour pyrometer, with optical head and fibre cable, with a temperature range from 250–1350 °C. One evident advantage of this pyrometer is a higher maximum temperature than that of IP 140-LO; however, its minimum temperature is also higher.

Another advantage is that its spot size is smaller: 1.2 mm diameter with the optical head type 1. This can be compared to the 3.4 mm diameter of the IP 140-LO with the same optical head.

During the experiments its performance was similar to that of the pyrometer IP 140-LO. The emissivity of the IGA 50-LO plus was set to 0.4 for the metal deposition done

without the argon-atmosphere enclosure and 0.31 for the metal deposition done inside the enclosure. These values were found with a procedure similar to the one described above for the pyrometer IP 140-LO. Figure 5.11 shows the temperature measurements with the pyrometers IGAR 12-LO and IGA 50-LOplus. It is important to note that a second order low-pass filter (cut-off frequency of 2 Hz) was used in the data acquisition of the melt pool temperature in order to reduce the noise of this signal.

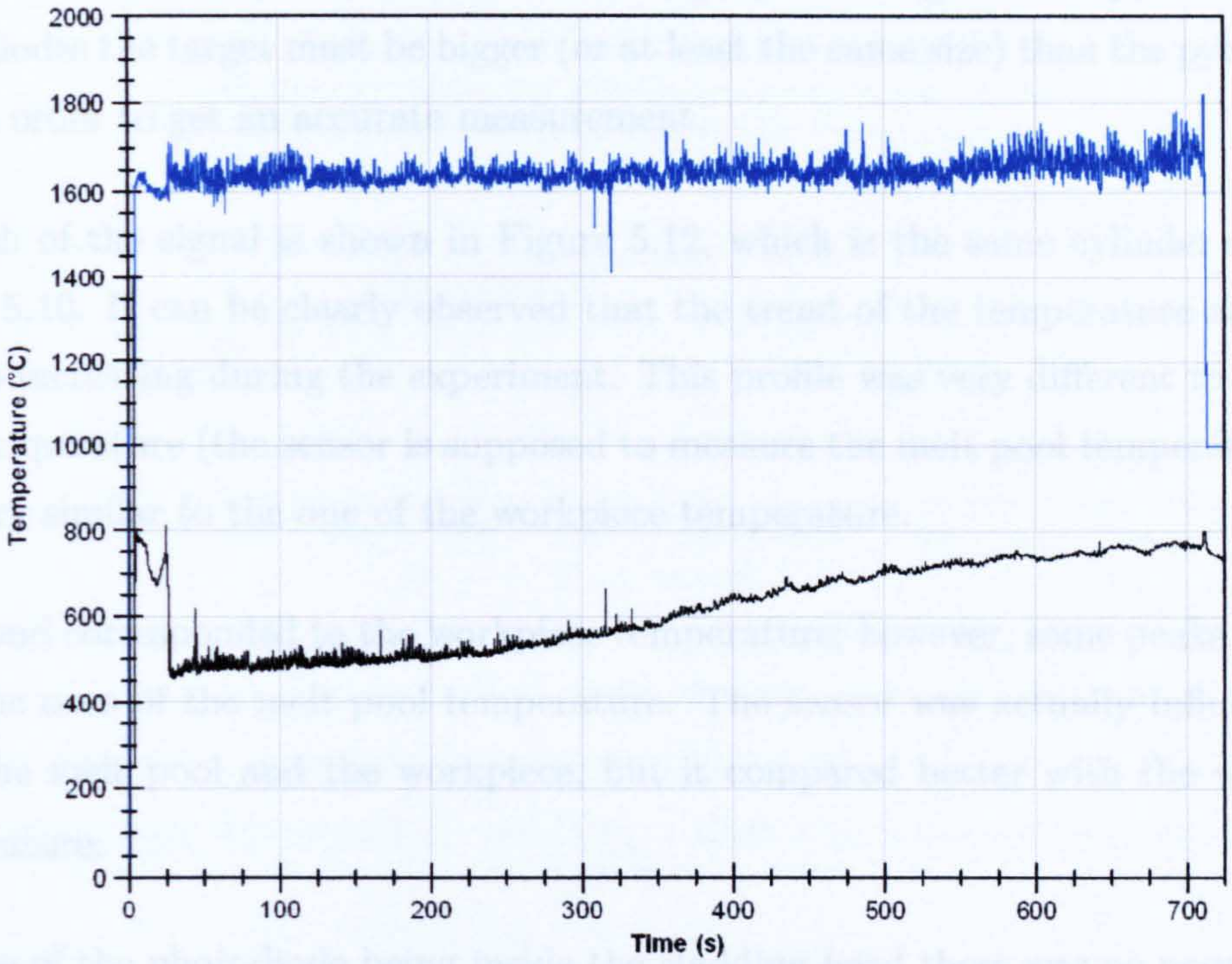

Figure 5.11: Measurements with pyrometers IGAR 12-LO and IGA 50-LOplus Blue: IGAR 12-LO MB 22. Black: IGA 50-LOplus MB 13.5

5.2.7 Precitec Photodiode

This sensor is a photodiode with a wavelength range from 1.3 to 1.6 μm. It is integrated in the cladding head and aims coaxially to the laser beam. The sensor is connected to an amplifier, which gives a voltage signal from 0 to 10 V. During this experiment the maximum amplification was used (lower amplifications did not

provide any signal). It does not give a temperature value, so it would need to be calibrated in order to interpret the signal as a temperature.

According to the supplier, this sensor was designed to have the smallest spot size when the laser is in focus, but the spot size itself was not provided. This experiment was undertaken at 20 mm out of focus and the pyrometer's spot size may be (much) bigger than the melt pool. It is worth noticing that for single-colour pyrometers and photodiodes the target must be bigger (or at least the same size) than the pyrometer's spot in order to get an accurate measurement.

A graph of the signal is shown in Figure 5.12, which is the same cylinder shown in Figure 5.10. It can be clearly observed that the trend of the temperature signal was to keep increasing during the experiment. This profile was very different to the melt pool temperature (the sensor is supposed to measure the melt pool temperature) but was very similar to the one of the workpiece temperature.

The trend corresponded to the workpiece temperature; however, some peaks matched with the ones of the melt pool temperature. The sensor was actually influenced by both the melt pool and the workpiece, but it compared better with the workpiece temperature.

Because of the photodiode being inside the cladding head there was no possibility to bring it closer to the melt pool in order to get a smaller spot size. The cladding head does not provide any means to change the focus distance of the photodiode (such as focusing lens, etc). For this reason, this sensor is not suitable for the process.

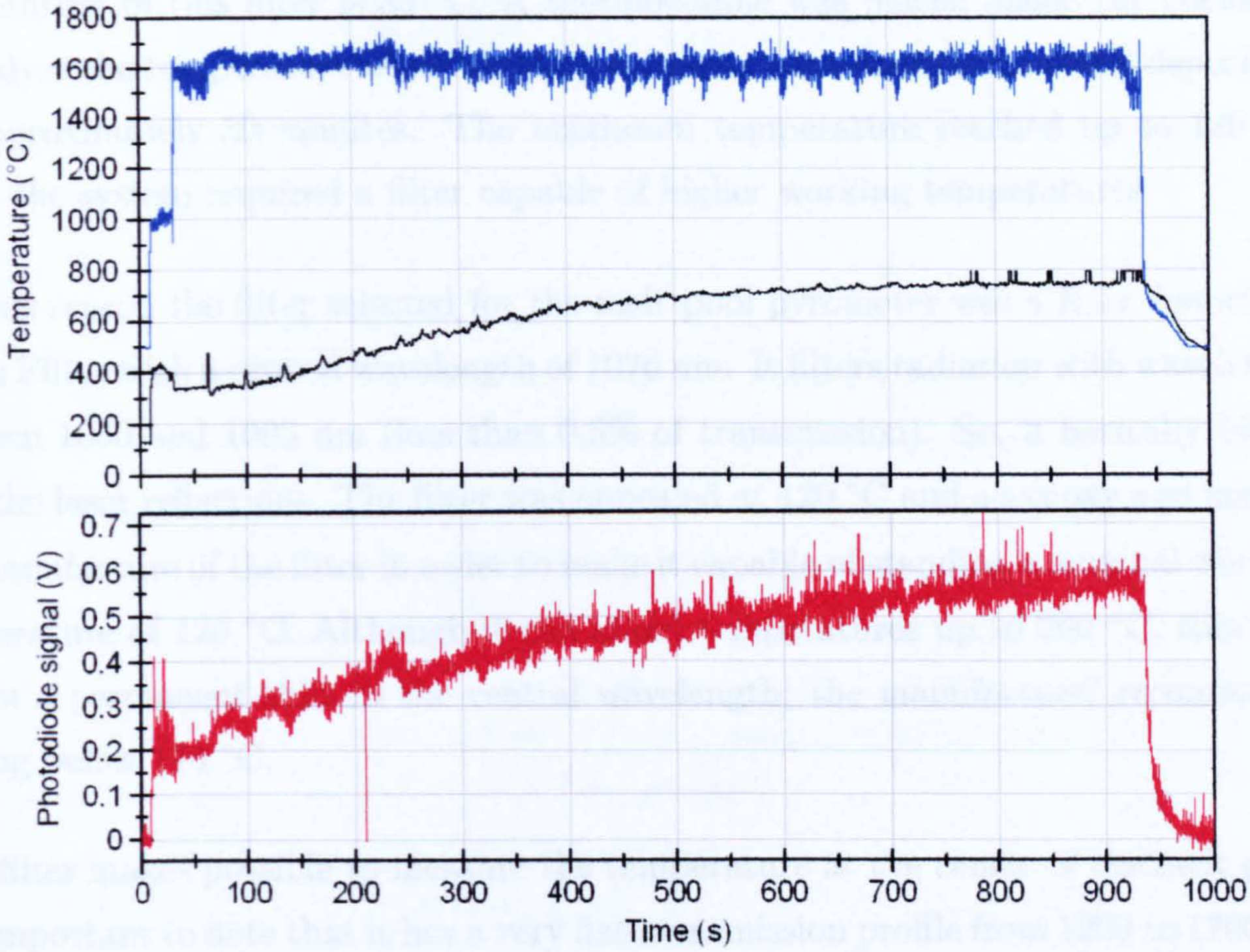

Figure 5.12: Comparison of Precitec photodiode and pyrometers Blue: Melt pool temperature (pyrometer IGAR 12-LO). Black: Workpiece temperature (pyrometer IP 140-LO). Red: Photodiode voltage signal.

5.3 Optical Filters for Rejection of Laser Reflections

As it was explained above, when the melt pool pyrometer was aiming at the centre of the laser spot the temperature measurement was very unstable. It was realised that the laser reflections had a strong influence on the pyrometer's reading, and that an optical filter was needed to reject those reflections.

Initially a Thor Labs FEL1150 Long-pass filter was used, which rejects radiation with wavelength lower than 1150 nm. It is important to note that the maximum working

temperature of this filter is 85 °C. A thermocouple was placed inside the enclosure to analyse the temperature when building cylinders with continuous metal deposition for approximately 30 minutes. The maximum temperature reached up to 120 °C. Thus, the system required a filter capable of higher working temperatures.

For this reason the filter selected for the melt pool pyrometer was a Barr Associates Notch Filter with a central wavelength of 1076 nm. It filters radiation with wavelength between 1060 and 1095 nm (less than 0.5% of transmission). So, it basically blocks only the laser reflections. The filter was annealed at 120 °C and an epoxy was used in the manufacture of the filter in order to make it capable of standing a nominal working temperature of 120 °C. Although it can stand temperatures up to 200 °C, this may induce a permanent shift in the central wavelength; the manufacturer recommends staying below 170 °C.

This filter makes possible to measure the temperature at the centre of the melt pool. It is important to note that it has a very flat transmission profile from 1200 to 1700 nm and that this characteristic minimizes the influence of the filter on the temperature reading, for it affects in the same way both wavelengths of the two-colour pyrometer. The transmission graph of the filter is shown in Figure 5.13. For the workpiece pyrometer (IGA 50-LO plus MB 13.5) the filter selected was NDC 1140 Long-pass. It rejects radiation with wavelength lower than 1140 nm. An epoxy has also been used in the manufacture of this filter for high-temperature applications. This filter affects the temperature reading of the one-colour pyrometer and a new calibration was performed, giving an emissivity value of 0.20 (i.e. 20%). The transmission graph of the filter is shown in Figure 5.14.

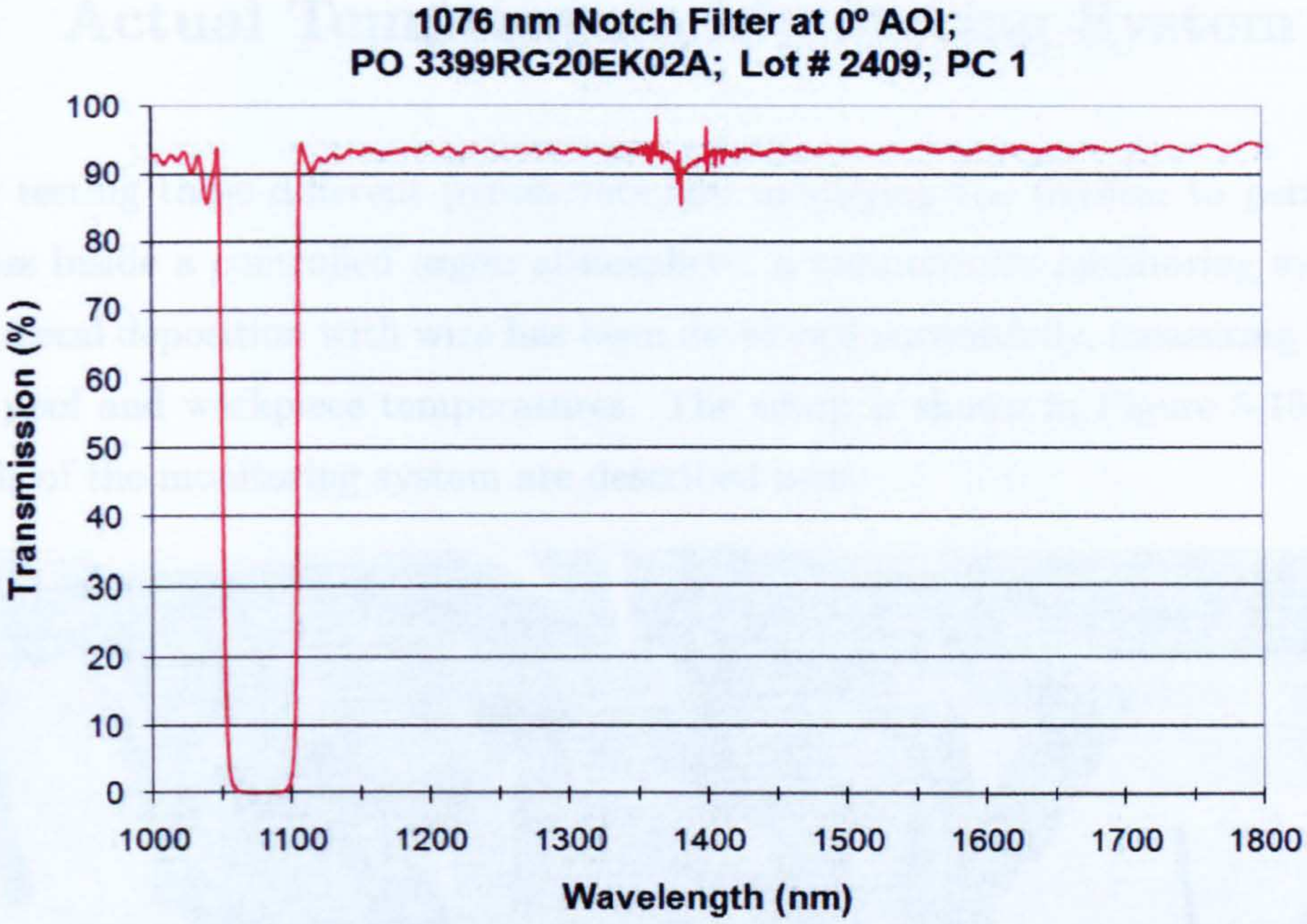

Figure 5.13: Transmission graph of notch filter (from supplier)

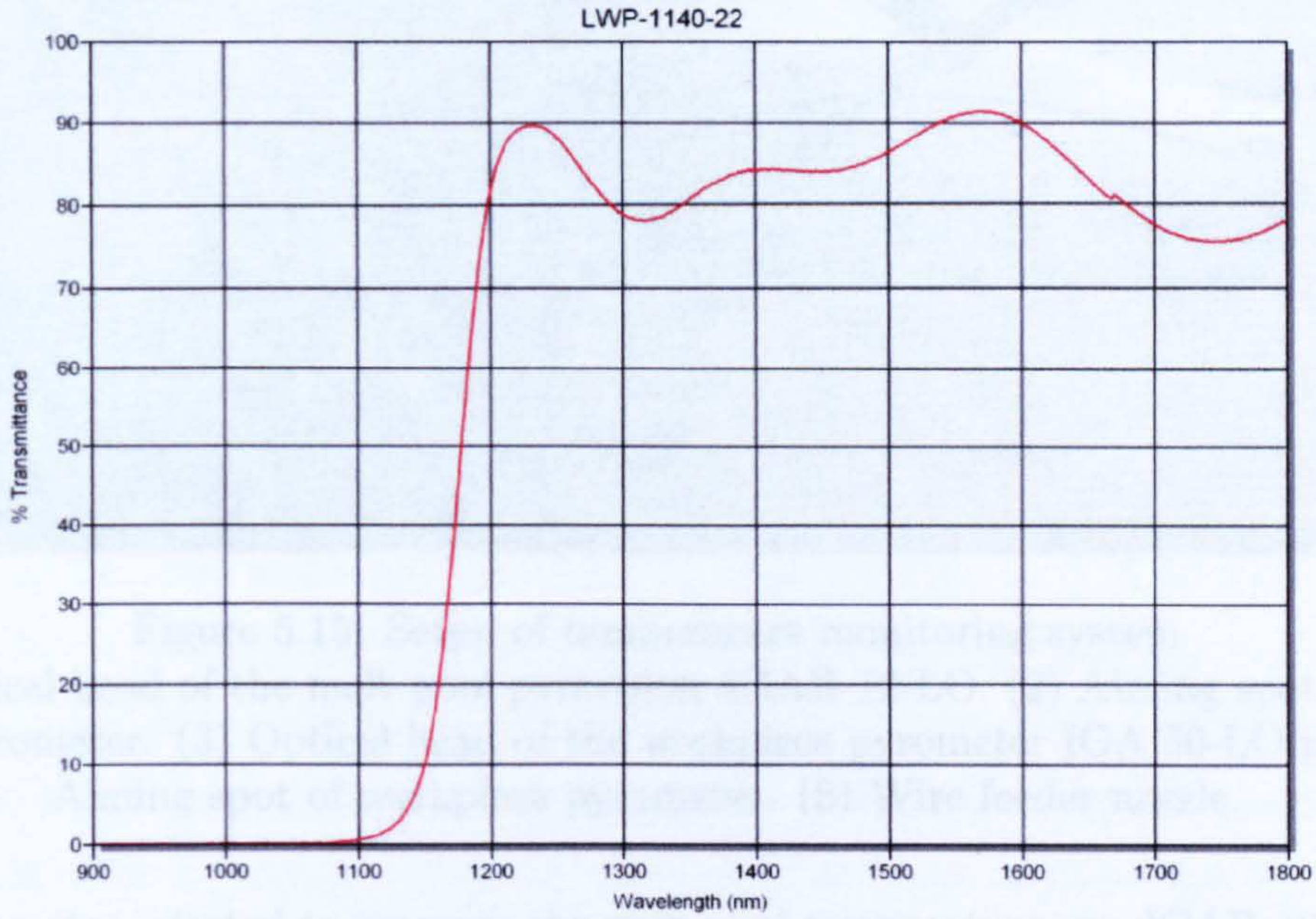

Figure 5.14: Transmission graph of long-pass filter (from supplier)

5.4 Actual Temperature Monitoring System

After testing these different pyrometers and modifying the fixtures to perform the process inside a controlled argon atmosphere, a temperature monitoring system for laser metal deposition with wire has been developed successfully, measuring both the melt pool and workpiece temperatures. The setup is shown in Figure 5.15 and the details of the monitoring system are described next.

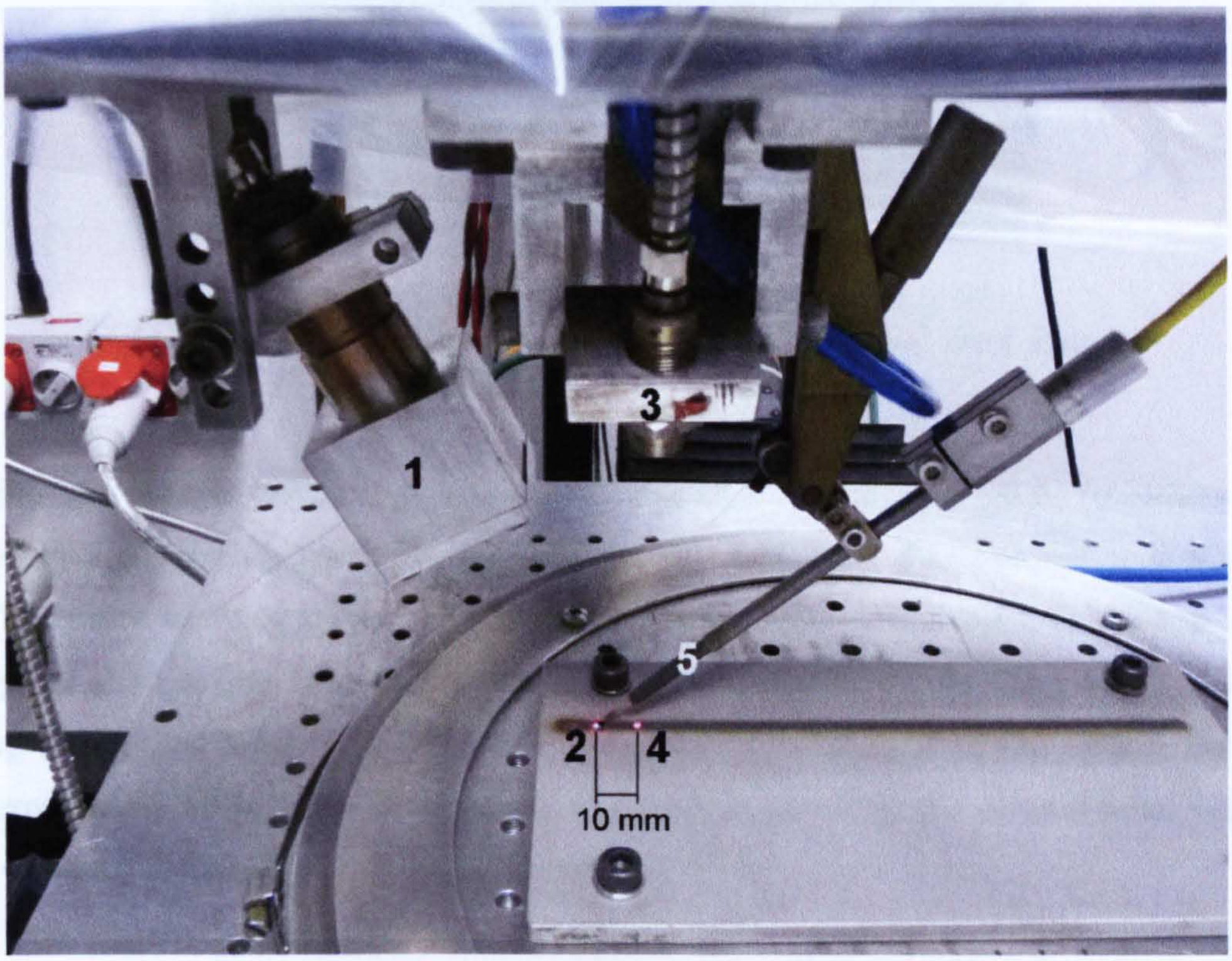

Figure 5.15: Setup of temperature monitoring system
(1) Optical head of the melt pool pyrometer IGAR 12-LO. (2) Aiming spot of melt pool pyrometer. (3) Optical head of the workpiece pyrometer IGA 50-LO plus. (4) Aiming spot of workpiece pyrometer. (5) Wire feeder nozzle.

The pyrometer selected to measure the melt pool temperature was IGAR 12-LO MB 22. It uses a Barr Associates Notch Filter with a central wavelength of 1076 nm, in order to reject the laser reflections; there is a glass window that protects the filter from any spatter that could come from the process. The optical head is situated

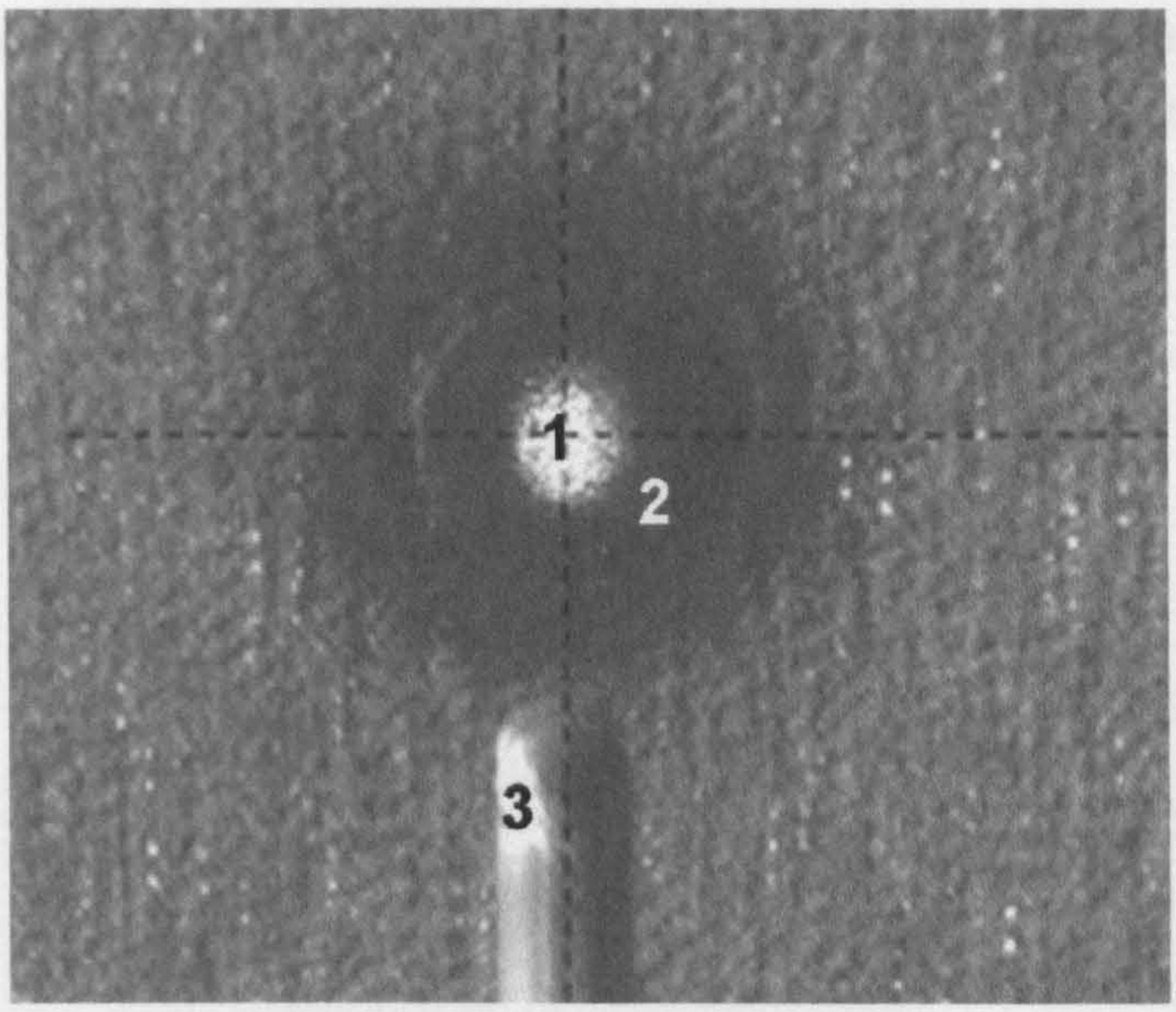

Figure 5.16: Alignment of melt pool pyrometer
(1) Aiming spot of melt pool pyrometer. (2) Melt pool area.
(3) Wire (1.2 mm diameter).

in line with the deposition process, from the back of the melt pool, to reduce the possibility of missing the melt pool; see Figure 5.15 (1). The pyrometer is aiming at the centre of the melt pool, as it is shown in Figure 5.16, which is the top view image of the process taken with a camera that is coaxial to the laser beam. When using the optical head type 1 the distance from the melt pool to the optical head is approximately 90 mm (as in Figure 5.15), and when using the optical head type 2 the distance is 120 mm.

The pyrometer that measures the workpiece temperature is IGA 50-LO plus MB 13.5. It uses a NDC 1140 Long-pass filter to reject the laser reflections; its cut-on wavelength is 1140 nm and it also has a glass window to protect the filter from spatter. The optical head is situated from one side of the melt pool. During the experiments it normally aims at 10 mm before the melt pool, in order to know the temperature just before the deposition takes place, but this can be modified if required. This pyrometer is normally used with the optical head type 2, and the distance between the aiming spot and the optical head is 120 mm. The emissivity value is set to 20% for metal deposition of stainless steel.

A DAQ card acquires the temperature signals from the pyrometers (0–20 mA) with a sampling rate of 50 Hz. Using a program developed in LabVIEW™, this signal is filtered, displayed graphically online and saved for offline analysis.

Chapter 6

Development of Temperature Control System

One of the main objectives of this project is the development of a temperature control system for wire metal deposition. This chapter explains the development of such a system.

First, the derivation of the transfer function of the plant is explained, followed by its transformation to the discrete domain and the design of the controller using the root locus method.

6.1 Development of the Model of the System

The proposed system aims to control the melt pool temperature by means of modifying the laser power. It is based on the principle that the melt pool temperature depends on the laser power, i.e. that increasing the laser power will increase the melt pool temperature, and decreasing the laser power will decrease the melt pool temperature.

A basic block diagram of the closed-loop control system is shown in Figure 6.1. The pyrometer reads the temperature from the melt pool and sends the signal to the computer. This signal is filtered and compared to the desired temperature. Then the controller applies a corrective action, setting a new value for the laser power, in order to achieve the desired temperature.

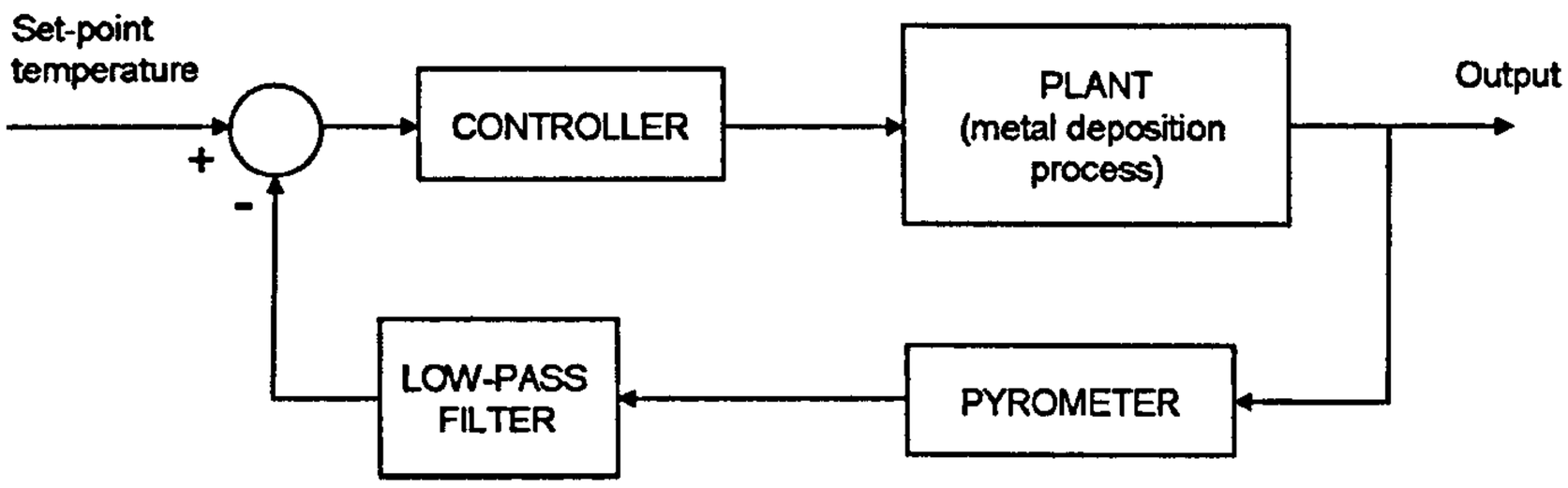

Figure 6.1: Basic block diagram of temperature control system

6.1.1 Derivation of the Transfer Function

Thermal system models can be described using a heat balance equation. Making the assumption that the temperature of a body is uniform, then a number of thermal systems can be represented by linear differential equations [88]. Thus, the heat that goes into the system equals the heat stored plus the heat lost, according to the law of conservation of energy. Then,

$$Q_{in} = Q_{storage} + Q_{out} \tag{6.1}$$

This equation can be expressed also in terms of heat rate q, with units J/s, i.e. watts.

$$q_{in} = q_{storage} + q_{out} \tag{6.2}$$

The system under analysis is shown in Figure 6.2. In this model the control volume (whose temperature is to be controlled) is the melt pool.

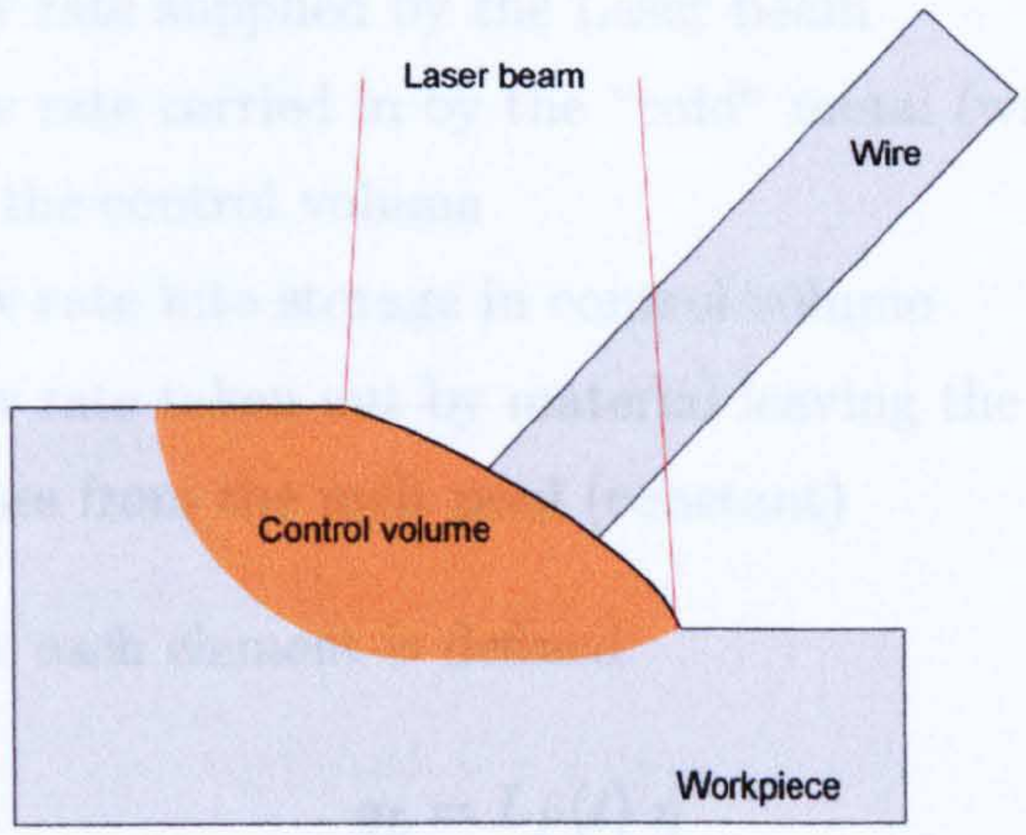

Figure 6.2: Control volume

In order to simplify the model, some assumptions have been made:

- At initial conditions the melt pool is already formed
- The control volume (melt pool) has a constant mass
- The control volume is at a uniform temperature T_{MP}
- The material leaves the control volume at the same temperature T_{MP}
- The system will operate within small deviations from the steady state condition
- Heat losses from the melt pool are considered constant

The heat rate balance equation can be expressed as:

$$q_L + q_I = q_{MP} + q_O + q_{LOSS} \tag{6.3}$$

Where

q_L = Heat flow rate supplied by the Laser beam

q_I = Heat flow rate carried in by the "cold" metal (wire and substrate) entering the control volume

q_{MP} = Heat flow rate into storage in control volume

q_O = Heat flow rate taken out by material leaving the control volume

q_{LOSS} = Heat losses from the melt pool (constant)

Then, the equation for each element is defined:

$$q_L = L_P(t)\,\eta \tag{6.4}$$

Where

L_P = Laser power (W)

η = Absorptivity

$$q_I = m_{FW}\,C_S\,T_W + m_{FS}\,C_S\,T_S \tag{6.5}$$

Where

m_{FW} = Mass flow rate of the wire (kg/s)

m_{FS} = Mass flow rate of the substrate going into the melt pool (kg/s)

C_S = Specific heat of solid material (J/[kg K])

T_W = Temperature of the wire before the metal deposition process (K)

T_S = Temperature of the substrate before the metal deposition process (K)

$$q_{MP} = m_{MP}\,C_L\,\frac{dT_{\Delta MP}(t)}{dt} \tag{6.6}$$

Where

m_{MP} = Mass of the control volume (kg)

C_L = Specific heat of liquid material (J/[kg K])

$T_{\Delta MP}$ = Temperature of the of the melt pool above the melting point (K)

$$q_O = m_{FT}\,[C_L\,T_{\Delta MP}(t) + L_F + C_S\,T_M] \tag{6.7}$$

Where

m_{FT} = Mass flow rate total

$m_{FT} = m_{FW} + m_{FS}$

L_F = Latent heat of fusion (J/kg)

T_M = Temperature of the melting point (liquidus) (K)

Thus the model of the system is:

$$L_P(t)\,\eta + m_{FW}\,C_S\,T_W + m_{FS}\,C_S\,T_S = m_{MP}\,C_L\,\frac{dT_{\Delta MP}(t)}{dt} + m_{FT}\,[C_L\,T_{\Delta MP}(t) + L_F + C_S\,T_M] + q_{LOSS} \tag{6.8}$$

It can also be expressed as:

$$L_P(t)\,\eta = m_{MP}\,C_L\,\frac{dT_{\Delta MP}(t)}{dt} + m_{FT}\,C_L\,T_{\Delta MP}(t) + m_{FT}\,[L_F + C_S\,T_M] - [m_{FW}\,C_S\,T_W + m_{FS}\,C_S\,T_S] + q_{LOSS} \tag{6.9}$$

Considering the terms m_{FW}, m_{FS}, T_W and T_S as constants, then they can be grouped in a single constant K_M

$$K_M = m_{FT}\,[L_F + C_S\,T_M] - [m_{FW}\,C_S\,T_W + m_{FS}\,C_S\,T_S] \tag{6.10}$$

This constant is the power needed to take the material flow from the solid state to the liquid state. The equation becomes:

$$L_P(t)\,\eta = m_{MP}\,C_L\,\frac{dT_{\Delta MP}(t)}{dt} + m_{FT}\,C_L\,T_{\Delta MP}(t) + K_M + q_{LOSS} \tag{6.11}$$

It is important to note that this is not a linear system, because it does not satisfy the homogeneity property due to the constants K_M and q_{LOSS} (see section 2.6.2). However, it can be linearized.

Assuming that at the initial conditions the melt pool is already formed, and that there are only small deviations from the steady state condition (frequent assumption in control engineering [46, 89]), then the model will consider only the relationship of the variation of the melt pool temperature to the variation of the laser power, above the melting point temperature, for all the metal deposition process takes place at temperatures above the melting point of the material. In other words, the system can be assumed linear above the melting point temperature.

This situation is similar to a system described with the equation $y = m\,x + b$, which does not satisfy the homogeneity condition. As stated by Dorf and Bishop [46], such a system can be considered linear about an operating point x_0, y_0 for small changes Δx and Δy.
Defining

$$x = x_0 + \Delta x$$

$$y = y_0 + \Delta y$$

The system $y = m\,x + b$ can be expressed as

$$y_0 + \Delta y = m\,x_0 + m\,\Delta x + b$$

Then it becomes

$$\Delta y = m\,\Delta x$$

Which satisfies the homogeneity property.

Applying a similar procedure to the metal deposition system, in order to make the model linear for temperatures close to the operation point (above the melting point), let us define:

$$L_P(t) = L_{OP} + L_{\Delta OP}(t) \tag{6.12}$$

Where

L_{OP} = Total laser power needed to take the flow of material to the operating point, including the heat loss (constant)

$L_{\Delta OP}(t)$ = Change in the laser power from the operating point

In the same way, let us define:

$$T_{\Delta MP}(t) = T_{MPOP} + T_{\Delta OP}(t) \tag{6.13}$$

Where

T_{MPOP} = The difference of the operating point temperature and the melting point temperature (constant)

$T_{\Delta OP}(t)$ = Change in the temperature from the operating point

The model can be expressed as:

$$L_{OP}\,\eta + L_{\Delta OP}(t)\,\eta = m_{MP}\,C_L\,\frac{dT_{\Delta OP}(t)}{dt} + m_{FT}\,C_L\,T_{\Delta OP}(t) + K_M + m_{FT}\,C_L\,T_{MPOP} + q_{LOSS} \tag{6.14}$$

It is important to remember that L_{OP} is the total laser power needed to melt the material and to take it to the operating point, including the heat loss of the system. It requires that

$$L_{OP}\,\eta = K_M + m_{FT}\,C_L\,T_{MPOP} + q_{LOSS} \tag{6.15}$$

The model becomes then:

$$L_{\Delta OP}(t)\,\eta = m_{MP}\,C_L\,\frac{dT_{\Delta OP}(t)}{dt} + m_{FT}\,C_L\,T_{\Delta OP}(t) \tag{6.16}$$

This model satisfies the homogeneity condition.

The transfer function of a linear system is defined as "the ratio of the Laplace transform of the output variable to the Laplace transform of the input variable, with all

initial conditions assumed to be zero" [46]. In order to obtain the transfer function it is necessary to transform the model to the Laplace domain. The result of this transformation is:

$$L_{\Delta OP}(s)\,\eta = m_{MP}\,C_L\,[s\,T_{\Delta OP}(s) - T_{\Delta OP}(0)] + m_{FT}\,C_L\,T_{\Delta OP}(s) \tag{6.17}$$

After applying zero initial conditions,

$$L_{\Delta OP}(s)\,\eta = m_{MP}\,C_L\,s\,T_{\Delta OP}(s) + m_{FT}\,C_L\,T_{\Delta OP}(s) \tag{6.18}$$

The transfer function of the system is:

$$\begin{aligned} \frac{T_{\Delta OP}(s)}{L_{\Delta OP}(s)} &= \frac{\eta}{C_L\,[s\,m_{MP} + m_{FT}]} \\ &= \frac{\frac{\eta}{C_L\,m_{FT}}}{1 + \frac{m_{MP}}{m_{FT}}\,s} \end{aligned} \tag{6.19}$$

If the constants are grouped in order to give the standard form of a first-order system, then

$$\frac{T_{\Delta OP}(s)}{L_{\Delta OP}(s)} = K_{PL}\left[\frac{1}{1+\tau\,s}\right] \tag{6.20}$$

Where τ is the system time constant

$$\begin{aligned} \tau &= \frac{m_{MP}}{m_{FT}} \\ K_{PL} &= \frac{\eta}{C_L\,m_{FT}} \end{aligned}$$

6.1.2 Constants of the System

In order to continue developing the transfer function it is necessary to find the constants of the system. They have been obtained by literature review or by practical approximations.

The absorptivity η of a material to an incident laser light depends on different parameters such as the laser wavelength, angle of incidence, chemical composition of the

material, temperature, roughness, oxide layers, contamination, etc. [90]. Bergstrom et al. [90] reported a value of reflectance R for stainless steel (bright annealed, grades 304 and 430) of $R = 0.65$ for the Nd:YLF laser wavelength of 1053 nm. This wavelength is very close to that of the fibre laser (1070 nm) and the reflectance value can be considered valid also for the fibre laser. The absorptivity η is calculated as $\eta = 1 - R$. Then its value is:

$$\eta = 0.35$$

The specific heat of liquid material C_L has been calculated by Miettinen [91] for stainless steel 304 at 1600 °C (maximum temperature shown on that study). Although the metal deposition was carried out at 1750 °C, the value is considered close enough and is the one used for this calculation:

$$C_L = 839 \text{ J/[kg K]}$$

Smooth metal deposition was obtained when performing the process at a traverse speed of 200 mm/min with a wire feed rate of 0.8 m/min. This condition has been used to calculate some of the constants of the system. As previously explained, the total mass flow rate m_{FT} is the sum of the mass flow rate of the wire m_{FW} and that of the substrate m_{FS} going into the melt pool. They are calculated by:

$$m_{FW} = \frac{\Pi\, D^2}{4}\, W_{FR}\, \rho \tag{6.21}$$

$$m_{FS} = A_S\, S_T\, \rho \tag{6.22}$$

Where,

D = Diameter of the wire (m)

W_{FR} = Wire feed rate (m/s)

ρ = Density (Kg/m^3)

A_S = Melted cross-sectional area of the substrate (m^2), from micrograph

S_T = Traverse speed (m/s)

Applying the following values:

D	=	1.2 mm	=	0.0012 m
W_{FR}	=	0.8 m/min	=	$1.3333 \cdot 10^{-2}$ m/s
ρ	=	8000 Kg/m^3		
A_S	=	1.916 mm^2	=	$1.9157 \cdot 10^{-6}$ m^2
S_T	=	200 mm/min	=	$3.3333 \cdot 10^{-3}$ m/s

The results are:

m_{FW}	=	$1.2064 \cdot 10^{-4}$ Kg/s
m_{FS}	=	$5.1085 \cdot 10^{-5}$ Kg/s
m_{FT}	=	$1.7172 \cdot 10^{-4}$ Kg/s

The volume of the melt pool has been approximated using micrographs that show the solidification front of the deposition process, in both transversal and longitudinal orientations, as shown in Figure 6.3. The value obtained is $1.78395 \cdot 10^{-8}$ m^3. Multiplying this value by a density of 8000 Kg/m^3, the mass of the melt pool is approximately

$m_{MP} = 1.4272 \cdot 10^{-4}$ Kg.

With these values, one can calculate τ and K:

τ	=	0.8311 s
K	=	2.4293 K/W

The transfer function of the plant is:

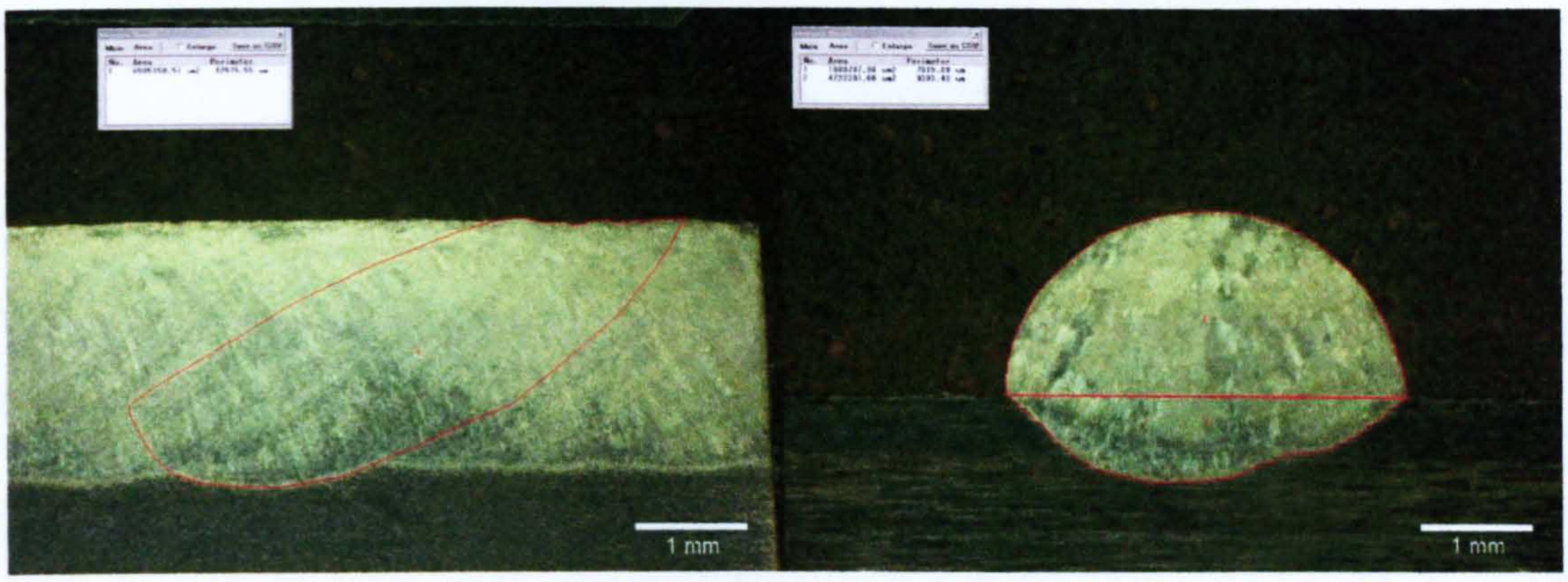

Figure 6.3: Longitudinal and transversal sections of the melt pool

$$\frac{T_{\Delta OP}(s)}{L_{\Delta OP}(s)} = 2.4293 \left[\frac{1}{1 + 0.8311\ s} \right] \tag{6.23}$$

This simplified model provides a means to analyse the behaviour of the system and can be used to design a controller. Simulation can be used to analyse different controller parameters and their influence on the performance of the system.

6.1.3 Transformation to the Discrete Domain

The transfer function has to be transformed to the discrete domain, for the controller has to be implemented in a computer. The system works at a frequency of 50 Hz, i.e. the sample period T is 0.02 seconds.

It is necessary to consider also the pyrometer and the low pass filter in the model. According to the manufacturer, the pyrometer has a response time of 2 ms. It will be modelled as a time delay of 0.002 s. It is important to note that this delay is shorter than one sample period.

The filter will cause a delay of "n" sampling periods according to the order of the filter. Because it is a second order filter, it will cause a delay of two sampling periods.

The transfer function of a first-order system with a time delay is:

$$G(s) = \frac{1}{1+\tau\, s}\, e^{-sT_D} \tag{6.24}$$

Where T_D is the time delay and can be expresed in two parts: a multiple of T and a fractional part δ:

$$T_D = kT + \delta$$

Golten and Verwer [45] show how to obtain and solve the pulse transfer function for a sampled-data first-order system with a time delay. The function is obtained by the equation:

$$G(z) = \frac{(z-1)}{z} z^{-k} Z_m \left\{ \frac{G(s)\, e^{-s\delta}}{s} \right\} \tag{6.25}$$

And the solution is:

$$G(z) = \frac{(1-\Gamma)\, z + (\Gamma - \beta)}{z^{k+1}\,(z-\beta)} \tag{6.26}$$

Where

$$\begin{aligned} \beta &= e^{-T/\tau} \\ \Gamma &= e^{-(T-\delta)/\tau} \end{aligned}$$

Applying equation 6.25 to the system:

$$\frac{T_{\Delta OP}(z)}{L_{\Delta OP}(z)} = K_{PL} \frac{(z-1)}{z} z^{-k} Z_m \left\{ \frac{e^{-s\delta}}{s(1+\tau\, s)} \right\} \tag{6.27}$$

After equation 6.26, the solution is:

$$\frac{T_{\Delta OP}(z)}{L_{\Delta OP}(z)} = K_{PL}\frac{(1-\Gamma)\,z+(\Gamma-\beta)}{z^{k+1}\,(z-\beta)} \tag{6.28}$$

The values of the constants are:

$$\begin{aligned} K_{PL} &= 2.4293 \text{ K/W} \\ \tau &= 0.8311 \text{ s} \\ T &= 0.02 \text{ s} \\ \delta &= 0.002 \text{ s} \\ k &= 2 \\ \beta &= e^{-0.02/0.8311} = 0.9762 \\ \Gamma &= e^{-(0.02-0.002)/0.8311} = 0.9786 \end{aligned}$$

The pulse transfer function of the system, including the plant, the pyrometer and the filter is:

$$\frac{T_{\Delta OP}(z)}{L_{\Delta OP}(z)} = \frac{0.0520(z+0.1098)}{z^3\,(z-0.9762)} \tag{6.29}$$

6.1.4 Root Locus Analysis and Controller Design

The root locus method traces the path of the roots of the closed-loop characteristic equation (i.e. closed-loop poles) in the s-plane (or the z-plane) as a system parameter is varied [46]. The parameter varied is normally the controller gain. The location of the roots gives important information on the performance of the closed-loop system.

In this case the system is analyzed in the z-plane. It is important to remember that:

- The locus of the roots starts at the open-loop poles and ends at the open-loop zeros or at infinity
- The roots of the numerator of the transfer function are called "Zeros"
- The roots of the denominator of the transfer function are called "Poles"

- In the z-plane the system is stable if all the closed-loop poles lay inside the unit circle

- A transfer function to be implemented in real-time must have equal or more poles than zeros, i.e. it must be a proper (or strictly proper) function

NI LabVIEW Control Design and Simulation Module is the software used in this project for the root locus analysis and the controller design. The controller has been designed in the zero-pole-gain form, in which transfer function is specified by indicating the gain and the location of the zeros and poles.

For this system, the pulse transfer function is described in equation 6.29. The poles are obtained from the equation:

$$z^3\,(z - 0.9762) = 0 \tag{6.30}$$

There are four open-loop poles in the real axis, at

$$\begin{aligned} z_{p1} &= 0.9762 \\ z_{p2} &= 0 \\ z_{p3} &= 0 \\ z_{p4} &= 0 \end{aligned}$$

The zeros are obtained from the equation:

$$0.0520(z + 0.1098) = 0 \tag{6.31}$$

There is one zero in the real axis, at

z_{z1} = - 0.1098

Figure 6.4 shows the poles and zeros of the system in the z-plane. A pole is plotted as a small cross, whereas a zero is plotted as a small circle.

A proportional controller could be initially considered for the analysis. The root locus of the closed-loop system in the z-plane is shown in Figure 6.5. There are four

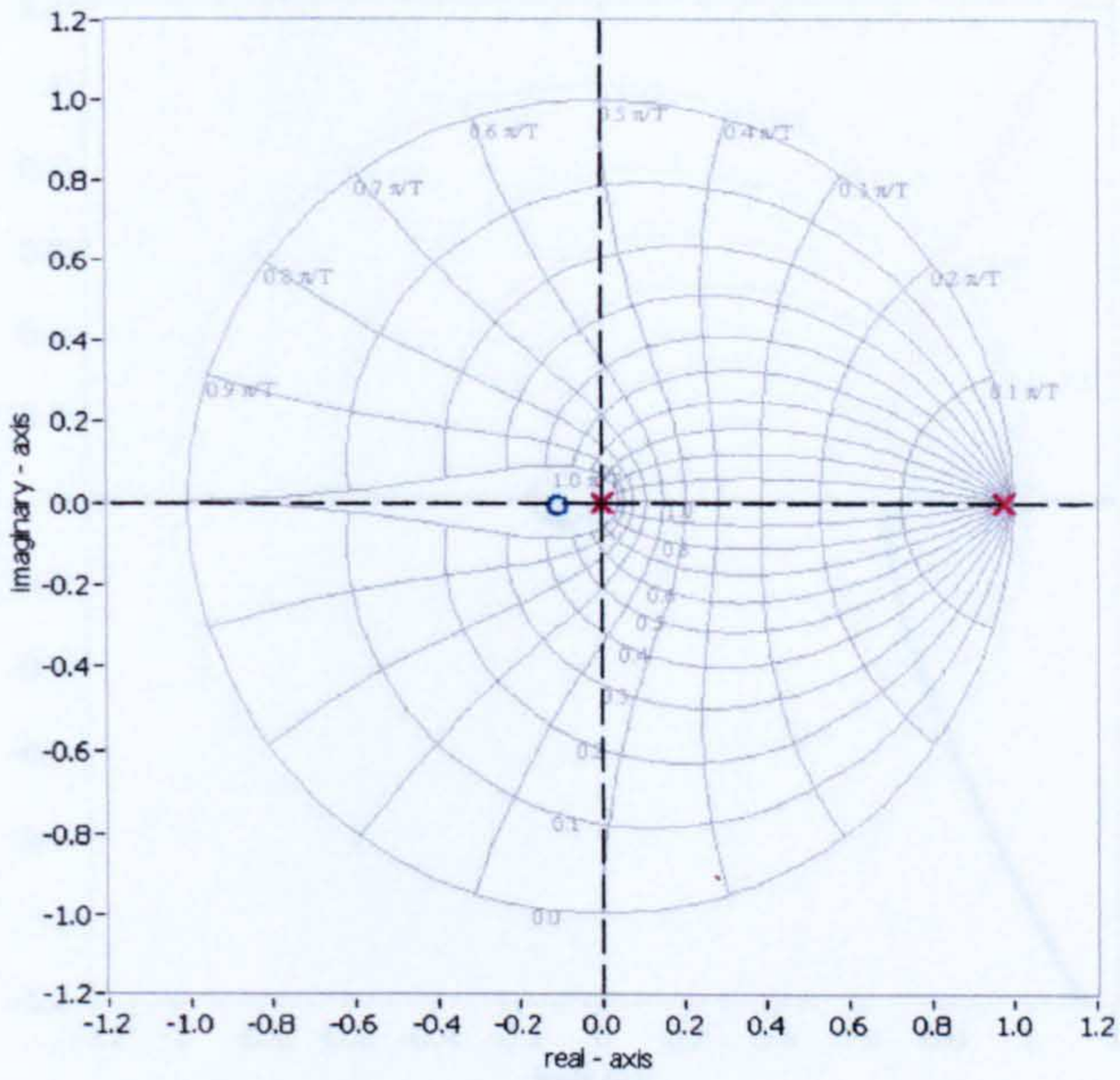

Figure 6.4: Poles and zeros in the z-plane

branches of the root locus (shown in different colours); they start at the poles and one of them will end at the zero whereas the other three will end at infinity.

However, this is a type–0 system i.e., it does not have a free integrator. In practice, it means that there will be a steady-state error or offset if there is a change in the set-point or a load disturbance [45].

In order to design an accurate controller, the first step is to add a free integrator in order to eliminate the steady state error. This is achieved by a pole in $z = 1$. In this case the pole is set at $z = 0.9999$ in order to ensure that it is inside the unit circle.

The dominant pole of the system is the one at $z = 0.9762$. The second step is to add a zero at the same location in order to cancel (or minimize) the effect of that pole.

Due to the zero at $z = -0.1098$ the root locus of two poles form a loop around the zero, as shown in Figure 6.5. The effect of this loop is very small compared to the effect of the dominant pole. The loop can be reduced by placing a pole close to the zero and placing a zero at the origin, although it does not make a significant change

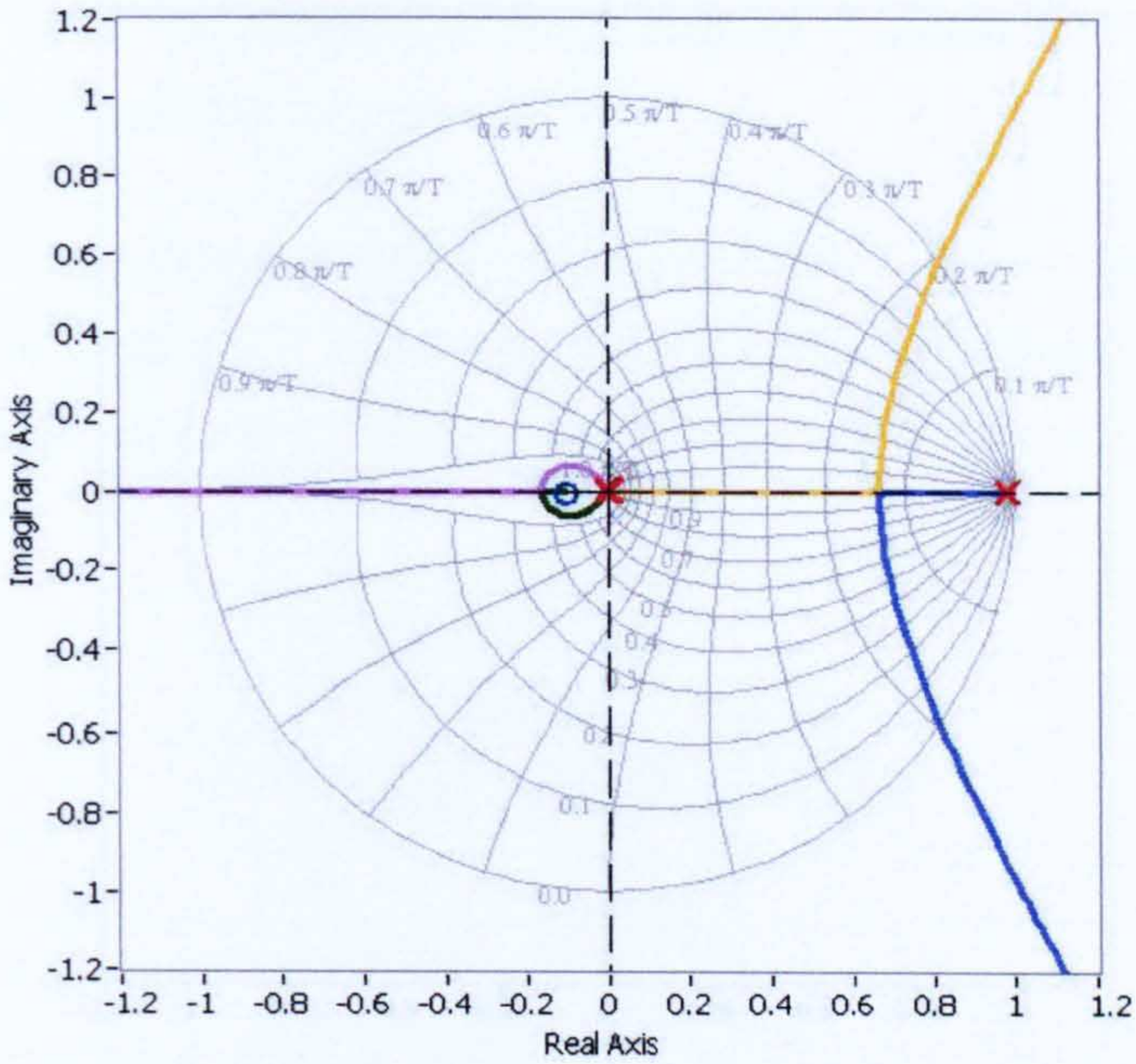

Figure 6.5: Root locus of the system with a proportional controller

in the time response of the system.

The proposed controller has two poles and two zeros in the real axis in these positions:

$$\begin{aligned} \text{Poles:} \quad z_{p1} &= 0.9999 \\ z_{p2} &= -0.05 \\ \text{Zeros:} \quad z_{z1} &= 0.9762 \\ z_{z2} &= 0 \end{aligned}$$

Having these poles and zeros, the next step is to find an adequate value for the gain K. Figure 6.6 shows the root locus plot of the system with this controller. Table 6.1 shows the time domain performance of the controller for different values of the gain.

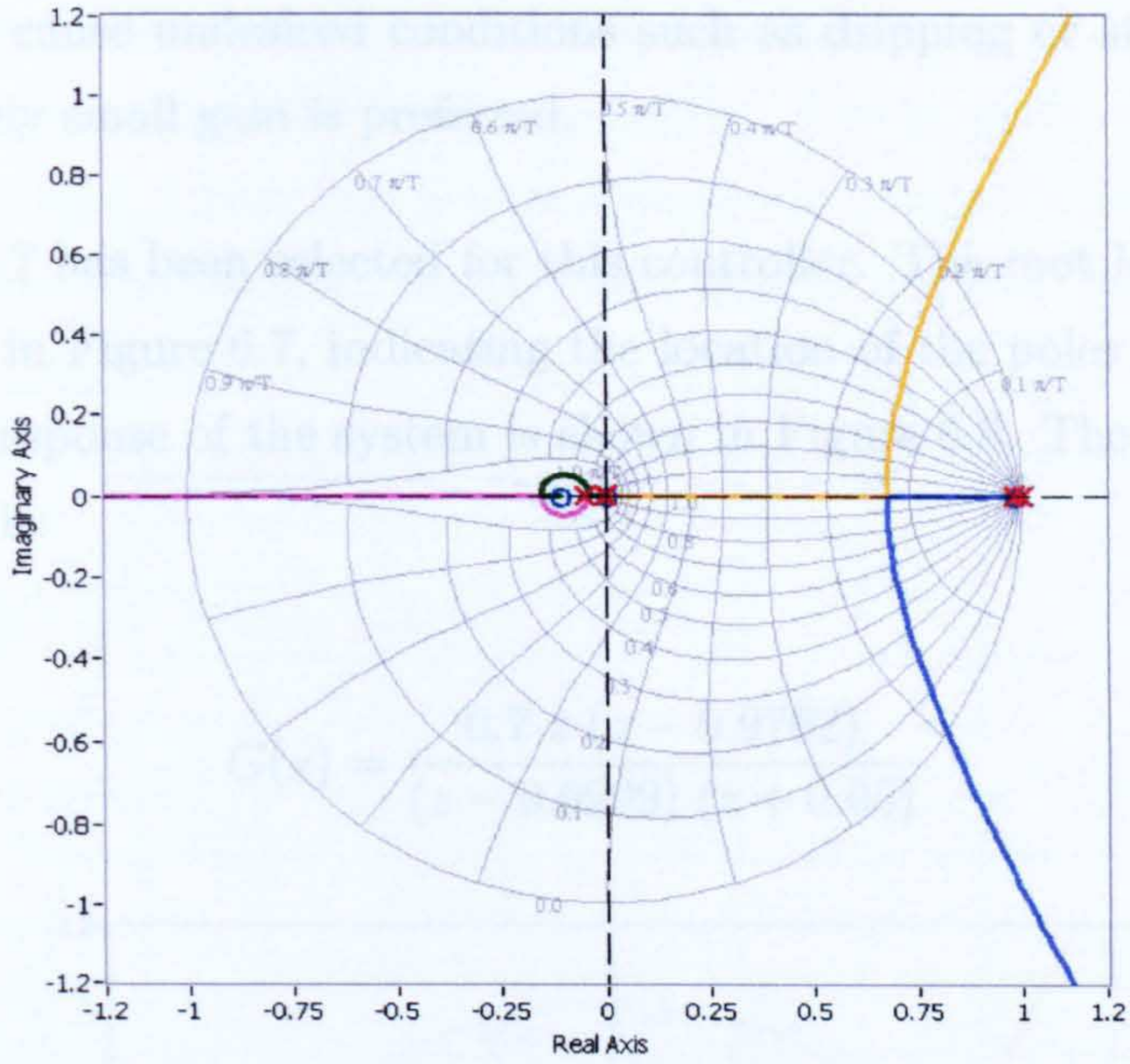

Figure 6.6: Root locus of the system with the proposed controller

Table 6.1: Time response characteristics of controller

Gain K	Rise time (s)	$\pm 1\%$ Settling time (s)	Overshoot (%)
0.2	3.88	8.18	0
0.3	2.54	5.38	0
0.4	1.88	3.98	0
0.5	1.48	3.14	0
0.6	1.20	2.58	0
0.7	1.02	2.18	0
0.8	0.88	1.88	0
0.9	0.76	1.66	0
1.0	0.68	1.46	0
2.0	0.28	0.60	0
3.0	0.14	0.26	0.39

It is important to consider that, from a practical point of view, the priority is to maintain the stability of the metal deposition process. Sudden large changes in the

laser power may cause undesired conditions such as dripping or stubbing. For this reason, a relatively small gain is preferred.

A gain of $K = 0.7$ has been selected for this controller. The root locus graph of the system is shown in Figure 6.7, indicating the location of the poles with the selected gain. The time response of the system is shown in Figure 6.8. The transfer function of the controller is:

$$G(z) = \frac{0.7\ z\ (z - 0.9762)}{(z - 0.9999)\ (z + 0.05)} \tag{6.32}$$

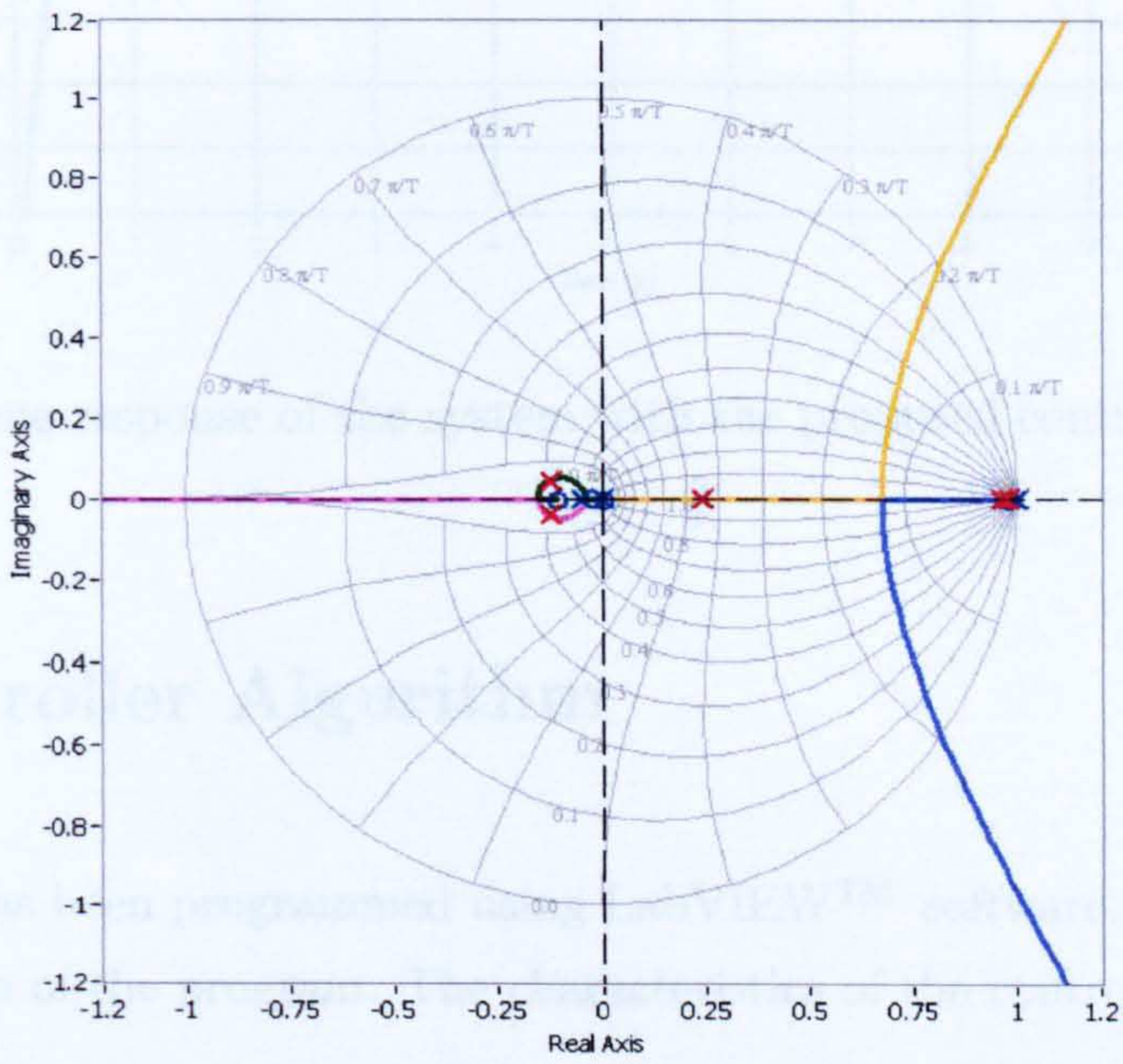

Figure 6.7: Root locus of the system with the proposed controller (K = 0.7)

It is important to note that this controller has been designed based on a simplified model of the metal deposition process. In reality, the process is more complex and the controller may not perform exactly with the time response described here. The controller has to be fine tuned based on the results on the experiments.

Regarding the experimental tunning of the controller, there are two factors that have

a strong influence on the performance of the system. The first of them is the gain. The other factor is the zero that is at $z = 0.9762$. If it is placed towards the right, the controller will have a smoother action. Conversely, if it is placed towards the left, the poles will form a loop around the pole and may produce an oscillatory response.

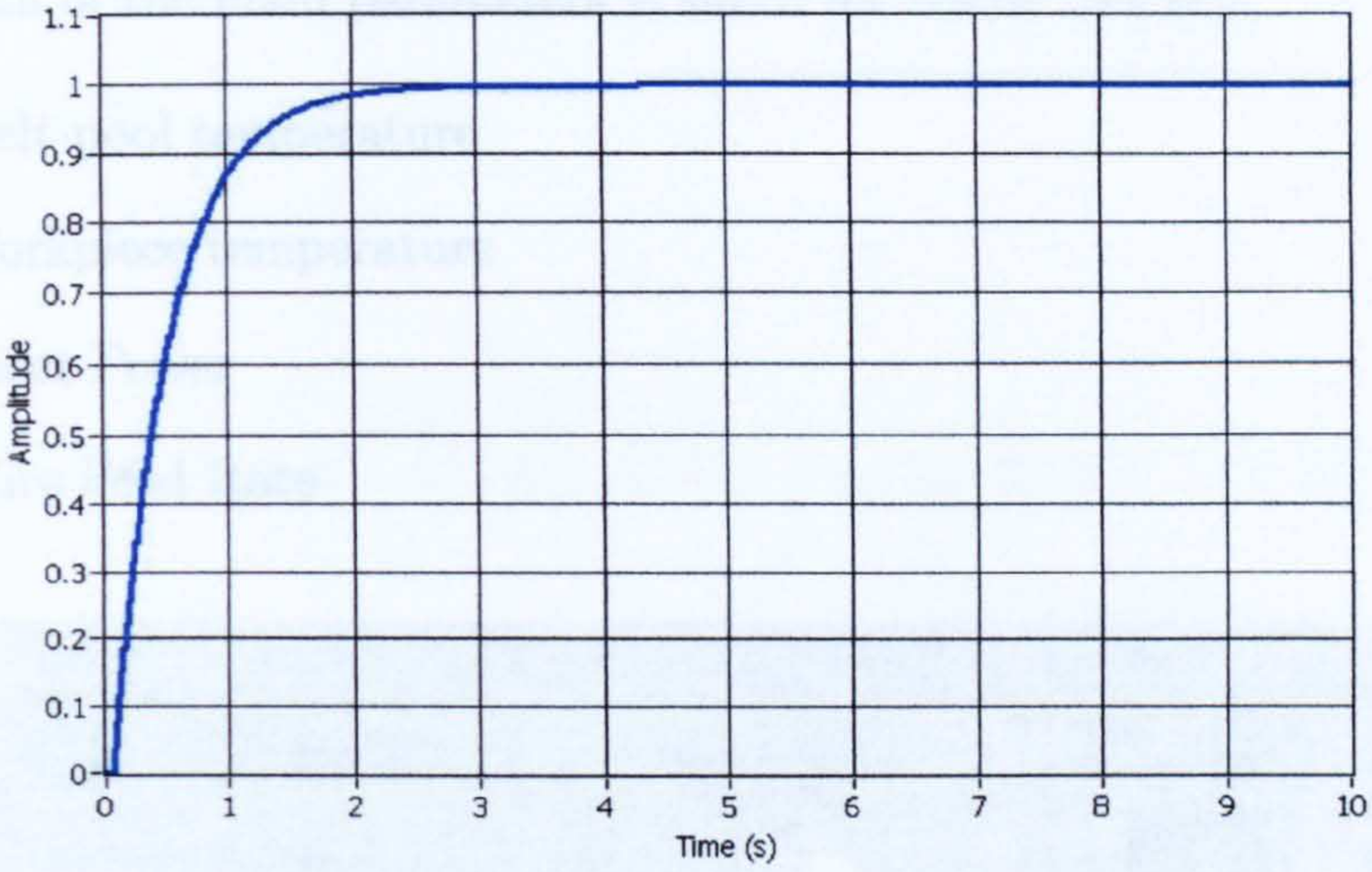

Figure 6.8: Time response of the system with the proposed controller (K = 0.7)

6.2 Controller Algorithm

The controller has been programmed using LabVIEW^{TM} software. Figure 6.9 shows the user interface of the program. The characteristics of the controller are:

- It uses the discrete zero-pole-gain form, in which the user has to specify the zeros, poles and gain of the controller function in the discrete domain
- The program is very flexible and can be used with a controller of order "n"
- It has a manual and an automatic mode, and is able to limit a maximum and minimum laser power output avoiding the wind-up effect
- It has a low-pass filter to reduce the noise of the temperature reading

- It shows the graphs of the temperatures and the laser power output so that the process can be monitored online
- It works at a frequency of 50 Hz
- The data of the main parameters is saved for offline analysis:
  - Melt pool temperature
  - Workpiece temperature
  - Laser Power
  - Wire Feed Rate

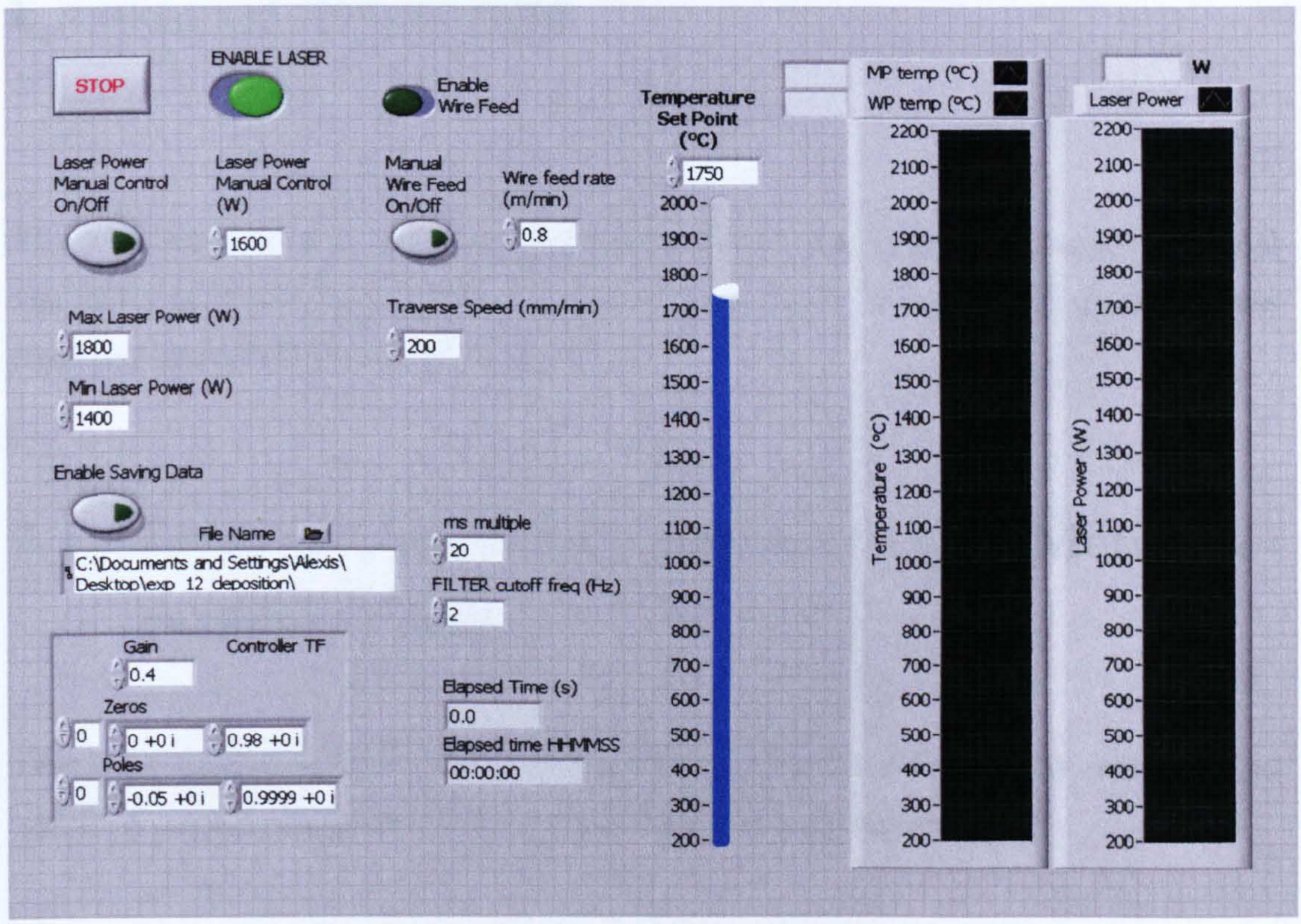

Figure 6.9: Interface of the controller

Chapter 7

Implementation of Temperature Control System

This chapter describes the implementation of the temperature controller in metal deposition of simple geometries such as single-bead walls and cylinders, using stainless steel and also titanium alloy Ti-6Al-4V.

7.1 Process Control of Non-continuous Metal Deposition (Walls)

This experiment consisted of the application of the controller to the deposition of multiple-layered single-bead-width walls, with these objectives:

- To deposit walls with controlled temperature and to analyse the performance of the system at different temperatures with austenitic stainless steel
- To make samples for tensile test and hardness test

- To analyse the suitability of the control system for metal deposition of Ti-6Al-4V

- To integrate the components of the system and to develop a strategy to stop and start automatically the wire feed, laser and CNC table movement

7.1.1 Experimental Conditions

Based on the controller design described in chapter 6, a number of trials were done to tune the controller for metal deposition of stainless steel. The resultant parameters for the controller were:

Gain	0.4
Pole:	0.9999 + 0i
Pole:	-0.05 + 0i
Zero:	0 + 0i
Zero:	0.98 + 0i
Frequency:	50 Hz

The melt pool temperature was filtered using a second-order low-pass filter with a cut-off frequency of 2 Hz. This frequency was selected after analysing graphically the raw signal and the desired filter action.

The process was performed inside the inert gas chamber, with an argon flow rate of 30 L/min. The melt pool temperature was measured at the centre of the melt pool. Other experimental conditions were:

Length of walls:	150 mm and 170 mm
Height of walls:	up to 115 mm
Traverse speed:	200 mm/min
Wire feed rate:	0.8 m/min
Step in Z:	1.2 mm

During the first trials of metal deposition of walls the laser power was controlled manually, monitoring the process in order to obtain a smooth and stable deposition. It was observed that the temperature was around 1750 °C. This temperature was then selected to build the first walls with automatic temperature control.

In the following sections the results of the experiments are explained as well as the strategies to achieve a more robust metal deposition system. These strategies were developed when depositing stainless steel at a temperature of 1750 °C.

7.1.2 First Layers of a Wall

During the first layers of the wall the plate acts as a heat sink. If the laser power is increased, the plate absorbs the extra heat and the melt pool temperature does not increase as much. So that, to some extent, the temperature does not depend on the laser power.

As the controller is based on the principle that the melt pool temperature depends on the laser power, then it does not perform properly. If the temperature is lower than the set-point, the controller may increase the laser power until it reaches its maximum. Vice versa, if the temperature is higher than the set-point, the controller may decrease the laser power until reaching its minimum. Figure 7.1 shows the deposition of the second layer of a wall with the temperature controller ON. In this bead the temperature was slightly above 1750 °C (set-point) and, although the laser power was reduced about 500 W, the temperature practically did not decrease.

After a few layers have been deposited the heat flow is reduced because the temperature of the workpiece is higher (i.e. lower temperature gradient) and the heat flow gradually changes from three-dimensional to bi-dimensional. If the laser power is increased, a greater part of the extra heat remains in the melt pool, raising its temperature. For this reason the melt pool temperature becomes more dependent on the laser power and the controller works properly.

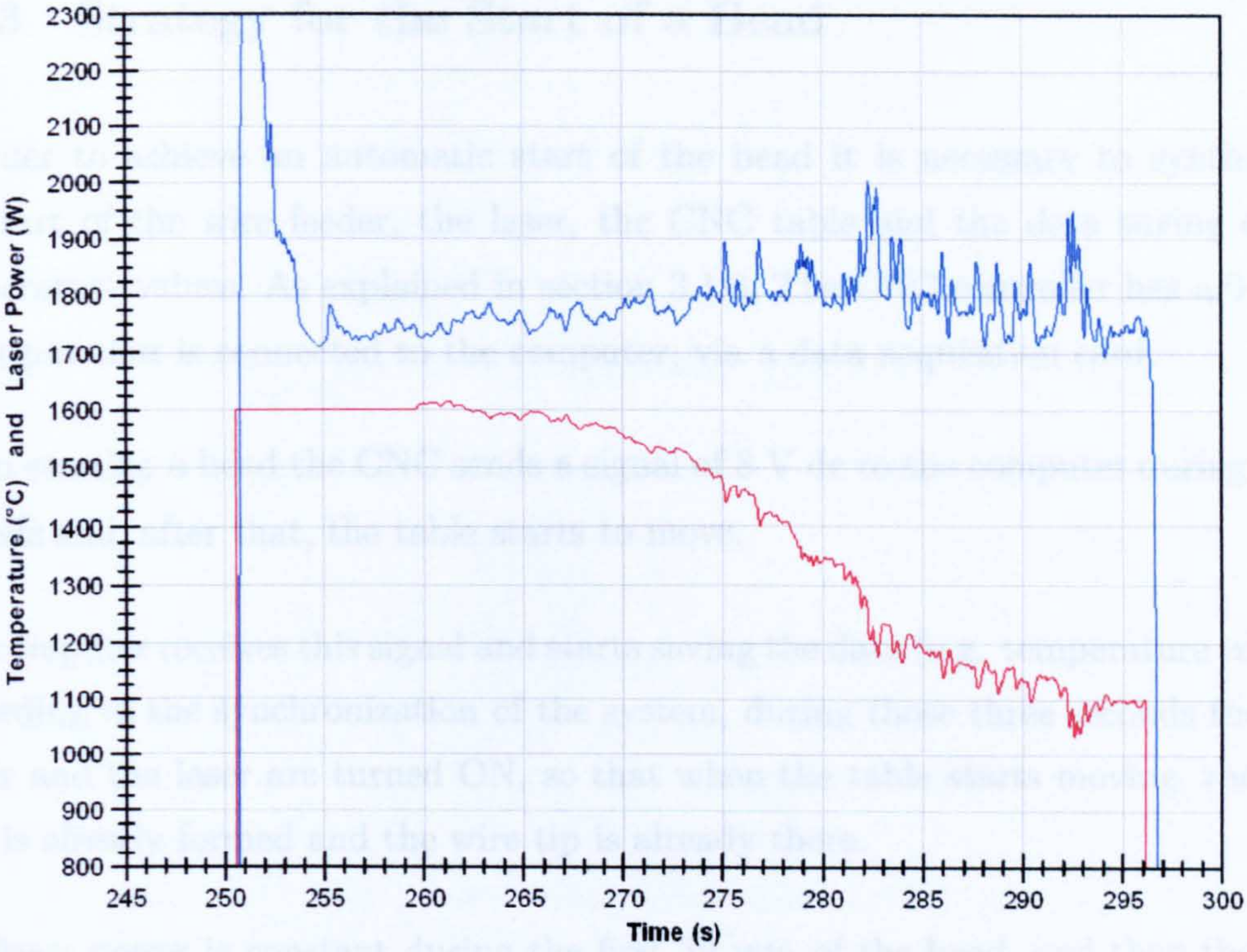

Figure 7.1: Deposition of second layer in a single-bead wall
Blue: Melt pool temperature. Red: Laser power.

In the experiments, in order to reduce the temperature gradient of the deposition of the first layer, a preheat run was made without wire feed. Then, for the first layers it was found convenient to set a constant laser power during the whole bead. For example, 1600 W during the first layer; 1500 W during layers 2, 3 and 4; 1400 W for the layer 5 and 6. Then turn ON the automatic controller from layer 7 onwards.

In section 8.4 it is shown that the hardness was greater in the first few millimetres from the bottom of the wall, due to the faster cooling rate. After that, the hardness decreased due to the slower cooling rate. This coincided with the performance of the temperature controller; it worked better once a slow cooling rate was achieved.

7.1.3 Strategy for the Start of a Bead

In order to achieve an automatic start of the bead it is necessary to synchronise the start of the wire feeder, the laser, the CNC table and the data saving of the temperature values. As explained in section 3.1.8, The CNC controller has a 0–10 V dc output that is connected to the computer, via a data acquisition card.

When starting a bead the CNC sends a signal of 8 V dc to the computer during three seconds and, after that, the table starts to move.

The computer receives this signal and starts saving the data (e.g. temperature values). According to the synchronization of the system, during those three seconds the wire feeder and the laser are turned ON, so that when the table starts moving, the melt pool is already formed and the wire tip is already there.

The laser power is constant during the first 30 mm of the bead, and then the temperature controller is automatically switched ON. This is in order to ensure that the temperature reading is in a stable condition before the controller is switched on.

The laser power used during these 30 mm is determined from the average laser power of a small segment of the previous bead in which the temperature is assumed to be stable. For example: if the length of the wall is 150 mm, the average laser power used during the segment 90–120 mm is calculated by the controller and is then used as the laser power setting for the start of the next bead. A different segment could be used if desired.

A typical graph of the temperature of one bead is shown in Figure 7.2. When the laser hits the material the melt pool is formed and there is a peak in the temperature reading. Then, the temperature reading becomes closer to the operating point. After 30 mm with constant laser power, the controller is turned ON and keeps the temperature around the set-point (in this case 1750 °C). At the end of the bead there is another peak in the temperature reading (see section 7.1.4).

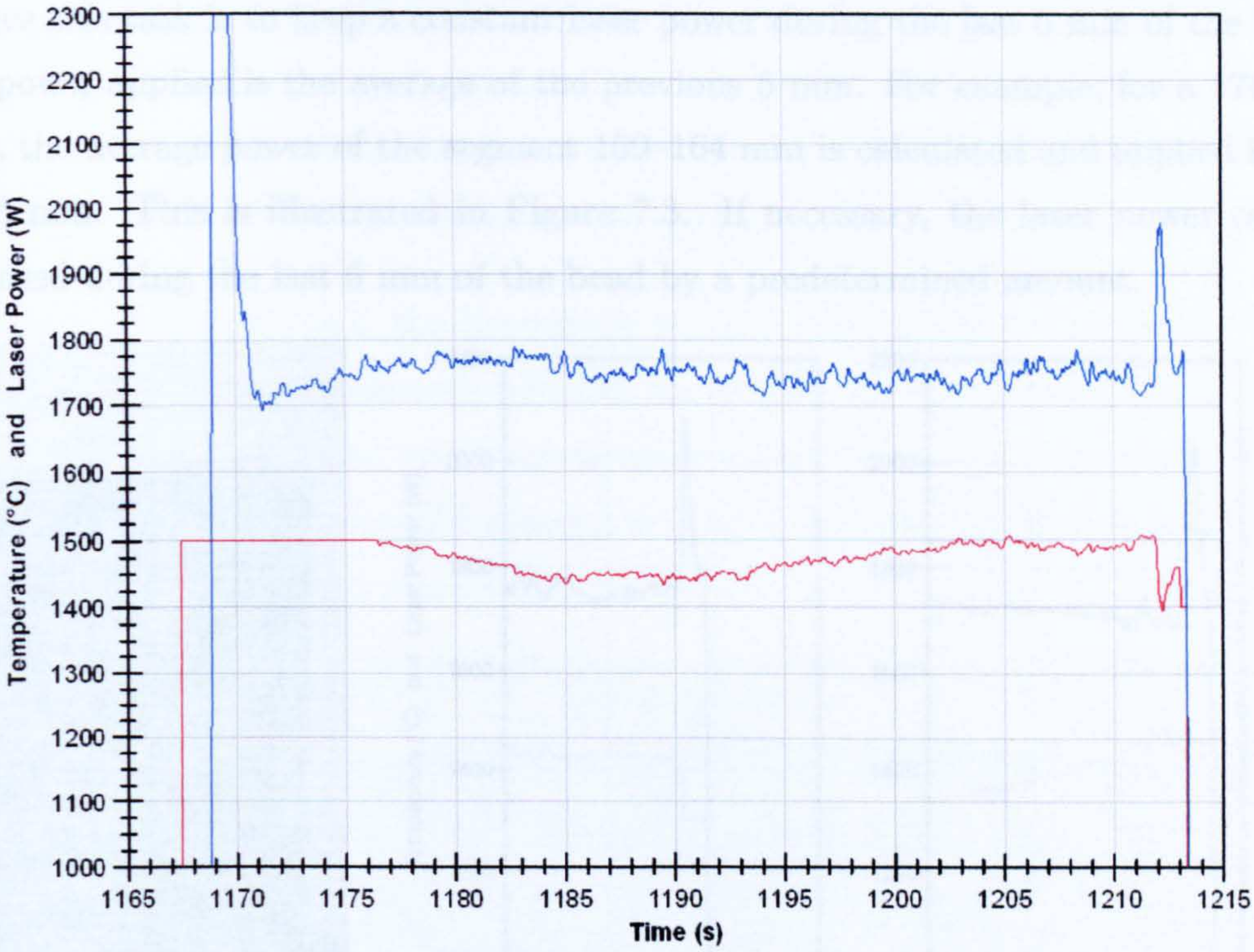

Figure 7.2: Deposition of a bead: melt pool temperature and laser power
Blue: Melt pool temperature. Red: Laser power.

7.1.4 Strategy for the End of a Bead

After few layers have been deposited on a wall, an excess deposit is formed at the end of every layer, as shown in Figure 7.3. When the metal deposition reaches this point, there is a very high temperature reading.

Because of this increase on the reading, the controller reduces the laser power (see Figure 7.3). As previously stated, a reduction on laser power produces a narrower/higher bead, then, the excess deposit will increase during the following layers. If this continues, there will be a point in which the wire tip will start hitting this lump without melting.

In order to deal with this problem it is necessary to ensure that the laser power is not reduced when the melt pool reaches the excess deposit. The strategy applied to

achieve this task is to keep a constant laser power during the last 6 mm of the bead. The power applied is the average of the previous 5 mm. For example, for a 170 mm bead, the average power of the segment 159–164 mm is calculated and applied in the last 6 mm. This is illustrated in Figure 7.3. If necessary, the laser power can be increased during the last 6 mm of the bead by a predetermined amount.

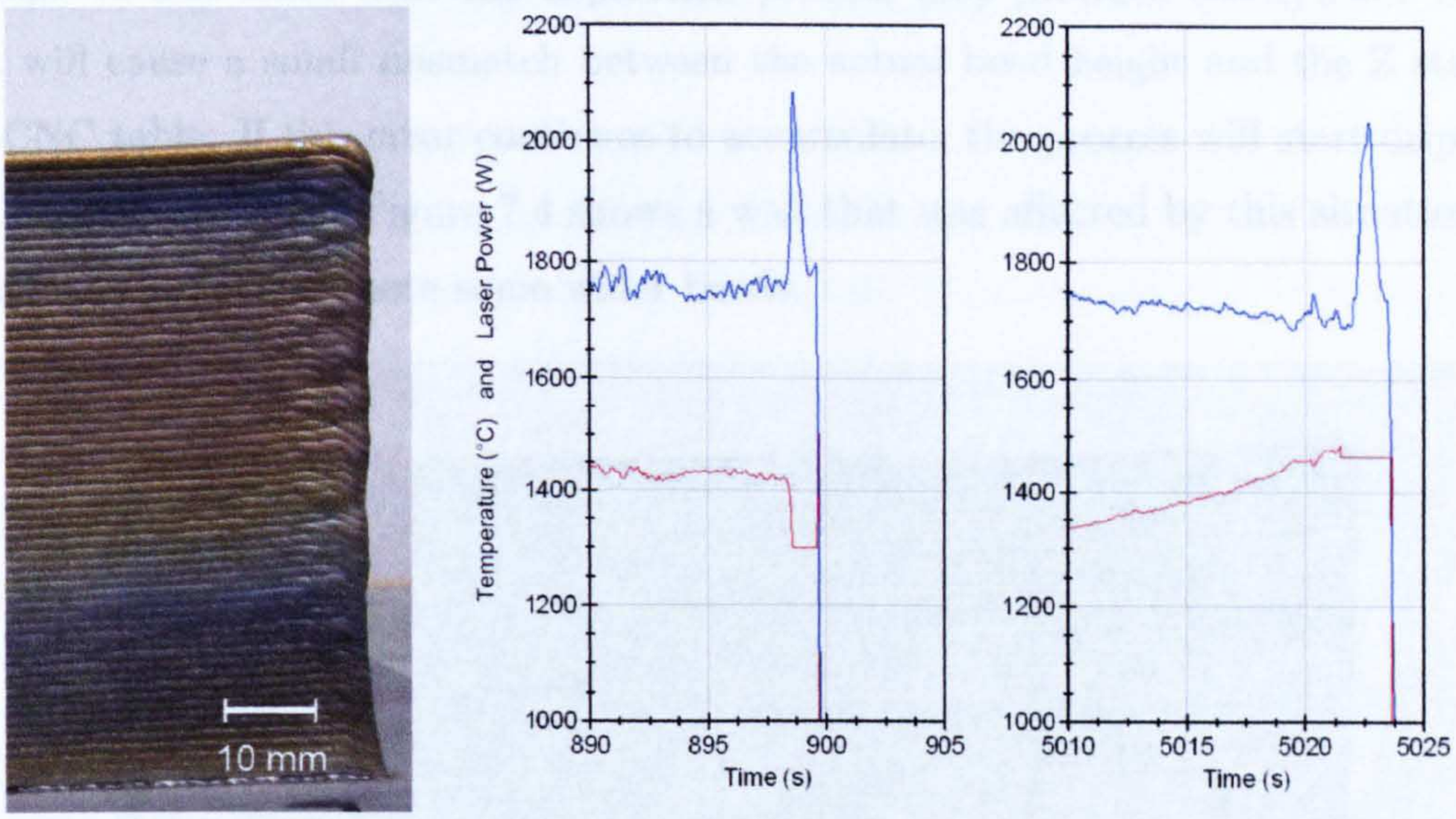

Figure 7.3: Excess deposit formed at the end of every layer and its effect
Blue: Melt pool temperature. Red: Laser power.
Left: Excess deposit at the end of the wall.
Centre: Effect on temperature measurement and laser power.
Right: Laser power with constant value at the end of the bead.

7.1.5 Strategy for Building Multiple Walls

The experiments explained so far consisted of building one wall per plate. When building two walls on the same plate, the first approach used was to build one complete wall and, after finishing that wall, the system would move to its side in order to build the second wall (provided that the components of the system do not crash with the wall).

This, however, affects the cooling of the second wall and its deposition process. Ap-

parently, the first wall obstructs the convection inside the argon chamber, reducing the cooling rate on the beads deposited on the second wall. Even more, the laser reflections that come from the deposition process and hit the first wall are reflected back to the second wall, increasing its temperature.

Because of this extra heat the deposition process may produce wider/lower beads that will cause a small mismatch between the actual bead height and the Z step of the CNC table. If this error continues to accumulate, the process will start dripping and become unstable. Figure 7.4 shows a wall that was affected by this situation, in which it is possible to note some wider beads.

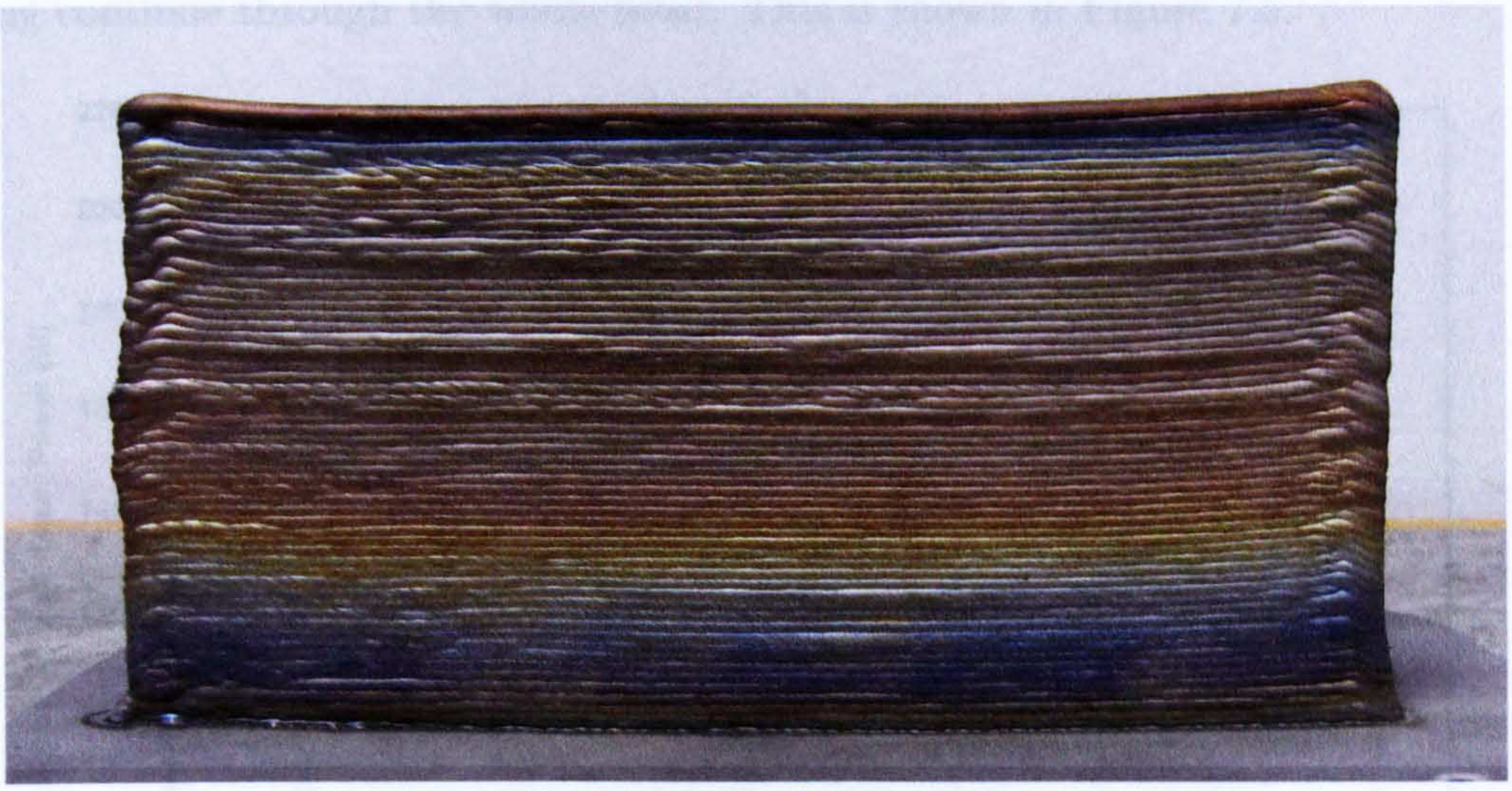

Figure 7.4: Problems when building multiple walls one at a time
The length of the wall is 150 mm.

This problem is avoided when the walls are built alternating the deposition of the beads, i.e. depositing a bead on "wall 1" and then a bead on "wall 2", and so on. This strategy also provides more cooling time for each bead, so that it reduces risk of overheating the walls. Using this approach, good quality deposition was achieved in both walls. The maximum workpiece temperature (at the start of the beads) was 412 °C, which is considerably lower than the 560 °C reached during the deposition of single walls.

7.1.6 Workpiece Temperature

The purpose of including the workpiece pyrometer in the system is to analyse whether there is any difference on the metal deposition process as the workpiece temperature is increased and whether it can be considered to improve the control system. As shown in chapter 5, the measuring point was 10 mm before the melt pool.

This temperature is measured at every layer. The data saving starts a few seconds before turning ON the laser, so that the initial temperature is taken without being influenced by the heat coming from the melt pool. Then the measurement and data saving continue through the whole bead. This is shown in Figure 7.5.

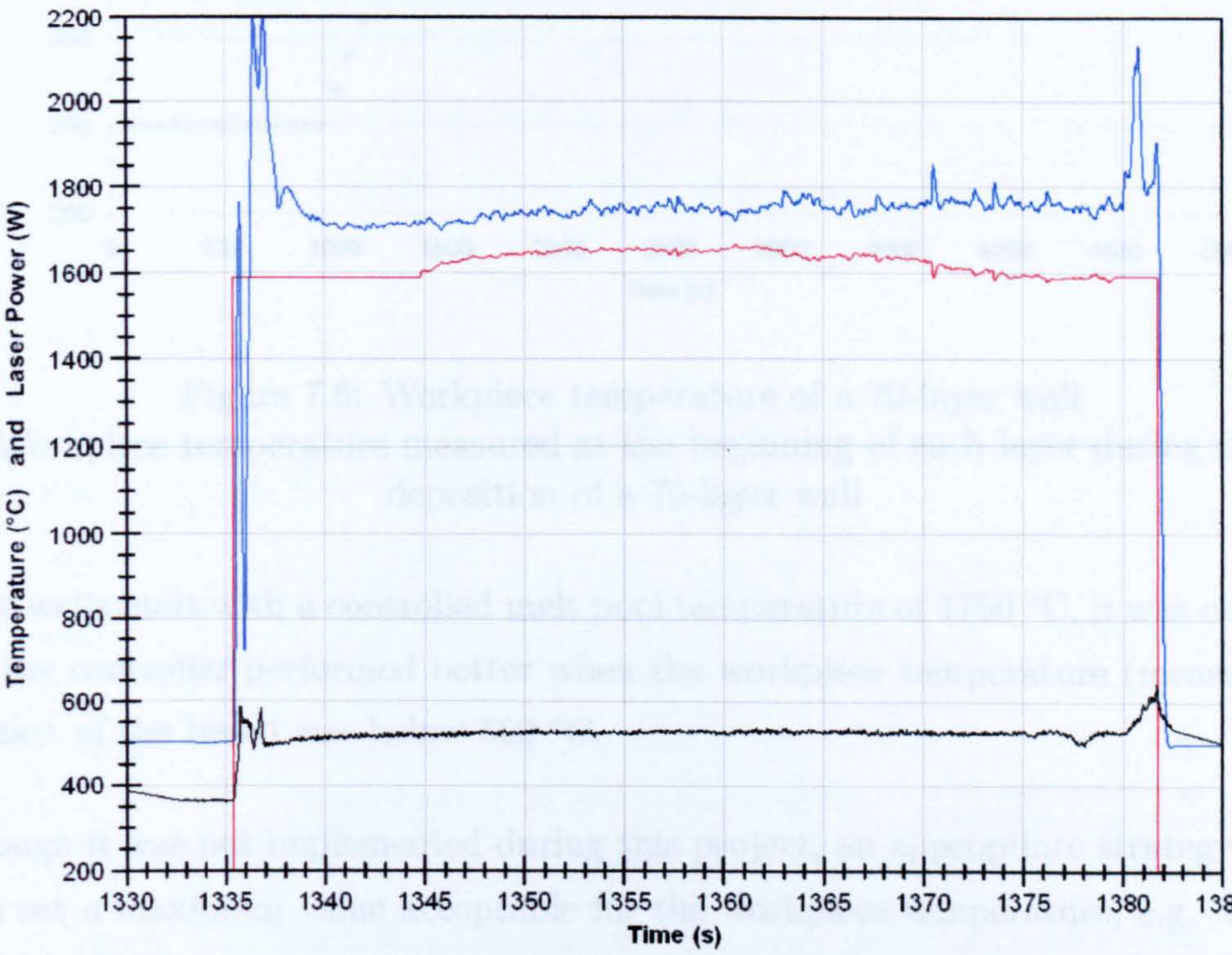

Figure 7.5: Workpiece temperature at the beginning of a bead
Blue: Melt pool temperature. Black: Workpiece temperature. Red: Laser power.
It can be noticed that, before the start of the bead, the workpiece temperature was 360 °C.

The temperature range of the workpiece pyrometer is 250–1350 °C. Figure 7.6 shows

the workpiece temperature, measured at the start of each layer, during the deposition of a 70-layer wall. It can be noticed that for this wall the temperature reached values of up to 560 °C, and that it settled down after approximately 50 layers.

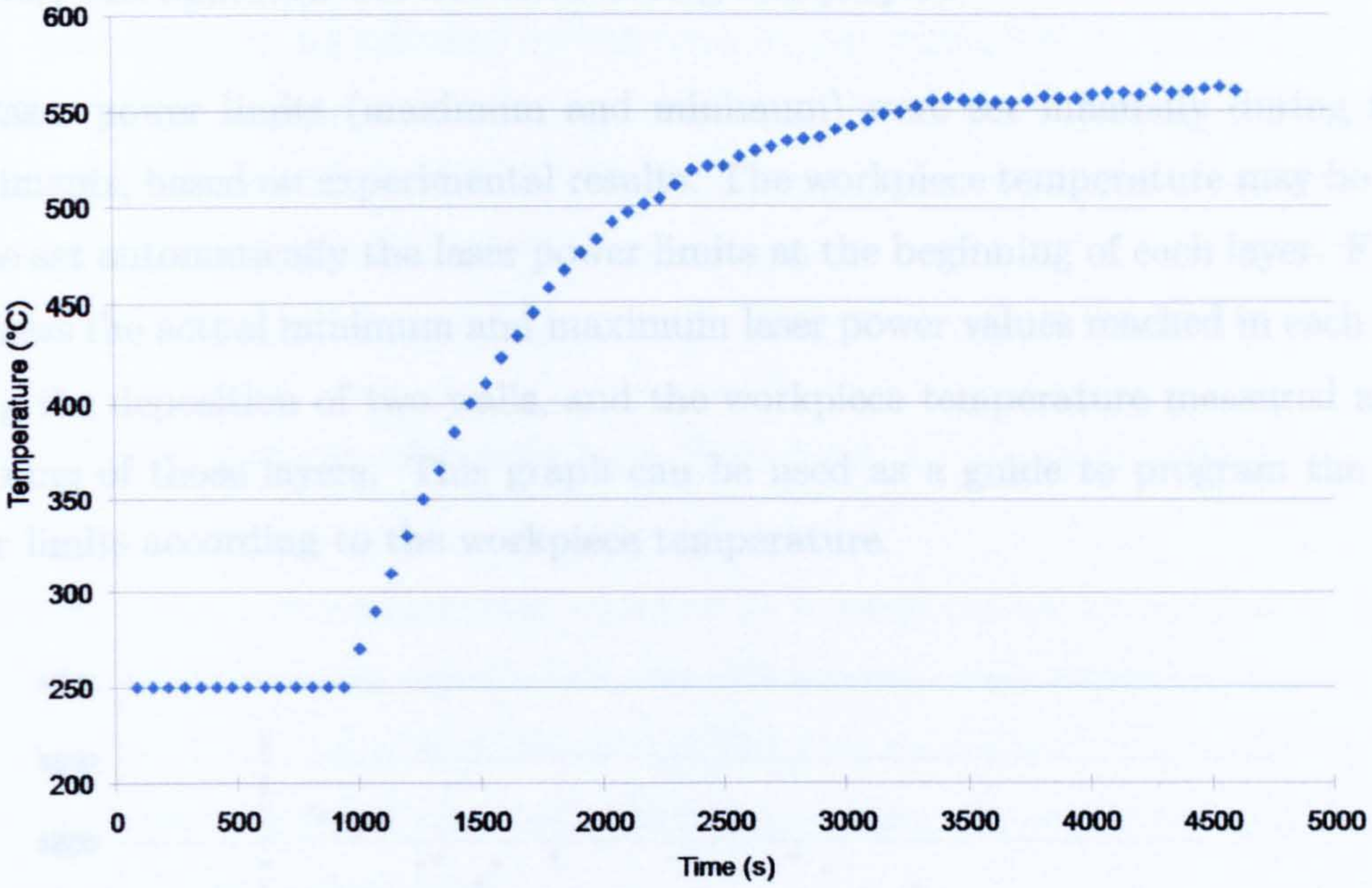

Figure 7.6: Workpiece temperature of a 70-layer wall
Workpiece temperature measured at the beginning of each layer during the deposition of a 70-layer wall

In the walls built with a controlled melt pool temperature of 1750 °C, it was observed that the controller performed better when the workpiece temperature (measured at the start of the bead) was below 500 °C.

Although it was not implemented during this project, an appropriate strategy would be to set a maximum value acceptable for the workpiece temperature, e.g. 450 °C, and measure the temperature at every bead, before the metal deposition starts. Thus, if the temperature is up to 450 °C, then start the deposition. If it is above that value, then wait until it cools down to 450 °C. This idea of setting a maximum workpiece temperature at which metal deposition is performed was previously suggested and applied by Spencer et al. [53]. This approach would also assist to maintain a lower temperature inside the inert gas chamber.

The workpiece temperature could be also used as an alternative approach to set a laser power value at the start of bead, i.e. that the initial laser power of the bead may be a function of the workpiece temperature (measured before the deposition starts). However, this approach was not tried during this project.

The laser power limits (maximum and minimum) were set manually during these experiments, based on experimental results. The workpiece temperature may be used also to set automatically the laser power limits at the beginning of each layer. Figure 7.7 shows the actual minimum and maximum laser power values reached in each bead during the deposition of two walls, and the workpiece temperature measured at the beginning of those layers. This graph can be used as a guide to program the laser power limits according to the workpiece temperature.

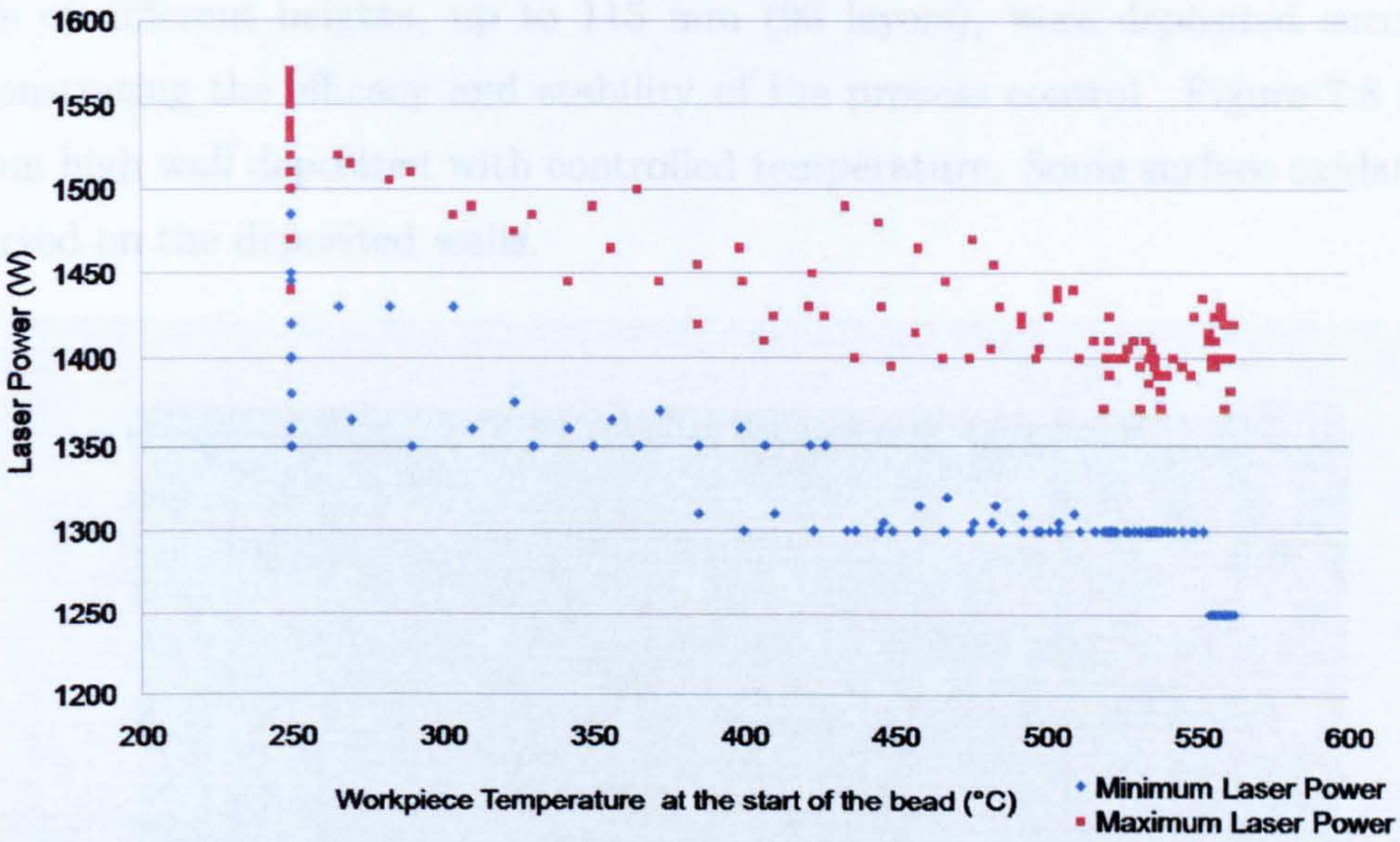

Figure 7.7: Workpiece temperature and laser power extreme values

The conditions of the metal deposition do vary depending on the heat, which changes depending on the geometry and temperature of the workpiece. Another possible application for the workpiece temperature would be to use it to set the controller parameters according to the temperature. For example, to have one set of controller parameters to use when the workpiece temperature is below a predetermined value

(e.g. 350 °C). Then use a second set of parameters when the temperature is above that value.

So far the analysis has been done on the workpiece temperature before the melt pool starts, because it is not affected by the heat of the melt pool. It is worth noticing that the workpiece temperature during the process (i.e. when the melt pool is already formed) varied from 450 to 580 °C. The measuring point was close to the melt pool (10 mm), so it received the heat conducted from it.

7.1.7 Deposition of Stainless Steel at 1750 and 2000 °C

Smooth and stable deposition was achieved at a temperature set-point of 1750 °C. Walls of different heights, up to 115 mm (96 layers), were deposited successfully, demonstrating the efficacy and stability of the process control. Figure 7.8 shows a 70 mm high wall deposited with controlled temperature. Some surface oxidation was observed on the deposited walls.

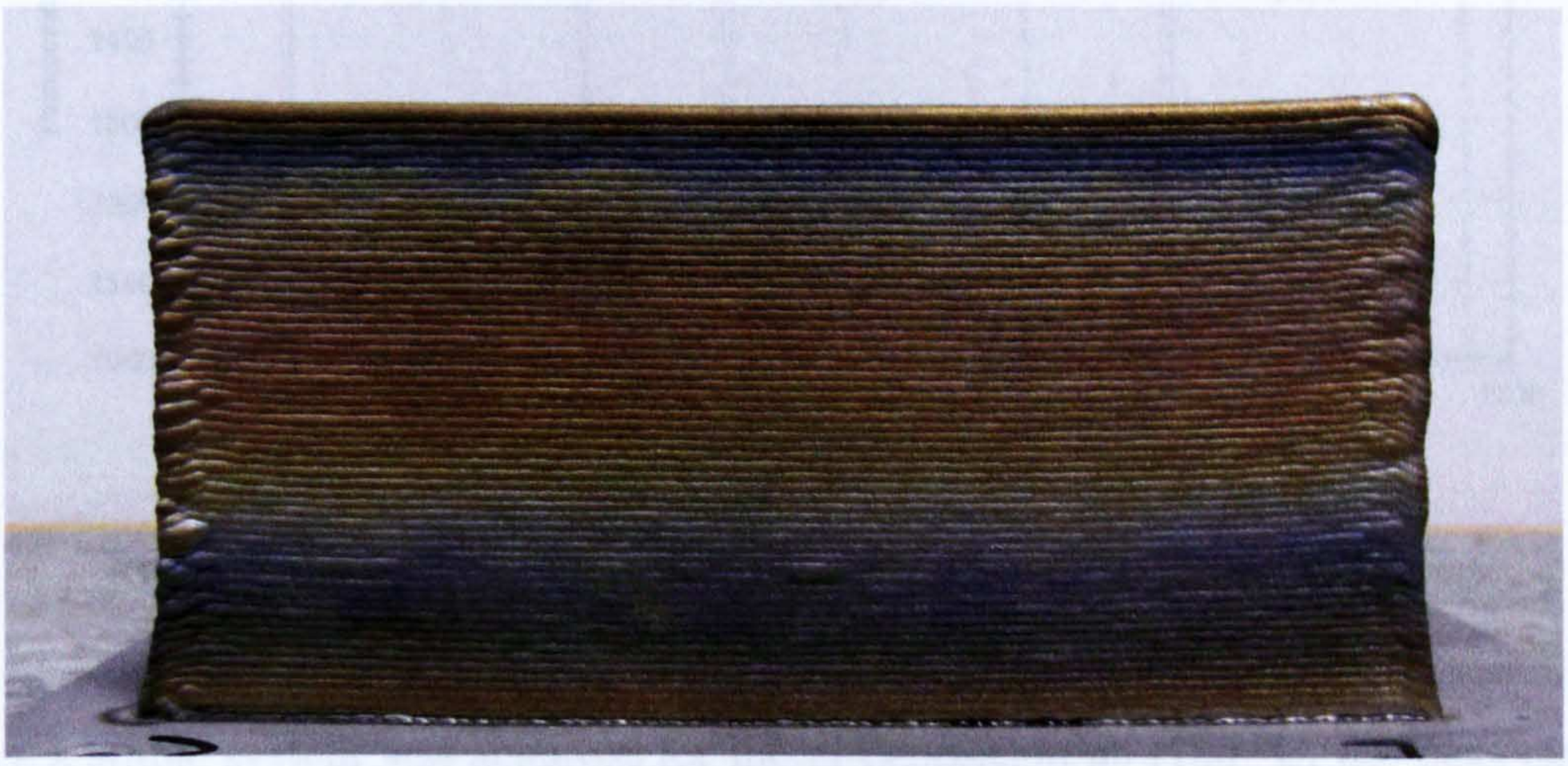

Figure 7.8: Stainless steel 308LSi wall deposited at 1750 °C
The length of the wall is 150 mm

Good temperature control was achieved with this system. Figure 7.9 shows the temperature and laser power of three consecutive beads of a wall deposited at 1750 °C,

whereas Figure 7.10 shows the same parameters during 20 layers. It can be seen how the controller maintains the temperature around the set-point and how the laser power is gradually reduced.

Apparently, the heat accumulates more in the central part of the wall than in the sides. This is reflected in the graphs, where the temperature tends to increase and the controller reduces the laser power because less heat is needed to deposit the material at the set-point temperature (see Figure 7.9).

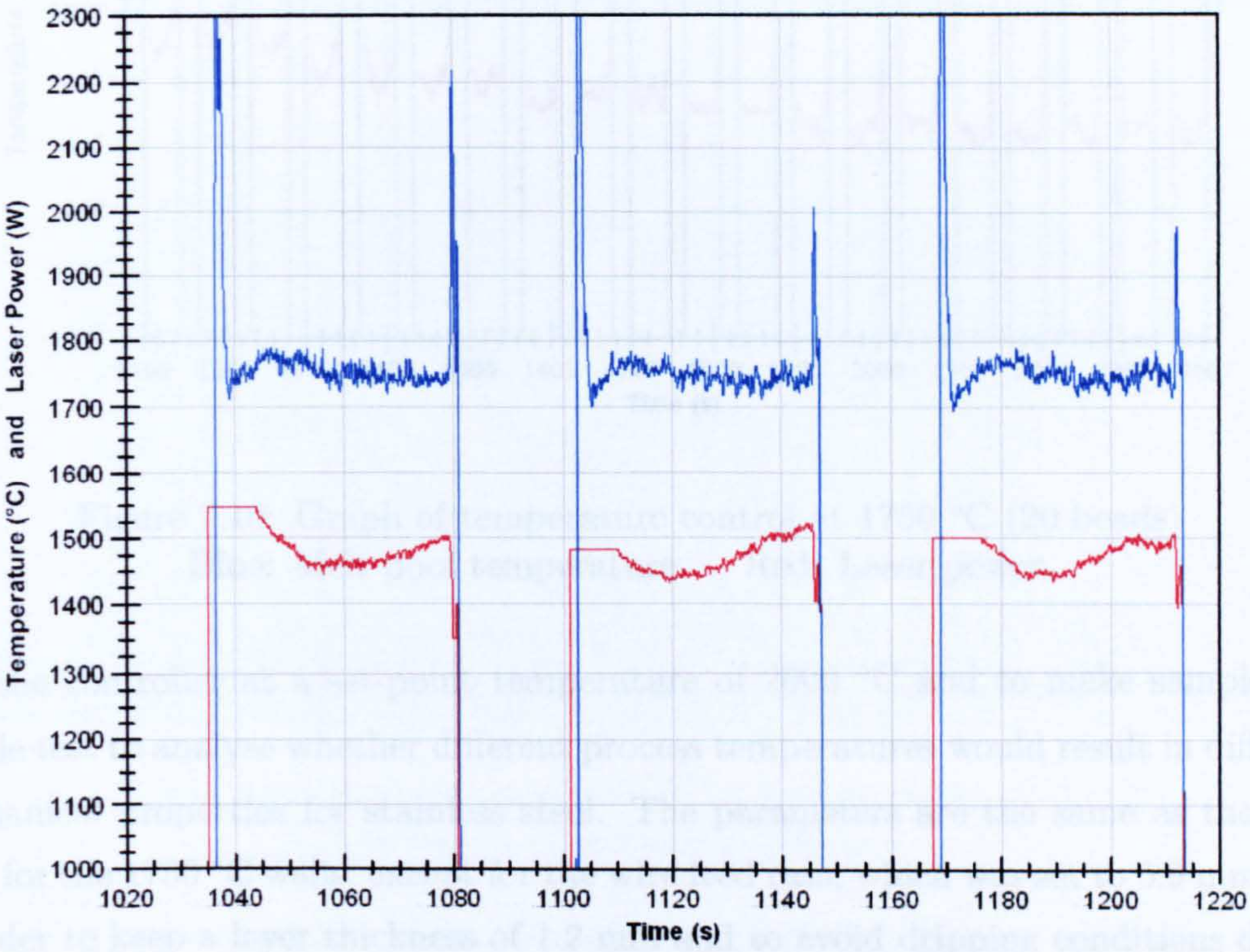

Figure 7.9: Graph of temperature control at 1750 °C (three beads)
Blue: Melt pool temperature. Red: Laser power.

Once a stable system was achieved for metal deposition at 1750 °C, the next experiment was to build walls controlling the melt pool temperature at a different temperature set-point. This temperature had to be higher than 1750 °C in order to ensure that all the material would melt. In this case the temperature chosen was 2000 °C.

The objectives of this experiment were to analyse the performance of the process

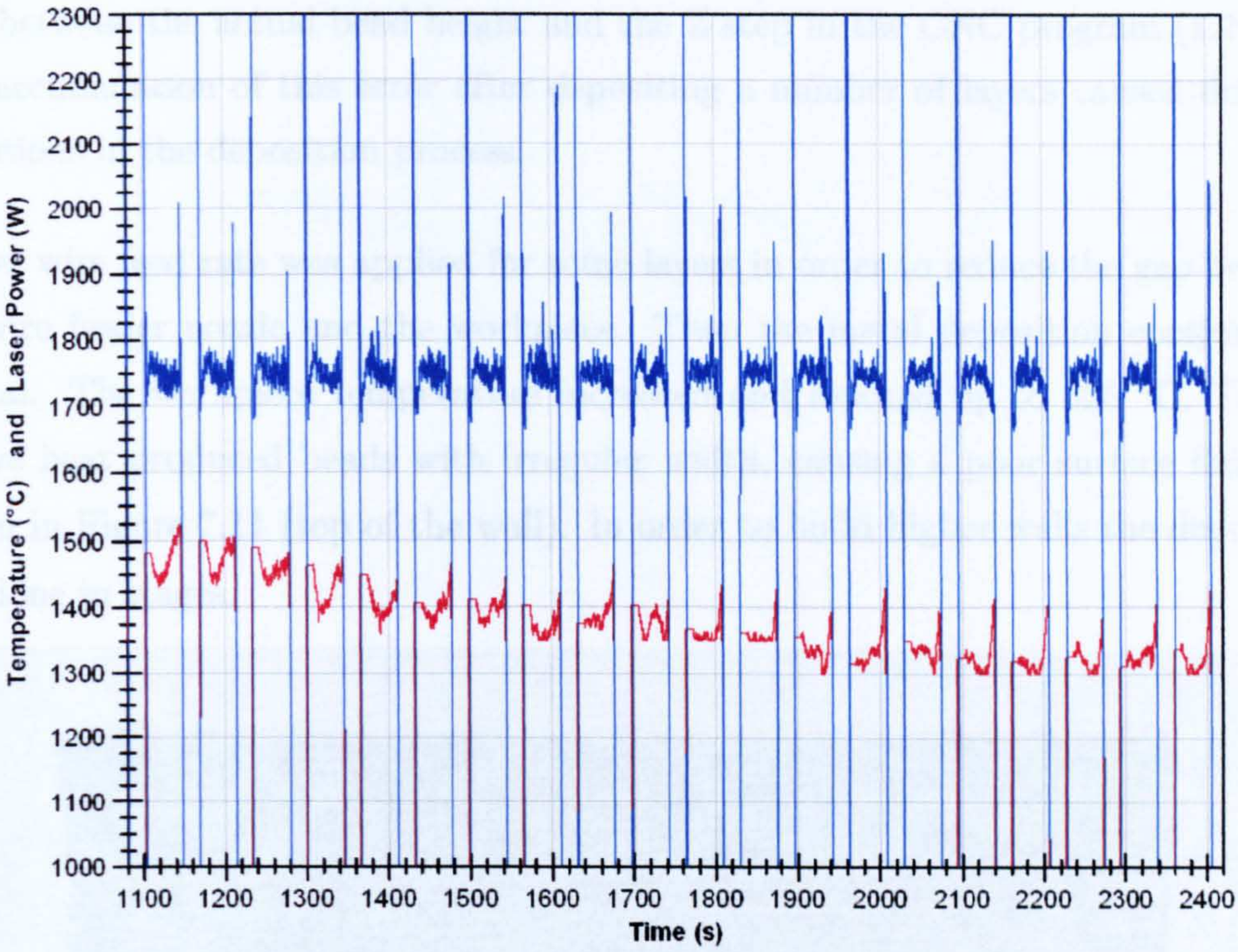

Figure 7.10: Graph of temperature control at 1750 °C (20 beads)
Blue: Melt pool temperature. Red: Laser power.

and the controller at a set-point temperature of 2000 °C and to make samples for tensile test to analyse whether different process temperatures would result in different mechanical properties for stainless steel. The parameters are the same as the ones used for the 1750 °C walls, except for the wire feed rate, which was set to 0.9 mm/min in order to keep a layer thickness of 1.2 mm and to avoid dripping conditions due to the higher laser power required to increase the temperature.

Good metal deposition was also achieved at 2000 °C for walls of approximately 60 mm of height. However, after that, the process became somehow unstable. The gap between the wire feeder nozzle and the workpiece increased and the process changed from smooth to dripping deposition.

The workpiece temperature reached up to 585 °C (measured at the start of the bead). The excessive heat produced wider beads with reduced height, causing a small differ-

ence between the actual bead height and the Z step in the CNC program (1.2 mm). The accumulation of this error after depositing a number of layers caused dripping conditions in the deposition process.

Higher wire feed rate was applied for some layers in order to reduce the gap between the wire feeder nozzle and the workpiece. Then the metal deposition continued as normal. The workpiece temperature increased and reached up to 625 °C. The excessive heat produced beads with irregular width, causing a poor surface finish, as shown in Figure 7.11 (top of the wall). In order to build higher walls the deposition was done in stages.

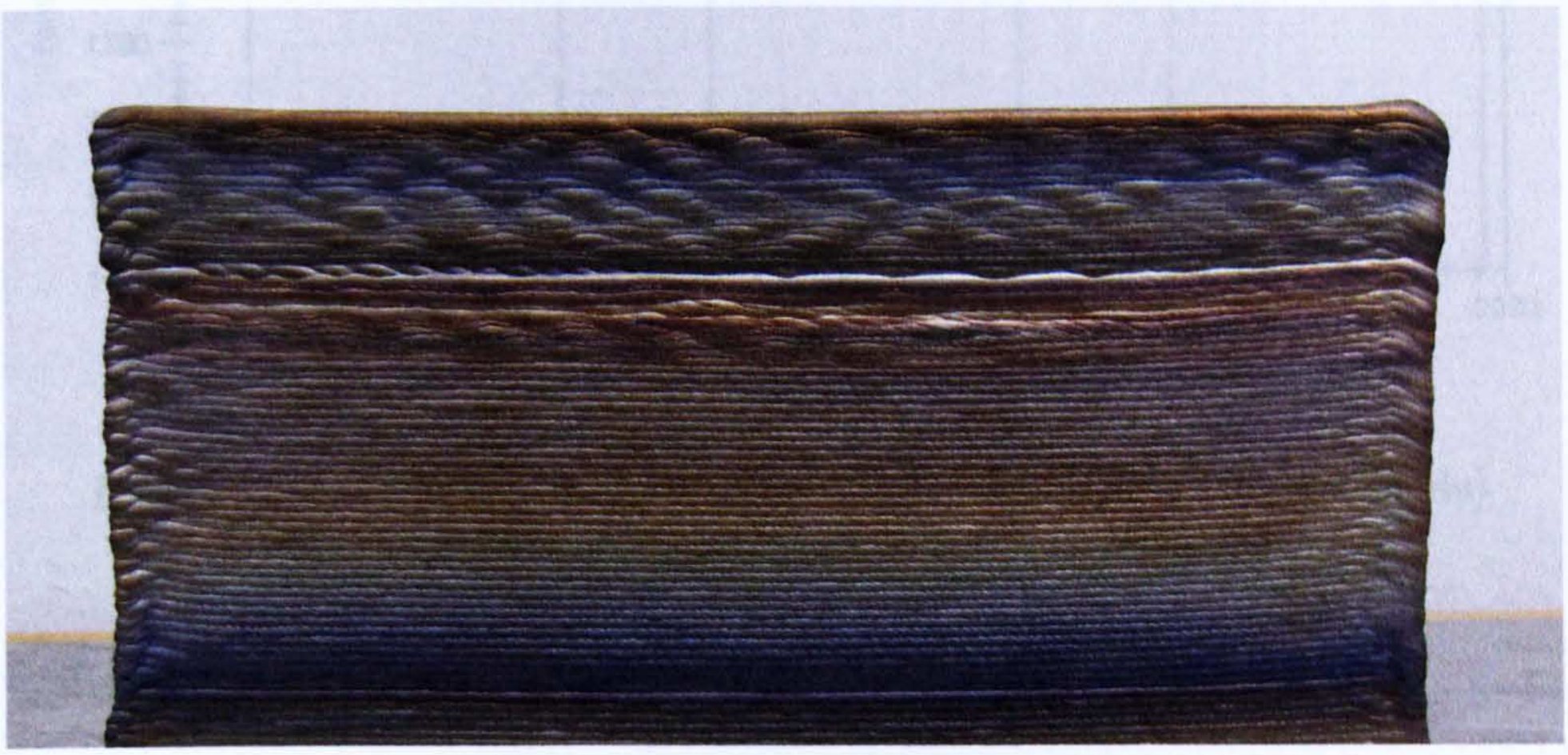

Figure 7.11: Stainless steel 308LSi wall deposited at 2000 °C
The length of the wall is 170 mm.

The system controlled the temperature around 2000 °C, but its performance was not as good as at 1750 °C i.e. the variation in temperature was higher at 2000 °C. Figure 7.12 shows the temperature and laser power of three consecutive beads of a wall deposited at this temperature.

From this experiment it can be concluded that a more stable and reliable process control is achieved at 1750 °C for stainless steel 308LSi. This temperature setting produces smooth and stable metal deposition, yet allowing the workpiece to remain at an acceptable temperature to avoid the creation of wider beads and dripping conditions for a high number of layers, without having to wait for long time to cool down

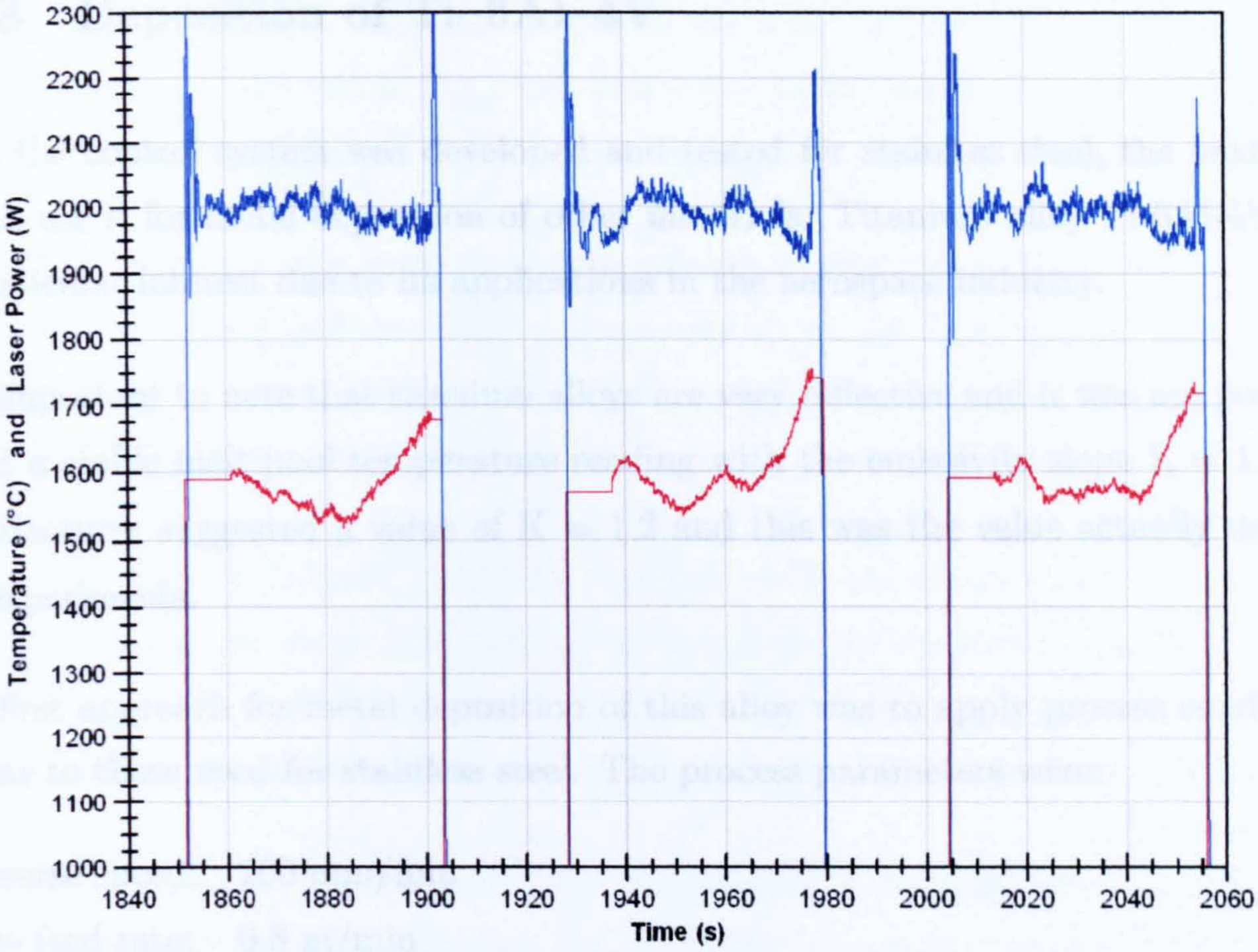

Figure 7.12: Graph of temperature control at 2000 °C (three beads)
Blue: Melt pool temperature. Red: Laser power.

the system between layers.

Although successful and controllable to a good extent, stainless steel metal deposition at 2000 °C produces some of disadvantages:

- Higher laser power is required for the metal deposition, so that the energy efficiency is lower
- It causes a higher workpiece temperature that can lead to an unstable process. The unstable conditions may be avoided by building the piece in stages or by waiting between each layer in order to allow the piece to cool down, however the total time for the fabrication of a piece will be longer than at 1750 °C
- It causes a higher temperature inside the chamber. This situation could affect the plastic enclosure and the optical filters.

7.1.8 Deposition of Ti–6Al–4V

Once the control system was developed and tested for stainless steel, the next step was to use it for metal deposition of other materials. Titanium alloy Ti-6Al-4V was of particular interest due to its applications in the aerospace industry.

It is important to note that titanium alloys are very reflective and it was not possible to get a stable melt pool temperature reading with the emissivity slope K = 1. The manufacturer suggested a value of K = 1.2 and this was the value actually used in the experiments.

The first approach for metal deposition of this alloy was to apply process conditions similar to those used for stainless steel. The process parameters were:

Traverse speed: 200 mm/min
Wire feed rate: 0.8 m/min
Step in Z: 1.2 mm

A stable process was quickly achieved with these parameters, needing to find only a suitable range for the laser power. The power required for Ti-6Al-4V was lower than that needed for stainless steel.

The controller parameters (gain, poles and zeros) were the same as those used for stainless steel. The temperature set-point was 1850 °C. This was selected on the basis of various trials building small walls with manual control of the laser power. A process temperature of about 1850 °C produced smooth deposition.

During the experiments, it was found that Ti-6Al-4V behaves in a different way than stainless steel 308LSi. At the end of the deposition of a bead, when the wire was retracting, a big drop formed and solidified at the wire tip (instead of being deposited to the bead).

When building a wall, this drop was then deposited at the beginning of the next layer. After depositing a few layers, this situation produced a lump at the beginning of the

wall. It also produced a slope at the end of the wall because the material was not being deposited at the end of the bead, and every bead tended to be slightly shorter than the previous one.

In order to overcome this problem it is necessary to find the right strategy and parameters to start and end the bead: when to start/stop the laser and the wire feeder; and whether it is necessary to modify the laser power and/or the wire feed rate at the start and/or at the end of the bead.

Figure 7.13 shows a 45-layer Ti-6Al-4V wall built with the temperature controller. It can be observed that there is a lump at the beginning of the wall and a slope at the lower half of the end of the wall. For the upper half the parameters were modified for the end of the beads and it can be seen that a more consistent end was achieved.

The central section of the wall, where the controller is actually active, shows good metal deposition, demonstrating that the controller is working properly in this material. Figure 7.14 shows a section of the temperature and laser power graph for metal deposition of Ti-6Al-4V using the temperature controller. From this experiment it can be concluded that the temperature controller performs well with Ti–6Al–4V, but it is necessary to find the right strategy and parameters to to optimize the start and end of the bead.

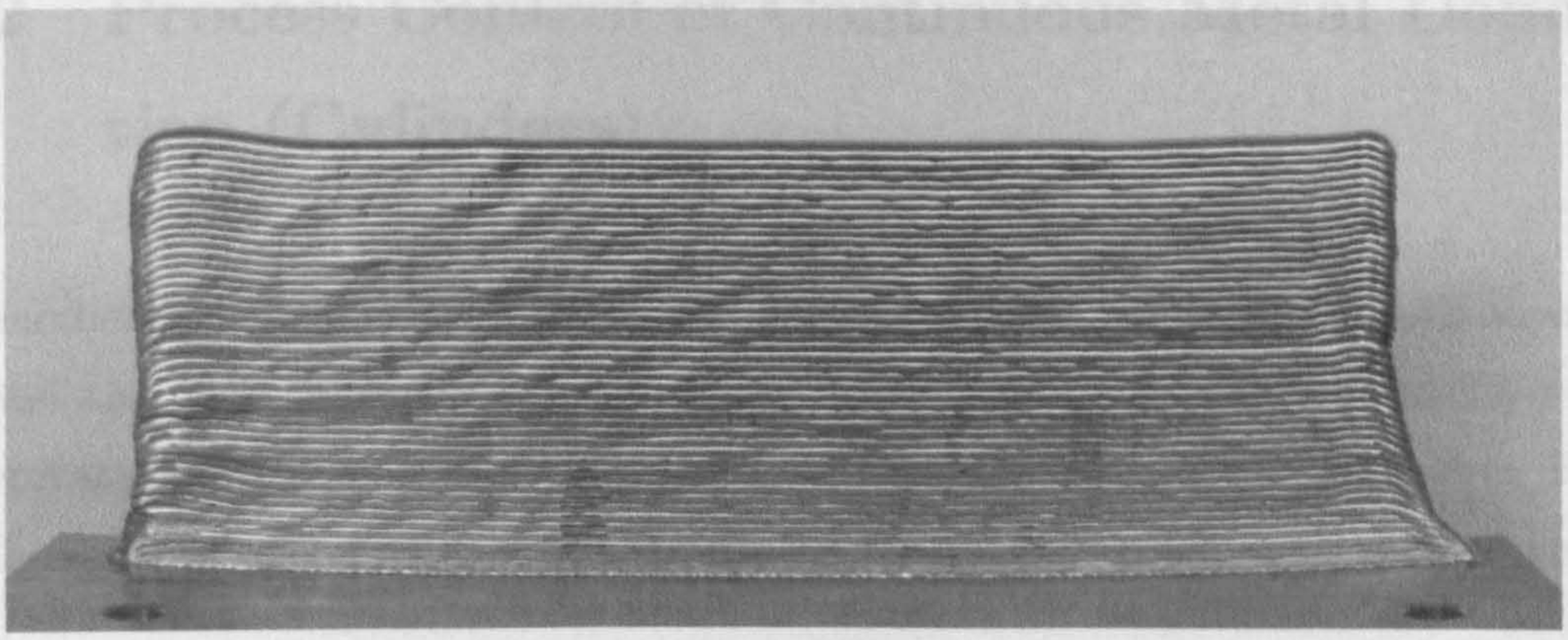

Figure 7.13: Ti–6Al–4V wall deposited at 1850 °C
The height of the wall is 54 mm.

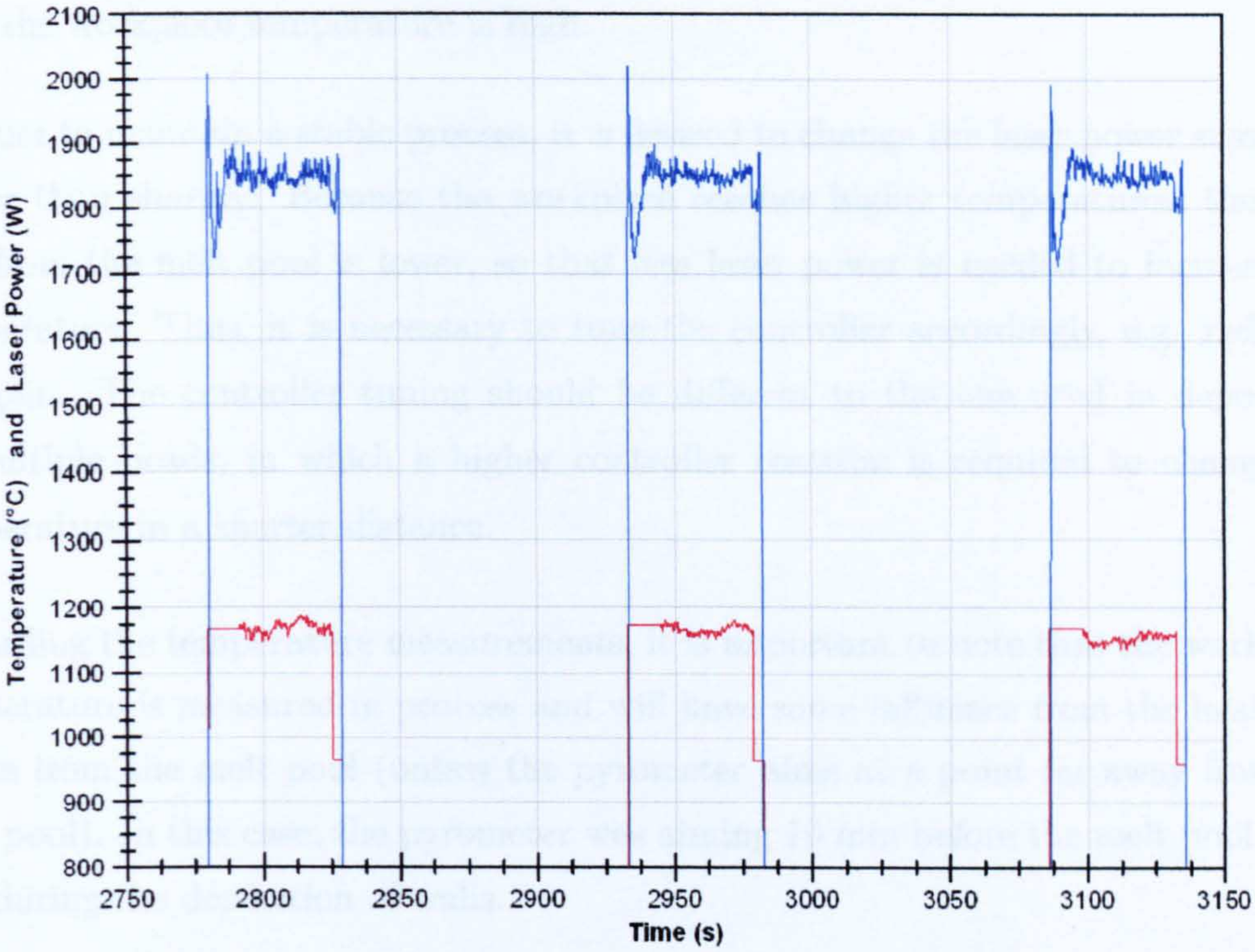

Figure 7.14: Graph of temperature control of Ti–6Al–4V at 1850 °C (three beads)
Blue: Melt pool temperature. Red: Laser power.

7.2 Process Control of Continuous Metal Deposition (Cylinders)

A number of cylinders were built in stainless steel and also in Ti-6Al-4V in order to test the performance of the control system in continuous deposition. There are important differences between continuous and non-continuous metal deposition. Some of the distinctive characteristics of continuous metal deposition are described next.

Because the deposition is not interrupted, there is not much time for the workpiece to cool down, so that it can reach very high temperatures (values of 750 °C were measured for stainless steel). For this reason, lower laser power is normally required

once the workpiece temperature is high.

In order to maintain a stable process, it is desired to change the laser power smoothly rather than sharply. Because the workpiece reaches higher temperatures, the heat loss from the melt pool is lower, so that less laser power is needed to increase the temperature. Thus, it is necessary to tune the controller accordingly, e.g. reducing the gain. The controller tuning should be different to the one used in deposition of multiple beads, in which a higher controller reaction is required to change the temperature in a shorter distance.

Regarding the temperature measurements, it is important to note that the workpiece temperature is measured in process and will have some influence from the heat that comes from the melt pool (unless the pyrometer aims at a point far away from the melt pool). In this case, the pyrometer was aiming 10 mm before the melt pool, as it was during the deposition of walls.

The experimental conditions are similar to those used for the deposition of walls. The process was performed inside the inert gas chamber, with an argon flow rate of 30 L/min, in order to avoid oxidation problems. This is shown in Figure 7.15. During these experiments the cylinders were built with the following characteristics:

Diameter of cylinders:	50 mm (centreline)
Height of cylinders:	49 mm (41 layers)
Traverse speed:	200 mm/min (tangential)
Wire feed rate:	0.8 m/min
Step in Z:	1.2 mm

The strategies for the deposition are explained in the next section.

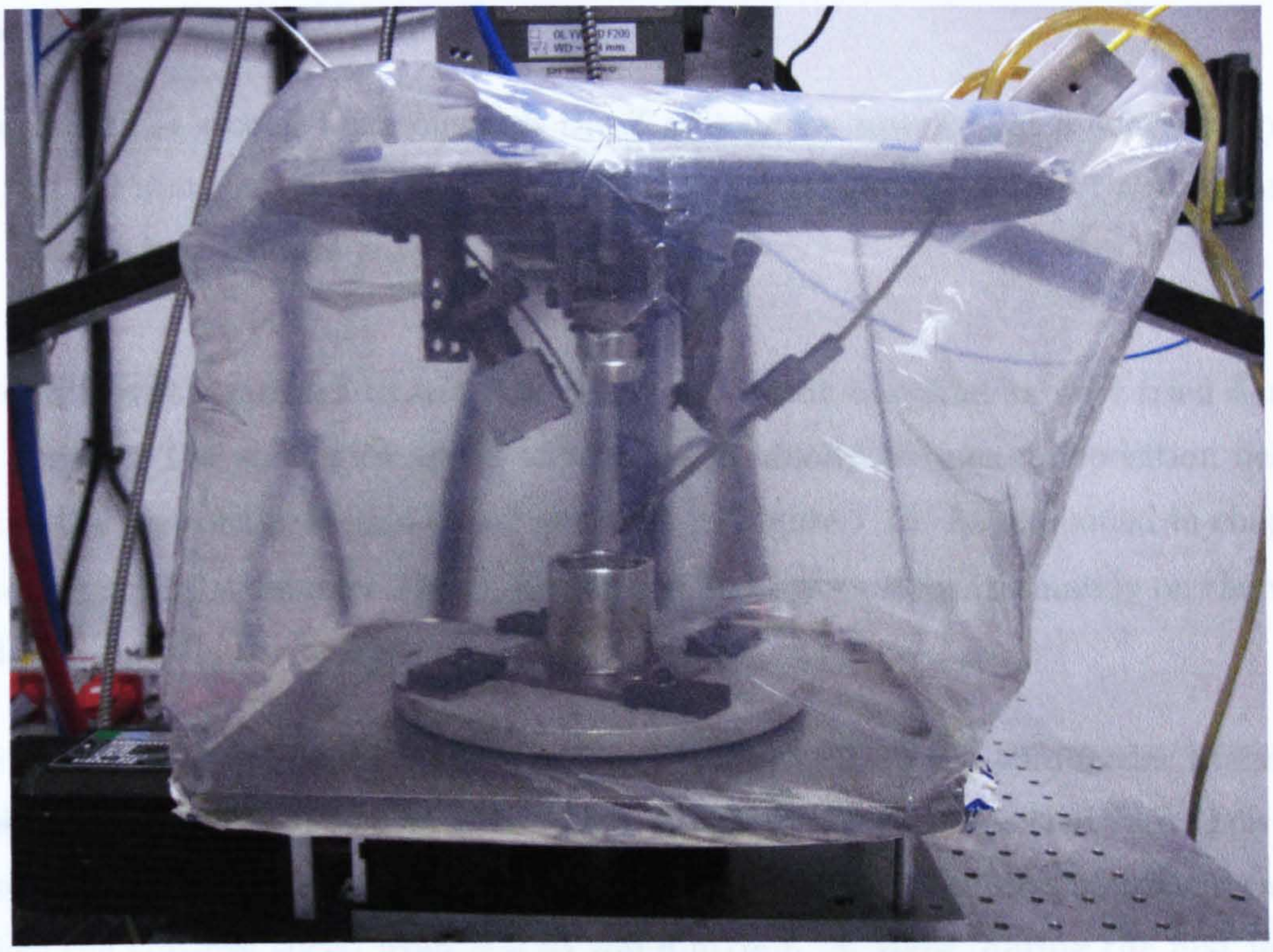

Figure 7.15: Deposition of a cylinder inside argon chamber
The diameter of the cylinder is 50 mm.

7.2.1 Strategy for Metal Deposition of Cylinders

As discussed in section 5.2.3 it is more convenient to build a cylinder in a continuous spiral path, in order to avoid disturbances in the temperature reading. It is necessary, then, to start this spiral movement from the beginning of the deposition of the cylinder. This means to increment (continuously or in steps) the height of the bead during one layer so that, when the next layer in deposited on top of it, the spiral path can be performed.

The movement of the rotary axis A and the Z axis produces the spiral path. The sequence is described here:

- A preheat run is made (one revolution with the laser ON, without wire feed)

- The first layer is deposited
- From the second layer onwards the Z axis moves upwards at a constant speed of 1.2 mm (or any predetermined Z step) per revolution of the A axis, in order to produce a spiral path

Three different strategies to start the spiral deposition of cylinders were tried during this project. The strategies aimed to increase gradually the metal deposition height during the first or the second layer, as shown in Figure 7.16. As explained in chapter 4 the height of the deposited bead, during the first layers, depends mainly on the wire feed rate and the traverse speed.

The first strategy was performed when the system utilized the wire feeder Planetics Jupiter 501, which did not have an external control for the wire feed rate. For this reason, the only variable to modify was the traverse speed. The first approach was to reduce the traverse speed from 500 to 200 mm/min, in steps, during the first layer, keeping the traverse speed at 200 mm/min during the rest of the cylinder deposition. The wire feed rate was constant.

Although it produced an increase in the height of the first layer, this approach did not give good metal deposition in the first layer. As explained in chapter 4, the process does not perform well at high traverse speeds, producing undesirable conditions such as wavy beads and the possibility of forming porosity. The deposition was good after the second layer.

The second approach was performed with the Redman Controls wire feeder, which can be controlled externally. The strategy consisted of keeping the traverse speed constant at 200 mm/min, while increasing the wire feeder rate gradually during the first layer, and then keeping a constant wire feed rate during the rest of the cylinder.

This approach gave better results than the first one. However, at the beginning of the deposition, because of the low wire feed rate, it produced dripping conditions. As the wire feed rate is increased, the process changes from dripping to smooth metal

deposition.

This issue is especially problematic when depositing Ti-6Al-4V, because this material tends to form big drops. This produces a very uneven first layer, so that the process will struggle to deposit a smooth second layer on top of it.

Attempting to avoid this formation of drops, the third approach consisted of depositing the first layer at a constant traverse speed (200 mm/min) and a constant wire feed rate (0.8 m/min). Then, at the beginning of the second layer, when the Z axis starts to move upwards, the wire feed rate is drastically reduced, and then it is increased gradually during that layer.

Because there is one layer already deposited and the Z axis is just starting to move upwards, the gap between the workpiece and the wire tip is reduced, decreasing the chance of dripping conditions when low wire feed rate is being applied. This approach is illustrated in Figure 7.16 (right). In practice, the wire feed rate was 0.4 m/min at the beginning of the second layer and it was gradually increased to 0.8 m/min. The formation of drops was reduced but not eliminated with this approach.

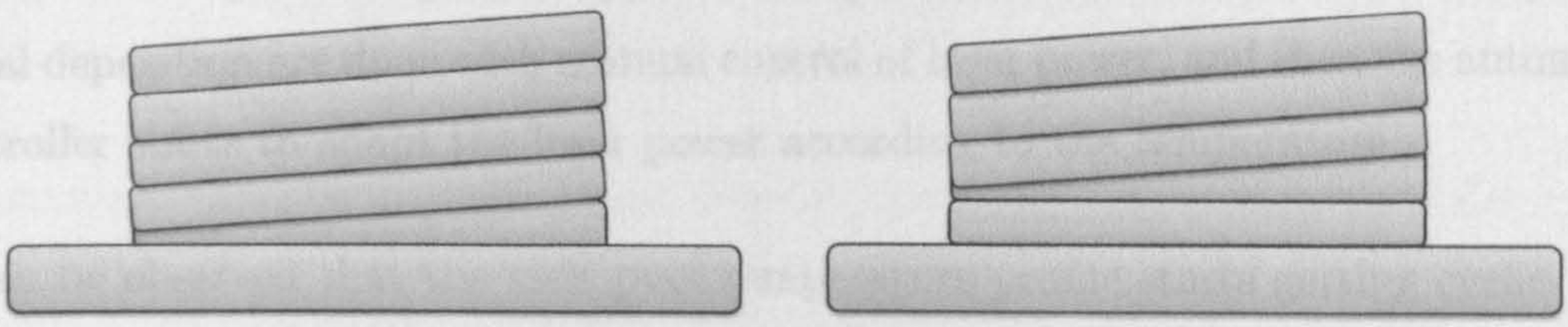

Figure 7.16: Start of the spiral path in the deposition of cylinders
Left: to increase gradually the height of the first layer.
Right: to increase gradually the height of the second layer.

Regarding the laser power, it was controlled manually during approximately the first four layers, and then the temperature controller was switched ON.

7.2.2 Deposition of Stainless Steel

As stated before, a smoother response of the control is desired for continuous metal deposition. This was achieved by tuning the controller accordingly: reducing the gain and moving a zero towards the right (i.e. increasing its value on the real axis).

After different trials to tune the controller, better results were obtained with these parameters:

Gain:	0.003 to 0.005
Pole:	0.9999 + 0i
Pole:	-0.05 + 0i
Zero:	0 + 0i
Zero:	0.99 + 0i
Frequency:	50 Hz

Figure 7.17 shows the graph of temperatures and laser power of a stainless steel cylinder. The experiment starts with a pre-heating pass. When the metal deposition starts, the temperature gets to approximately 1650–1900 °C. The first few layers of metal deposition are done with manual control of laser power, and then the automatic controller starts to adapt the laser power according to the temperature.

It can be observed that the melt pool temperature profile starts getting cyclic from the beginning of the cylinder, when the laser power is controlled manually. Then the controller reacts in order to get a constant temperature. Thus, the controller output (laser power) becomes also cyclic in order to counteract the temperature variation. After few layers a more constant temperature is indeed achieved and maintained.

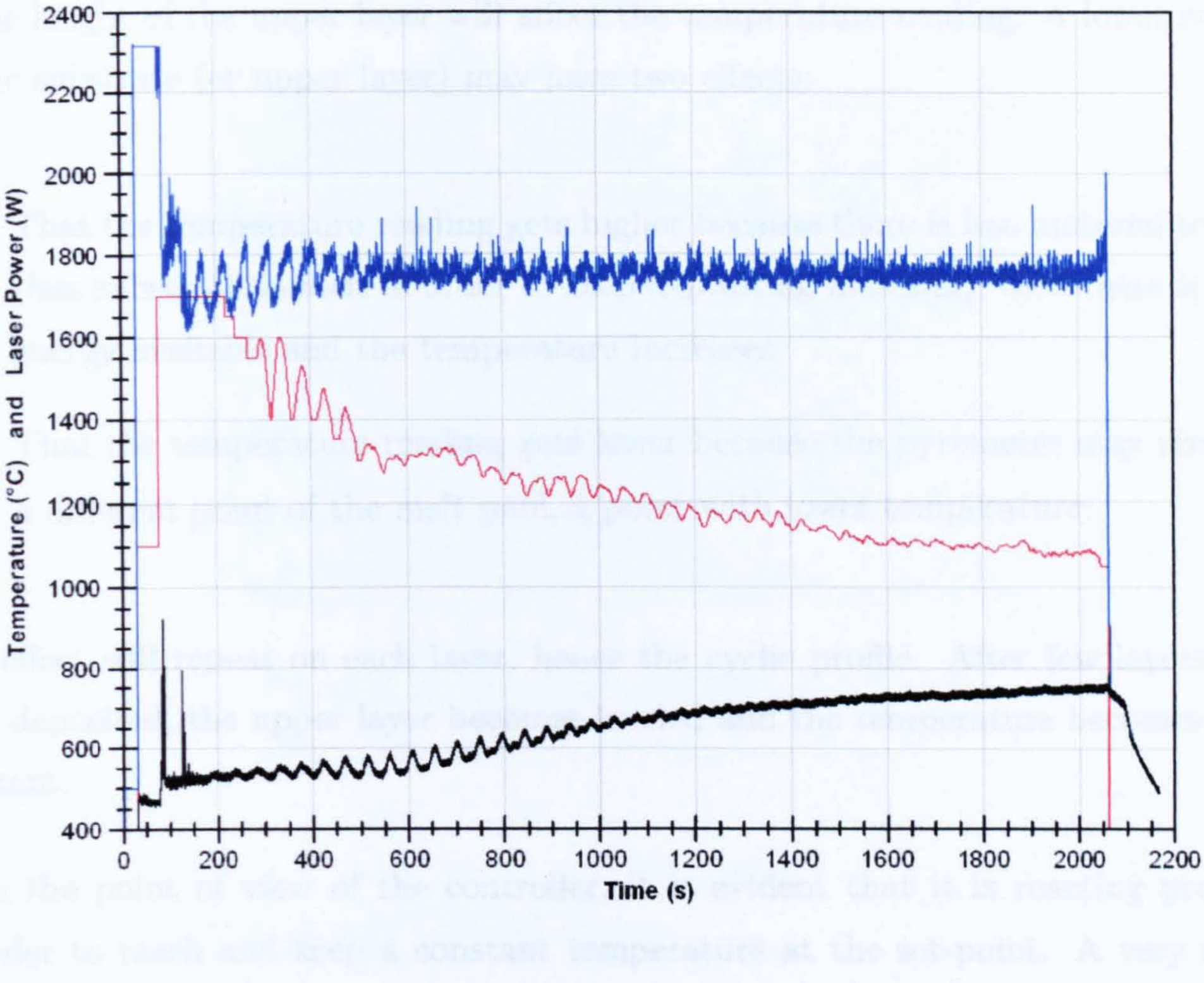

Figure 7.17: Deposition of a stainless steel 308LSi cylinder

Blue: Melt pool temperature. Black: Workpiece temperature. Red: Laser power.

As expected, the laser power is being reduced as the workpiece temperature increases. Due to this higher workpiece temperature, less power is required from the laser beam to keep melting the material.

Regarding the cyclic profile of the melt pool temperature, it is important to note that one cycle in the temperature graph corresponds to one layer in the cylinder (i.e. one revolution of the A axis). The stragety for building the cylinder appears to have an important effect on this issue.

The cyclic profile seems to start due to dripping conditions during the first or second layers, when the wire feed rate was varied and the laser power was manually controlled.

Dripping conditions on a section of the layer will cause an uneven layer. Variations

on the height of the upper layer will affect the temperature reading. A lower section on the substrate (or upper layer) may have two effects:

- That the temperature reading gets higher because there is less material to melt (less substrate to melt in order to keep depositing material), then there is more energy available and the temperature increases
- That the temperature reading gets lower because the pyrometer may aim into a different point of the melt pool, a point with lower temperature.

The effect will repeat on each layer, hence the cyclic profile. After few layers have been deposited, the upper layer becomes leveled and the temperature becomes more constant.

From the point of view of the controller, it is evident that it is reacting properly in order to reach and keep a constant temperature at the set-point. A very stable process is achieved and maintained, leading to good quality metal deposition.

However, in order to have a more repeatable process, it is necessary to optimise the start of the cylinder. This would include programming not only a change in the wire feeding rate but also in the laser power, in order to be able to optimize the combination of both factors and to avoid the variability of manual control so that a more repeatable start of the cylinder can be achieved.

It is also important to ensure that other factors do not affect the temperature reading. A height control system would help to overcome the variations on the upper layer, leading to a more robust process.

Figure 7.18 shows a cylinder built with controlled temperature at 1750 °C. The surface finish is very even, product of a very stable process.

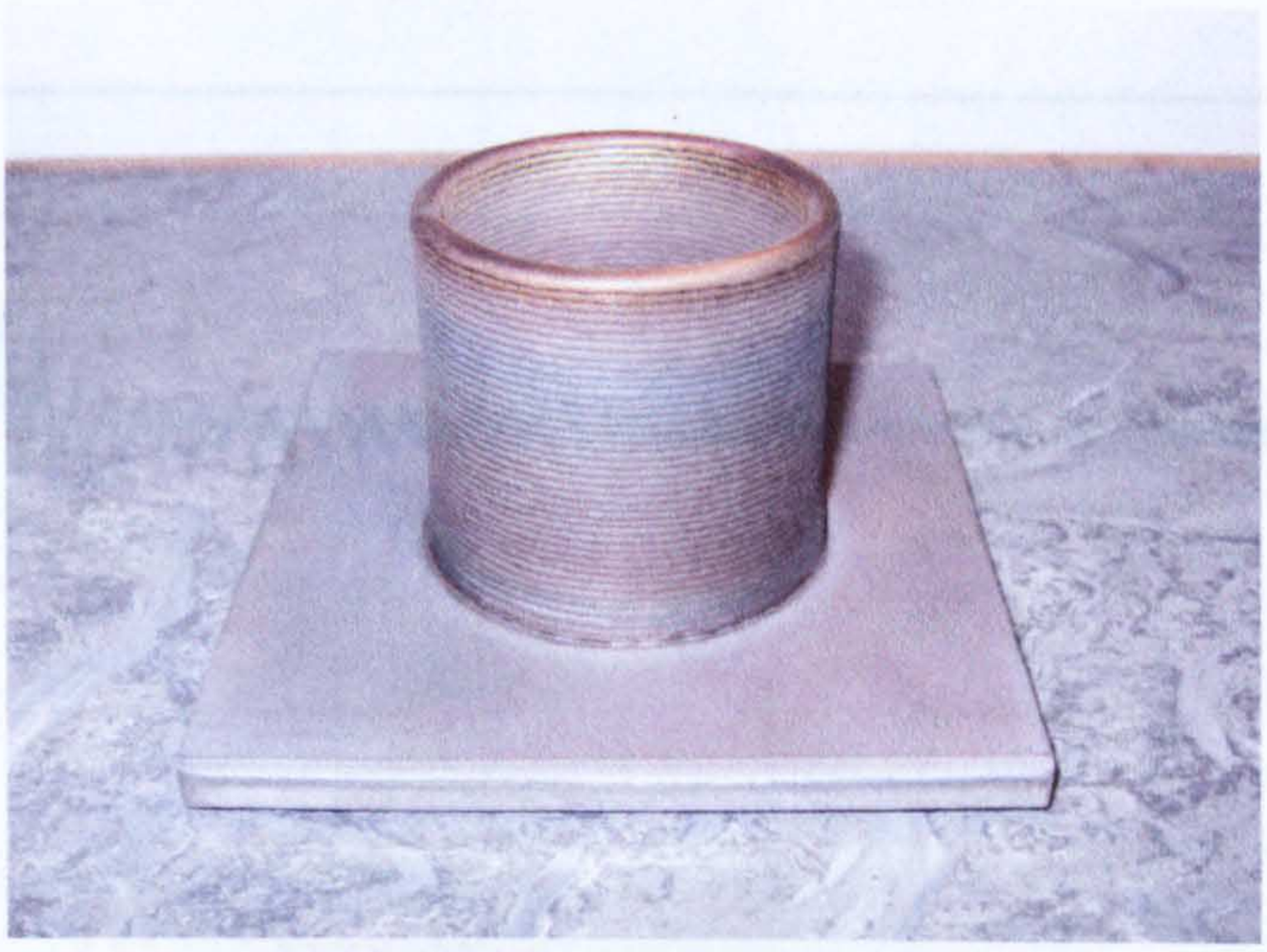

Figure 7.18: Stainless steel 308LSi cylinder
The diameter of the cylinder is 50 mm.

7.2.3 Deposition of Ti-6Al-4V

In a similar way, continuous metal deposition was performed with Ti–6Al–4V. For this material, good results were obtained with these controller parameters:

Gain	0.003
Pole:	0.9999 + 0i
Pole:	-0.05 + 0i
Zero:	0 + 0i
Zero:	0.99 + 0i
Frequency:	50 Hz

Figure 7.19 shows the graph of temperatures and laser power of a Ti–6Al–4V cylinder. The results are very similar to those obtained in the stainless steel cylinder. A cyclic profile of the melt pool temperature and the temperature controller reacting in order to achieve a constant temperature. The laser power is gradually reduced as the workpiece temperature increases. Figure 7.20 shows a Ti-6Al-4V cylinder built by this process at 1850 °C.

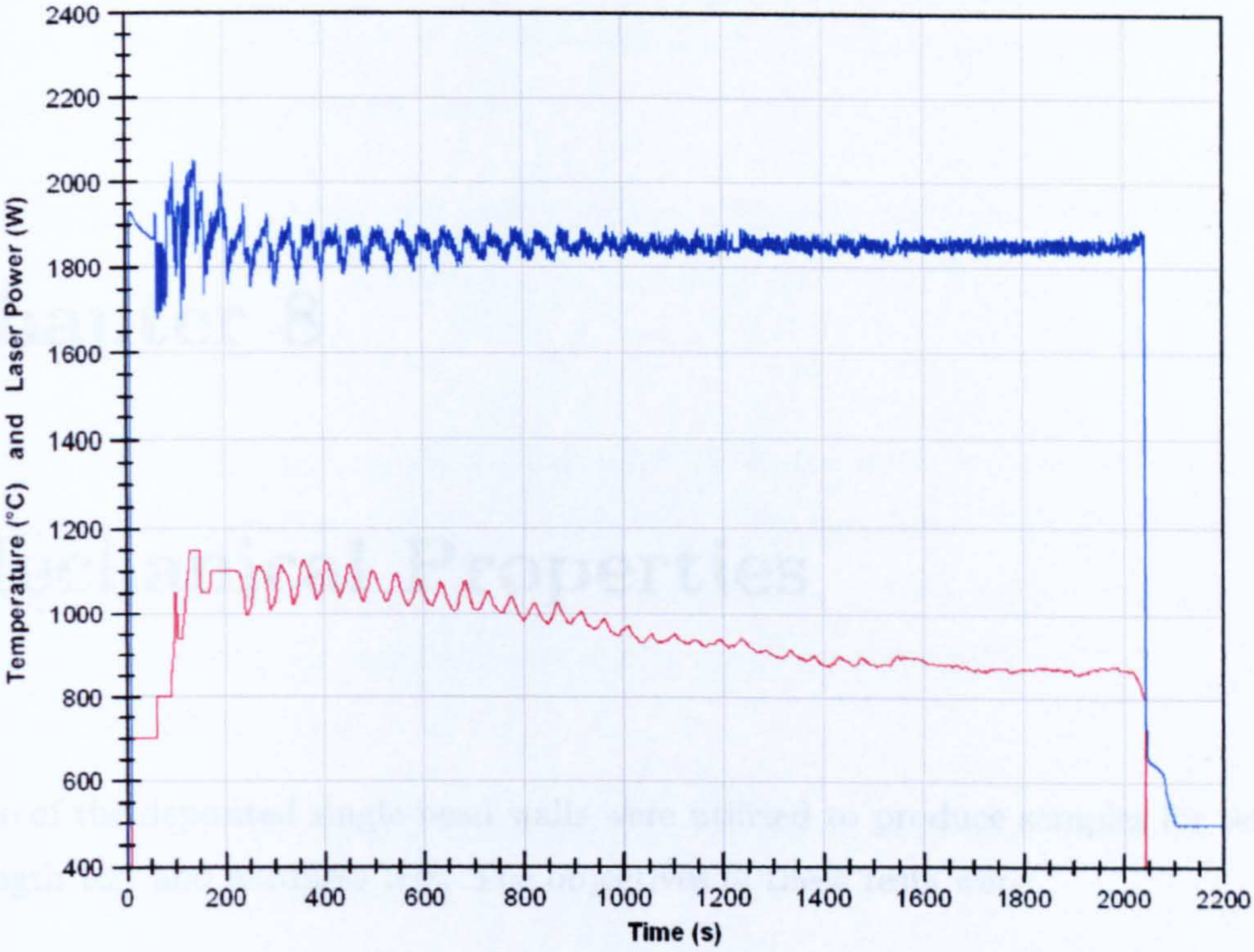

Figure 7.19: Deposition of a Ti–6Al–4V cylinder
Blue: Melt pool temperature. Red: Laser power.

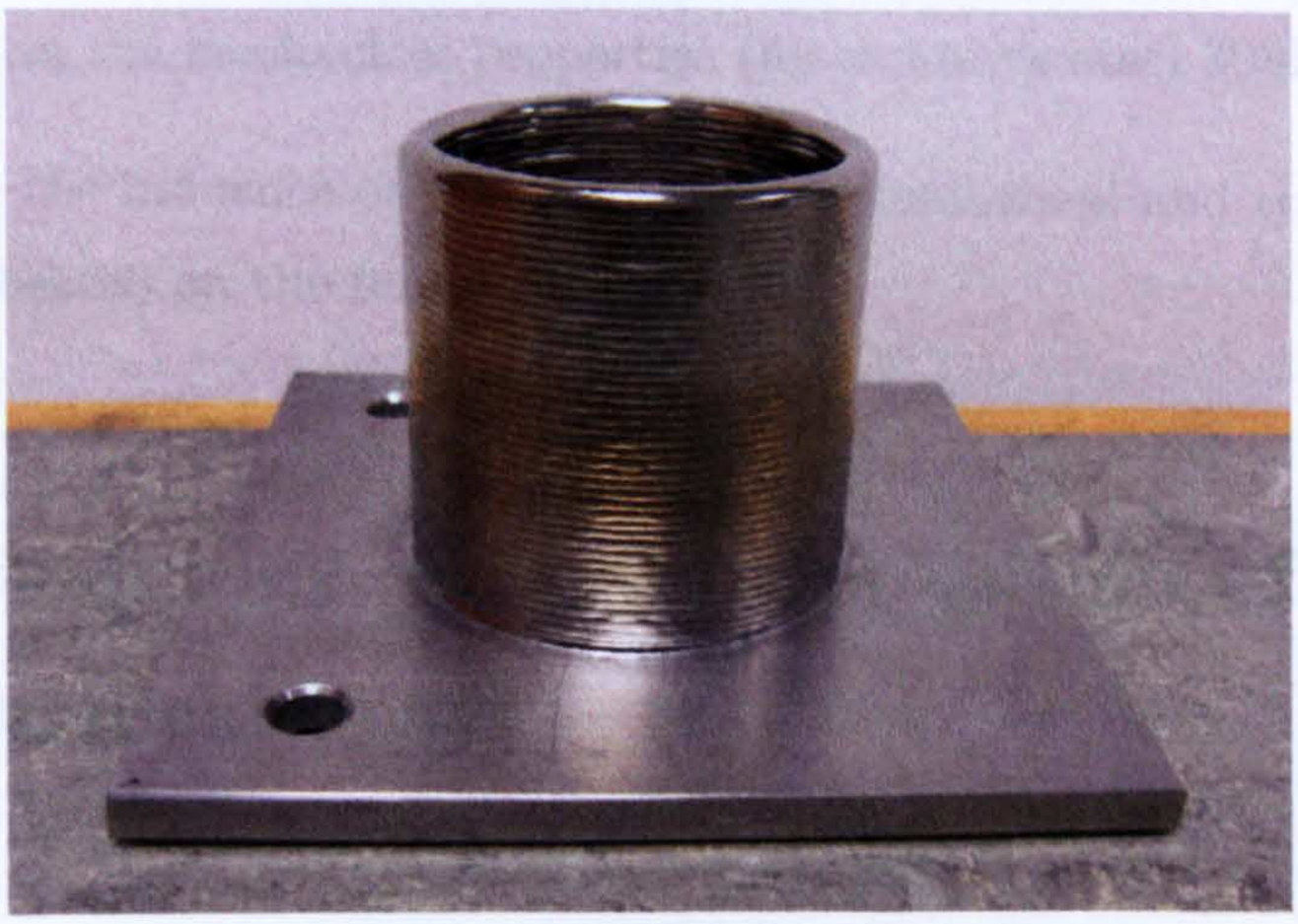

Figure 7.20: Ti–6Al–4V cylinder
The diameter of the cylinder is 50 mm.

Chapter 8

Mechanical Properties

Some of the deposited single-bead walls were utilized to produce samples for tensile strength test and hardness test. The objectives of these tests were:

- To obtain the ultimate tensile strength (UTS) of the deposited materials (stainless steel 308LSi and titanium alloy Ti–6Al–4V)
- To analyse whether different control conditions and temperatures would have an impact on the mechanical properties (for stainless steel 308LSi)
- To analyse the influence of the orientation (longitudinal and transversal to the deposited beads) on the tensile strength

8.1 Methodology of Metal Deposition of Walls for Mechanical Tests

The development of the strategy to deposit walls was explained in chapter 7. A brief summary of the method used to deposit these walls is described next:

A preheat run (i.e. only laser, without wire feed) is first made to reduce the temperature gradient of the deposition of the first layer. The first layer of the wall is then deposited with constant laser power.

The next few layers of the wall are deposited also with constant laser power during the whole bead. Then, the temperature controller is turned ON and the laser power is controlled automatically.

The first 30 mm of every bead are deposited with constant laser power (in order to achieve a stable condition before the controller is turned ON). Then the temperature controller is automatically turned ON. The laser power used during these 30 mm is determined from the average laser power of a small segment of the previous bead (as explained in section 7.1.3).

The start and stop of the system elements (wire feeder, laser and movement of CNC table) is done automatically by the system.

8.2 Tensile Test for Stainless Steel 308LSi

8.2.1 Conditions of the Test

In the experimental design for this test two factors are considered: the condition of the process control (three levels) and the orientation of the sample with respect to the deposition process (two levels). The levels are:

Condition of the process control:

- Manual control
- Automatic control at 1750 °C
- Automatic control at 2000 °C

Orientation of the sample (as shown in Figure 8.1):

- Longitudinal (horizontal)
- Transversal (vertical)

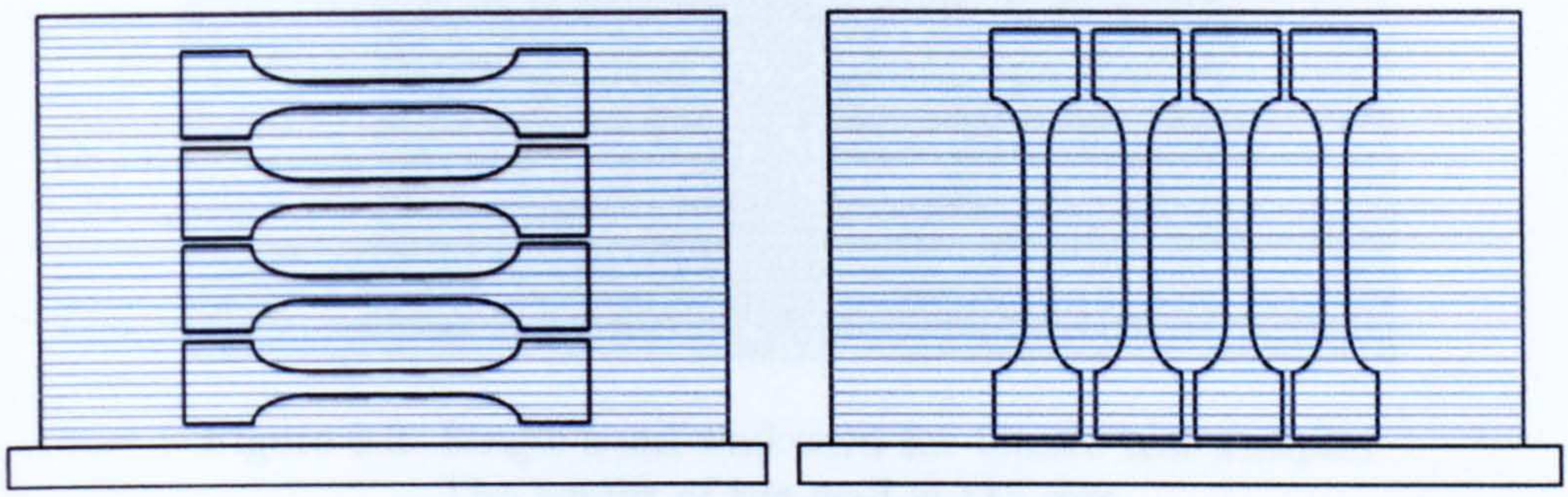

Figure 8.1: Orientation of tensile test samples in walls
Left: longitudinal (horizontal). Right: transversal (vertical).

Four samples were made for each treatment. However, two of the samples broke at one of the marks (for it acted as a crack initiator) and were discarded. Thus, three samples for each treatment were considered for the analysis of the results in order to keep the same number of runs for all the conditions. The response variables are the ultimate tensile strength and the elongation. The vertical samples were machined from single-bead walls with a height of 115 mm, one of these walls is shown in Figure 8.2. The horizontal samples were machined from smaller size single-bead walls.

8.2.2 Ultimate Tensile Strength

The results of the UTS test are shown in Table 8.1. The objective of this experiment is to determine whether there is any difference between the UTS in the different process control conditions and in the different directions of the test.

From Table 8.1 it can be seen that the samples deposited with manual control have lower UTS than those deposited with automatic control, and also that the samples

Figure 8.2: Single-bead wall used for tensile test samples
The height of the wall is 115 mm

Table 8.1: Results for UTS of stainless steel 308LSi

Condition	Direction	N	UTS results* (MPa)			Mean	St Dev
Manual	Longitudinal	3	507	521	525	517.67	9.45
	Transversal	3	480	482	488	483.33	4.16
Cont. 1750 °C	Longitudinal	3	526	537	565	542.7	20.1
	Transversal	3	498	498	498	498	≈ 0
Cont. 2000 °C	Longitudinal	3	534	539	546	539.67	6.03
	Transversal	3	502	503	504	503	1.0

* Ordered from minimum to maximum

tested in the longitudinal direction have higher UTS than the ones tested in the transversal one. However, it is important to perform an ANOVA in order to obtain more reliable conclusions from the analysis. The result of it is shown in Table 8.2, whereas the residual plots are presented in appendix D.

From the ANOVA table it can be seen that both the deposition condition and the direction of the test are important factors that affect the UTS.

Having an $\alpha = 0.01$, there is a statistical difference in the UTS value between walls deposited with manual control and with automatic temperature control (P-value = 0.002). The walls built with automatic controll show a higher UTS than those built

Table 8.2: Analysis of variance for UTS (factors and interaction)

Source	DF	SS	MS	F	P
Deposition Condition (DC)	2	1656.8	828.4	9.06	0.004
Direction of Test (DT)	1	6689.4	6689.4	73.20	< 0.001
Interaction DC DT	2	88.1	44.1	0.48	0.629
Error	12	1096.7	91.4		
Total	17	9530.9			
S = 9.55975 $R^2 = 0.8849$ R^2(adj) = 0.8370					

with manual control, as it is shown in the main effects plot (Figure 8.3) and in the interaction plot (Figure 8.4).

The automatic process control provides a smooth metal deposition throughout the wall, avoiding defects and achieving good mechanical properties. Conversely, with manual control it is difficult to maintain a smooth and even deposition throughout the whole wall.

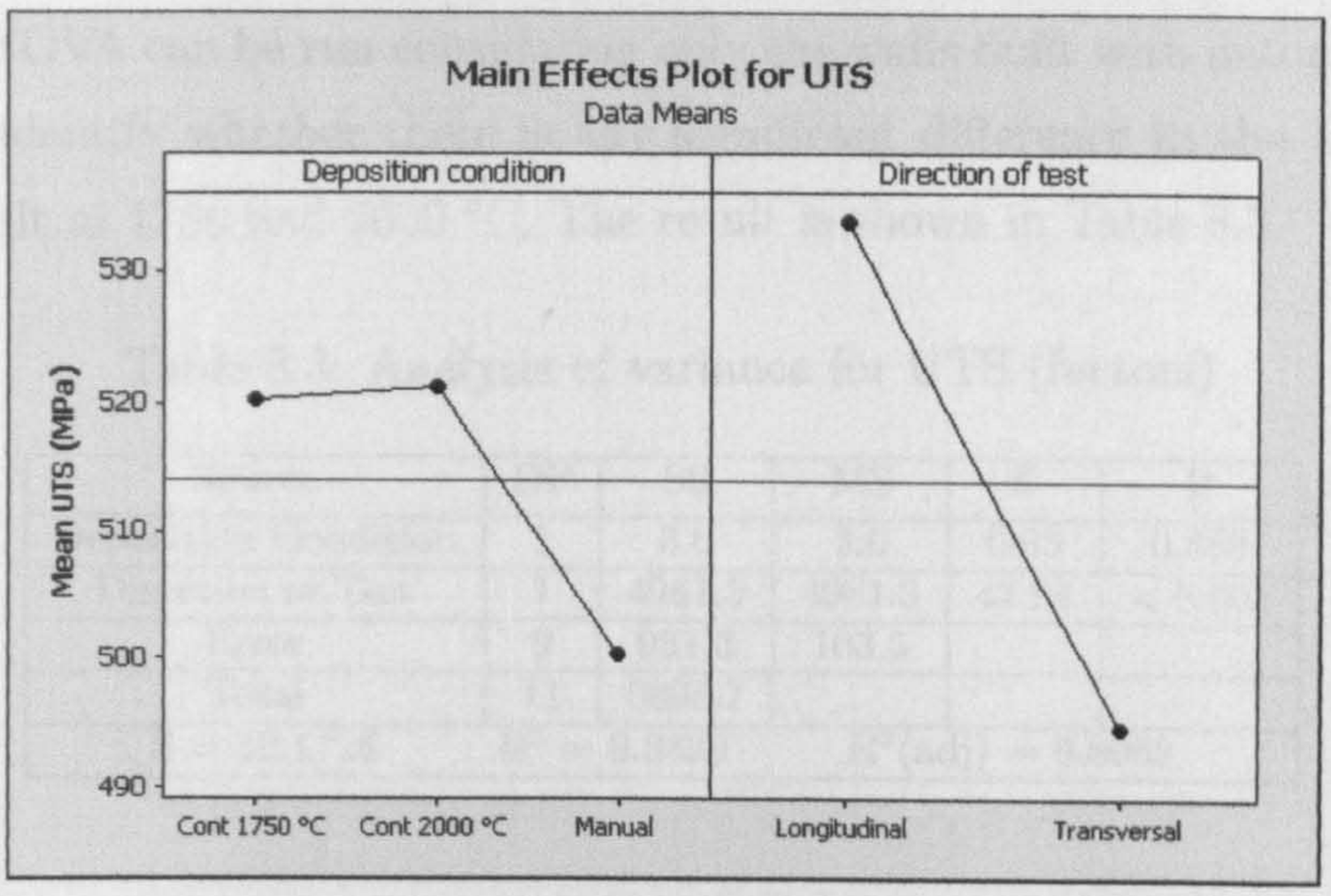

Figure 8.3: Main effects plot for UTS

There is also a statistical difference in the UTS value between samples tested in the longitudinal and the transversal directions (P-value < 0.001). Those tested in the longitudinal (horizontal) direction show a higher UTS.

Figure 8.4 shows a small interaction between the factors. However, this interaction is not significant (P-value = 0.629), as it can be seen in the ANOVA table.

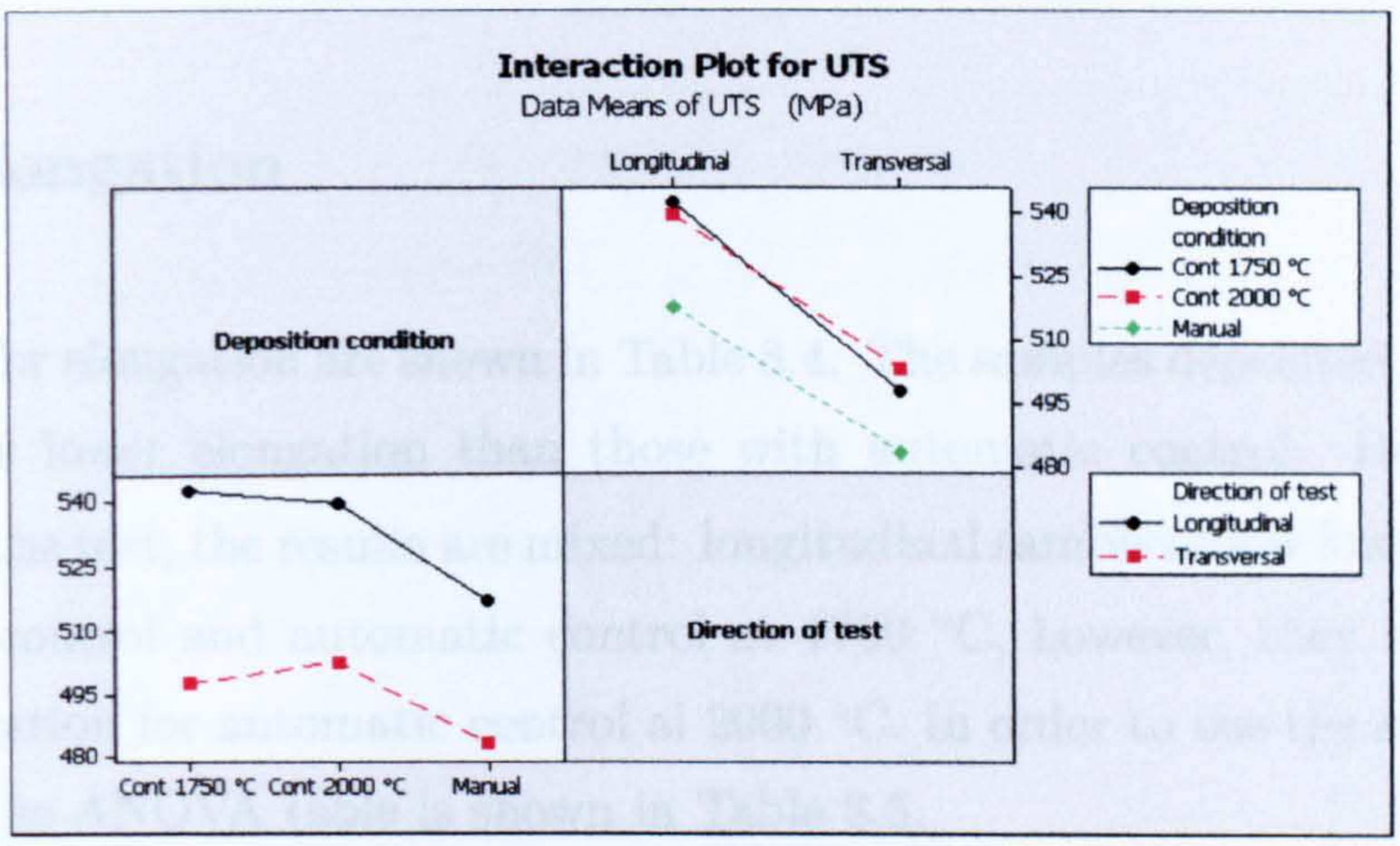

Figure 8.4: Interactions plot for UTS

A second ANOVA can be run considering only the walls built with automatic control, in order to identify whether there is any significant difference in the UTS between the walls built at 1750 and 2000 °C. The result is shown in Table 8.3.

Table 8.3: Analysis of variance for UTS (factors)

Source	DF	SS	MS	F	P
Deposition Condition	1	3.0	3.0	0.03	0.869
Direction of Test	1	4961.3	4961.3	47.94	< 0.001
Error	9	931.3	103.5		
Total	11	5895.7			
S = 10.1726	$R^2 = 0.8420$		R^2(adj) = 0.8069		

There is no evidence to support that there is a difference between the tensile strength of walls deposited at 2000 °C and those deposited at 1750 °C (P-value = 0.869). It can be concluded that the temperature set-point does not have a significant difference on the UTS of stainless steel 308LSi.

This second ANOVA confirms that there is statistical difference between samples

tested in the transversal direction and those tested in the longitudinal direction (P-value < 0.001).

8.2.3 Elongation

The results for elongation are shown in Table 8.4. The samples deposited with manual control show lower elongation than those with automatic control. Regarding the direction of the test, the results are mixed: longitudinal samples show lower elongation for manual control and automatic control at 1750 °C, however, they show slightly higher elongation for automatic control al 2000 °C. In order to use the same analysis procedure, the ANOVA table is shown in Table 8.5.

Table 8.4: Results for elongation of stainless steel 308LSi

Condition	Direction	N	Elongation results* (%)			Mean	St Dev
Manual	Longitudinal	3	35	38	43	38.67	4.04
	Transversal	3	38	45	47	43.33	4.73
Cont. 1750 °C	Longitudinal	3	52	52	52	52	≈ 0
	Transversal	3	52	53	65	56.67	7.23
Cont. 2000 °C	Longitudinal	3	50	53	57	53.33	3.51
	Transversal	3	48	50	58	52	5.29

* Ordered from minimum to maximum

Table 8.5: Analysis of variance for elongation (factors and interaction)

Source	DF	SS	MS	F	P
Deposition Condition (DC)	2	633.33	316.67	14.47	0.001
Direction of Test (DT)	1	32.00	32.00	1.46	0.250
Interaction DC DT	2	36.00	18.00	0.82	0.463
Error	12	262.67	21.89		
Total	17	964.00			
S = 4.67856 $R^2 = 0.7275$ R^2(adj) = 0.6140					

There is a statistical difference between the elongation of walls deposited with manual control and with automatic temperature control (deposition condition), indicated by a P-value = 0.001. In contrast, there is no evidence to support that there is any difference between the elongation of samples tested in the transversal direction and

those tested in the longitudinal direction (P-value = 0.241). The interaction between both factors is not significant (P-value = 0.463) and can be ignored. The main effects and the interaction plots of this ANOVA are shown in figures 8.5 and 8.6 respectively.

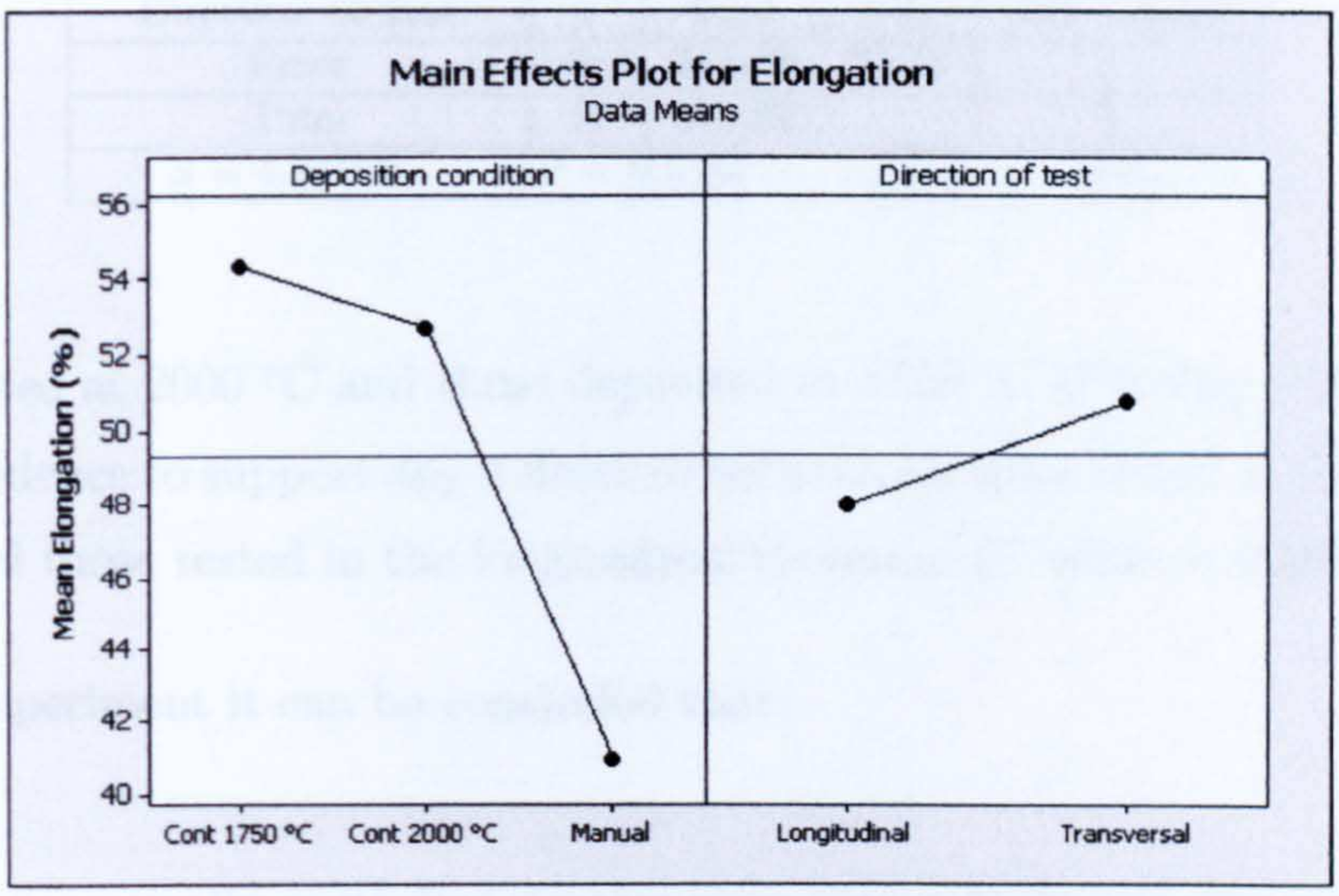

Figure 8.5: Main effects plot for elongation

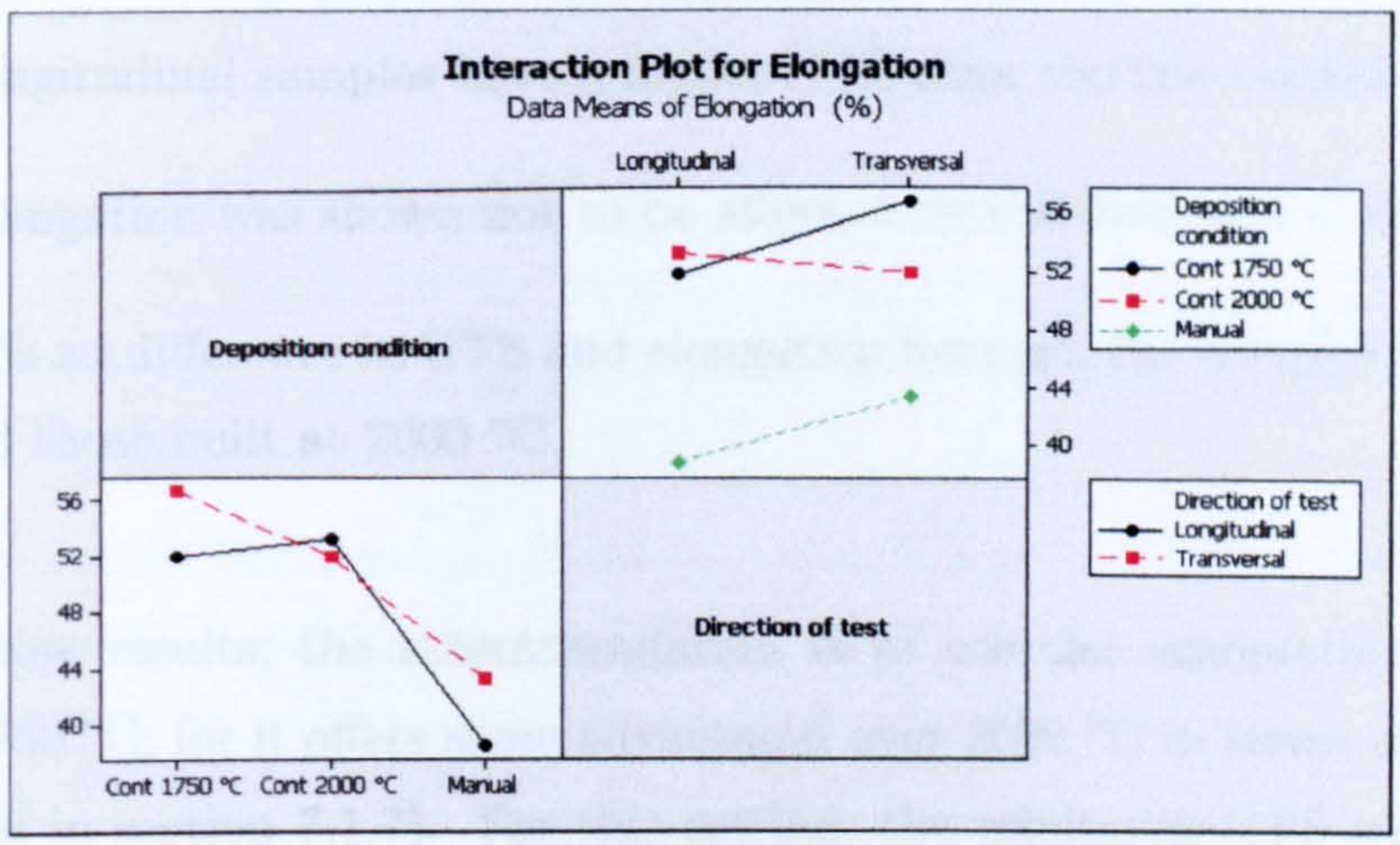

Figure 8.6: Interactions plot for elongation

A second ANOVA was done to identify any significant difference in elongation between the samples built at 1750 °C and those built at 2000 °C. The ANOVA is shown in Table 8.6.

There is no evidence to support that there is any difference between the elongation of

Table 8.6: Analysis of variance for elongation (factors)

Source	DF	SS	MS	F	P
Deposition Condition	1	8.33	8.33	0.35	0.567
Direction of Test	1	8.33	8.33	0.35	0.567
Error	9	212.33	23.59		
Total	11	229.00			
S = 4.85722	$R^2 = 0.7280$		R^2(adj) = 0.00		

walls deposited at 2000 °C and those deposited at 1750 °C (P-value = 0.567). There is also no evidence to support any difference between samples tested in the transversal direction and those tested in the longitudinal direction (P-value = 0.567).

From this experiment it can be concluded that:

- The automatically controlled process gives higher UTS and elongation than the manually controlled one
- The longitudinal samples have a higher UTS than the transversal ones
- The elongation was shown not to be affected by the direction of the test
- There is no difference in UTS and elongation between the samples built at 1750 °C and those built at 2000 °C

Based on these results, the recommendation is to use the automatic temperature control at 1750 °C, for it offers some advantages over 2000 °C in terms of the process (as explained in section 7.1.7). For this setting, the minimum UTS were 526 MPa (longitudinal) and 498 MPa (transversal), whereas the minimum elongation was 52% (longitudinal and transversal samples).

Table 8.7 offers a reference of the UTS and elongation of some austenitic stainless steels with chemical composition close to that of 308LSi, both wrought (annealed) and deposited by a LMD system. Although chemical compositions are different, it

can be seen that the UTS is within the range of other austenitic stainless steels, and that the elongation is higher than that of other deposited stainless steels.

Table 8.7: Mechanical properties of wrought and deposited stainless steel [24, 61]

Material	Condition	Tensile Strength (MPa)	Elongation (%)
SS 304	Wrought (annealed)	515 min.	40
SS 308	Wrought (annealed)	515 min.	40
SS 316L	Laser Consolidation *	540–560	35–43
SS 316	Directed Light Fabrication *	580	41
SS 308LSi	Fibre Laser + wire **	498–565	52–65

* Laser Powder Deposition process, ref. [61]
** Temperature control at 1750 °C, transversal and longitudinal samples

8.3 Tensile Test for Ti-6Al-4V

8.3.1 Conditions of the Tests

Tensile tests were made also for Ti-6Al-4V, following the same procedure as for stainless steel 308LSi. For Ti-6Al-4V the walls were deposited with automatic temperature control at 1850 °C. Only one factor is considered in the analysis: the orientation of the sample with respect to the deposition process. The same orientations are considered: longitudinal and transversal, as shown in Figure 8.1. Three samples of each orientation are considered for the analysis.

8.3.2 Ultimate Tensile Strength

The results for the tensile strength are in Table 8.8. It can be seen that the UTS is higher for the samples tested in the longitudinal direction. The results of the ANOVA are in Table 8.9.

The ANOVA shows that there is no statistical evidence to support a difference in

Table 8.8: Results for UTS of Ti-6Al-4V

Direction	N	UTS results* (MPa)			Mean	St Dev
Longitudinal	3	930	964	975	956.3	23.5
Transversal	3	902	906	939	915.7	20.3

* Ordered from minimum to maximum

Table 8.9: Analysis of variance for UTS

Source	DF	SS	MS	F	P
Direction of Test	1	2480.7	2480.7	5.15	0.086
Error	4	1925.3	481.3		
Total	5	4406.0			
S = 21.9393	$R^2 = 0.5630$		R^2(adj) = 0.4538		

the UTS between the samples tested in the longitudinal direction and those tested in the transversal one. The P-value for the test is 0.086 and is higher than the α value (0.01). Although the UTS mean is higher in the longitudinal direction, the variability in the test is also high and does not allow a sound statistical conclusion on the influence of the orientation on the UTS. More replicates would be needed to achieve a conclusion in this test. The main effects plot is shown in Figure 8.7.

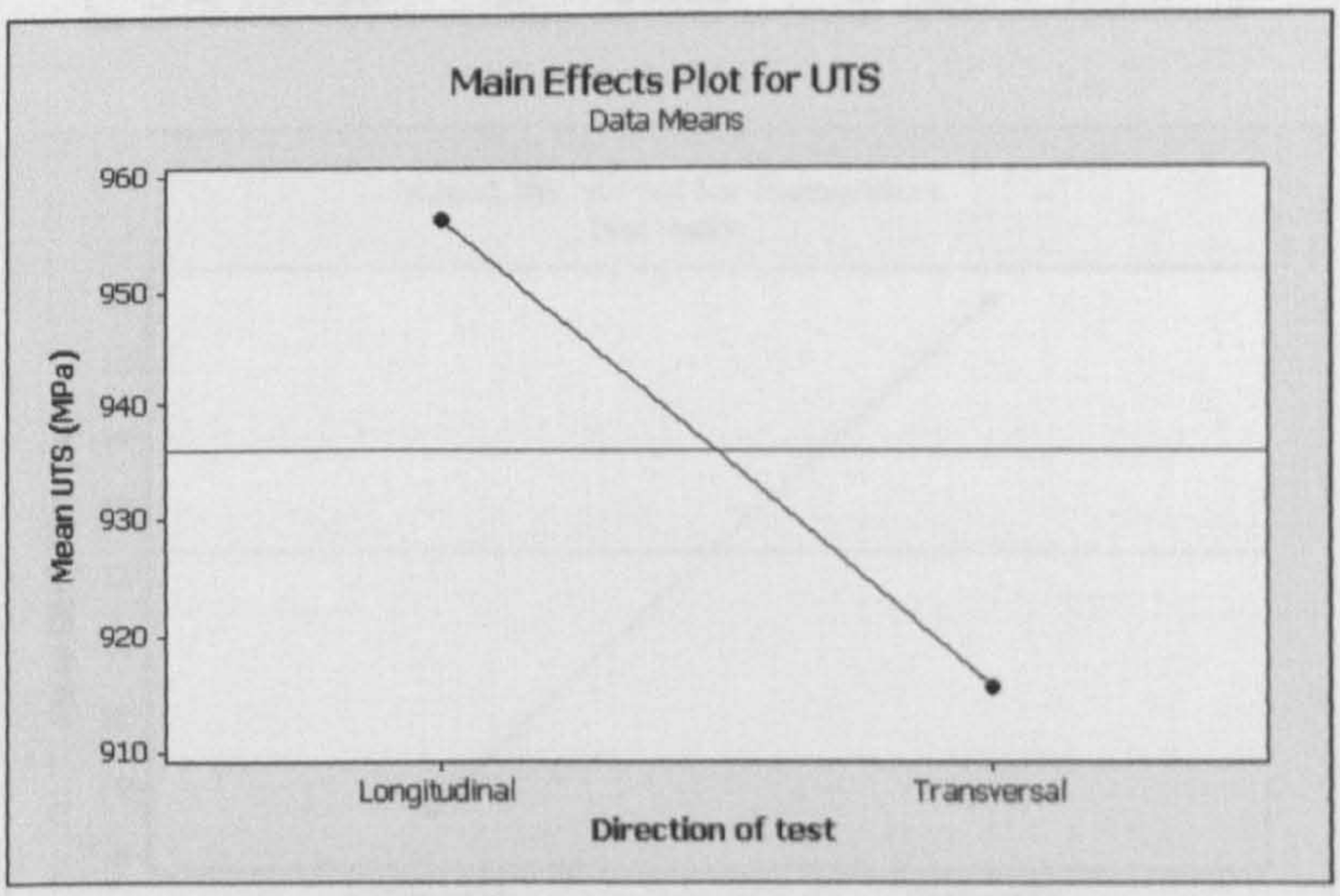

Figure 8.7: Main effects plot for UTS

8.3.3 Elongation

The results for the elongation are in Table 8.10. It can be seen that the elongation is higher for the samples tested in the transversal direction.

Table 8.10: Results for elongation of Ti-6Al-4V

Direction	N	Elongation results* (%)			Mean	St Dev
Longitudinal	3	8	8	10	8.67	1.16
Transversal	3	15	15	18	16.0	1.73

* Ordered from minimum to maximum

The results of the ANOVA are in Table 8.11. It shows that the direction of test is an important factor that influences the elongation (P-value = 0.004). The main effects plot for elongation is shown in Figure 8.8.

Table 8.11: Analysis of variance for elongation

Source	DF	SS	MS	F	P
Direction of Test	1	80.667	80.667	37.23	0.004
Error	4	8.667	2.167		
Total	5	89.333			
S = 1.47196	$R^2 = 0.9030$		R^2(adj) = 0.8787		

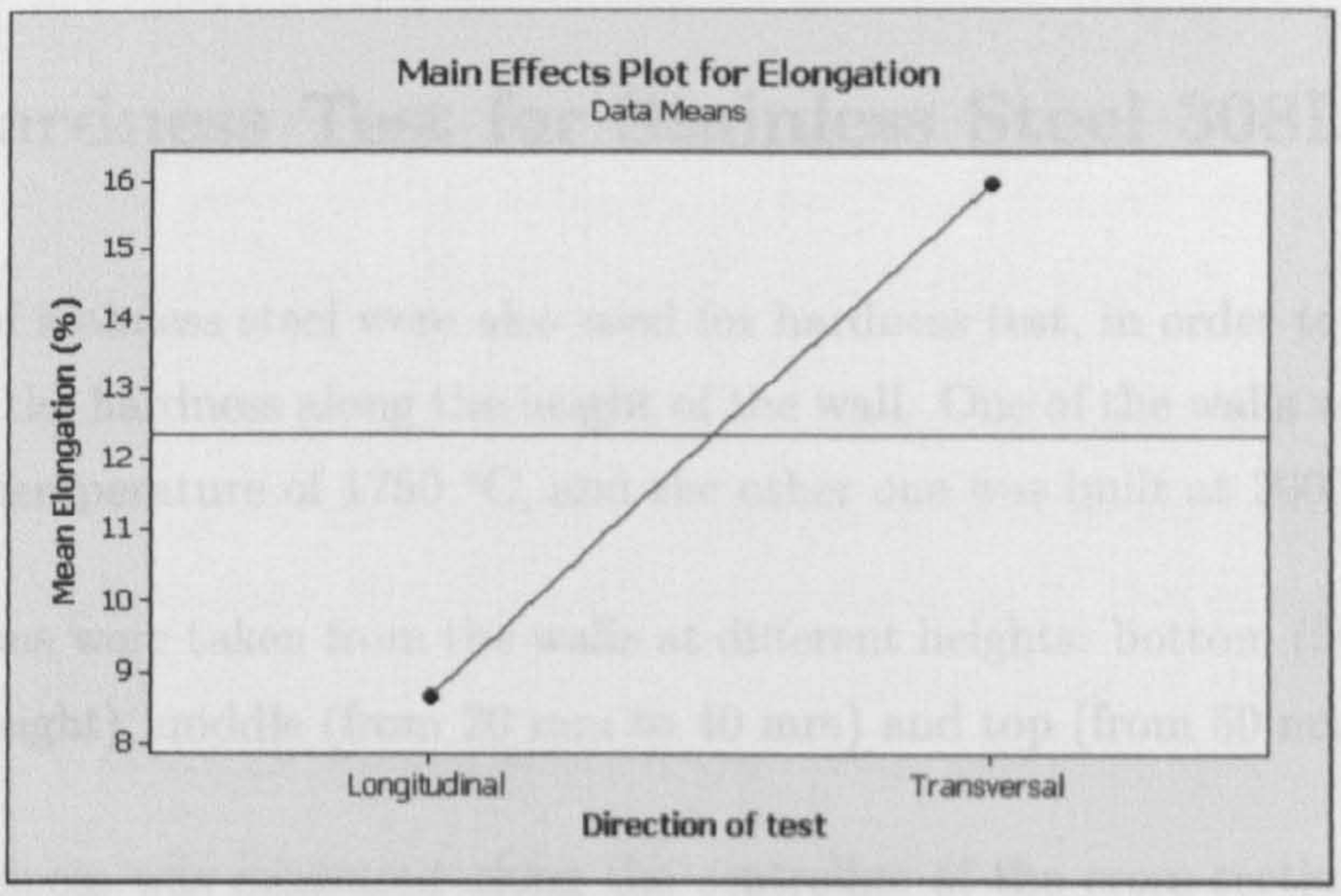

Figure 8.8: Main effects plot for elongation

The samples tested in the transversal direction showed higher elongation than those tested in the longitudinal direction. However, this result should be taken with some caution because the residual plots do not show a proper normal distribution. More runs would be required to confirm the results. The residual plots are shown in appendix D.

Table 8.12 offers a comparison of the UTS and elongation of wrought (annealed) and deposited Ti-6Al-4V. Both UTS and elongation of the material deposited by fibre laser and wire with temperature control are within the range of the properties of Ti-6Al-4V annealed or deposited by other systems.

Table 8.12: Mechanical properties of wrought and deposited Ti-6Al-4V [24, 61]

Material	Condition	Tensile Strength (MPa)	Elongation (%)
Ti-6Al-4V	Wrought (annealed)	931	15
Ti-6Al-4V	Laser Forming *	900	12
Ti-6Al-4V	Laser Consolidation *	1160	6
Ti-6Al-4V	Directed Light Fabrication *	1125	6
Ti-6Al-4V	Fibre Laser + wire **	902–975	8–18

* Laser Powder Deposition process, ref. [61]
** Temperature control at 1850 °C, transversal and longitudinal samples

8.4 Hardness Test for Stainless Steel 308LSi

Two walls of stainless steel were also used for hardness test, in order to measure the variation of the hardness along the height of the wall. One of the walls was built with a set-point temperature of 1750 °C, and the other one was built at 2000 °C.

Three sections were taken from the walls at different heights: bottom (from the plate to 15 mm height), middle (from 20 mm to 40 mm) and top (from 50 mm to 70 mm).

Vickers hardness was measured along the centreline of the cross section of the wall applying a load of 20 Kg. The measurements were spaced 4 mm from each other.

The results are shown in Table 8.13.

Table 8.13: Hardness of stainless steel walls

Section of wall	Height (mm)	Vickers Hardness, HV(20)	
		Wall built at 1750 °C	Wall built at 2000 °C
Top	64	173	167
	60	172	169
	56	178	169
	52	171	174
Average	52–64	173.5	169.8
Middle	36	176	177
	32	178	176
	28	180	177
	24	177	174
Average	24–36	177.8	176.0
Bottom	12	183	180
	8	187	181
	4	185	191
	0	187	200
Average	0–12	185.5	188.0
Plate		213	210

As expected, the hardness of the deposited material is highest at the bottom of the wall, in the first few millimetres. In this region, the plate acts as a heat sink that removes quickly the heat from the melt pool, causing a fast cooling rate, which is frequently associated to a finer microstructure and a higher hardness. Majumdar et al. [92] reported an increase of microhardness, attributed the refinement of the grain, due to rapid solidification in LPD of austenitic stainless steel 316L.

At higher regions of the wall the heat transfer from the melt pool is reduced because the conduction changes from three-dimensional to bi-dimensional. Also the temperature of the wall increases as the heat is accumulated in it, this causes a reduction in the temperature gradient (between the solidification front of the melt pool and the workpiece), therefore a lower heat transfer. This reduction in the heat transfer produces a slower cooling rate, hence a lower hardness.

Both walls have similar hardness and show the same trend: the hardness is slightly

reduced as the height is increased, as it can be noticed in the average values of the sections in Table 8.13. The temperature set-point does not seem to have an effect on the hardness of the deposited material. Table 8.14 shows hardness values of some austenitic stainless steels (wrought annealed) of close chemical composition for comparison.

Table 8.14: Hardness of selected wrought stainless steels [24, 93]

Material	Condition	Hardness HRB max (HV equivalent *)
SS 304	Wrought (annealed)	92 (198)
SS 304L	Wrought (annealed)	88 (179)
SS 308	Wrought (annealed)	88 (179)

* Equivalent Vickers hardness calculated based on reference [93]

Chapter 9

Summary and Conclusions

As described in chapter 1, the aim of this research was the development of a fibre laser metal deposition system with wire feeding, and the objectives were focused on investigating the process window, process characterisation and melt pool temperature control.

The aim and objectives of the project have been accomplished. The previous chapters described the steps undertaken to achieve the objectives. This final chapter brings together the conclusions obtained from the study on process parameters (chapter 4), the development of a system for monitoring and control of melt pool temperature (chapters 5, 6 and 7) and the characterization on mechanical properties of the deposited material (chapter 8).

Finally, recommendations are given for the future work that can be undertaken based on this research.

9.1 Summary and Conclusions

9.1.1 System Development

A Fibre laser metal deposition system with wire feeding has been developed successfully. The key features of this system are:

- The system consists of a 2 kW fibre laser, a CNC table, a wire feeder and a temperature control system
- Closed-loop control system for the melt pool temperature using a two-colour pyrometer for the feedback signal: the laser power is modified in order to maintain the set-point temperature
- Monitoring of the workpiece (upper layer) temperature is carried out using a single-colour pyrometer
- An algorithm developed in LabVIEW^{TM} software performs the control action and displays online the temperatures and laser power. It saves the data from temperatures, laser power and wire feed rate
- A flexible enclosure chamber is used for controlled atmosphere
- The system has a flexible structure and can be expanded by adding more sensors or input/output signals if needed

Temperature-controlled metal deposition has been performed with stainless steel 308LSi and also with titanium alloy Ti-6Al-4V. Deposited geometries include single-bead walls and cylinders.

9.1.2 Effect of Parameters on the Process Condition

The effect of the main factors on the process condition was studied, depositing stainless steel 308LSi wire (1.2 mm diameter).

The process window has been found, identifying the parameter combinations that lead to four deposition conditions: smooth deposition, droplet formation, stubbing and wave-like deposition. Although the parameters have individual effects, it is the combination of them that causes the process to fall in one or another deposition condition.

The positioning of the wire tip was identified as a very important factor. Only front feeding was used in this research. For the range of parameters used, best results were obtained when the wire tip was positioned at the centre of the melt pool (i.e. the spot where the laser beam hits the substrate). With this setup and a good combination of parameters, smooth deposition is achieved.

If the wire tip was positioned towards the back of the melt pool (i.e. leaving a relative large distance between the wire and the melt pool), the deposition occurred with formation of droplets. This condition can also occur when too high laser power and/or too low wire feed rate is used.

Stubbing occurred when an excess of wire feed was used (for a particular combination of traverse speed and laser power). Too much material is fed into the melt pool and starts hitting the material that is already there. This can lead to oscillations in the deposition.

Wave-like deposition occurred when the traverse speed was too high in combination with a relatively low wire feed rate. The interaction time between the substrate and the laser was not enough to form a wide-enough melt pool.

9.1.3 Influence of Parameters on Bead Geometry

The influence of the main three process parameters (laser power, traverse speed and wire feed rate) on the bead geometry has been analysed using the Design of Experiments methodology. The response variables were the bead height and width. A 3^3 full factorial design was used, and the levels of the factors were:

Laser power (W):	1700	1850	2000
Traverse speed (mm/min):	175	200	225
Wire feed rate (m/min):	0.8	1.0	1.2

The conclusions from this analysis were:

- Increasing the wire feed rate increased the bead height
- Increasing the traverse speed decreased the height
- Increasing the laser power decreased the height

Wire feed rate had the highest influence on the bead height, followed by the traverse speed. The least influential was the laser power.

For bead width:

- Increasing the traverse speed decreased the width
- Increasing the wire feed rate increased the bead width
- Increasing the laser power increased the width

Traverse speed had the highest impact on the bead width, followed by the wire feed rate. Whereas the laser power was the least significant factor.

The interactions between the factors have a small influence and can be neglected. Two regression equations were calculated from the experimental results. These are valid within the process conditions used (setup, material and process parameters), but with a good process understanding, they can give an insight of how it would perform in other conditions (e.g. with a different material). The equations are:

$$Height = 1.91 - 0.000153LP - 0.00528TS + 1.28WFR$$

$$Width = 3.437 + 0.000433\ LP - 0.00774\ TS + 0.837\ WFR$$

Where

LP	=	Laser Power	(W)
TS	=	Traverse Speed	(mm/min)
WFR	=	Wire Feed Rate	(m/min)

9.1.4 Temperature Monitoring

During the development of the temperature monitoring system six infrared sensors (one photodiode, four single-colour pyrometers and one two-colour pyrometer) were tested to analyse their suitability for the process. The two-colour pyrometer was found most suitable for temperature measuring of the melt pool. A single-colour pyrometer was found suitable for temperature monitoring of the workpiece. Both of them have the configuration of fibre cable and optical head.

It was found that the positioning of the pyrometer spot is a crucial factor for melt pool temperature measuring. More consistent result were obtained when the spot was positioned at the centre of the melt pool (i.e. on the same spot where the laser hits the substrate).

It was also observed that more stable results were obtained by locating the pyrometer optical head in line with the deposition process (on the opposite side of the wire feeder nozzle). This way, small variations in the stand-off distance will not cause the pyrometer to aim outside the melt pool.

Optical filters are needed in order to reject the laser reflections, so that they do not affect the temperature measurement. The filters were located at the optical heads of the pyrometers.

9.1.5 Temperature Control

A theoretical model of the melt pool was developed starting from a heat balance equation. This model was linearized and converted to the Laplace domain in order to obtain the transfer function. It was then converted into the discrete domain (z) to obtain the pulse transfer function, which was utilized to design a controller, using the root locus method in the discrete domain with a sampling frequency of 50 Hz.

A control algorithm was developed in LabVIEW^{TM} software using the zero-pole-gain form. The control system was utilized to deposit two different multi-layered structures: single-bead walls and cylinders.

During the deposition of the first layers of a piece the cool substrate acts as a heat sink. If the laser power is increased, the extra heat is absorbed by the substrate and the temperature does not increase as much. For this reason, the controller action is not very effective during the initial layers. In the deposition of single-bead walls it was observed that more consistent deposition was achieved by selecting adequate laser power values for the first six or seven layers and keeping that power constant during the whole layer.

After that, the heat flow is reduced because the temperature of the workpiece is higher (i.e. lower temperature gradient) and the heat flow gradually changes from three-dimensional to bi-dimensional. If the laser power is increased, a greater part of

the extra heat remains in the melt pool, rising its temperature. For this reason the melt pool temperature becomes more dependent on the laser power and the controller works properly.

The control system achieves a very stable deposition process, maintaining the set-point temperature. Strategies for the automation of the deposition of stainless steel 308LSi were developed and implemented for the start and end of a bead.

In single-bead walls deposition of stainless steel 308LSi:

- A very stable process with smooth deposition was achieved by controlling the temperature at a set-point of 1750 °C. Walls of 115 mm height and 150 mm length were successfully produced
- For control temperature at a set-point of 2000 °C, good control was achieved to a height of approximately 60 mm. After that, the controller did not perform well due to the excessive heat accumulation.
- A set-point of 1750 °C is recommended
- The workpiece (upper layer) temperature was measured at the start of every layer. The performance of the process was affected when this temperature was above 500 °C due to the excessive accumulation of heat.

In single-bead walls deposition of titanium alloy Ti-6Al-4V:

- The emissivity slope of the two-colour pyrometer was set to K = 1.2 in order to get a stable melt pool temperature reading
- The controller accomplished a very smooth and stable deposition at a set-point of 1850 °C
- The formation of a melted (and then solidified) droplet at the wire tip at the end of a bead was observed

- A different strategy for the end of the bead was required to avoid the formation of this droplet at the wire tip

Continuous metal deposition:

- Continuous deposition of stainless steel 308LSi and titanium alloy Ti-6Al-4V was also achieved successfully by means of building cylinders
- The controller parameters had to be modified to reduce the control action due to the accumulation of heat
- It is important to develop an adequate strategy to start the cylinder to avoid the formation of droplets
- A cyclical temperature profile was observed at the beginning of the cylinders, which was corrected by the control action, accomplishing very smooth and stable metal deposition

9.1.6 Mechanical Properties of Deposited Walls

Single-bead walls were used to make samples for tensile test of both stainless steel 308LSi and titanium alloy Ti-6Al-4V. The samples were tested in two orientations: longitudinal and transversal to the bead direction.

For stainless steel 308LSi, three different control conditions were tested: manual control, automatic control at 1750 °C and automatic control at 2000 °C. Three samples were tested for each treatment, and the results were analysed by an ANOVA. The results were:

- Samples deposited by automatic control (both at 1750 and 2000 °C) showed higher UTS than those deposited with manual control

- Samples tested longitudinally to the beads showed higher UTS than those tested transversally

- There was no statistical difference between the UTS of the samples deposited with automatic control at 1750 °C and those deposited at 2000 °C

For titanium alloy Ti-6Al-4V, the walls were deposited with controlled temperature at 1850 °C and tested in the longitudinal and transversal orientation. Although the UTS mean was higher in the longitudinal direction, the ANOVA showed no statistical difference between the UTS of the samples tested at these two orientations. More replicates would be needed to analyse the difference between the two orientations.

Vickers hardness tests were performed on stainless steel 308LSi walls deposited at 1750 and 2000 °C. Hardness values were similar for both walls. They were in a range of 167–200 HV. The tests at the bottom of the walls (0–12 mm) showed a higher hardness than those at 52–64 mm height.

9.2 Future Work

After the successful development of this fibre laser metal deposition system with temperature control, several possibilities for research can be explored. Some of them are suggested in this section.

Research on the Process

- To implement an automatic upper limit for the workpiece temperature (upper layer) in such a way that: before the start of a bead the system measures the workpiece temperature and, if the temperature is above the pre-defined limit, the deposition does not start until the temperature is below the limit.

- The use of a heater to preheat the plate (substrate) before the deposition is

also an interesting line of research. This could improve the performance of the controller in the first layers and also reduce the geometrical inaccuracies (e.g. warping) due to uneven thermal expansion/contraction

- The use of hot wire can increase the metal deposition rate
- If the process conditions are likely to increase significantly the temperature inside the enclosure chamber, the optical filters need to be protected. This could be done by a jacket with air (or argon) flow.
- Explore strategies for automatic deposition of different geometries, analysing the performance of the controller on them
- The influence of the process factors on the bead height and width has been analysed. The wire feed rate has the highest influence on the bead height. This factor could be used for closed-loop control of the height. In the same line, the traverse speed has the highest influence on the bead width, so that it could be used for closed-loop control purposes. From these options, height control would have a greater effect on the system stability, for it would avoid the droplet-formation deposition (which occurs when the distance between the wire and the melt pool is large)
- Explore the use for process control of electric-arc based wire metal deposition systems such as GTAW, PTA. It is important to note that radiation from the electric-arc plasma may affect the melt pool temperature measurement and that, if the welding current is pulsed, the temperature reading may have a cyclic profile. Thus, modifications to the system should be done to reduce the effect of these factors
- Deposition of other materials and analysis of the controller performance
- Signal analysis of the stored data can be performed for identification of a change in the process condition by detecting changes in the temperature signals. It was observed in the experiments that the formation of droplets had an effect on both temperature signals. If this is identified online, an automatic corrective action can be implemented, such as an increment in the wire feed rate

Research on the Materials

- Research on microstructure characterization of the deposited material, analysing differences between the material deposited on (or close to) the substrate (fast cooling rate) and material deposited at a higher position (slower cooling rate)
- Investigate the influence of the microstructure on the materials properties
- Investigate the anisotropic properties such as the tensile strength (e.g. the influence of the solidification, grain growth, interface between two layers, etc.)
- Deposition of other materials and analysis of their properties

9.3 Publications Resulting from the Work

The work carried out over the course of this project has resulted in a paper being published in a conference:

Alexis Medrano, Janet Folkes, Joel Segal and Ian Pashby, "Fibre laser metal deposition with wire: parameters study and temperature monitoring system", *XVII International Symposium on Gas Flow, Chemical Lasers, and High-Power Lasers, Lisbon, Portugal*, September 2008. Proceedings SPIE Vol. 7131, 713122 (2008); doi:10.1117/12.816831

References

[1] G. Bi, A. Gasser, K. Wissenbach, A. Drenker, and R. Poprawe, "Identification and qualification of temperature signal for monitoring and control in laser cladding," *Optics and lasers in engineering*, vol. 44, pp. 1348–1359, 2006.

[2] S. H. Mok, G. Bi, J. Folkes, and I. Pashby, "Deposition of Ti-6Al-4V using a high power diode laser and wire, part I: Investigation on the process characteristics," *Surface & Coatings Technology*, vol. 202, pp. 3933–3939, 2008.

[3] A. Heralic, A. K. Christiansson, M. Ottosson, and B. Lennartson, "Increased stability in laser metal wire deposition through feedback from optical measurements," *Optics and Lasers in Engineering*, vol. 48, pp. 478–485, 2010.

[4] J. D. Kim and Y. Peng, "Plunging method for Nd:YAG laser cladding with wire feeding," *Optics and lasers in engineering*, pp. 299–309, 2000.

[5] W. U. H. Syed and L. Li, "Effects of wire feeding direction and location in multiple layer diode laser direct metal deposition," *Applied Surface Science*, vol. 248, pp. 518–524, 2005.

[6] W. U. H. Syed, A. J. Pinkerton, and L. Li, "A comparative study of wire feeding and powder feeding in direct diode laser deposition for rapid prototyping," *Applied Surface Science*, vol. 247, pp. 268–276, 2005.

[7] R. M. Miranda, G. Lopes, L. Quintino, J. P. Rodrigues, and S. Williams, "Rapid prototyping with high power fibre lasers," *Materials and Design*, vol. 29, pp. 2072–2075, 2008.

[8] A. Heralic, "Towards full automation of robotized laser metal-wire deposition," 2009, Thesis for the degree of Licentiate of Engineering, Chalmers University of Technology, Goteborg, Sweden.

[9] T. Wohlers, "10 methods that will impact the next 10 years," http://wohlersassociates.com/SepOct08TCT.htm, Sep 2008, accessed on 20 Mar 2010.

[10] L. Song and J. Mazumder, "Sensing and experimental base modeling of direct metal deposition," in *ICALEO Congress Proceedings*, Scottsdale, AZ, USA, 2006, pp. 449–454.

[11] AWS Committee, "Laser beam welding," in *Welding Processes*, vol. 2 of *AWS Welding Handbook*, pp. 713–738. American Welding Society, Miami, FL, 8 edition, 1991.

[12] "How fibre lasers work," http://www.orc.soton.ac.uk/61.html#, accessed on 25 Feb 2010.

[13] "Laser sources," www.ailu.org.uk/laser_technology/information_sheets.html, accessed on 28 Feb 2010.

[14] W. Steen, *Laser Material Processing*, Springer, London, 3 edition, 2003.

[15] "IPG photonics," http://www.ipgphotonics.com/faqs.htm, accessed on 28 Feb 2010.

[16] J. Hecht, *Understanding Lasers: an entry level guide*, IEEE Press and John Wiley & Sons Inc., New Jersey, 3 edition, 2008.

[17] J. Hecht, *Understanding Lasers: an entry level guide*, IEEE Press, New York, 2 edition, 1993.

[18] "Rofin dl 025s industrial diode laser operating manual," .

[19] "Solid-state lasers," http://www.rp-photonics.com/solid_state_lasers.html, accessed on 08 Mar 2010.

[20] "YAG lasers," http://www.rp-photonics.com/yag_lasers.html, accessed on 26 Feb 2010.

[21] "Fiber lasers," http://www.rp-photonics.com/fiber_lasers.html, accessed on 26 Feb 2010.

[22] "Q-switched lasers," http://www.rp-photonics.com/q_switched_lasers.html, accessed on 08 Mar 2010.

[23] "IPG photonics - high power fiber lasers for industrial applications," http://www.ipgphotonics.com/apps_materials_multi.htm, accessed on 09 Mar 2010.

[24] S. D. Washko and G. Aggen, "Wrought stainless steel," in *Properties and selection : irons, steels, and high-performance alloys*, vol. 1 of *ASM Handbook*, pp. 841–907. ASM International, Metals Park, Ohio, 10 edition, 1990.

[25] D. J. Kotecki, "Welding of stainless steels," in *Welding, brazing, and soldering*, vol. 6 of *ASM Handbook*, pp. 677–705. ASM International, Metals Park, Ohio, 10 edition, 1993.

[26] W. R. Oates and A. M. Saitta, "Stainless and heat-resisting steels," in *Materials and Applications Part 2*, vol. 4 of *AWS Welding Handbook*, pp. 257–296. American Welding Society, Miami, FL, 8 edition, 1998.

[27] "Application of the schaeffler diagram," http://www.dacaposteel.com/filer/schaeffler_diagram.pdf, accessed on 11 Mar 2010.

[28] "Stainless steel - grade 304," http://www.azom.com/Details.asp?ArticleID=965, accessed on 15 Jun 2008.

[29] "Nexus 308L/308LSi datasheet," http://www.nexusweld.com, accessed on Nov 2007.

[30] AWS Committee, "Titanium and titanium alloys," in *Materials and Applications Part 2*, vol. 4 of *AWS Welding Handbook*, pp. 487–540. American Welding Society, Miami, FL, 8 edition, 1998.

[31] S. Lampman, "Wrought titanium and titanium alloys," in *Properties and selection : nonferrous alloys and special-purpose materials*, vol. 2 of *ASM Handbook*, pp. 592–633. ASM International, Metals Park, Ohio, 10 edition, 1990.

[32] R. T. Webster, "Welding of titanium alloys," in *Welding, brazing, and soldering*, vol. 6 of *ASM Handbook*, pp. 783–786. ASM International, Metals Park, Ohio, 10 edition, 1993.

[33] D. Eylon, J. R. Newman, and J. K. Thorne, "Titanium and titanium alloy castings," in *Properties and selection : nonferrous alloys and special-purpose materials*, vol. 2 of *ASM Handbook*, pp. 634–646. ASM International, Metals Park, Ohio, 10 edition, 1990.

[34] "Titanium Ti-6Al-4V (grade 5) datasheet," http://www.matweb.com/, accessed on Jul 2009.

[35] "Thermocouples - an introduction," http://www.omega.com/thermocouples.html, accessed on 15 Mar 2010.

[36] "Introduction to temperature measurement," http://www.omega.com/prodinfo/temperaturemeasurement.html, accessed on 15 Mar 2010.

[37] "Pyrometer-handbook: Non-contact thermometry," Also available as http://www.impacinfrared.com/EN/application-solution/basics/.

[38] "Spectrum," Also available as http://www.raytek.com/Raytek/en-r0.

[39] "Principles of noncontact temperature measurement," http://www.raytek.com/Raytek/en-r0/IREducation/Principlesof+IR.htm, accessed on 17 Mar 2010.

[40] "Non-contact temperature measurement," 1998, Also available as http://www.omega.com/literature/transactions/.

[41] D. Montgomery, *Design and Analysis of Experiments*, John Wiley & Sons, Hoboken, NJ, 6 edition, 2005.

[42] "Nist/sematech e-handbook of statistical methods," http://www.itl.nist.gov/div898/handbook/index.htm, accessed on 21 Mar 2010.

[43] M. Anderson and S. Kraber, "Keys to successful designed experiments," http://www.statease.com/pubs/doe-keys.pdf, 2007, accessed on 10 Jun 2007.

[44] "Factorial plots," http://www.processma.com/resource/factorial_plots.htm, accessed on 23 Mar 2010.

[45] J. Golten and A. Verwer, *Control system design and simulation*, McGraw-Hill, London, 1991.

[46] R. C. Dorf and R. H. Bishop, *Modern control systems*, Pearson Prentice Hall, Upper Saddle River, NJ, 10 edition, 2005.

[47] R. C. Dorf and R. H. Bishop, "Modern control systems companion website," http://www.prenhall.com/dorf/, accessed on 17 Feb 2010.

[48] "Understanding poles and zeros," http://web.mit.edu/2.14/www/Handouts/PoleZero.pdf, accessed on 30 Mar 2010.

[49] F. White, *Principles of control engineering*, Edward Arnold, London, 1995.

[50] I. Gibson, D. Rosen, and B. Stucker, *Additive Manufacturing Technologies*, Springer, New York, 2010.

[51] E. Grenda, "Rapid manufacturing; what RP will be when it grows up," http://home.att.net/~castleisland/rm_c.htm, accessed on 17 April 2005.

[52] ASTM Committee, "ASTM F2792–09 Standard terminology for additive manufacturing technologies," in *Annual Book of ASTM Standards*, vol. 10.04, pp. 663–664. ASTM International, West Conshohocken, PA, 2010.

[53] J. D. Spencer, P. M. Dickens, and C. M. Wykes, "Rapid prototyping of metal parts by three-dimensional welding," *IMechE*, vol. 212, pp. 175–182, 1998.

[54] S. Jones, "Apparatus and method for forming a body," Application Number: GB 0107561.3Patent Version Number: 2373749.

[55] H. Wang, W. Jiang, J. Ouyang, and R. Kovacevic, "Rapid prototyping of 4043 Al-alloy parts by VP-GTAW," *Journal of Materials Processing Technology*, vol. 148, pp. 93–102, 2004.

[56] H. Zhang, J. Xu, and G.Wang, "Fundamental study on plasma deposition manufacturing," *Surface and Coatings Technology*, vol. 171, pp. 112–118, 2003.

[57] "Electron beam melting," http://www.arcam.com/, accessed on 05 May 2006.

[58] M. L. Griffith, D. M. Keicher, C. L. Atwood, J. A. Romero, J. E. Smugeresky, L. D. Harwell, and D. L. Green, "Free form fabrication of metallic components using laser engineered net shaping (LENS)," in *Solid Freeform Fabrication Symposium Proceedings*, Austin, TX, USA, 1996.

[59] J. Mazumder, D. Dutta, N. Kikuchi, and A. Ghosh, "Closed loop direct metal deposition: art to part," *Optics and Lasers in Engineering*, vol. 34, pp. 397–414, 2000.

[60] Y. Li, X. Huang, Y. Liu, and H. Peng, "Laser net shape manufacturing of metallic materials with CO_2 and fiber laser," in *ICALEO Congress Proceedings*, Miami, FL, USA, 2005, pp. 320–325.

[61] L. Costa and R. Vilar, "Laser powder deposition," *Rapid Prototyping Journal*, vol. 15/4, pp. 264–279, 2009.

[62] W. Hofmeister, M. Wert, J. Smugeresky, J. A. Philliber, M. Griffith, and M. Ensz, "Investigating solidification with the laser-engineered net shaping (LENS) process," *JOM*, vol. 51, Jul 1999.

[63] W. U. H. Syed, A. J. Pinkerton, and L. Li, "Combining wire and coaxial powder feeding in laser direct metal deposition for rapid prototyping," *Applied Surface Science*, vol. 252, pp. 4803–4808, 2006.

[64] G. Bi, B. Schurmann, A. Gasser, K. Wissenbach, and R. Poprawe, "Development and qualification of a novel laser-cladding head with integrated sensors," *International Journal of Machine Tools & Manufacture*, vol. 47, pp. 555–561, 2007.

[65] W. U. H. Syed, A. J. Pinkerton, Z. Liu, and L. Li, "Coincident wire and powder deposition by laser to form compositionally graded material," *Surface & Coatings Technology*, vol. 201, pp. 7083–7091, 2007.

[66] F. Wang, J. Mei, H. Jiang, and X. Wu, "Laser fabrication of Ti6Al4V/TiC composites using simultaneous powder and wire feed," *Materials Science and Engineering A*, vol. 445–446, pp. 461–466, 2007.

[67] H. Qi, M. Azer, and J. Deaton, "Development of transfer functions for controlling fabrication of components by laser net shape deposition (lnsd)," in *ICALEO Congress Proceedings*, Miami, FL, USA, 2005, pp. 869–877.

[68] L. Song and J. Mazumder, "Predictive control for direct metal deposition," in *ICALEO Congress Proceedings*, Orlando, FL, USA, 2007, pp. 829–834.

[69] A. Heralic, A. K. Christiansson, K. Hurtig, Mattias Ottosson, and Bengt Lennartson, "Control design for automation of robotized laser metal-wire deposition," in *17th International Federatin of Automatic Control World Congress*, Seoul, Korea, 2008, pp. 14785–14971.

[70] P. A. Kobryn, E. H. Moore, and S. L. Semiatin, "The effect of laser power and traverse speed on microstructure, porosity and build height in laser deposited Ti-6Al-4V," *Scripta Mater*, vol. 43, pp. 299–305, 2000.

[71] W. H. Hofmeister, D. O. MacCallum, and G. A. Knorovsky, "Video monitoring and control of the LENS process," in *Proceedings of the AWS 9th International Conference on Computer Technology in Welding*, 1998, pp. 187–196.

[72] D. Hu and R. Kovacevic, "Sensing, modeling and control for laser-based additive manufacturing," *International Journal of Machine Tools & Manufacture*, vol. 43, pp. 51–60, 2003.

[73] P. Aubry, M. Guiraud, T. Malot, and K. Verdier, "Process control on laser cladding by coaxial vision for direct manufacturing of 3d metallic structures," in *PICALO Conference Proceedings*, 2008, pp. 402–407.

[74] J. T. Hofman, D. F. de Lange, and J. Meijer, "Camera base feedback control of the laser cladding process," in *ICALEO Congress Proceedings*, Scottsdale, AZ, USA, 2006, pp. 456–460.

[75] L. Song and J. Mazumder, "Robust sensing and control of direct metal deposition," in *PICALO Conference Proceedings*, 2008, pp. 582–586.

[76] D. Salehi and M. Brandt, "Melt pool temperature control using Lab VIEW in Nd:YAG laser blown powder cladding process," *International Journal of Advanced Manufacturing Technology*, vol. 29, pp. 273–278, 2006.

[77] G. Bi, A. Gasser, K. Wissenbach, A. Drenker, and R. Poprawe, "Investigation on the direct laser metallic powder deposition process via temperature measurement," *Applied Surface Science*, vol. 253, pp. 1411–1416, 2006.

[78] G. Bi, A. Gasser, K. Wissenbach, A. Drenker, and R. Poprawe, "Characterization of the process control for the direct laser metallic powder deposition," *Surface & Coatings Technology*, vol. 201, pp. 2676–2683, 2006.

[79] K. H. Leong, K. L. Ho, and H. C. Man, "Monitoring laser cladding," in *ICALEO Congress Proceedings*, Miami, FL, USA, 2005, pp. 895–899.

[80] D. Krantz and S. Nasla, "Intelligent process control for laser direct metal deposition," in *ICALEO Conference Proceedings*, 2000, pp. D1–D10.

[81] "Triangulation laser sensors rf605 series," http://www.riftek.com/resource/download/rf605_riftek_eng.pdf, accessed on 05 Mar 2010.

[82] G. Vander-Voort, G. M. Lucas, and E. P. Manilova, "Metallography and microstructures of stainless steels and maraging steels," in *Metallography and microstructures*, vol. 9 of *ASM Handbook*, pp. 670–705. ASM International, Metals Park, Ohio, 10 edition, 2004.

[83] I. Pashby, G. Bi, S. H. Mok, and J. Folkes, "Deposition of Ti-6Al-4V using a high power diode laser and wire," in *Proceedings of the 5th LANE 2007*, Erlangen, Germany, Sep 2007, pp. 345–356, Meisenbach Bamberg.

[84] C. F. Hung and J. Lin, "Solidification model of laser cladding with wire feeding technique," *Journal of Laser Applications*, vol. 16, pp. 140–146, Aug 2004.

[85] D. Montgomery, *Design and Analysis of Experiments*, John Wiley & Sons, New York, 5 edition, 2001.

[86] "Raytek marathon series mm 1m 2m datasheet," http://support.fluke.com/raytek-sales/Download/Asset/9250015_ENG_C_W.PDF, accessed on 17 Mar 2010.

[87] "Iga 50-lo plus," http://www.lumasenseinc.com/EN/products/pyrometer/series-50/iga-50-lo-plus.html, accessed on 17 Mar 2010.

[88] S. Shinners, *Modern control system theory and design*, John Wiley & Sons, New York, 2 edition, 1998.

[89] K. Ogata, *Modern control engineering*, Prentice Hall, Upper Saddle River, NJ, 4 edition, 2002.

[90] D. Bergstrom, J. Powell, and A. Kaplan, "The reflectance of steels and non-ferrous alloys to Nd:YAG and Nd:YLF laser light," in *PICALO Conference Proceedings*, Melbourne, AU, 2006, pp. 140–145.

[91] J. Miettinen, "Calculation of solidification-related thermophysical properties for steels," *Metallurgical and materials transactions B*, vol. 28B, pp. 281–296, Apr 1997.

[92] J. D. Majumdar, A. Pinkerton, Z. Liu, I. Manna, and L. Li, "Mechanical and electrochemical properties of multiple-layer diode laser cladding of 316l stainless steel," *Applied Surface Science*, vol. 247, pp. 373–377, 2005.

[93] "Stainless steel - approximate hardness conversions for austenitic stainless steels," http://www.azom.com/details.asp?ArticleID=1152, accessed on 28 Apr 2010.

[94] "Primes focusmonitor - user manual," 2008.

[95] "Laser engineered net shaping," http://www.optomec.com/site/lens_home, accessed on 05 May 2006.

[96] "CO_2 lasers," http://www.rp-photonics.com/co2_lasers.html, accessed on 26 Feb 2010.

[97] "Laser diodes," http://www.rp-photonics.com/laser_diodes.html, accessed on 26 Feb 2010.

[98] "IPG Ytterbium fiber laser YLR-2000-p user manual," .

[99] K. Niles, "Most practical DOE explained," http://www.isixsigma.com/library/content/c030616a.asp, accessed on 21 Jan 2007.

[100] R. Dull, "Advantages of plasma welding: Often-overlooked PAW offers speed and affordability," http://www.thefabricator.com/ArcWelding/ArcWelding_Article.cfm?ID=135, accessed on 07 May 2006.

[101] V. Easton and J. McColl, "Statistics glossary: Design of experiments and ANOVA," http://www.cas.lancs.ac.uk/glossary_v1.1/dexanova.html#expdes, accessed on 21 Jan 2007.

[102] P. Fuerschbach, "Energy transfer efficiencies (ETE) for fusion welding processes," http://www.sandia.gov/soar/Pdf_docs/Ener_trans_effic.pdf, 2004, accessed on 12 Nov 2006.

[103] T. Wohlers, "New developments and trends in rapid and high-performance tooling," http://wohlersassociates.com/EuroMold-2002-paper.html, Dec 2002, accessed on 11 Apr 2005.

[104] L. Smith, "The fundamentals of gas tungsten arc welding: Preparation, consumables, and equipment necessary for the process," http://www.thefabricator.com/ArcWelding/ArcWelding_Article.cfm?ID=518, accessed on 07 May 2006.

[105] J. D. Destefani, "Introduction to titanium and titanium alloys," in *Properties and selection : nonferrous alloys and special-purpose materials*, vol. 2 of *ASM Handbook*, pp. 586–591. ASM International, Metals Park, Ohio, 10 edition, 1990.

[106] J. Mazumder, "Laser-beam welding," in *Welding, brazing, and soldering*, vol. 6 of *ASM Handbook*, pp. 262–269. ASM International, Metals Park, Ohio, 10 edition, 1993.

[107] AWS Committee, *Welding Technology*, vol. 1 of *AWS Welding Handbook*, American Welding Society, Miami, FL, 8 edition, 1991.

[108] AWS Committee, *Welding Processes*, vol. 2 of *AWS Welding Handbook*, American Welding Society, Miami, FL, 8 edition, 1991.

[109] C. Asfahl, *Robots and manufacturing automation*, John Wiley & Sons, New York, 1992.

[110] A. C. Davies, *The practice of welding*, vol. 2 of *The science and practice of welding*, Cambridge University Press, Cambridge, 10 edition, 1993.

[111] W. Lucas, *TIG and Plasma Welding*, Abington Publishing, Cambridge, 1990.

[112] F. Raven, *Automatic control engineering*, McGraw-Hill, New York, 5 edition, 1995.

[113] G. Franklin, *Feedback control of dynamic systems*, Prentice Hall, Upper Saddle River, NJ, 4 edition, 2002.

[114] R. Stefani, Bahram Shahian, Clement Savant, and Gene Hostetter, *Design of feedback control systems*, Oxford University Press, Oxford, 4 edition, 2002.

[115] *LabVIEW Getting Started with LabVIEW*, National Instruments Corporation, 2006.

[116] *LabVIEW Control Design Toolkit User Manual*, National Instruments Corporation, 2006.

[117] A. Heralic, M. Ottosson, K. Hurtig, and A. K. Christiansson, "Visual feedback for operator interaction in robotized laser metal deposition," in *22nd Conference on Surface Modification Technologies*, Trollhattan, Sweden, 2008.

[118] A. Medrano, J. Folkes, J. Segal, and I. Pashby, "Fibre laser metal deposition with wire: parameters study and temperature monitoring system," in *Proceedings SPIE*, Lisbon, PT, Sep 2008, vol. 7131, XVII International Symposium on Gas Flow, Chemical Lasers, and High-Power Lasers.

[119] S. Barnes, N. Timms, B. Bryden, and I. Pashby, "High power diode laser cladding," *Journal of Materials Processing Technology*, vol. 138, pp. 411–416, 2003.

[120] M. Doubenskaia, P. Bertrand, and I. Smurov, "Optical monitoring of nd:yag laser cladding," *Thin Solid Films*, vol. 453–454, pp. 477–485, 2004.

[121] D. Coleman and D. Montgomery, "A systematic approach to planning for a designed industrial experiment (with discussion)," *Technometrics*, vol. 35, pp. 1–27, 1993.

[122] D. Farson, R. Richardson, and X. Li, "Infrared measurement of base metal temperature in gas tungsten arc welding," *Welding Journal Supplement*, 1998, Also available as http://www.aws.org/wj/supplement/Farson/farson.htmlaccessed on 24 Jan 2007.

[123] S. C. Juang and Y. S. Tarng, "Process parameter selection for optimizing the weld pool geometry in the tungsten inert gas welding of stainless steel," *Journal of Materials Processing Technology*, vol. 122, pp. 33–37, 2002.

[124] I. S. Kim, K. J. Son, Y. S. Yang, and P. K. D. V. Yaragada, "Sensitivity analysis for process parameters in gma welding processes using a factorial design method," *International Journal of Machine Tools & Manufacture*, vol. 43, pp. 763–769, 2003.

[125] S. H. Mok, G. Bi, J. Folkes, I. Pashby, and J. Segal, "Deposition of Ti-6Al-4V using a high power diode laser and wire, part II: Investigation on the mechanical properties," *Surface & Coatings Technology*, vol. 202, pp. 4613–4619, 2008.

[126] Y. Songa, S. Parka, D. Choib, and H. Jee, "3d welding and milling: part I - a direct approach for freeform fabrication of metallic prototypes," *International Journal of Machine Tools & Manufacture*, vol. 45, pp. 10571062, 2005.

[127] Y. Songa, S. Parka, and S. Chaeb, "3d welding and milling: part II - optimization of the 3d welding process using an experimental design approach," *International Journal of Machine Tools & Manufacture*, vol. 45, pp. 1063–1069, 2005.

[128] S. Y. Tu, M. D. Jean, J. TingWang, and C. SenWu, "A robust design in hardfacing using a plasma transfer arc," *Int J Adv Manuf Technol*, vol. 27, pp. 889–896, 2006.

[129] W. Hofmeister, M. Griffith, M. Ensz, and J. Smugeresky, "Solidification in direct metal deposition by LENS processing," *JOM*, pp. 30–34, Sep 2001.

[130] T. Koseki and M. C. Flemings, "Solidification of undercooled Fe-Cr-Ni alloys part II - microstructural evolution," *Metallurgical and Materials Transactions A*, pp. 3226–3240, 1996.

[131] P. Aubry, M. Guiraud, T. Malot, and K. Verdier, "Parameter study and process control on laser cladding for direct manufacturing of 3d metallic structures," in *ICALEO Congress Proceedings*, Orlando, FL, USA, 2007, pp. 841–849.

[132] L. Tang and R. G. Landers, "Melt pool temperature control for laser metal deposition processes – part I: Online temperature control," *Journal of Manufacturing Science and Engineering*, vol. 132, pp. 011010–1–011010–9, Feb 2010.

[133] L. Tang and R. G. Landers, "Melt pool temperature control for laser metal deposition processes – part II: Layer-to-layer temperature control," *Journal of Manufacturing Science and Engineering*, vol. 132, pp. 011011–1–011011–9, Feb 2010.

Appendix A

Laser Power Measurement

This appendix shows the results of the power measurements of the 2 kW IPG fibre laser performed on 03 of June 2009, after the 600 μm process fibre.

Table A.1: Laser power measurement after 600 μm process fibre

Current (%)	Power_{ind} (kW)	Power_{meas} (kW)
10	0.10	96
20	0.31	295
30	0.52	495
40	0.74	695
50	0.95	893
60	1.17	1095
70	1.38	1295
80	1.60	1506
90	1.82	1715
100	2.02	1910

Appendix B

Laser Focus Measurement

The analysis of the laser beam was performed using the PRIMES FocusMonitor. The automatic caustic measurement was used to measure the focal distance and the beam radius. The laser had the 600 μm fibre. Laser power was varied from 250 to 2000 W in steps of 250 W.

The software of the FocusMonitor provides 2 ways to calculate the beam radius: 86% and Second order moments.

86% definition: "The radius of the laser beam is calculated by estimating the beam area containing 86% of the total measured laser power. This value allows one to determine the radius of the circle with the same area. This definition is valid only when the laser beam is rotationally-symmetric and there are no areas with deep modulation of laser intensity (very low laser intensity) in the beam area" [94].

Second order moments definition: "The radius of the laser beam is calculated from the second order moment of the power density distribution - according to ISO 11146" [94].

Caustic Measurement

In this mode the device scans the laser beam in different positions (Z axis) in order to find the beam radius at every Z position and the focal distance of the beam.

Measurements were performed on 11th March 2008 and on 10th July 2008. On the 10th July the PRIMES FocusMonitor of Cranfield University was used. Results of both measurements are presented.

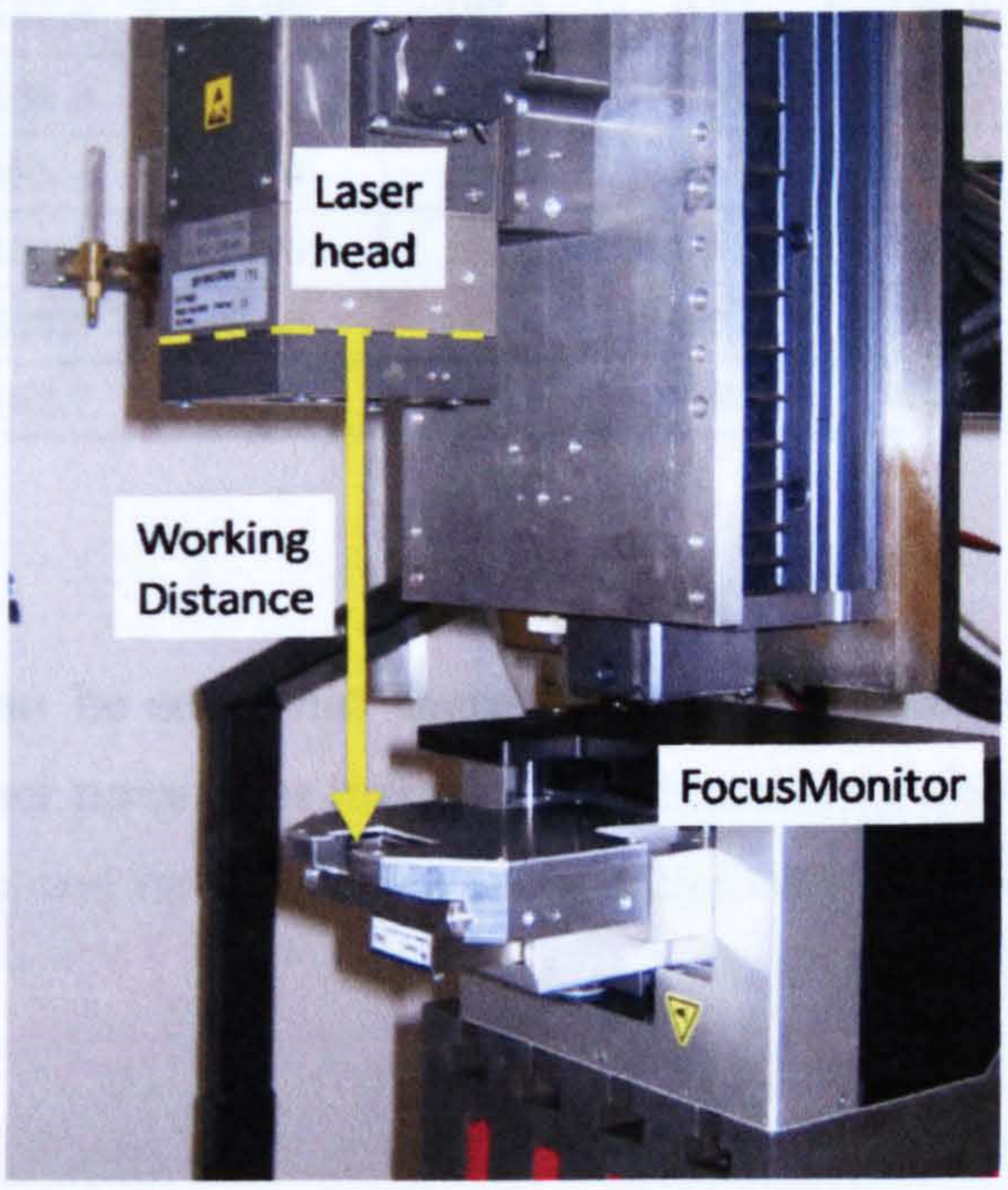

Figure B.1: Setup for beam analysis

The beam diameter was analysed as a function of the working distance. This distance was measured from a reference edge in the laser head to the measuring tip of the FocusMonitor. The reference in the laser head is shown in Figure B.1.

Focal distance and laser power

The results of the measurements are shown in Table B.1.

Table B.1: Focal distance and diameter (in focus) at different laser power settings

	11th March 2008				10th July 2008			
	86% radius		2nd order moments		86% radius		2nd order moments	
Laser Power (W)	Beam diameter (mm)	Focus position (mm)	Beam diameter (mm)	Focus position (mm)	Beam diameter (mm)	Focus position (mm)	Beam diameter (mm)	Focus position (mm)
250	0.90	190.2	0.96	190.7	0.92	189.6	0.95	189.7
500	0.90	188.9	0.94	189.2	0.91	188.6	0.95	188.7
750	0.90	187.9	0.95	187.9	0.91	186.9	0.95	187.1
1000	0.90	186.9	0.95	186.9	0.90	185.6	0.95	185.8
1250	0.90	185.8	0.94	186.0	0.91	183.8	0.96	184.1
1500	0.91	184.5	0.96	184.6	0.92	182.2	0.95	182.2
1750	0.92	183.3	0.96	183.4	0.92	181.1	0.96	181.2
2000	0.91	182.7	0.96	183.0	0.94	180.4	0.98	180.6

From Table B.1 it can be seen that there was a considerable variation in the focal distance when the laser power was increased. This is shown also in Figure B.2 for the 86% radius definition and in Figure B.3 for the 2nd order moments definition.

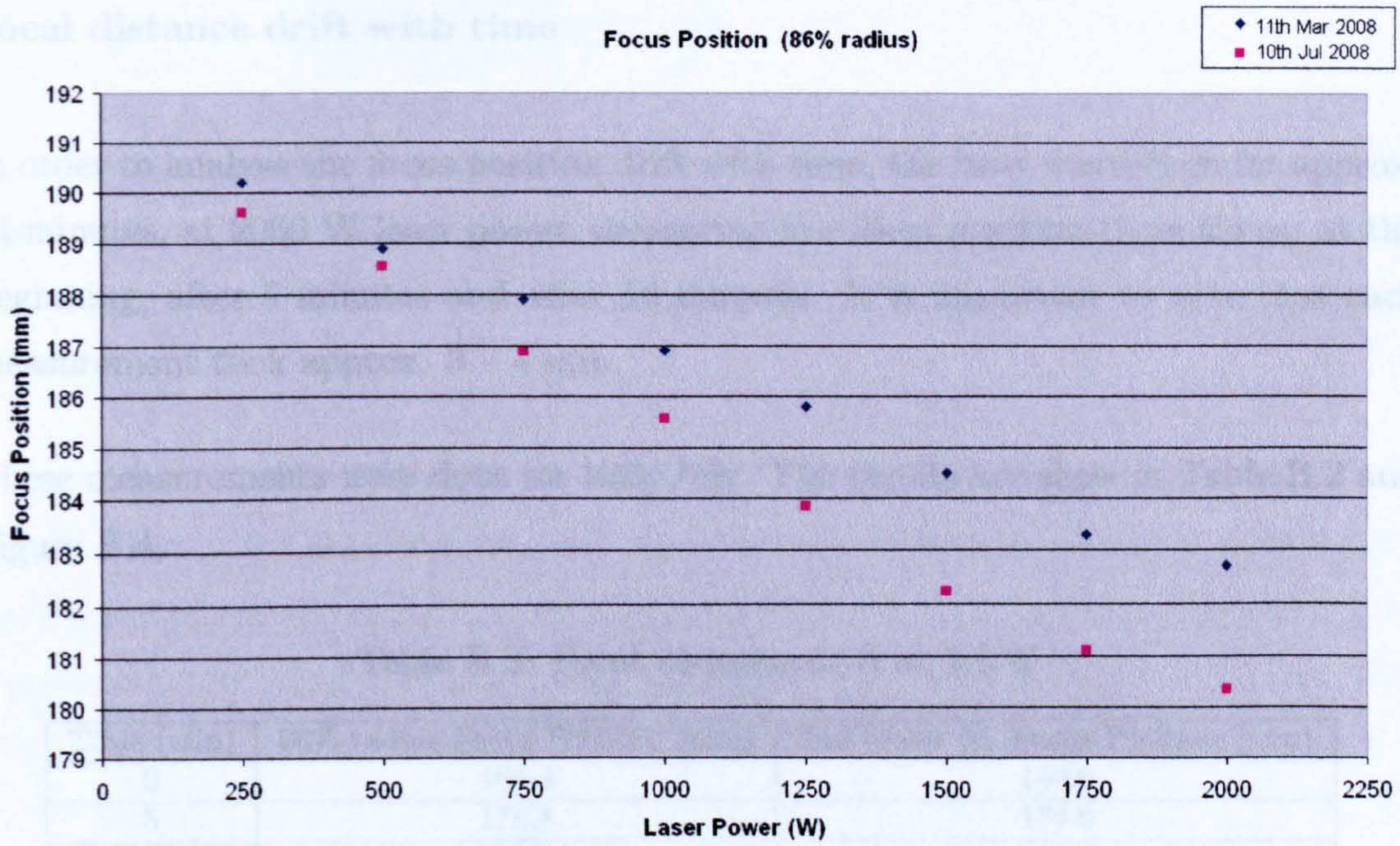

Figure B.2: Focal distance vs laser power (86% radius definition)

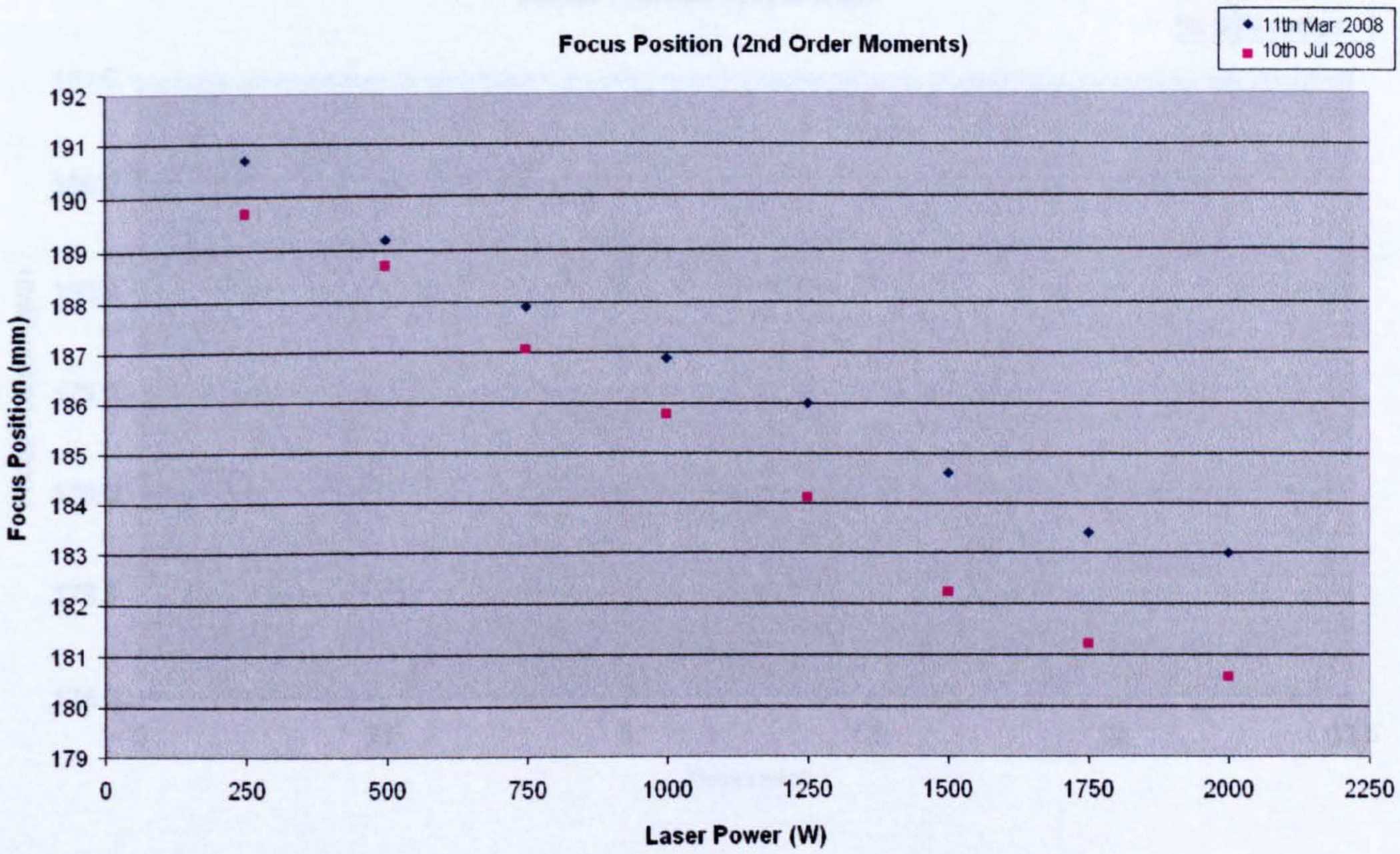

Figure B.3: Focal distance vs laser power (Second order moments)

Focal distance drift with time

In order to analyse the focus position drift with time, the laser was left on for approx. 14 minutes, at 2000 W laser power, measuring the focus position three times: at the beginning, after 5 minutes and after 10 minutes. It is important to note that each measurement took approx. 3 – 4 min.

These measurements were done on 10th July. The results are show in Table B.2 and Figure B.4.

Table B.2: Focal distance drift at 2 kW

Time (min)	86% radius Focus Position (mm)	2nd Order M. Focus Position (mm)
0	180.4	180.6
5	178.8	179.0
10	178.8	178.9

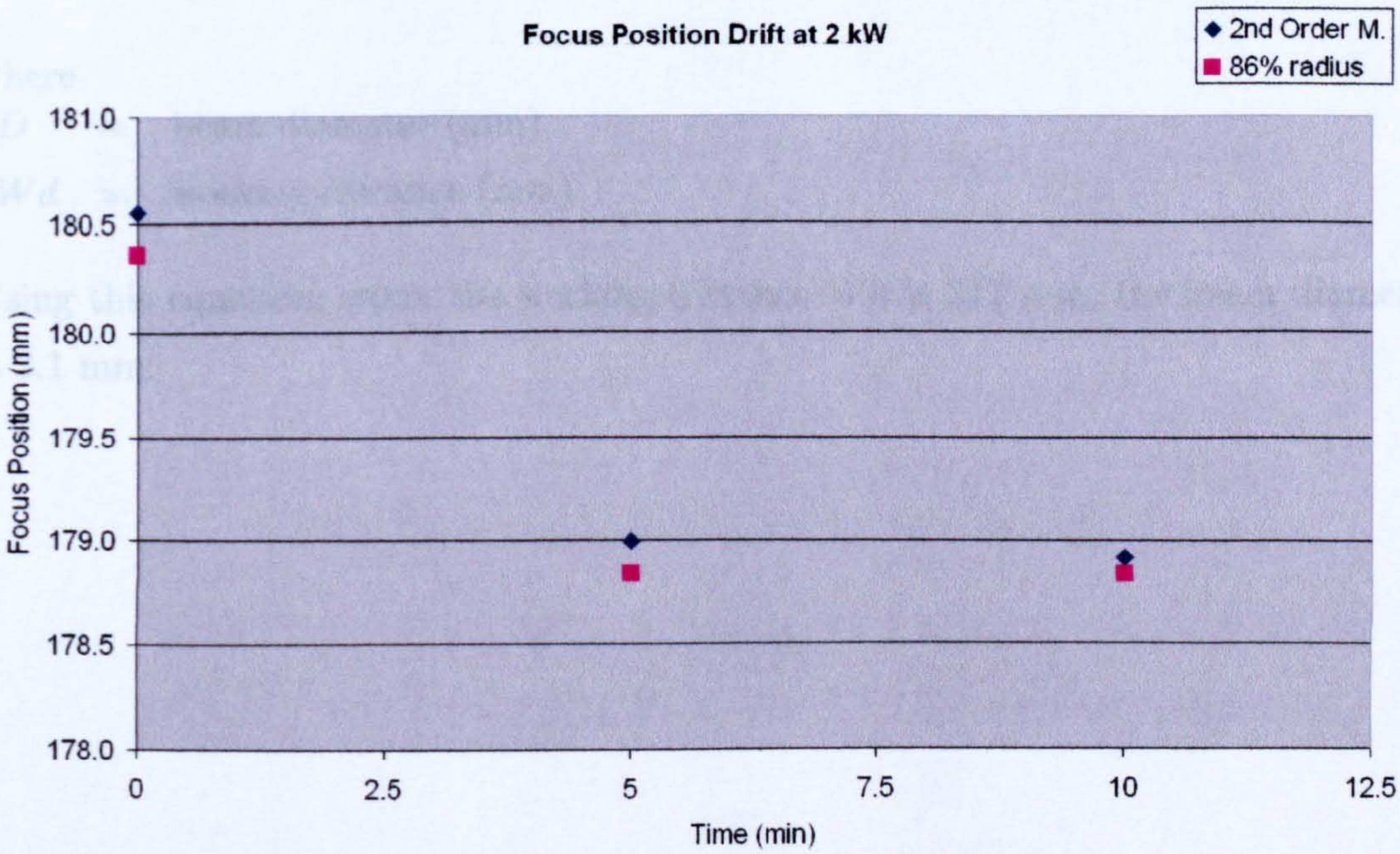

Figure B.4: Focal distance drift at 2 kW

Measurements at 1500 W out of focus

Laser metal deposition experiments had been done at 212 mm working distance, with a laser power around 1500 W. For this reason the beam was also analysed out of focus in order to know the beam diameter at different distances, applying a laser power of 1500 W.

The result is shown in Figure B.5. In order to find the relationship between the distance form laser head and the beam diameter, the trend lines of both measurements have been calculated using the data from 191 to 213 mm (working distance). The equations of the trend lines have been averaged to calculate an overall trend line. The resulting equation is:

$$D = 0.0944\,Wd - 16.906$$

where

D = beam diameter (mm)

Wd = working distance (mm)

Using this equation, when the working distance Wd is 212 mm, the beam diameter is 3.1 mm.

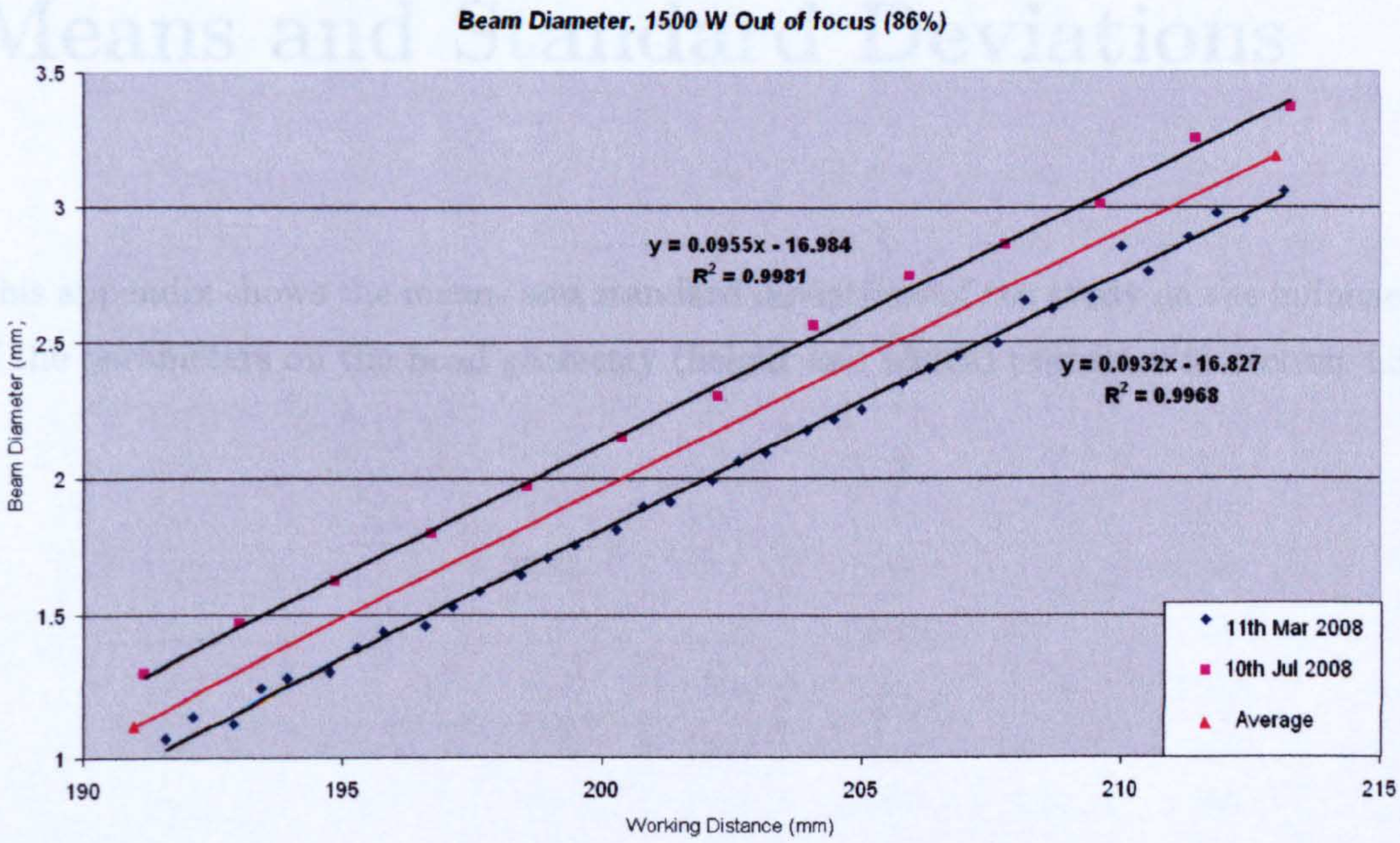

Figure B.5: Beam diameter out of focus at 1.5 kW

Appendix C

Means and Standard Deviations

This appendix shows the means and standard deviations of the study on the influence of the parameters on the bead geometry (height and width) presented in section 4.3.

Table C.1: Means and standard deviations of bead height and width

Laser Power (W)	Traverse Speed (mm/min)	Wire Feed Rate (m/min)	Mean Height (mm)	Standard Deviation Height	Mean Width (mm)	Standard Deviation Width
1700	175	0.8	1.73	0.056	3.46	0.110
1700	175	1.0	1.98	0.021	3.75	0.049
1700	175	1.2	2.33	0.035	3.78	0.071
1700	200	0.8	1.63	0.087	3.22	0.204
1700	200	1.0	1.83	0.015	3.60	0.046
1700	200	1.2	2.15	0.031	3.55	0.015
1700	225	0.8	1.50	0.042	3.11	0.111
1700	225	1.0	1.73	0.035	3.27	0.164
1700	225	1.2	1.98	0.060	3.42	0.125
1850	175	0.8	1.72	0.040	3.57	0.040
1850	175	1.0	2.00	0.035	3.65	0.091
1850	175	1.2	2.27	0.031	3.90	0.075
1850	200	0.8	1.60	0.035	3.38	0.123
1850	200	1.0	1.84	0.060	3.49	0.115
1850	200	1.2	2.07	0.030	3.73	0.076
1850	225	0.8	1.51	0.012	3.15	0.060
1850	225	1.0	1.75	0.015	3.31	0.104
1850	225	1.2	1.93	0.032	3.55	0.015
2000	175	0.8	1.69	0.051	3.48	0.035
2000	175	1.0	1.93	0.025	3.92	0.088
2000	175	1.2	2.26	0.035	3.88	0.095
2000	200	0.8	1.54	0.025	3.55	0.066
2000	200	1.0	1.80	0.032	3.64	0.048
2000	200	1.2	2.08	0.062	3.78	0.059
2000	225	0.8	1.50	0.030	3.21	0.094
2000	225	1.0	1.69	0.045	3.33	0.108
2000	225	1.2	1.95	0.021	3.55	0.023

Appendix D

Residual Plots

This appendix shows the residual plots of the ANOVA tests of this thesis.

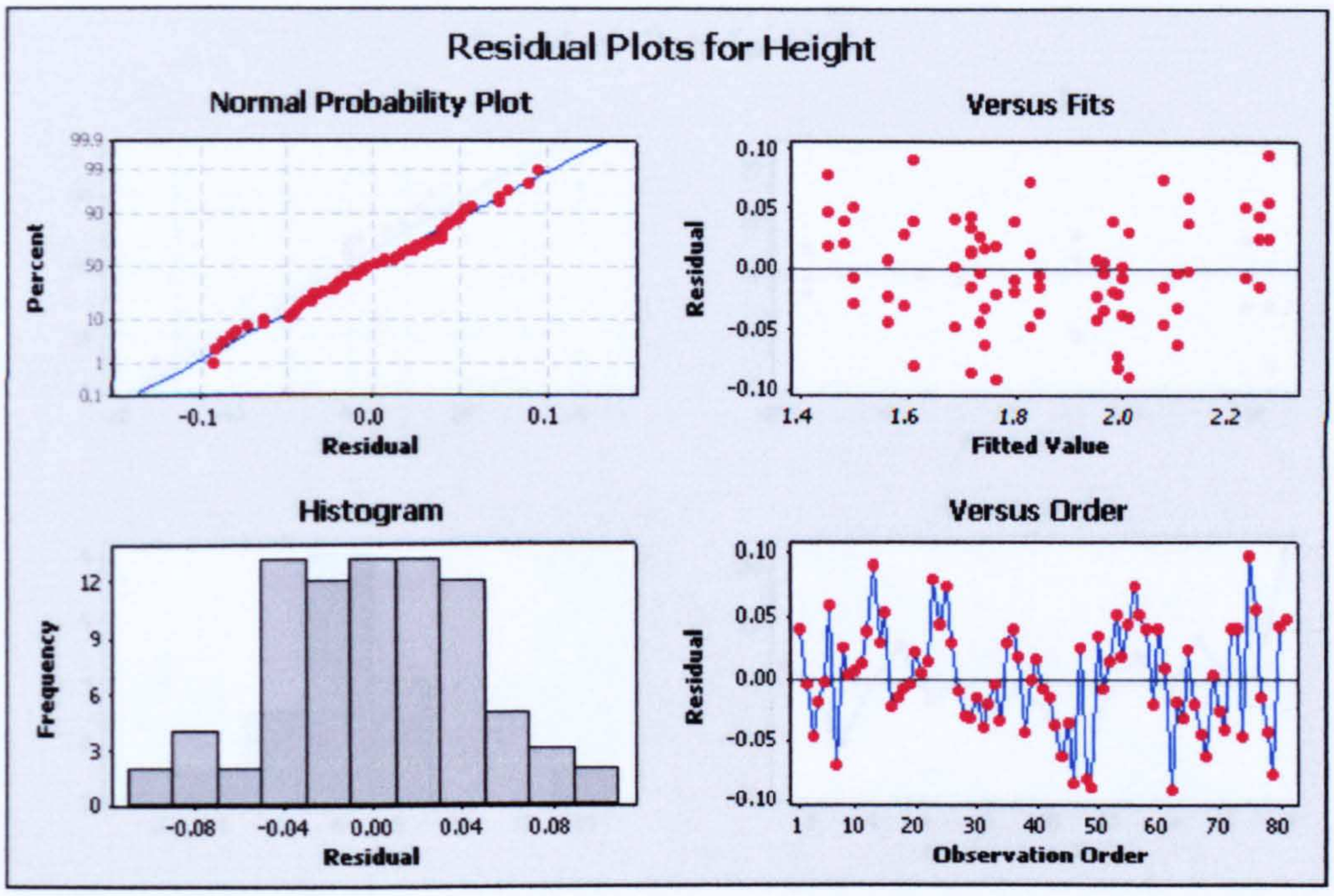

Figure D.1: Residual plots for bead height

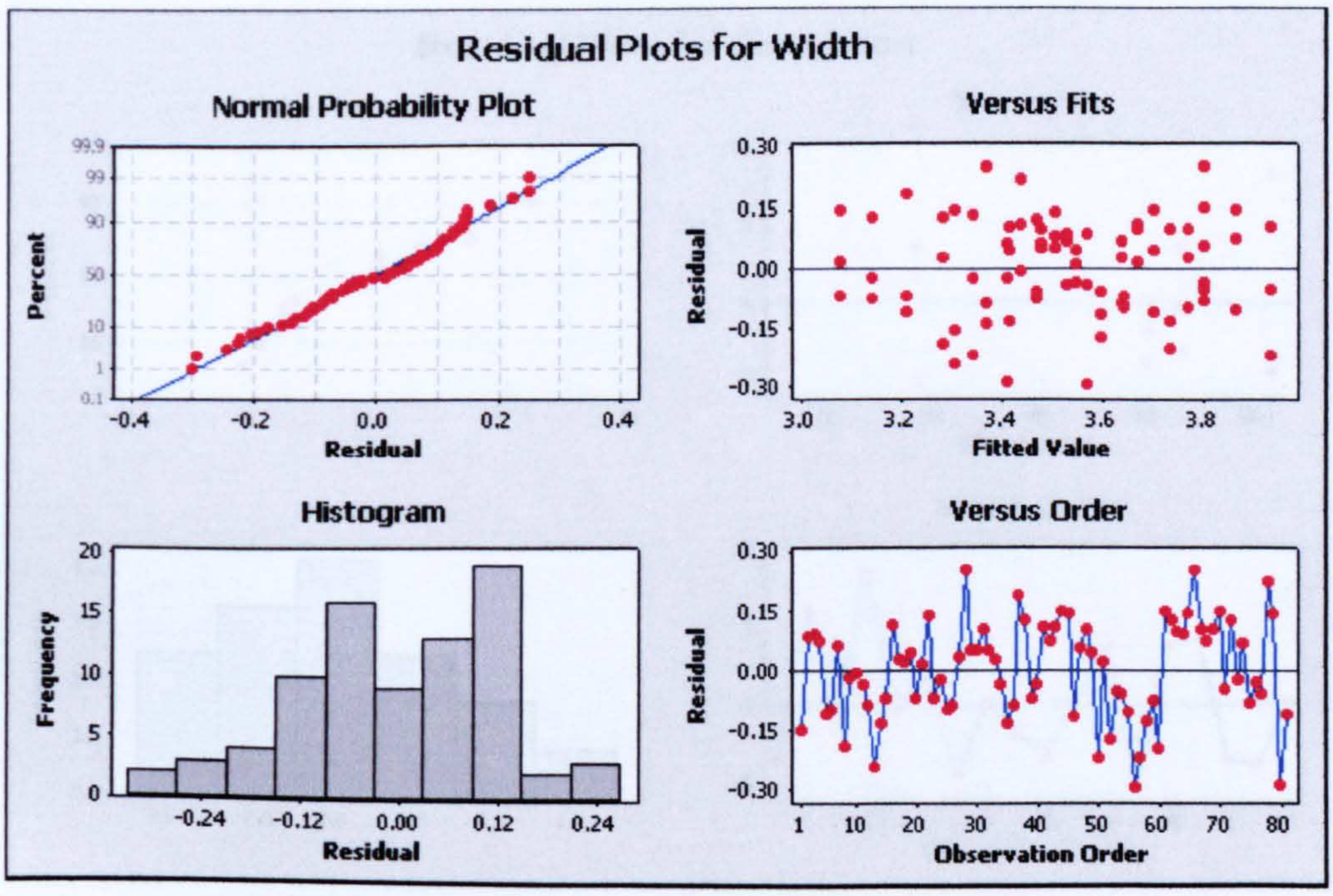

Figure D.2: Residual plots for bead width

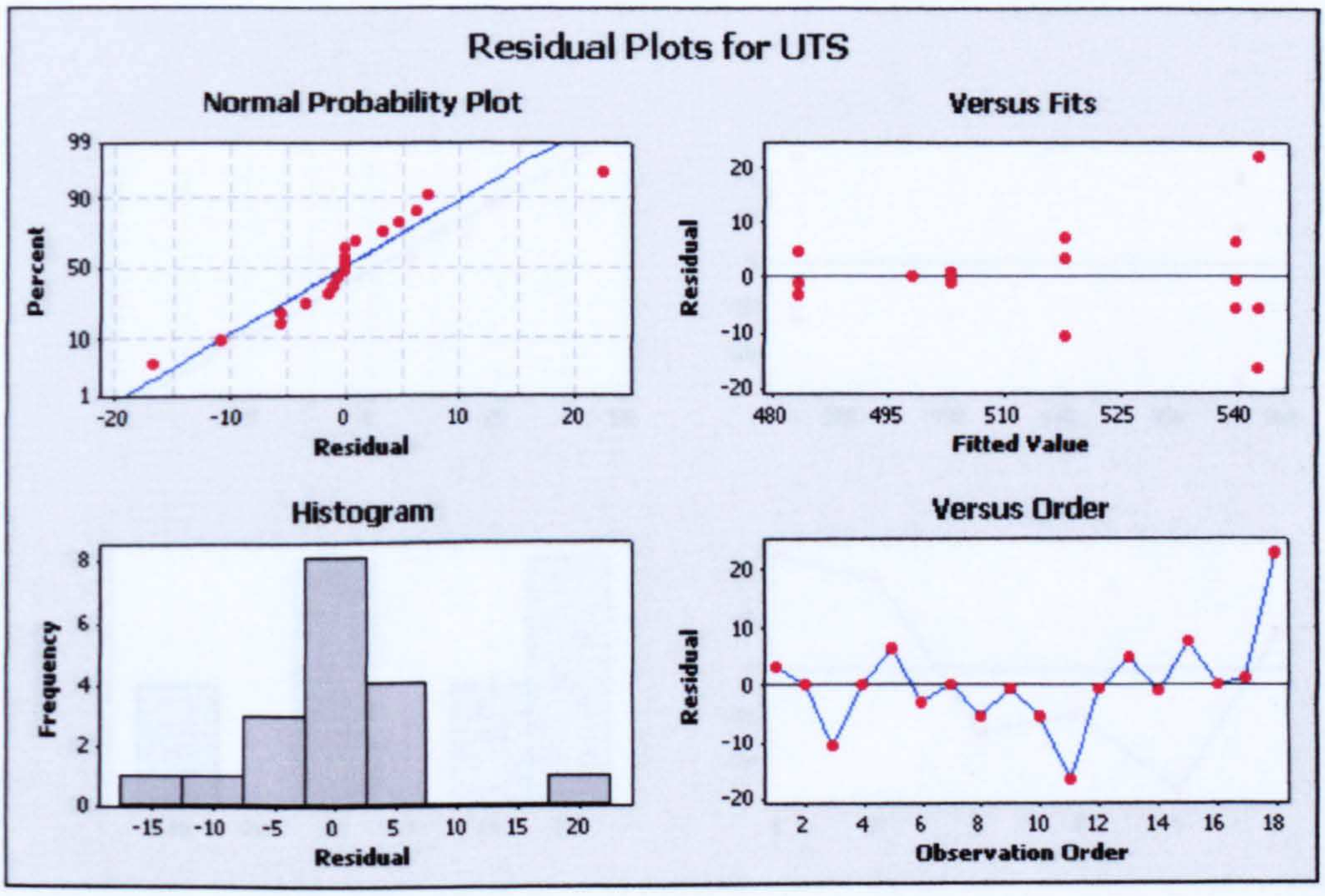

Figure D.3: Residual plots for UTS of stainless steel 308LSi

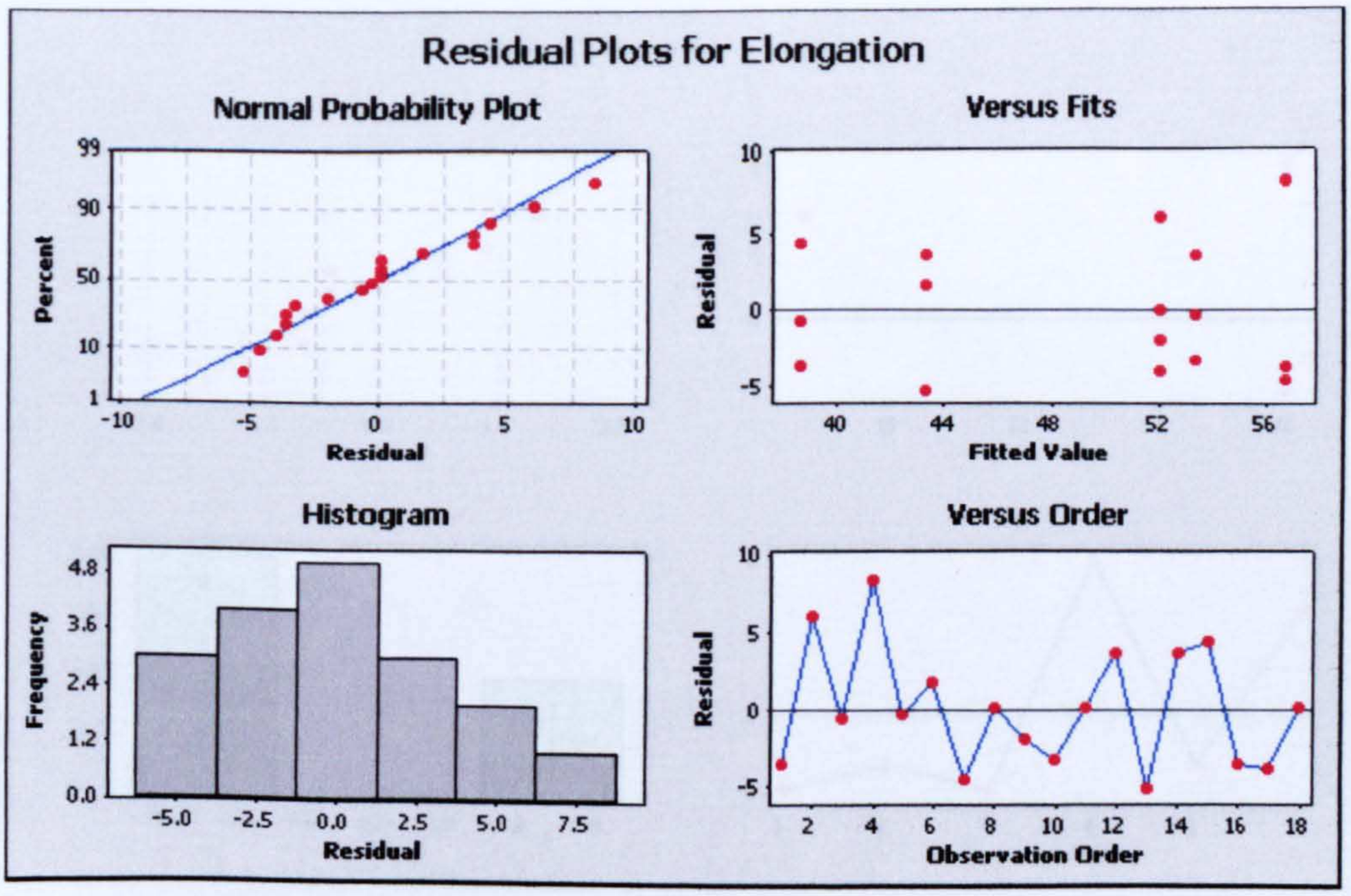

Figure D.4: Residual plots for elongation of stainless steel 308LSi

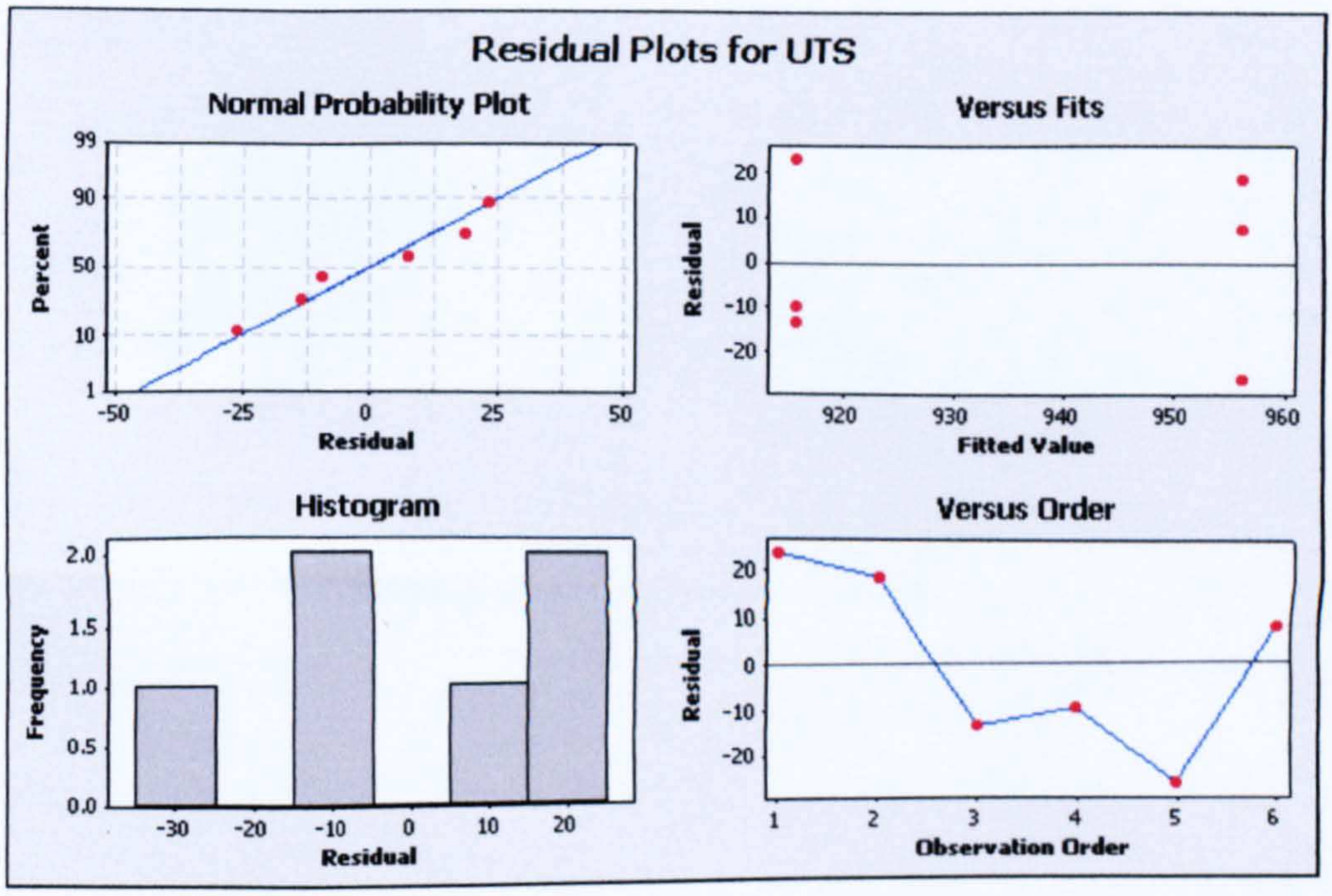

Figure D.5: Residual plots for UTS of Ti-6Al-4V

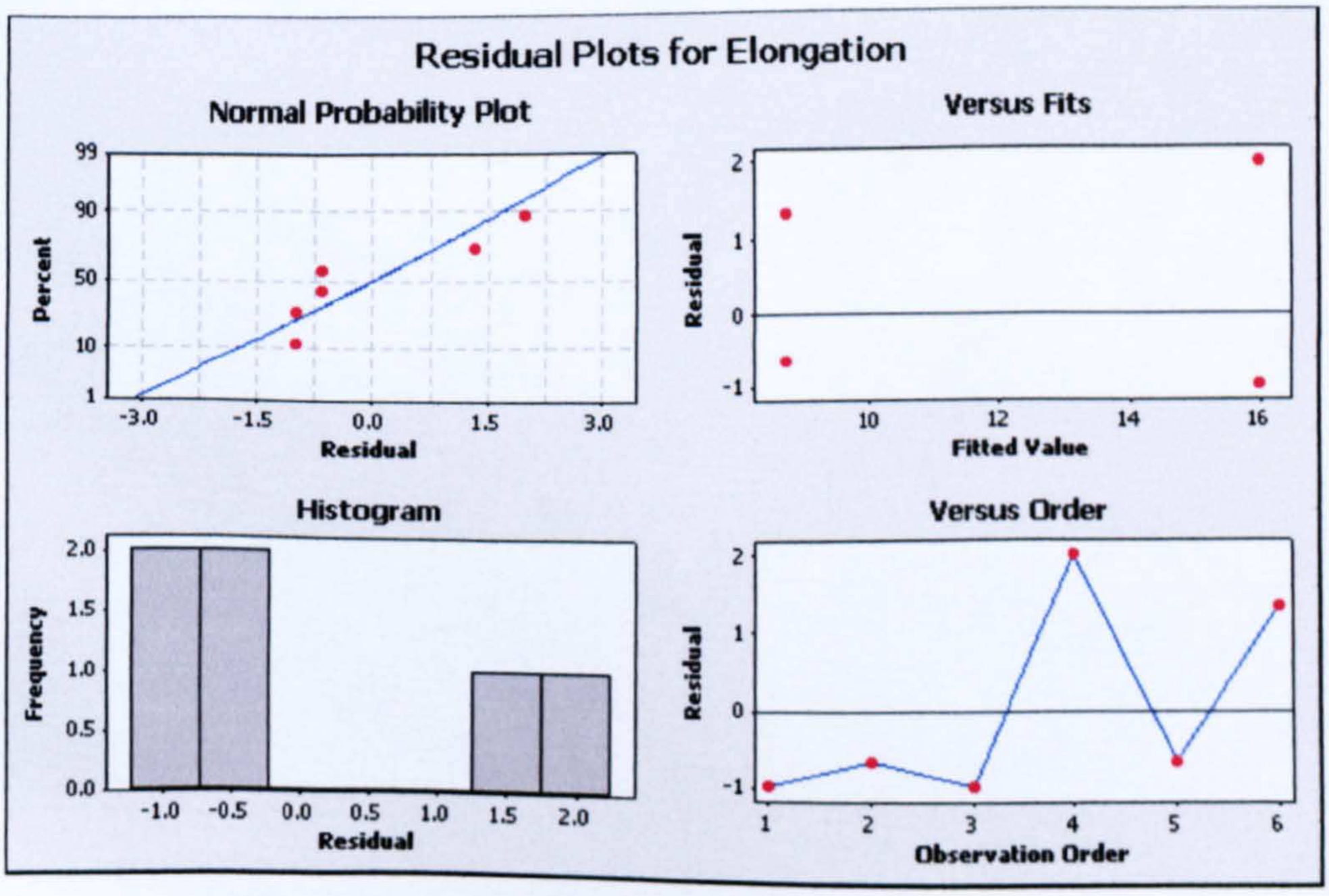

Figure D.6: Residual plots for elongation of Ti-6Al-4V